ENERGY CONSERVATION MECHANISMS AND ELECTRON TRANSFER IN SYNTROPHIC PROPIONATE-OXIDIZING MICROBIAL CONSORTIA

VICENTE T. SEDANO NÚÑEZ

PROPOSITIONS

1. Reverse electron transfer, exocellular electron transfer and confurcation mechanisms are all necessary for syntrophic growth on propionate (This thesis)

2. In *Syntrophobacter fumaroxidans*, molybdenum-containing formate dehydrogenases are key enzymes for interspecies electron transfer during syntrophic propionate oxidation (This thesis)

3. Anaerobic digestion is no longer a black-box but rather an over-exposed photo.

4. The circadian rhythm in archaea and bacteria will become essential in the planning of experiments. (Johnson et al., 2017. Nature Reviews Microbiology)

5. The discovery of the existence of water as two fluids with different densities at the same time, as described by Perakis et al. (PNAS. 2017), has major implications in metabolism.

6. Scientists are to blame for the wave of antiscientific policies around the world.

7. The title of *Philosophiae Doctor* (PhD) does not describe the current aptitudes of PhD graduates.

8. In the quest for practicality and universal understanding, the scientific language has become tedious.

Prepositions belonging to the PhD thesis entitled "Energy conservation mechanisms and electron transfer in syntrophic propionate-oxidizing microbial consortia".

Vicente T. Sedano Núñez

Wageningen, 3 April 2018

ENERGY CONSERVATION MECHANISMS AND ELECTRON TRANSFER IN SYNTROPHIC PROPIONATE-OXIDIZING MICROBIAL CONSORTIA

VICENTE T. SEDANO NÚÑEZ

Thesis committee

Promotor

Prof. Dr Alfons J.M. Stams
Personal chair at the Laboratory of Microbiology
Wageningen University & Research

Co-promotor

Dr Caroline M. Plugge
Associate professor, Laboratory of Microbiology
Wageningen University & Research

Other members

Prof. Dr Willem J.H. van Berkel, Wageningen University & Research
Prof. Dr Huub J.M. Op den Camp, Radboud University Nijmegen, The Netherlands
Dr Robbert Kleerebezem, Delft University of Technology, The Netherlands
Prof. Dr Inês Cardoso Pereira, Universidade Nova de Lisboa, Portugal

This research was conducted under the auspices of the Graduate School for Socio-Economic and Natural Sciences of the Environment (SENSE).

Energy conservation mechanisms and electron transfer in syntrophic propionate-oxidizing microbial consortia

Vicente T. Sedano Núñez

Thesis

submitted in fulfilment of the requirements for the degree of doctor
at Wageningen University
by the authority of the Rector Magnificus,
Prof. Dr A.P.J. Mol,
in presence of the
Thesis Committee appointed by the Academic Board
to be defended in public
on Tuesday 3 April 2018
at 1:30 p.m. in the Aula.

Vicente Tonamellotl Sedano Núñez
Energy conservation mechanisms and electron transfer in syntrophic propionate-oxidizing microbial consortia,
206 pages.

PhD thesis, Wageningen University, Wageningen, the Netherlands (2018)
With references, with summary in English
ISBN: 978-94-6343-263-4
DOI: 10.18174/441473

To the two people that inspired me to begin a doctorate:

S.S.R. & A.H.G.

And to the two people that inspired me to complete it:

G.S.C. & N.A.O.

Table of contents

"There are two mistakes one can make along the road...

Not going all the way, and not starting"

S. G.

Chapter 1

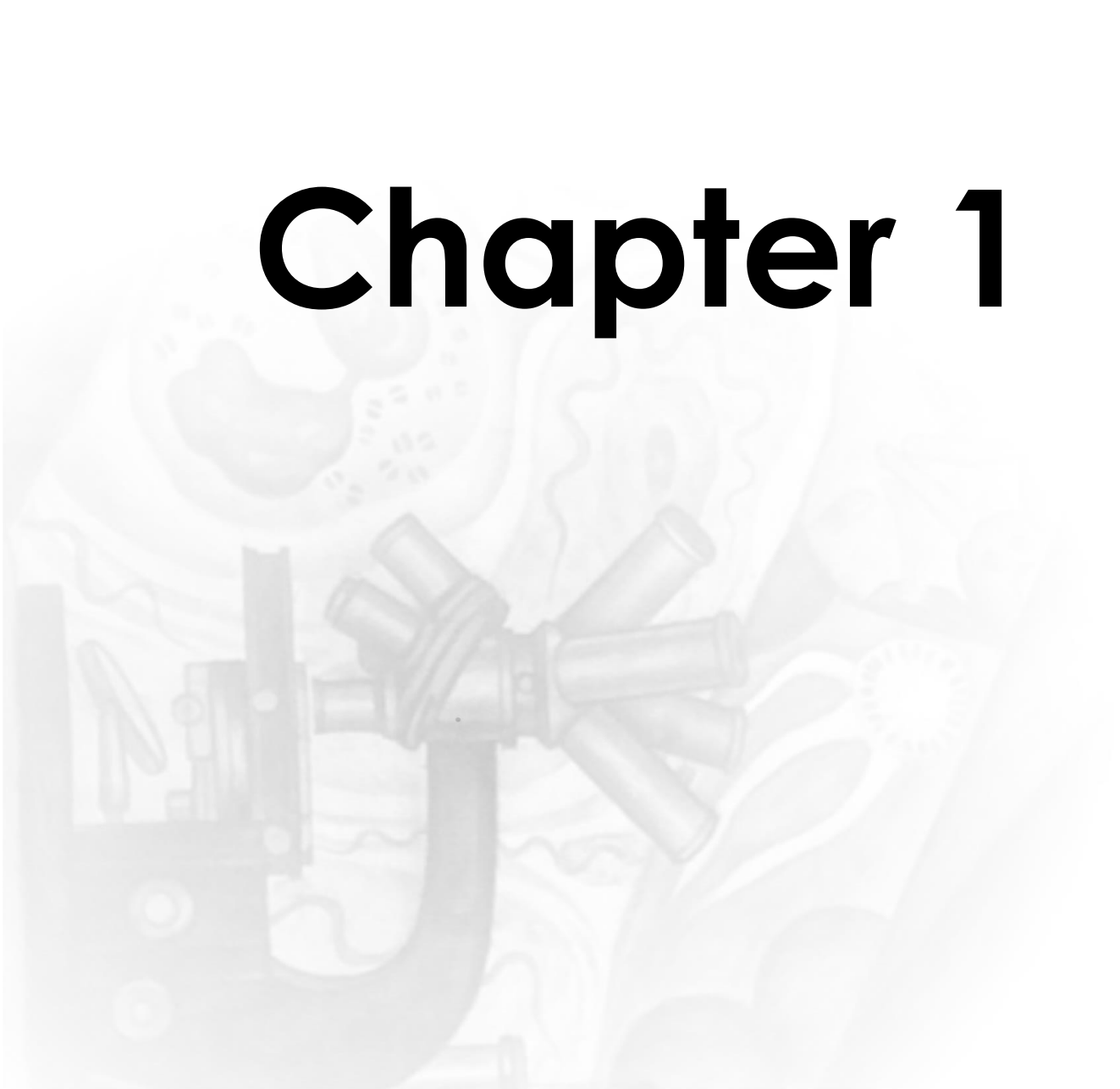

General introduction

and thesis outline

Anaerobic degradation of organic matter to carbon dioxide and methane requires the interaction of different microbial groups along a series of four stages: hydrolysis, acidogenesis, acetogenesis and methanogenesis (McInerney et al., 2008; Sieber et al., 2012; Shrestha and Rotaru, 2014) (**Figure 1.1**). During **hydrolysis** and **acidogenesis**, complex organic structures like polysaccharides, proteins and lipids are converted to smaller moieties such as organic acids, alcohols, simple sugars and amino acids, among others. Several of these products can be directly mineralized to CO_2 by microorganisms using inorganic electron acceptors such as iron (Fe^{3+}), manganese (Mn^{2+}), nitrate (NO_3^-), sulfate (SO_4^{2-}), selenate (SeO_4^{2-}) or arsenate (AsO_4^{3-}) (Kristensen et al., 1995; Stams et al., 2006).

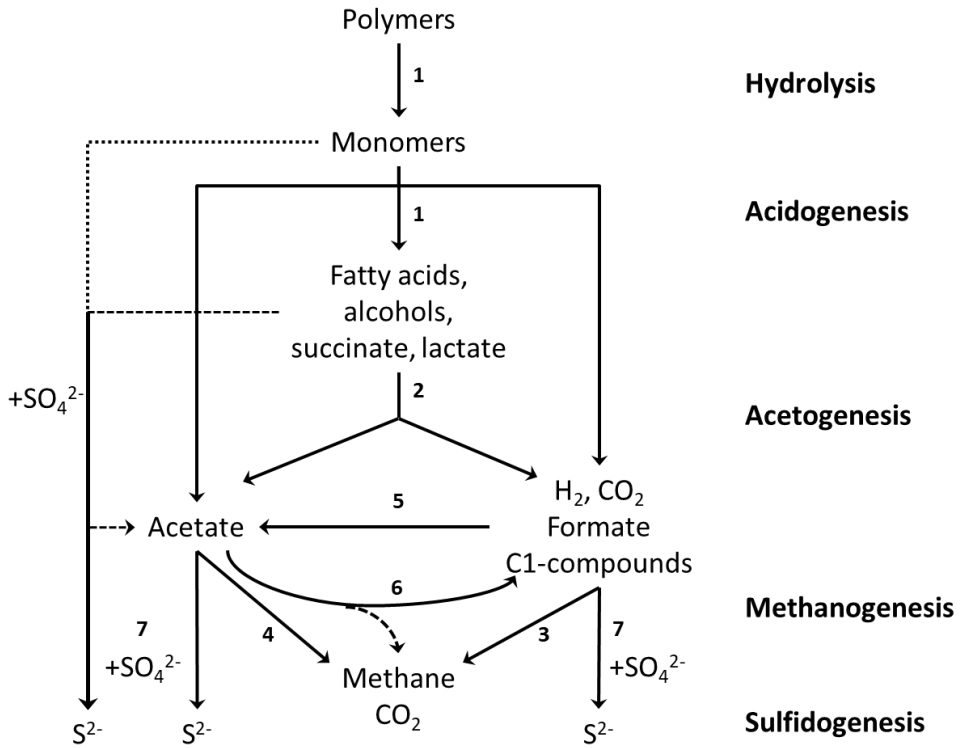

Figure 1.1. Anaerobic degradation of organic matter by cooperation of different metabolic groups. Primary fermenters (1), secondary fermenters or acetogens (2), hydrogenotrophic methanogens (3), acetoclastic methanogens, homoacetogenic bacteria (5), syntrophic acetate oxidizers (6) and sulfate reducers (7).

However, in some environments, microcosms or even in man-made environments, such as paddy fields, landfills and anaerobic bioreactors, inorganic electron acceptors are not always sufficiently available, or the products of their reduction are not desirable, for instance, sulfide production from sulfate reduction. In such

environments, where inorganic electron acceptors are limited, the degradation of organic matter is channelled to methane production. Consequently, syntrophic associations between secondary fermentative bacteria and methanogens become important. These associations occur since the degradation of fatty acids by acetogenic bacteria, requires that the products, typically hydrogen, formate and acetate, are maintained at very low concentrations by methanogenic archaea (Stams et al., 2005; McInerney et al., 2009; Schink and Stams, 2013).

Energetic constraints in methanogenic ecosystems

During hydrolysis, polymeric compounds such as carbohydrates, proteins and lipids are converted to sugars, amino acids and fatty acids. These monomeric compounds are in turn fermented in the acidogenic stage to volatile fatty acids, alcohols, succinate, lactate, H_2, CO_2, and H_2S. The subsequent degradation of these products is an important limiting step in anaerobic digestion due to thermodynamic constrains. Most of the secondary fermentative conversions proceed close to thermodynamic equilibrium with **Gibbs energy changes** close to zero (**Table 1.1**) (Thauer et al., 1977; Schink, 1997; Kleerebezem and Stams, 2000).

It can be noticed from **Table 1.1** that the energetic barriers for anaerobic lactate and ethanol oxidation are easier to overcome than those for butyrate, propionate and acetate degradation. Degradation of butyrate, propionate and acetate in the absence of inorganic electron acceptors can only occur when the concentrations of hydrogen and formate are low, <10 Pa and <10 μM, respectively (Stams, 1994). When oxidation of these organic acids is coupled to methane production in a tight association with a methanogenic partner, the acetogenic reactions mentioned above become thermodynamically favourable (**Equations 1 and 2**). Having this in mind, a complete oxidation of butyrate and propionate into methane and CO_2 requires the interaction of at least three different groups of microorganisms: acetogenic bacteria, acetotrophic archaea and hydrogenotrophic archaea. This interaction is more than simple mutualism as it is based on providing trophic benefits for all the involved partners.

$$2\ \text{Butyrate}^- + 5\ H_2O \rightarrow 5\ CH_4 + 3\ HCO_3^- + H^+ \qquad \Delta G^{o'} = -177\ \text{kJ/reac} \qquad \textbf{Eq. 1}$$

$$4\ \text{Propionate}^- + 7\ H_2O \rightarrow 7\ CH_4 + 5\ HCO_3^- + H^+ \qquad \Delta G^{o'} = -249\ \text{kJ/reac} \qquad \textbf{Eq. 2}$$

Not only acetogenic bacteria depend on efficient removal of the products formed by oxidation of organic acids, but methanogenic archaea rely on the acetogenic partner for substrate supply since methanogens are able to convert only a small number of one-carbon compounds (e.g. methanol, formate, methylamines and methylsulfides) besides acetate (Zinder, 1993; Liu and Whitman, 2008; Thauer et al., 2008).

Table 1.1. Equations and standard free energy changes for acetogenic and methanogenic reactions. Values were calculated from the Gibbs free energies of formation of the reactants at a concentration of 1 M, pH 7.0, 298 K and a partial pressure of gas of 10^5 Pa according to Thauer et al. 1977.

Acetogenic reactions		$\Delta G^{o'}$ (kJ/mol)
$Lactate^- + 2\ H_2O$	$\rightarrow Acetate^- + HCO_3 + H^+ + 2\ H_2$	-7.7
$Ethanol + H_2O$	$\rightarrow Acetate^- + H^+ + 2\ H_2$	+9.6
$Butyrate^- + 2\ H_2O$	$\rightarrow 2\ Acetate^- + H^+ + 2\ H_2$	+48.6
$Butyrate^- + 2\ HCO_3^-$	$\rightarrow 2\ Acetate^- + H^+ + 2\ Formate^-$	+45.6
$Propionate^- + 3\ H_2O$	$\rightarrow Acetate^- + HCO_3^- + H^+ + 3\ H_2$	+76.1
$Propionate^- + 2\ HCO_3^-$	$\rightarrow Acetate^- + H^+ + 3\ Formate^-$	+72.2
Hydrogen/formate formation reactions		**$\Delta G^{o'}$ (kJ/mol)**
$Acetate^- + 4\ H_2O$	$\rightarrow 4\ H_2 + 2\ HCO_3^- + H^+$	+95.0
$Acetate^- + 2\ HCO_3^-$	$\rightarrow 4\ Formate^- + H^+$	+109
$Formate^- + H_2O$	$\rightarrow H_2 + HCO_3^-$	+1.3
Methanogenic reactions		**$\Delta G^{o'}$ (kJ/reac)**
$4\ Formate^- + H^+ + H_2O$	$\rightarrow CH_4 + 3\ HCO_3^-$	-130.4
$4\ H_2 + HCO_3^- + H^+$	$\rightarrow CH_4 + 3\ H_2O$	-135.6
$Acetate^- + H_2O$	$\rightarrow CH_4 + HCO_3^-$	-31.0

Methanogenic syntrophy

Methanogenic syntrophy is an essential process in the global carbon cycle and fundamental for the complete mineralization of organic carbon (Thauer et al., 2008; McInerney et al., 2009). The mutual dependence of syntrophic partners with respect to energy limitations can go, in some cases, so far that neither partner can operate without the other, and together they exhibit a metabolic activity that neither one could accomplish on its own (de Bok et al., 2005; Qiu et al., 2006; Sousa et al., 2007; McInerney et al., 2008).

A balanced performance among the trophic groups of microorganisms involved in syntrophy depends on many factors such as the concentration of substrates and products as well as their diffusion, intermicrobial distances, formation of aggregates, etc. (Seitz et al., 1988; Thiele et al., 1988; Boone et al., 1989; Ozturk et al., 1989; Stams and Dong, 1995).

Although the driving force for the establishment of syntrophic associations is the small amount of energy available in methanogenic environments, these associations seems to be very difficult to achieve and easy to disrupt. The mechanisms by which syntrophic microorganisms thrive with a very low energy gain, which furthermore must be shared among different cells, are very complex and have not been completely understood yet.

Interspecies electron transfer (IET)

The transfer of reducing equivalents in syntrophic consortia is denoted as **interspecies electron transfer** (Stams, 1994; Schink, 1997; Stams and Plugge, 2009; Sieber et al., 2014). Several redox shuttles have been recognized to be involved in IET, among them, humic substances (Lovley et al., 1999), sulfur compounds (Milucka et al., 2012), cysteine-cystine shuttles (Kaden et al., 2002), flavins (Von Canstein et al., 2008; Brutinel and Gralnick, 2012) and conductive particles (Chen et al., 2014; Cruz Viggi et al., 2014; Kato, 2015; Rotaru et al., 2017). However, the interspecies exchange of hydrogen and formate has been the most widely studied. **Hydrogen and formate** are formed by secondary fermenting bacteria to release the excess of electrons during the oxidative degradation of organic acids (Schink, 1997; McInerney et al., 2009; Stams and Plugge, 2009; Schink et al., 2017).

Reducing equivalents are formed along different oxidation steps in the anaerobic degradation of organic compounds. The reduced forms of electron carriers, such as NADH or reduced ferredoxin (Fd_{red}) need to be re-oxidized to keep the different pathways functioning. During **acidogenesis** the oxidation of NADH (E' of -320 mV) coupled to the reduction of acetaldehyde (E' of -197 mV), pyruvate (E' of -190 mV), enoyl-CoA (E' of -10mV), or fumarate (E' of +33 mV), is energetically favourable, allowing primary fermentative bacteria to form ethanol, lactate, butyrate, or propionate, respectively.

However, in **acetogenesis** the re-oxidation of the electron carriers, in the absence of nitrate, sulfate or other external electron acceptor, needs to be coupled to protons and CO_2 reduction leading to the formation of hydrogen and formate. (McInerney et al., 2008). It is energetically difficult to reduce protons using the redox mediators NADH and ferredoxin. The midpoint redox potential ($E^{\circ\prime}$) of the redox couples NAD^+/NADH and Fd_{ox}/Fd_{red} is -320 and -398 mV, respectively; while the $E^{\circ\prime}$ of the redox couples H^+/H_2 and $CO_2/HCOO^-$ is much lower with -414 mV and -432 mV, respectively (Thauer et al., 1977). This causes an energetic problem under standard conditions (for comparison, the $E^{\circ\prime}$ of the redox couple O_2/H_2O, which is important for aerobic respiration, is +818 mV). In nature however, methanogens can maintain hydrogen threshold values below 10 Pa and formate concentrations as low as 10 µM (Stams, 1994). At these levels, the redox potential for hydrogen and formate production changes from -414 and -432 mV to -260 and -290 mV, respectively (Sieber et al., 2012). Thus, hydrogen and formate production from NADH and Fd_{red} becomes thermodynamically favourable. Consequently, in anaerobic environments, long-chain fatty acids, butyrate, propionate, alcohols, and some amino acids and aromatic compounds are syntrophically degraded to the methanogenic substrates, H_2, formate, and acetate (McInerney et al., 2008).

Hydrogen and formate as electron carriers

Since Bryant and co-workers discovered that their cultures of *Methanobacillus omelianskii* did not contain one species but a syntrophic coculture of two types of microorganisms, hydrogen and formate were recognized from the very beginning as key metabolites in the electron transfer processes between the ethanol oxidizing bacterium and the methanogenic partner (Bryant et al., 1967). Since then, many syntrophic associations have been described and the debate over which compound is the main interspecies electron carrier between the diverse syntrophic associations continues (McInerney et al., 2009; Sieber et al., 2012; Morris et al., 2013; Schink et al., 2017).

Many studies in syntrophic metabolism have emphasized the role of **hydrogen** in IET because the methanogens used in partnerships with *Pelotomaculum thermopropionicum*, *Syntrophococcus sucromutans*, *Syntrophomonas wolfei*, *Syntrophobotulus glycolicus* and *Thermoacetogenium phaeum* among others, were only able to utilize H_2/CO_2 and not formate (Schink, 1997; Sieber et al., 2012). However, other studies have shown the significance of **formate transfer** in methanogenic communities (Thiele and Zeikus, 1988; Boone et al., 1989; Schmidt and Ahring, 1995; de Bok et al., 2003) and in cocultures with *Syntrophobacter fumaroxidans* (Dong and Stams, 1995; Stams and Dong, 1995; de Bok et al., 2002a; de Bok et al., 2003), *Desulfovibrio desulfuricans* strain G20 (Li et al., 2009), *Syntrophomonas wolfei* and *Syntrophus aciditrophicus* (Sieber et al., 2014). Thus, although the exclusive use of hydrogen has been reported for the butyrate-oxidizing coculture *Syntrophomonas wolfei* (Wofford et al., 1986), biochemical and genomic information supports the combined occurrence of hydrogen and formate transfer (Walker et al., 2009; Hillesland and Stahl, 2010; Müller et al., 2010; Li et al., 2011; Worm et al., 2011b; Rotaru et al., 2012; Schink and Stams, 2013).

Therefore, the production and oxidation of hydrogen and formate plays a crucial role in the metabolism of syntrophic methanogenic microorganisms. Hydrogen formation is one of the simplest redox reactions in nature, which nevertheless requires enzymes with complex active centres (Hedderich and Forzi, 2005; Vignais and Billoud, 2007). **Hydrogenases** are metalloenzymes that catalyse the reversible conversion of protons and electrons into molecular hydrogen (**Equation 3**) (Lubitz et al., 2014).

$$H_2 \rightleftharpoons 2H^+ + 2e^- \qquad \textbf{Eq. 3}$$

Hydrogenases are widespread in nature; they occur in bacteria, archaea, and eukarya. It is predicted that over 55 microbial phyla and over a third of all microorganisms harbour hydrogenases. There are three different types of hydrogenases known to date and their current classification is based on the active site metal composition (Søndergaard et al., 2016).

1. **[NiFe]-Hydrogenases.** Heterodimeric proteins consisting of small and large subunits. The large subunit contains the active site, a sulfur bridged bimetallic centre of iron and nickel typically with an open coordination site on one metal. The small subunit contains one or more Fe-S clusters.
2. **[FeFe]-Hydrogenases.** In these enzymes, which can be monomeric or heterodimeric, catalysis occurs at a unique di-iron centre containing a bridging dithiolate ligand, three CO ligands and two CN− ligands (Berggren et al., 2013). The active site of the [FeFe]-hydrogenase is the H cluster, which consists of a $[4Fe–4S]_H$ subcluster linked to an organometallic $[2Fe]_H$ subcluster (Suess et al., 2016).
3. **[Fe]-Hydrogenases.** Iron-only hydrogenases, also called iron–sulfur-cluster-free hydrogenases, these enzymes have been found only in some hydrogenotrophic methanogenic archaea, containing neither nickel nor iron-sulfur clusters but only an iron-containing cofactor.

[NiFe]-hydrogenases have been reported to be often more active towards H_2 oxidation and the [FeFe]-hydrogenases extremely active in H_2 generation (Wu and Mandrand, 1993; Vignais et al., 2001). Nevertheless, [FeFe]-hydrogenase have the highest H_2 production activities (Cammack, 1999; Hambourger et al., 2008; Brown et al., 2012). Although the catalytic activities reported for [NiFe]-hydrogenases are usually lower (Lubitz et al., 2014), these enzymes show much less sensitivity to oxygen inactivation and can generally recover from it, unlike [FeFe]-hydrogenases which are extremely sensitive and irreversible inactivated by oxygen in the reduced state (Vincent et al., 2007; Lenz et al., 2010).

A subgroup of the [NiFe]-Hydrogenases is formed by the **[NiFeSe]-Hydrogenases**, in which one of the cysteine ligands of the nickel is replaced by a selenocysteine (Sec) (Garcin et al., 1999). Although the chemical properties of selenium and sulfur are similar, the change of coordination caused by replacement of one cysteine by a selenocysteine modifies considerably the catalytic and spectroscopic features of the active site (Baltazar et al., 2011). Recent studies have shown that selenium has a crucial role in protection against oxidative damage and that [NiFeSe]-hydrogenases have a higher catalytic activity than [NiFe]-hydrogenases and a bias towards H_2 production (Ceccaldi et al., 2015; Marques et al., 2017; Ruff et al., 2017). Another classification (biochemical) of hydrogenases is often made according to its redox partner, which in many cases is $NAD(P)^+$, ferredoxin, coenzyme F_{420} or a-, b- or c-type cytochrome (Vignais and Billoud, 2007). The metal sites of the three types of hydrogenases involved in interspecies hydrogen transfer have unusual structural features in common, such as intrinsic CO ligands. Despite this, [NiFe]-hydrogenases, [FeFe]-hydrogenases, and [Fe]-hydrogenases are not phylogenetically related at the level of their primary structure or at the level of the enzymes involved in their active-site biosynthesis.

Formate dehydrogenases (FDHs) comprise a heterogeneous group of enzymes found in both prokaryotes and eukaryotes that catalyse the reversible oxidation of formate to CO_2 and H^+.

$$HCOO^- \rightleftharpoons CO_2 + H^+ + 2e^- \qquad \textbf{Eq. 4}$$

The most common class is present in aerobic organisms, monomeric, without cofactors in the active site and mainly $NAD(P)^+$-dependent (Ferry, 1990). However, the conversion of CO_2 to formate results difficult in aerobic conditions because the redox potential of $NADP^+$ is more positive than that of CO_2 (Reda et al., 2008). In prokaryotes, on the other hand, formate dehydrogenases reversibly interconvert CO_2 and formate; they can be found in heterodimeric form (in subunits α, ß, and γ), and contain a complex inventory of redox centres sensitive to oxygen (Reda et al., 2008; Bassegoda et al., 2014). The active sites of formate dehydrogenases from anaerobic prokaryotes include transition metals, such as molybdenum (Mo), tungsten (W) and non-heme iron, molybdopterin guanine dinucleotides as cofactors and in some cases a Sec residue. Inactivation by cyanide can be partially reversed by incubation with sulfide (Robinson et al., 2017). The cofactors are used to transfer the electrons from formate oxidation to an independent active site, to reduce quinone, protons, or $NAD(P)^+$ (Reda et al., 2008). The high efficiency and specificity of isolated bacterial formate dehydrogenases have become appealing for environmental and industrial applications. There is increasing interest in developing biocatalysts that remove CO_2 electrochemically from the atmosphere as a mean of relieving global warming while producing fuels or chemical feedstocks (El-Zahab et al., 2008; Yadav et al., 2012; Sakai et al., 2017)

Hydrogenases and formate dehydrogenases are located in the periplasm or cytoplasm, either in soluble form or membrane-bound. Their location is important when analysing their role in interspecies electron transfer. Depending on the location in the cell, these enzymes may either be tuned for hydrogen/formate production, removing reducing equivalents, or hydrogen/formate uptake, providing electrons to the cell.

The importance of hydrogen and formate as electron carriers is not limited to IET, but they are also used in other energy conservation mechanisms such as reverse electron transport and bifurcating/confurcating complexes that will be discussed below. Moreover, IET is not restricted either to methanogenic systems, as the research in other syntrophic cocultures indicate, for instance in *Pelobacter carbinolicus* and *Geobacter sulfurreducens* (Rotaru et al., 2012).

Direct interspecies electron transfer (DIET)

A **direct interspecies electron transfer** mechanism in a coculture of G*eobacter metallireducens* and *Geobacter sulfurreducens* growing on ethanol and fumarate has been described (Summers et al., 2010). Direct interspecies electron transfer (DIET) has been proposed before in *G. sulfurreducens* and *Shewanella oneidensis* (Reguera et al., 2005; Gorby et al., 2006), where the authors proposed that electrically conductive pili-like appendages, termed nanowires, were involved in electron transferring from the cell surface to the surface of Fe(III) oxides. The mechanisms underlying DIET are still being investigated and debated (Reguera et al., 2005; Lovley and Malvankar, 2015). Besides the production of pili or nanowires as the structures utilized to transfer the electrons among cells, the requirement of a multitude of extracellular and periplasmic cytochromes has also been suggested (Larsen et al., 2015; Lovley, 2017). The first studies in DIET were limited to interactions of metal-reducing bacteria, such as *Geobacter* and *Shewanella* species, in which one bacteria oxidized ethanol while the other reduced fumarate (Liu et al., 2012; Shrestha et al., 2013; Rotaru et al., 2014). More recently DIET has been investigated in methanogenic environments for syntrophic associations between *Geobacter* species and species of *Methanosaeta* and *Methanothrix* (Rotaru et al., 2014; Holmes et al., 2017; Rotaru et al., 2017).

Although DIET might indeed play a role in syntrophic communities of anaerobic microorganisms, hydrogen and formate transfer among acetogenic bacteria and methanogens remains the best-established mechanism for interspecies electron transfer.

Energy conservation mechanisms in anaerobic environments

Conservation of energy by chemotrophic microorganisms is based on both **substrate-level phosphorylation** and **electron transport phosphorylation** (Stams et al., 2006). We have explained the energetic limitations faced by acetogenic bacteria in the absence of inorganic electron acceptors; and how IET and the establishment of syntrophic associations makes, the otherwise thermodynamically unfavourable, reduction of protons with NADH possible. But even under optimal syntrophic growth conditions, when hydrogen, formate, and acetate are low, the Gibbs free energy change for syntrophic metabolism is very close to the minimum increment of energy required for ATP synthesis, which is predicted to be about -15 to -20 $kJ \cdot mol^{-1}$ (McInerney et al., 2009; Schink and Stams, 2013). Moreover, the available free energy must be shared by the different organisms (Schink, 1997). The energy conservation mechanisms used to establish and maintain a syntrophic lifestyle when the thermodynamic driving force is very low are not completely understood and have been subject of research over the last years. Research in anaerobic microorganisms has increased our understanding of the metabolic capabilities of bacteria and archaea

and helped to elucidate mechanisms such as **reverse electron transport**, flavin based electron **bifurcation** and its reversal, electron **confurcation** (Li et al., 2008; McInerney et al., 2011; Buckel and Thauer, 2013; Schink, 2015).

Reverse electron transport (RET)

Propionate and butyrate are important intermediates in the degradation of organic matter to methane (Dong et al., 1994; Schmidt and Ahring, 1995; Kleerebezem and Stams, 2000). Although propionate can be dismutated to acetate and butyrate by *Smithella propionica* (de Bok et al., 2001), the most common biochemical pathways of syntrophic propionate and butyrate oxidation are methylmalonyl-CoA pathway (MMC) and beta-oxidation, respectively (**Figure 1.2**). In MMC reducing equivalents are formed in the oxidation of succinate to fumarate, malate to oxaloacetate, and pyruvate to acetyl-CoA + CO_2. These equivalents are released at the level of $FADH_2$ (enzyme bound), NADH and Fd_{red}, respectively. In beta-oxidation the oxidation of hydroxybutyryl-CoA is NADH-dependent, but the oxidation of butyryl-CoA to crotonyl-CoA is the energetically most difficult step in butyrate conversion due to the high redox potential of this electron pair ($E^{\circ\prime}$ = -125 mV) (Losey et al., 2017), as the oxidation of succinate is the most energy-consuming step in MMC (Stams and Plugge, 2009). NADH oxidation coupled to hydrogen/formate formation is energetically feasible when the concentration of these compounds is kept low by methanogens. However, the oxidation of $FADH_2$/FAD ($E^{\circ\prime}$= -220 mV) would require much lower hydrogen or formate concentrations than those that can be achieved by methanogens (Stams et al., 2005). It has been estimated that to couple this step to proton or CO_2 reduction would require a partial pressure of hydrogen (pH_2) of 10^{-10} Pa (Schink, 1997); while the minimal pH_2 that methanogens can maintain is between 1 to 10 Pa (Thauer et al., 2008). Therefore, by means of a reverse electron flow mechanism, acetogenic bacteria invest metabolic energy to make protons accessible to accept electrons from $FADH_2$. This mechanism is known as **reverse electron transport** (RET) (Schink, 1997; van Kuijk et al., 1998b; Schink and Stams, 2013).

During RET energy is invested in the form of ATP to generate a proton gradient across the membrane which allows butyryl-CoA and succinate oxidation to proceed (Stams and Plugge, 2009). Several membrane-bound proteins like butyryl-CoA dehydrogenase, succinate dehydrogenases, Ech and Rnf to cytochromes and periplasmic formate dehydrogenases and hydrogenases, have been reported to be involved in RET (Müller et al., 2009; Sieber et al., 2012; Grein et al., 2013; Schmidt et al., 2013; Sieber et al., 2015). Therefore, reverse electron transport makes use of membrane-associated respiratory chains (Müller et al., 2010). However, the discovery in the last decade of soluble enzyme complexes that use the energy of a favourable redox reaction to drive an unfavourable redox reaction established the bases for the recognition of a third mechanism of biological energy conservation (McInerney et al., 2009; Stams and Plugge, 2009; Peters et al., 2016).

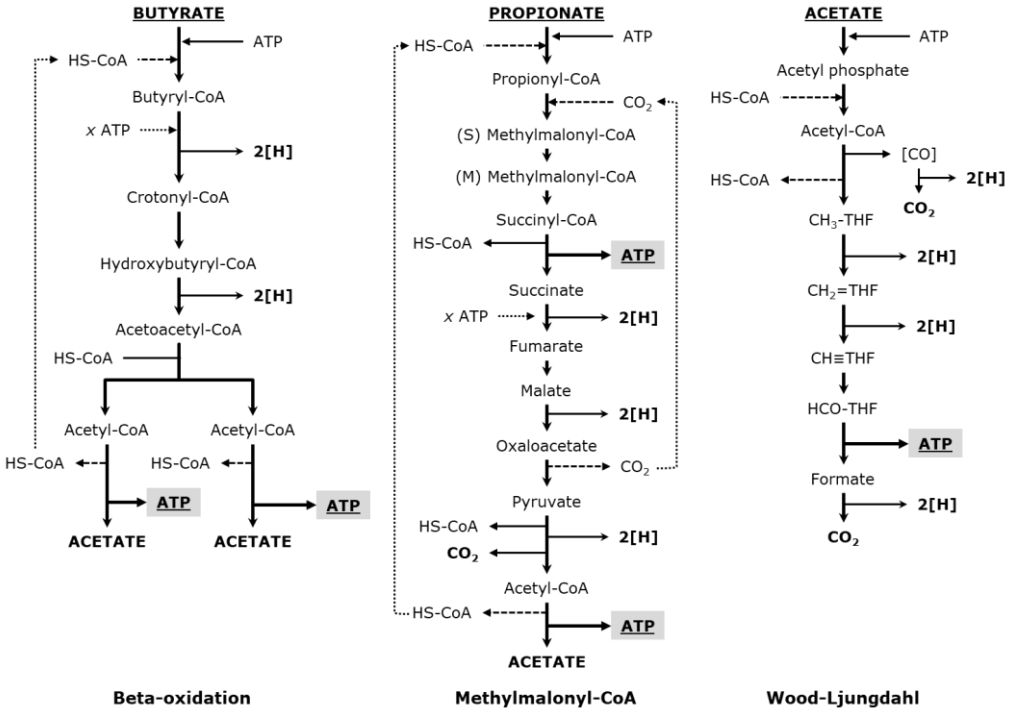

Figure 1.2. Metabolic pathways for acetate, propionate and butyrate conversion by bacteria that can grow in syntrophy with methanogens. Modified from (Worm et al. 2014)

Electron bifurcation and electron confurcation

Electron bifurcation is an energy conservation mechanism in which an endergonic reduction reaction is catalysed by coupling it to two exergonic oxidation reactions (Herrmann et al., 2008). Electron confurcation is the reversal of electron bifurcation (Buckel and Thauer, 2013; Schink, 2015). Hence, in electron bifurcation a pair of electrons is acquired at intermediate reduction potential (intermediate reducing power) and each electron is passed to a different acceptor, one with lower and the other with higher reducing power, leading to 'bifurcation'. While in electron confurcation a two-electron acceptor of intermediate reduction potential simultaneously accepts electrons from electron donors with more negative and more positive potentials (**Figure 1.3**) (Peters et al., 2016; Hoben et al., 2017).

The principle of electron bifurcation was originally proposed for a butyryl-CoA dehydrogenase/electron transferring flavoprotein complex (Bcd-Etf) in *Clostridium kluyveri* (Li et al., 2008). Later, three more flavin-containing complexes from anaerobic bacteria and archaea were described: [FeFe]-hydrogenases (Hyd), transhydrogenases (NfnAB) and [NiFe]-hydrogenase/heterodisulfide reductases

(MvhADG–HdrABC) (Schut and Adams, 2009; Kaster et al., 2011b; Huang et al., 2012; Buckel and Thauer, 2013). Up to date, at least seven types of reactions are known to be catalysed by bifurcating flavoenzymes (Peters et al., 2016; Zhang et al., 2017).

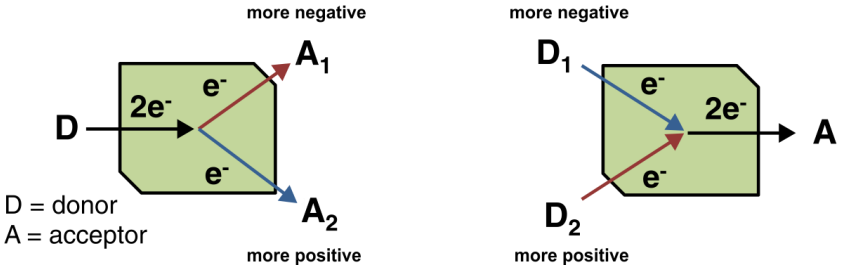

Figure 1.3. Scheme depicting electron transfer in bifurcating (left) and confurcating (right) complexes. In bifurcation a two-electron donor (D) of intermediate reduction potential (E°') simultaneously provides electrons to electron acceptors with more negative (A_1) and more positive (A_2) potentials. While in confurcation a two-electron acceptor (A) of intermediate E°' simultaneously accepts electrons from electron donors with more negative (D1) and more positive (D2) E°'. Modified from (Peters et al., 2016)

The discovery of the bifurcating complex Bcd-Etf in *C. kluyveri* opened the possibility and quest to find similar complexes that could perform the reverse during syntrophic fatty acid oxidation (Müller et al., 2009). After the description of the confurcating hydrogenase that couples the energetically unfavourable formation of hydrogen from NADH with the energetically favourable formation of hydrogen from reduced ferredoxin (Schut and Adams, 2009), homologs to this hydrogenase complex were found in *Syntrophomonas wolfei* and *S. fumaroxidans* genomes (Müller et al., 2010; Sieber et al., 2010). Currently confurcating hydrogenases are found in the genomes of all hydrogen-generating syntrophs described to date (Sieber et al., 2012; Worm et al., 2014). Electron bifurcation from formate has also been described (Costa et al., 2010; Costa et al., 2013b; Wang et al., 2013b)

Hydrogenotrophic methanogens use electron bifurcation as a primary energy coupling step in methanogenesis from CO_2 (Costa et al., 2010; Kaster et al., 2011b). In the case of the hydrogenotrophic methanogenic pathway the bifurcation process involves a formylmethanofuran dehydrogenase (Fmd), an heterodisulfide reductase (Hdr) complex and an F420-non-reducing hydrogenase (Mvh) or a formate dehydrogenase (Fdh) that connects the final step of methanogenesis to the initial reduction of CO_2 (Lie et al., 2012; Costa and Leigh, 2014).

The details of how these flavoprotein complexes couple energetically downhill and uphill redox reactions are still under research, but the process is remarkable from

both thermodynamic and kinetic perspectives (Lubner et al., 2017). How can proteins drive two electrons from a redox active donor onto two acceptors at very different potentials and distances? And how can this transaction be conducted without dissipating energy very much or violating the laws of thermodynamics? (Zhang et al., 2017). Moreover, it was proposed that bifurcation is mediated by a flavin, however there are numerous flavoenzymes that can carry two-electrons but cannot perform electron bifurcation (Garcia Costas et al., 2017; Hoben et al., 2017); it remains important to identify factors required for a flavin site to execute bifurcation. The number of genes encoding bifurcating/confurcating proteins found in many anaerobic microorganisms, indicates that the presently known flavin-based electron-bifurcating enzyme complexes are only the tip of an iceberg.

Anaerobic degradation of propionate

Syntrophy and sulfate reduction

Propionate oxidation coupled to hydrogen or formate production is endergonic under standard conditions (**Table 1.1**). However, when propionate oxidation is coupled to methane production the conversion is energetically feasible (**Eq. 2**). The oxidation of propionate coupled to sulfate reduction is also an energy yielding reaction, **Equation 5**:

$$4\ \text{Propionate}^- + 3\ SO_4^{-2} \rightarrow 4\ \text{Acetate}^- + 4\ HCO_3^- + 3\ HS^- + H^+$$

$$\Delta G^{\circ\prime} = -37.7\ \text{kJ/mol}$$

Consequently, syntrophic fatty acid-degrading communities in anaerobic environments may be affected by the presence of sulfate. When sulfate is present, sulfate-reducing bacteria (SRB) compete with methanogens for hydrogen, formate and acetate, and with syntrophic methanogenic communities for substrates like propionate and butyrate (Muyzer and Stams, 2008). While many SRB can grow without sulfate and are engaged in syntrophic associations with methanogens, others lack this ability (Worm et al., 2014). For instance, *Syntrophobacter* species can use propionate in syntrophy with hydrogenotrophic methanogens, or alone if sulfate is available (Plugge et al., 2011; Liu and Conrad, 2017). *Pelotomaculum* species on the other hand do not possess the ability to couple propionate oxidation with sulfate reduction (Imachi et al., 2007).

Sulfate reduction is a respiratory process which includes oxidative phosphorylation through a still incompletely understood electron transfer pathway (Muyzer and Stams, 2008). Analysis of distinct organisms capable of sulfate reduction has helped to identify the minimal set of proteins required for this metabolic activity: Sulfate adenylyltransferase (Sat), APS reductase (AprAB), dissimilatory sulfite reductase

(DsrAB) and DsrC and sulfate transporters (Pereira et al., 2011). Genomic studies have revealed that sulfate-reducing microorganisms use diverse processes for energy conservation involving membrane-based chemiosmotic or soluble flavin-based electron bifurcation mechanisms. Many of these proteins such as proton-translocating pyrophosphatase (HppA) or DsrC are also present in other non-sulfate-reducing bacteria, whereas others like heterodisulfide reductases-related proteins are shared with methanogens (Grein et al., 2013).

One of the remaining important questions about sulfate reduction was the nature of the electron donors to the terminal reductases AprAB and DsrAB (Pereira et al., 2011). Recent studies have shown that a QmoABC membrane complex might serve as the physiological electron donor for AprAB, coupling the quinone-pool to sulfate reduction (Duarte et al., 2016). Moreover, the role of the DsrC trisulfide as the product of sulfite reduction by DsrAB and its link to energy conservation has also been reported recently (Santos et al., 2015). A glance into the versatile redox machinery of SRB involving membrane complexes such as Qrc, Qmo, DsrMKJOP, Nuo, Tmc, Hmc as well as cytoplasmic energy-conserving enzymes such as Hdr and Flox is helping to better understand the nature of prokaryotic energy metabolism (Grein et al., 2013; Rabus et al., 2015; Ramos et al., 2015; Santos et al., 2015).

Thesis outline

The aim of this thesis is to gain insight into the molecular mechanisms used in anaerobic propionate degradation. In this thesis, the capacity of a model bacterium, *Syntrophobacter fumaroxidans*, to degrade propionate in syntrophy with methanogens, and in pure culture with different electron acceptors, was investigated. Special emphasis was given to the enzyme complexes used for energy conservation and interspecies electron transfer. Moreover, an in-depth analysis of the methanogenic partners and a sulfate-reducing partner was included in this work.

Chapter 2 addresses the fundamental and ecologically important question of why some microorganisms are able to engage in syntrophy with methanogens while others are not. A functional analysis of protein domains of a selected group of bacteria was performed. The bacterial strains were selected based on genome availability and their ability to grow on short chain fatty acids alone or in syntrophic association with methanogens. The research shows, at genomic level, the molecular mechanisms available in syntrophic bacteria that could facilitate syntrophic interactions with methanogens. The presence of periplasmic formate dehydrogenases and their maturation protein FdhE was found to be a typical difference between syntrophic and non-syntrophic butyrate and propionate degraders. Furthermore, a domain (CapA) putatively involved in capsule or biofilm production and another domain (FtsW/RodA/SpoVE) involved in cell division, shape-determination or sporulation seemed to be associated with the ability of syntrophic growth.

In **Chapter 3** the metabolic flexibility of *Syntrophobacter fumaroxidans* to grow in syntrophy or as sulfate-reducing bacterium was assessed. The metabolic flexibility of sulfate-reducing bacteria to form syntrophic associations, despite their ability to reduce sulfate and oxidize fatty acids on their own, is an important topic that has been investigated to gain knowledge about the dynamics and resilience of anaerobic microbial communities. Perturbations in sulfidogenic pure cultures of *S. fumaroxidans* and in methanogenic cocultures of the bacteria with *Methanospirillum hungatei* were performed. *Desulfovibrio desulfuricans* was also used as an alternative syntrophic partner of *S. fumaroxidans* in sulfate rich environments. Growth of *D. desulfuricans* in the coculture with *S. fumaroxidans*, would only be possible if *Syntrophobacter* transferred electrons to *D. desulfuricans* via hydrogen or/and formate. Although growth of *D. desulfuricans* in the coculture was verified, it could not be clearly shown that *S. fumaroxidans* switched its metabolism from sulfidogenesis to syntrophy.

In **Chapter 4** a proteomic comparison of five growing conditions of *Syntrophobacter fumaroxidans* is discussed. Proteomic data of *S. fumaroxidans* growing with propionate axenically with sulfate or fumarate, and in syntrophy with *Methanospirillum hungatei*, *Methanobacterium formicicum* or *D. desulfuricans* was

analysed. Confurcating enzymes, formate dehydrogenases, hydrogenases, and other IET complexes and energy conservation mechanisms were scrutinized. Enzymes associated with sulfate reduction were also widely discussed. A brief proteomic analysis of the sulfate-reducing partner *D. desulfuricans* is also included in the chapter.

Chapter 5 completes and widens the proteomic analysis of the propionate-degrading syntrophic bacterium *S. fumaroxidans* by analysing the genome and proteome of the two methanogenic partners. The enzymes used in methanogenesis and energy conservation are discussed for *M. hungatei* and *M. formicicum*. Differences between the methanogens and among the cultured conditions (growth in H_2/CO_2, formate and in syntrophy with *S. fumaroxidans*) are described in detail. *M. formicicum* uses a F_{420}-non-reducing hydrogenase (MvhADG) for bifurcation with the formylmethanofuran dehydrogenase (Fmd) and heterodisulfide reductase (Hdr). *M. hungatei* on the other hand employs an F_{420}-reducing hydrogenase (FrhADGB). Differential production of enzymes involved in the methanogenic pathway as well as in diverse extracellular structures such as archaellum and pili are described in the analysis. Although both methanogens can grow on hydrogen and formate, the mechanisms available in their genome and the produced proteins, point to the use of hydrogen, in *M. formicicum*, and of formate, in *M. hungatei*, as electron carriers in their metabolism.

Throughout the thesis it is emphasized that formate and hydrogen are important intermediates in the anaerobic degradation of organic matter for which different microbes compete. In **Chapter 6** the performance and robustness to high loading tests of an anaerobic membrane bioreactor (AnMBR) was evaluated. Considering that an increase in hydrogen might be useful to predict disturbances between fermentative processes and methanogenesis, we investigated if monitoring hydrogen can be used as an early warning indicator of process instability. The study analysed microbial community composition with next-generation sequencing techniques., process parameters and performance during the start-up and stable operation of a mesophilic AnMBR treating pot ale, as well as the resilience of the bioreactor and its biomass to overloading events.

Chapter 7 summarizes the findings of this thesis, discusses the outcome in a broader setting and provides future perspectives for research. The molecular mechanisms used by bacteria and archaea in syntrophy, methanogenesis and sulfate reduction are discussed in an integrative way.

"ipse se nihil scire id unum sciat"

P.? S.?

Chapter 2

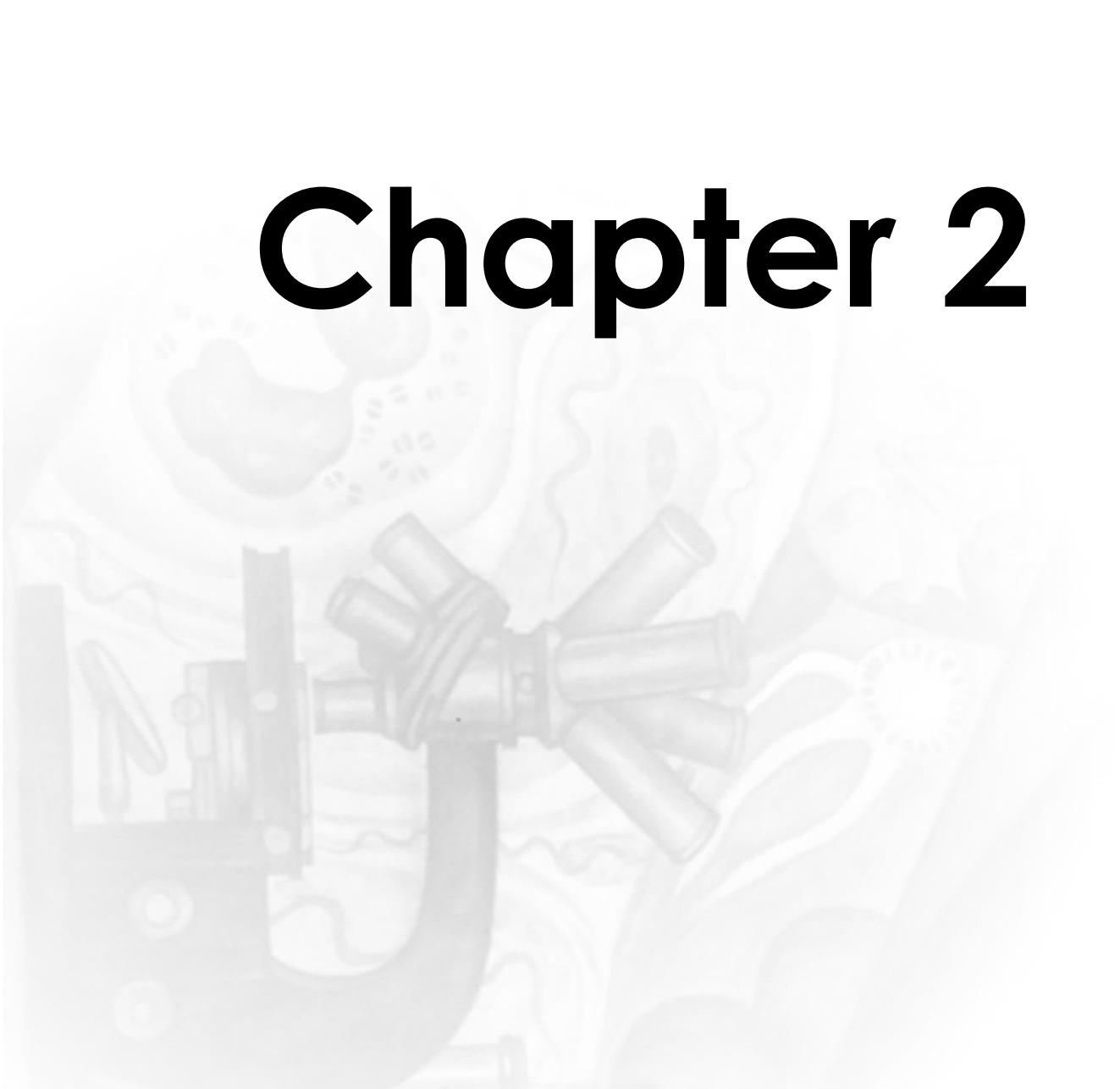

CHAPTER 2

A genomic comparison of syntrophic and non-syntrophic butyrate- and propionate-degrading bacteria points to a key role of formate in syntrophy

This chapter is adapted from Worm P., Koehorst J.J., Visser M., Sedano-Núñez V.T., Schaap P.J., Plugge C.M., Sousa D.Z. and Stams A.J.M. (2014) A genomic view on syntrophic versus non-syntrophic lifestyle in anaerobic fatty acid degrading communities. 1837:12, 2004–2016

Abstract

In sulfate-reducing and methanogenic environments complex biopolymers are hydrolysed and degraded by fermentative microorganisms that produce hydrogen, carbon dioxide and short chain fatty acids. Degradation of short chain fatty acids can be coupled to methanogenesis or to sulfate reduction. Here we study from a genome perspective why some of these microorganisms are able to grow in syntrophy with methanogens and others are not. Bacterial strains were selected based on genome availability and upon their ability to grow on short chain fatty acids alone or in syntrophic association with methanogens. Systematic functional domain profiling allowed us to gain insight on this fundamental and ecologically important question. Extra-cytoplasmic formate dehydrogenases (InterPro domain number; IPR006443), including their maturation protein FdhE (IPR024064 and IPR006452) is a typical difference between syntrophic and non-syntrophic butyrate and propionate degraders. This also implies that formate is an important electron carrier in syntrophic butyrate and propionate degradation. Furthermore, two domains with a currently unknown function seem to be associated with the ability of syntrophic growth. One is putatively involved in capsule or biofilm production (IPR019079) and a second in cell division, shape-determination or sporulation (IPR018365). The sulfate reducing bacteria *Desulfobacterium autotrophicum* HRM2, *Desulfomonile tiedjei* and *Desulfosporosinus meridiei* were never reported for syntrophic growth, but all crucial domains were found in their genomes, which suggests their possible ability to grow in syntrophic association with methanogens. In addition, profiling domains involved in electron transfer mechanisms revealed the important role of the Rnf-complex and the formate transporter in syntrophy, and indicates that DUF224 may have a role in electron transfer in bacteria other than *Syntrophomonas wolfei* as well.

Keywords: Syntrophy, propionate, butyrate, formate, interspecies electron transfer, functional profiling.

Introduction

Environments with a low redox potential are abundantly present on earth, especially in the deeper zones of marine and freshwater sediments. The low redox potential is created by the depletion of oxygen and the formation of hydrogen sulfide in the anaerobic degradation of organic matter. In the decomposition of sulfur-containing organic compounds such as the amino acids (cysteine and methionine) and cofactors (biotin and thiamine) hydrogen sulfide is released. Additionally, hydrogen sulfide is formed by anaerobic microorganisms that respire with sulfate or other sulfur compounds, such as thiosulfate and elemental sulfur. This respiratory type of sulfidogenesis is quantitatively most important (Blank, 2009; Shao et al., 2010; Offre et al., 2013).

Respiratory sulfate reduction is an important process in nature, especially in marine sediments where the sulfate concentration is high (about 20 mM) (Muyzer and Stams, 2008). In freshwater environments that are generally low in sulfate, sulfate reduction does not play an important role unless hydrogen sulfide is rapidly oxidized by sulfide-oxidizing microbes (Lovley and Klug, 1983; Luther et al., 2011). In sulfate-depleted anoxic environments methanogenesis is the most abundant process (Laanbroek et al., 1982), (Stams and Plugge, 2009). Interestingly, in marine environments methanogenesis occurs as well, especially in zones where the available sulfate is not sufficient to degrade organic matter (Ferry and Lessner, 2008). In both marine and freshwater environments microbes involved in sulfate-reduction and methanogenesis interact strongly with each other, and this interaction is strongly depending on the availability of sulfate. Generally, sulfate reduction is favoured over methanogenesis when sufficient sulfate is present (Muyzer and Stams, 2008; Stams and Plugge, 2009).

In sulfate-reducing and methanogenic environments organic material is degraded in a cascade process. Complex biopolymers are first hydrolysed and degraded by fermentative microorganisms that produce hydrogen, carbon dioxide and organic compounds, typically organic acids (butyrate, propionate, acetate and formate) as products. In sulfate-reducing environments these compounds are the common substrates for sulfate-reducing microorganisms. Phylogenetically and physiologically sulfate reducing microorganisms are very diverse (Muyzer and Stams, 2008). Phylogenetically they occur in the bacterial and archaeal domain of life. Some sulfate reducers have the ability to grow autotrophically with H_2 and sulfate as energy substrates. Often these autotrophs are the sulfate reducers that are also able to degrade acetate completely to CO_2, employing the reversible Wood-Ljungdahl pathway for acetate degradation and acetate formation (Hansen, 1994).

In methanogenic environments, methanogens use H_2/CO_2, formate and acetate as the main substrates (Liu and Whitman, 2008). Methanogenic archaea belong to

different phylotypes. The ability to use acetate is restricted to archaea belonging to the order *Methanosarcinales*, with *Methanosarcina* and *Methanosaeta* as important genera. The ability to grow with H_2/CO_2 and formate occurs in most of the currently described orders of methanogens (Liu and Whitman, 2008). Higher organic compounds such as propionate and butyrate, that are typical intermediates in methanogenic environments, are not degraded by methanogens. Therefore, acetogenic bacteria are required to degrade such compounds to the methanogenic substrates acetate, formate and H_2/CO_2 (McInerney et al., 2008; Stams and Plugge, 2009). For thermodynamic reasons such bacteria can only degrade propionate and butyrate when the products are efficiently taken away by methanogens. Thus, these acetogenic bacteria grow in obligate syntrophy with methanogens. The methanogenic substrates acetate and formate may be degraded by syntrophic communities as well (Dolfing et al., 2008; Hattori, 2008). Syntrophic acetate degradation especially occurs under conditions at which the activity of acetoclastic methanogens is low such as a high temperature and high levels of ammonium (Hattori, 2008).

Though the basic concepts of sulfate reduction and methanogenesis are clear, it is not very clear how sulfate-reducing and methanogenic communities in freshwater and marine sediments are responding to changes in the sulfate availability. The metabolic flexibility of sulfate reducing bacteria has been addressed recently (Plugge et al., 2010; Plugge et al., 2011; Meyer et al., 2013). Several sulfate reducers are able to grow acetogenically in syntrophic association with methanogens which is for instance the case for *Syntrophobacter fumaroxidans* growing with propionate. Nevertheless, not all sulfate reducers possess the ability to switch from a sulfate-dependent lifestyle to a syntrophic lifestyle. For instance, *Desulfobulbus propionicus* is a bacterium that grows with propionate and sulfate, but it is not able to grow with propionate in syntrophy with methanogens. Similarly, the thermophilic sulfate reducer *Desulfotomaculum kuznetsovii* is able to degrade propionate with sulfate, but it is not able to grow in syntrophy with methanogens, while the phylogenetically closely related non-sulfate-reducing bacterium *Pelotomaculum thermopropionicum* grows with propionate in syntrophy with methanogens (Imachi et al., 2002).

This study focusses on syntrophic degradation of short chain fatty acids (SCFA) such as butyrate, propionate and acetate. In contrast to syntrophic degradation of ethanol and lactate, syntrophic SCFA degradation occurs at the limit of what is thermodynamically possible and requires at least one step with reversed electron transport (Schink, 1997). Here we address a fundamental and ecologically important question: “what are the key properties that make a SCFA degrading bacterium able to grow in syntrophy with methanogens and another not”. The availability of genome sequences of bacteria that can and bacteria that cannot grow with SCFA in syntrophic association may allow to identify key genes in syntrophy.

Microbial functions required for syntrophic growth

Functional profiling strategies

Bacterial strains were selected based on genome availability, and ability to grow on short chain fatty acids syntrophically or not. Sulfate reducers that grow on short chain fatty acids, whose genomes are available and currently have not been tested for syntrophic growth were included in our analysis (**Table 2.1**). Correct codon usage of sequences coding for selenocysteine-containing formate dehydrogenases and hydrogenases was verified. Our strategy was to compare first bacteria that degrade propionate and butyrate, and then to identify if similarities can also be found in acetate degraders. Functional domain profiles were obtained with InterProScan 5 (version 5RC7, 27th January 2014). To get more insight into microbial functions required for syntrophic growth, domain based functional profiles of five butyrate and or/ propionate-degrading syntrophs were compared with the non-syntrophs *Desulfobulbus propionicus* and *Desulfotomaculum kuznetsovii*. Domains only present in syntrophs are listed in **Table 2.1**. Genomes of sulfate reducers that degrade butyrate and/or propionate, but were never tested for syntrophy, were screened for these domains (**Table 2.1**).

Functional domains assigned to proteins involved in electron transport were separately analysed. Domains that were unique for each protein were selected. Genomes of short chain fatty acid degrading syntrophs, non-syntrophs and sulfate reducers that never have been tested for syntrophy were screened for these domains (**Table 2.2**). Electron transport mechanisms in short chain fatty acid degrading syntrophs and non-syntrophs were predicted from their genomes by using the tools described below.

Electron transfer complexes predicted from genome analysis

Gene analysis started with automatic annotations of genomes from DOE-Joined Genome Institute (Markowitz et al., Version 4.2. November 2013). NCBI-pBLAST analysis with sequences from biochemically confirmed active subunits, was used to indicate the presence of gene clusters coding for formate dehydrogenases, hydrogenases, Electron transfer flavoprotein (Etf) and Rnf complexes in the genomes of *Syntrophomonas wolfei, Syntrophus aciditrophicus*, *Syntrophothermus lipocalidus*, *Syntrophobacter fumaroxidans, Pelotomaculum thermopropionicum, Desulfotomaculum kuznetsovii, and Desulfobulbus propionicus.* N-terminal amino acid sequences that corresponded to formate dehydrogenase 1 and -2 of *S. fumaroxidans* were used to find the gene clusters that code for these enzymes. To identify cofactor binding motifs, transmembrane helices, and twin-arginine translocation motifs in the N-terminus we used the Pfam protein families database version 27.0 (March 2013) (Punta et al., 2012), TMHMM Server v. 2.0 (Moller et al.,

2001) and the TatP 1.0 Server (Bendtsen et al., 2005) respectively. RNA loop predictions with Mfold version 3.2. were used to predict incorporation of selenocysteine (Mathews et al., 1999; Zuker, 2003). We compared the predicted RNA loop in the 50-100 bp region downstream of the UGA-codon with the consensus loop by (Zhang and Gladyshev, 2005). Sequences with similarity to iron-only or [FeFe]-hydrogenases, were manually analysed for the presence of conserved H-cluster residues (Stothard, 2000). Bifurcation of electrons can occur via FAD, without the presence of iron-sulfur clusters (Buckel and Thauer, 2013). When a FAD binding domain was predicted by Pfam we propose that electrons from reduced ferredoxin and NADH can confurcate. In some cases, also an NADH binding site and/or iron sulphur cluster binding motifs were found with Pfam. Cofactor binding to NADH: ubiquinone oxidoreductase subunits in bacteria as listed by Yano and co-workers (Yano, 2002) was predicted based on domain similarity as determined by Pfam. We predict that enzyme complexes with an NADH binding domain, iron-sulfur clusters and a domain binding Mo/W, Se or hydrogen and not necessarily flavin, might have electron confurcating functions. Iron-only hydrogenases ([Fe]-hydrogenases) do not contain Fe-S clusters nor Ni or Fe and were initially referred to as "metal-free" hydrogenases. They are present mainly in methanogens, belong to a phylogenetically distinct class and their function in bacteria is not clear (Vignais and Billoud, 2007).

Domain based genome comparison of syntrophic and non-syntrophic propionate and/or butyrate degraders

Six domains are present in the genomes of all analysed butyrate and/or propionate degrading syntrophs and not in non-syntrophs (**Table 2.1**). Domain "IPR006443" is exclusively present in the extra-cytoplasmic formate dehydrogenase (FDH) alpha subunit. Domains "IPR024064 and IPR006452" both belong to FdhE. The gene *fdh*E in *Escherichia coli* is required for maturation of the membrane bound FDH-complex (Schlindwein et al., 1990). The fact that extra-cytoplasmic formate dehydrogenases are only present in syntrophs and not in non-syntrophs strongly indicates that extra-cytoplasmic formate production is essential for syntrophic propionate and butyrate oxidation, and that formate plays a major role in interspecies electron transfer. The redox potential of the couple proton / hydrogen ($E^{0'}$= -414 mV) is slightly higher than the redox potential of the couple CO_2 / formate (-432 mV). The preference in syntrophic fatty acid-degrading communities has not been clear thus far, but a syntrophic relationship in which both hydrogen and formate can be transferred would be more flexible than when only hydrogen is transferred (Sieber et al., 2014). Moreover, multiple studies indicate that interspecies formate transfer is of significant importance in syntrophic degradation of butyrate and propionate. For example, *Syntrophobacter fumaroxidans* and *Syntrophospora bryantii* oxidize propionate and butyrate, respectively, in syntrophy with hydrogen and formate-using methanogens such as *Methanospirillum hungatei* and *Methanobacterium*

formicicum, but not with the hydrogen only-using *Methanobrevibacter arboriphilus* (Jackson et al., 1999). In analogy with this, *S. wolfei* oxidizes butyrate faster with the formate and hydrogen-using *M. hungatei* than with the hydrogen-only using *M. arboriphilus* (McInerney et al., 1981). The importance of formate transfer in *S. wolfei* cocultures is supported further by the observed involvement of an extra-cytoplasmic formate dehydrogenase in the final reduction of CO_2 with electrons generated by the butyryl-CoA to crotonyl-CoA conversion (Schmidt et al., 2013). Moreover, this extra-cytoplasmic formate dehydrogenase was more expressed during syntrophic growth compared to axenic growth (Schmidt et al., 2013).

Domain "IPR019079", named CapA, was found in genomes of all short chain fatty acid degrading syntrophs (including acetate oxidizers, data not shown) and was not present in the genomes of the two non-syntrophs (**Table 2.1**). CapA is part of a membrane bound complex that synthesizes poly-γ-glutamate to form a capsule or biofilm in *Bacillus subtilis*, *B. anthracis*, *Staphylococcus epidermidis* and *Fusobacterium nucleatum* (Candela and Fouet, 2006; Morikawa et al., 2006; Candela et al., 2009). The presence of this domain in SCFA degrading bacteria may contribute to the formation of exopolymeric substances that may facilitate syntrophic growth. Domain "IPR018365" is present in FtsW, RodA, SpoVE, that are membrane integrated proteins involved in cell division, shape-determination and sporulation in *Escherichia coli* and *Bacillus subtilis* (Ikeda et al., 1989; Joris et al., 1990; Mohammadi et al., 2014). What the exact function of this domain is in syntrophic butyrate and propionate degraders is unclear. The domain "IPR020539" that seems exclusively present in syntrophs in our analysis belongs to the protein Ribonuclease P which removes extra residues at the 5'- side from precursor tRNA, resulting in mature tRNA. However, what its function could be in syntrophic growth is unclear, but just coincidence cannot be excluded. As can be seen from **Table 2.1**, only one copy of this domain is present in the genome of a syntrophic bacterium, whereas for the domains involved in periplasmic formate dehydrogenases, CapA-domains and Cell cycle FtsW / RodA / SpoVE- domains, more copies are present. Furthermore, domain co-occurrence suggests that *D. autotrophicum* HRM2*, D. tiedjei* and *D. meridiei* are able to adopt a syntrophic lifestyle on SCFA.

Domain based functional profiling of electron transfer mechanisms

For syntrophic butyrate and propionate degradation, electron transfer mechanisms are required to transfer electrons to the terminal acceptor, which can be sulfate during sulfidogenic lifestyle or protons and/or CO_2 during syntrophic lifestyle. As the previous paragraph focussed on functional domains that are present in all syntrophic and not in non-syntrophic propionate and/or butyrate degraders, here we profile the functional domains involved in electron transfer mechanisms (**Table 2.2**).

Table 2.1. Domain based genome comparison of syntrophic and non-syntrophic butyrate and/or propionate degraders. Domains present in genomes of all butyrate and/or propionate degrading syntrophs and absent in those of non-syntrophs are listed and domain abundance is indicated. Syntrophs are shaded white, non-syntrophs are shaded black and sulfate reducers that were never tested for syntrophic growth are shaded grey.

		Syntrophomonas wolfei	*Syntrophus aciditrophicus*	*Syntrophothermus lipocalidus*	*Syntrophobacter fumaroxidans*	*Pelotomaculum thermopropionicum*	*Desulfotomaculum kuznetsovii*	*Desulfobulbus propionicus*	*Desulfobulbus japonicus*	*Desulfatibacillum alkenivorans*	*Desulfatirhabdium butyrativorans*	*Desulfobacterium autotrophicum*	*Desulfospira joergensenii*	*Desulfotignum balticum*	*Desulfomonile tiedjei*	*Desulfarculus baarsii*	*Desulfosporosinus meridiei*	*Desulfotalea psychrophila*	*Desulfatibacillum aliphaticivorans*	*Desulfotomaculum gibsoniae*
Growth on butyrate[¥]																				
Growth on propionate[¥]																				
Extra-cytoplasmic FDH α subunit	IPR006443	1	2	1	3	1	0	0	0	2	1	5	2	0	2	0	1	0	0	1
FdhE-like protein	IPR024064	4	6	2	5	3	0	0	0	0	0	4	4	0	2	1	2	0	0	2
FDH accessory protein	IPR006452	2	3	1	2	1	0	0	0	0	0	2	2	0	1	0	1	0	0	1
Capsule synthesis protein, CapA	IPR019079	2	2	4	2	1	0	0	0	0	0	4	2	0	2	0	4	4	0	2
Cell cycle, FtsW / RodA / SpoVE,	IPR018365	1	2	2	2	1	0	0	0	2	1	3	0	1	1	2	2	0	0	0
Ribonuclease P, conserved site	IPR020539	1	1	1	1	1	0	0	0	2	1	1	0	0	1	1	1	1	0	0

[¥]The ability of substrate conversion was retrieved from literature (Widdel, 1980; McInerney et al., 1981; Brysch et al., 1987; Nazina et al., 1988; Deweerd and Suflita, 1990; K. et al., 1997; Harmsen et al., 1998; Jackson et al., 1999; Knoblauch et al., 1999; Kuever et al., 1999; Sekiguchi et al., 2000; Robertson et al., 2001; Imachi et al., 2002; Cravo-Laureau et al., 2004; Ommedal and Torsvik, 2007; Suzuki et al., 2007; Balk et al., 2008).

Table 2.2. Profiles of functional domains involved in electron transfer mechanisms. Profiles of functional domains involved in electron transfer mechanisms are shown. Profiles of functional domains involved in electron transfer mechanisms are shown and abundance indicated. Syntrophic butyrate and/or propionate degraders are shaded white, non-syntrophic butyrate and/or propionate degraders are shaded black and sulfate reducers that were never tested for syntrophic growth are shaded grey.

			Syntrophomonas wolfei	*Syntrophus aciditrophicus*	*Syntrophothermus lipocalidus*	*Syntrophobacter fumaroxidans*	*Pelotomaculum thermopropionicum*	*Desulfotomaculum kuznetsovii*	*Desulfobulbus propionicus*	*Desulfobulbus japonicus*	*Desulfatibacillum alkenivorans*	*Desulfatirhabdium butyrativorans*	*Desulfobacterium autotrophicum*	*Desulfospira joergensenii*	*Desulfotignum balticum*	*Desulfomonile tiedjei*	*Desulfarculus baarsii*	*Desulfosporosinus meridiei*	*Desulfotalea psychrophila*	*Desulfatibacillum aliphaticivorans*	*Desulfotomaculum gibsoniae*
Growth on SCFA[¥]		Butyrate																			
		Propionate																			
Protein (complex)	Subunit	InterPro number																			
Cytoplasmic FDH	Alpha	IPR027467	4	2	2	3	1	2	0	0	5	3	10	2	5	2	3	4	2	2	2
		IPR006655	2	4	0	5	2	2	2	1	9	5	9	3	4	7	1	7	4	1	6
		IPR006478	0	0	1	3	0	1	0	0	1	1	1	0	0	2	0	2	0	1	1
	NUO 51kDa	IPR019575	12	12	4	8	6	12	8	2	12	4	6	0	12	9	8	6	8	6	12
		IPR001949	8	6	3	4	3	5	4	1	6	2	3	0	6	4	4	1	2	3	4
Extra-cytoplasmic FDH	alpha	IPR006443	3	4	1	5	2	0	0	1	3	2	5	4	0	2	0	2	0	1	2
Formate transporter	-	IPR000292	2	1	0	1	1	0	0	0	4	0	4	0	0	0	2	2	0	2	0
		IPR024092	2	0	0	1	0	0	0	0	4	0	2	0	0	0	2	2	0	2	0

f

			Syntrophomonas wolfei	*Syntrophus aciditrophicus*	*Syntrophothermus lipocalidus*	*Syntrophobacter fumaroxidans*	*Pelotomaculum thermopropionicum*	*Desulfotomaculum kuznetsovii*	*Desulfobulbus propionicus*	*Desulfobulbus japonicus*	*Desulfatibacillum alkenivorans*	*Desulfatirhabdium butyratixorans*	*Desulfobacterium autotrophicum*	*Desulfospira joergensenii*	*Desulfotignum balticum*	*Desulfomonile tiedjei*	*Desulfarculus baarsii*	*Desulfosporosinus meridiei*	*Desulfotalea psychrophila*	*Desulfatibacillum aliphaticivorans*	*Desulfotomaculum gibsoniae*
FeFe-hydrogenase	alpha	IPR004108	4	1	3	3	4	8	3	0	0	0	4	1	2	1	1	5	4	0	7
		IPR009016	5	1	3	3	5	8	3	0	0	0	6	1	2	1	1	5	6	0	7
		IPR003149	9	3	9	6	9	12	6	0	0	0	9	3	3	3	0	9	6	0	9
		IPR013352	3	1	3	2	3	4	2	0	0	0	3	1	1	1	0	3	2	0	3
NiFe-hydrogenase		IPR001501†	0	2	3	17	2	0	10	7	12	1	12	2	6	3	2	7	14	8	8
		IPR018194†	0	1	2	6	2	0	6	4	9	2	8	2	4	4	4	5	13	7	2
Rnf complex	RnfB	IPR007202	2	2	0	9	6	10	2	0	22	7	30	10	10	14	13	6	4	4	13
		IPR010207	0	1	0	1	0	0	0	0	1	0	5	1	0	1	0	0	2	1	0
	RnfC	IPR026902	0	1	0	1	0	0	0	1	4	0	2	2	1	1	1	3	6	1	0
		IPR010208	0	2	0	2	0	0	0	0	0	0	4	0	0	2	2	0	4	0	0
	RnfD	IPR004338	0	1	0	1	0	0	0	0	2	1	4	1	2	1	1	0	4	0	0
		IPR011303	0	1	0	1	0	0	0	0	2	1	2	1	1	1	1	0	2	0	0
	RnfG	IPR007329	2	2	0	2	0	0	0	0	4	2	14	2	6	2	2	0	8	0	6
DUF224	-	IPR003816	1	1	1	1	2	1	2	0	5	4	6	2	5	8	3	4	2	2	1
		IPR004017	6	15	10	27	13	26	17	8	58	25	54	24	34	39	18	34	33	10	31
		IPR023234	1	1	1	5	3	3	4	0	19	6	27	6	14	15	9	8	8	6	3

Ech complex	EchA	IPR001750	0	0	4	6	0	3	14	0	4	9	8	6	9	6	0	7	11	0	3
		IPR001516	0	0	2	2	0	1	3	0	0	1	0	2	2	2	0	1	0	0	1
	EchB	IPR001694	0	0	3	4	0	2	8	0	0	2	2	0	1	4	0	4	6	0	2
	EchC	IPR006137	0	2	6	16	2	2	19	6	12	6	12	4	8	8	4	12	22	6	9
	EchD	IPR001268	0	0	2	2	0	1	3	0	0	2	1	0	1	2	0	3	4	0	1
		IPR012179	0	0	0	0	0	0	0	0	0	0	0	0	0	0	0	0	0	0	0
	EchE	IPR001135	0	0	4	3	0	2	5	0	0	3	1	0	1	2	0	4	6	0	2
Etf alpha	-	IPR014731	3	1	4	4	6	4	2	0	10	4	7	4	7	3	3	3	3	0	1
Etf beta	-	IPR012255	3	1	4	4	7	4	2	0	10	4	5	4	7	3	3	3	2	0	1
Bcd	-	IPR006089	7	6	17	7	8	12	6	0	54	9	18	4	10	21	22	15	0	15	20
		IPR009075	18	13	28	14	20	20	6	0	*	36	64	17	36	45	44	22	0	34	30
		IPR006092	7	6	10	6	9	8	3	0	82	15	31	7	16	19	18	8	0	15	15
		IPR006091	18	13	27	14	20	18	6	0	*	36	68	17	36	45	43	22	0	36	30
		IPR013786	8	6	12	6	9	9	3	0	90	15	31	7	17	19	19	9	0	18	15
		IPR009100	9	7	14	8	11	9	3	0	*	18	34	9	19	25	23	12	0	18	15
Cytochrome	c	IPR023155	1	1	0	6	0	0	12	0	12	4	10	4	4	20	11	1	3	2	0
		IPR024673	0	0	0	3	0	0	0	0	10	3	2	0	4	0	0	0	6	0	0
	cIII	IPR020942	0	0	0	2	0	0	4	2	10	5	11	4	10	4	2	0	0	1	0
		IPR002322	0	0	0	0	0	0	8	4	24	16	40	16	24	8	4	0	0	4	0
	b561	IPR016174	6	6	6	3	1	2	1	1	4	2	0	4	2	6	1	13	11	0	1
		IPR000516	0	0	4	2	0	0	0	0	4	2	0	0	0	0	0	10	10	0	2
	b5	IPR001199	0	3	0	3	0	0	0	0	0	3	0	4	0	3	0	0	0	0	0

Abbreviations are explained as formate dehydrogenase (FDH); NADH: ubiquinone oxidoreductase subunit 51 kDa (NUO 51kDa); membrane-bound ferredoxin:NAD^+ oxidoreductase (Rnf) complex; Butyryl-CoA dehydrogenase (Bcd); Domain of unknown function 224 (DUF224).

¥ The ability of substrate conversion was retrieved from literature (Widdel and Pfennig, 1977; Widdel, 1980; McInerney et al., 1981; Widdel and Pfennig, 1981; Brysch et al., 1987; Widdel, 1987; Nazina et al., 1988; Schnell et al., 1989; Deweerd and Suflita, 1990; Ollivier et al., 1991; Schnürer et al., 1996; K. et al., 1997; Harmsen et al., 1998; Jackson et al., 1999; Knoblauch et al., 1999; Kuever et al., 1999; Oude Elferink et al., 1999; Sekiguchi et al., 2000; Robertson et al., 2001; Imachi et al., 2002; Cravo-Laureau et al., 2004; Ommedal and Torsvik, 2007; Suzuki et al., 2007; Balk et al., 2008; Westerholm et al., 2011; Oehler et al., 2012).

*more than 99

†These IPR numbers were unique for NiFe hydrogenase alpha subunits. As the Ech complex also contains a NiFe hydrogenase alpha subunit, corresponding domains were also found in this EchE.

As can be seen from **Table 2.2**, cytoplasmic and extra-cytoplasmic formate dehydrogenases contain InterPro domains that are unique for each protein. "IPR006443" is only present in extra-cytoplasmic FDH's, not in cytoplasmic FDH's whereas "IPR027467", "IPR006655" and "IPR006478" of cytoplasmic FDH, are not present in extra-cytoplasmic FDH's. Domains of cytoplasmic FDH's are present in genomes of syntrophs and non-syntrophs, whereas the domain of extra-cytoplasmic FDH's is present only in syntrophs. Formate transporter linked domains are absent in genomes of non-syntrophs whereas they are present in a number of syntrophs. These observations again point to the importance of formate as interspecies electron carrier.

The membrane bound Rnf complex that can conserve energy by the reversible translocation of protons or sodium ions from ferredoxin oxidation with NAD^+ (Tremblay et al., 2012) was not found in non-syntrophs but is present in several syntrophs. As syntrophs live at the limit of what is energetically possible (Schink, 1997; Scholten and Conrad, 2000; McInerney et al., 2007) they contain mechanisms to conserve energy from ferredoxin oxidation with NAD^+. Furthermore, recently the domain with unknown function "DUF224" was shown to play a role in electron transport from an electron transfer flavoprotein (ETF) towards membrane-bound electron transfer components in *S. wolfei* (Schmidt et al., 2013). DUF224 is present in 18 genomes from which 17 also contain domains linked to ETF complexes. This indicates that DUF224 may have a role in electron transfer in bacteria other than *S. wolfei* as well.

Energetics and metabolism of syntrophic butyrate and propionate degradation.

Energy conservation mechanisms

For microbial maintenance and growth, the energy that is released from catabolic reactions has to be converted into energy that can be used to perform anabolic reactions. Therefore, energy is conserved as ATP by substrate level phosphorylation or via a proton or sodium gradient over the cytoplasmic membrane, termed electron transport phosphorylation. Membrane bound enzyme complexes are required to build a proton gradient over the membrane while other membrane bound enzyme complexes are required to use the proton gradient. The membrane bound enzyme complex ATP synthase can either use the proton gradient for ATP synthesis or ATP hydrolysis to build the proton gradient.

In addition to substrate level phosphorylation and the proton gradient over the cytoplasmic membrane, an only recently discovered process called flavin-based electron bifurcation has been considered as a third mechanism for energy conservation (Buckel and Thauer, 2013). In the last decade, several of such

cytoplasmic bifurcation complexes were determined in Bacteria and Archaea (Li et al., 2008; Schut and Adams, 2009; Wang et al., 2010; Kaster et al., 2011b; Huang et al., 2012; Buckel and Thauer, 2013; Costa et al., 2013b; Wang et al., 2013a; Wang et al., 2013b). Instead of coupling two redox reactions, as is performed by commonly known redox proteins, bifurcation (and the reversed reaction termed confurcation) enzyme complexes couple three redox reactions. With this concept, energy that would otherwise have been lost can be conserved or endergonic reactions can be coupled to exergonic reactions and reducing equivalents that are generated can be re-oxidized efficiently. For instance, endergonic reduction of ferredoxin with NADH is coupled to the exergonic reduction of crotonyl-CoA to butyryl-CoA by the butyryl-CoA / electron transfer flavoprotein complex of *Clostridium kluyveri* (Li et al., 2008). Another example is the [FeFe]-hydrogenase complex of *Thermotoga maritima* that couples reversible ferredoxin reduction with hydrogen to NAD^+ reduction (Schut and Adams, 2009). In addition to cytoplasmic bifurcating enzyme complexes, membrane bound complexes (Rnf-complexes) were recently shown to conserve energy by the reversible translocation of protons or sodium from ferredoxin oxidation with NAD^+ (Biegel et al., 2011). The energy conserving hydrogenase (Ech) has a similar function, but performs the proton or sodium translocation by ferredoxin oxidation with hydrogen production (Hedderich and Forzi, 2005).

Syntrophic butyrate degradation

Butyrate oxidation coupled to hydrogen or formate production is endergonic under standard conditions. This is shown by the positive Gibbs free energy changes; + 48 kJ and + 45 kJ, respectively (**Table 1.1**). When butyrate oxidation is coupled to methane production the conversion is energetically feasible. To share this energy between the syntrophic butyrate oxidizer and the methanogen in such a manner that both organisms gain enough energy to grow, the hydrogen and formate concentrations have to be kept in a low range (Schink, 1997). *Syntrophomonas wolfei*, *Syntrophus aciditrophicus* and *Syntrophothermus lipocalidus* can couple butyrate oxidation to syntrophic growth with methanogens and cannot grow in pure culture with any electron acceptor (Beaty and McInerney, 1990; Jackson et al., 1999; Sekiguchi et al., 2000).

All known syntrophic butyrate degraders oxidize butyrate via the beta-oxidation pathway (**Table 2.4, Figure 1.2**) (McInerney et al., 2007; Stams and Plugge, 2009). This pathway includes two reactions that generate electron pairs and one reaction that generates ATP. This ATP partially has to be invested in the endergonic conversion of butyryl-CoA to crotonyl-CoA. The biochemical mechanism that enables investment of a fraction of ATP for the endergonic conversion of butyryl-CoA to crotonyl-CoA has recently been revealed in *S. wolfei*. Electrons that are generated by the conversion of butyryl-CoA to crotonyl-CoA travel via butyryl-CoA dehydrogenase (encoded by genes with locus tags Swol_1933 and Swol_2053), an electron transfer

flavoprotein (encoded by Swol_0696-7) and a membrane anchored protein that was annotated as DUF224 (encoded by Swol_0698) to the menaquinone pool in the membrane. Oxidation of reduced menaquinone is then coupled to formate generation by a membrane anchored extra-cytoplasmic formate dehydrogenase (encoded by Swol_0797-800) (Schmidt et al., 2013). This reaction is driven by the proton motive force. The produced formate is used by the methanogen. The second reaction that generates electrons and protons is the conversion of hydroxybutyryl-CoA to acetoacetyl-CoA which is endergonic when coupled via NAD^+ to hydrogen or formate production. Most likely in *S. wolfei* this involves the [FeFe]-hydrogenase (encoded by Swol_1017-19) that forms a cytoplasmic complex with a formate dehydrogenase (Swol_0783-6) (Müller et al., 2009).

Syntrophic propionate degradation

Propionate oxidation coupled to hydrogen or formate production is endergonic under standard conditions. This is shown by the positive Gibbs free energy changes; + 76 kJ and + 72 kJ respectively (**Table 1.1**). However, when propionate oxidation is coupled to methane production the conversion is energetically feasible. To share energy between the syntrophic propionate oxidizer and the methanogen in such a manner that both organisms gain enough energy to grow, the hydrogen and formate concentrations have to be kept in a low range (around 40 Pa) (Schink, 1997). *Smithella propionica*, *Syntrophobacter fumaroxidans* and *Pelotomaculum thermopropionicum* are able to couple propionate oxidation to syntrophic growth with methanogens (Harmsen et al., 1998; Liu et al., 1999; Imachi et al., 2002; Kosaka et al., 2006). *Smithella propionica* degrades propionate via a dismutating pathway to acetate and butyrate, which is subsequently oxidized to acetate (de Bok et al., 2001). All other known syntrophic propionate-degrading bacteria use the methylmalonyl-CoA pathway to oxidize propionate to acetate and CO_2 (**Figure 1.2**). In this pathway one ATP is formed via substrate level phosphorylation, 2/3 ATP have to be invested and three conversions in the methylmalonyl-CoA pathway generate each two electrons and two protons.

One of the reactions that generates two electrons and two protons is the endergonic oxidation of succinate to fumarate that requires investment of 2/3 ATP (Schink, 1997). Van Kuijk et al. (1998) proposed that succinate oxidation could be coupled to extra-cytoplasmic hydrogen or formate formation via a menaquinone loop between a cytoplasmic oriented membrane-bound succinate dehydrogenase and a periplasmic oriented membrane bound hydrogenase or formate dehydrogenase (van Kuijk et al., 1998b)

Table 2.4. Physiological characteristics of butyrate and propionate degrading syntrophs and non-syntrophs. *Syntrophomonas wolfei subsp. wolfei (A), Syntrophus aciditrophicus (B), Syntrophothermus lipocalidus (C), Syntrophobacter fumaroxidans (D), Pelotomaculum thermopropionicum (E), Desulfotomaculum kuznetsovii (F), Desulfobulbus propionicus (G).*

	A	B	C	D	E	F	G
Gram reaction	-	-	-[a]	-	-[a]	-[a]	-
Motility	+	-	+	-	-	+	-
Spore formation	-	-	-	-	+	+	-
Growth pH (range /optimum)	ND/7.2?	ND/7.0?	5.8-7.5 (6.5-7)	6.0-8.0/7	6.5-8.0/7.0	ND	6.0-8.6 (7.1-7.5)
Growth temperature (°C) (range/optimum)	ND/35	25-42/35	45-60/55	20-40/37	45-65/55	50-85/60-65	10-43/39
Growth rate (d^{-1})	0.27 in coculture on butyrate with *Methanospirillum hungatei*	0.22 in coculture with *Desulfovibrio desulfuricans* G11	0.93 in pure culture on crotonate 1.06 in coculture on butyrate	0.17 in coculture	0.19 coculture on propionate 2.4 coculture on ethanol	ND	0.42 (propionate + sulfate)
Cytochrome b and - c Menaquinone	Cyt C MK-7	MQ	Not found	Cyt b & Cyt c MK-6 & MK-7	MK	ND	Cyt b & Cyt c MK-4&MK-5
Metabolic pathway used	ß-oxidation	ß-oxidation	ß-oxidation	Methylmalonyl-CoA (MMC)	Methylmalonyl-CoA (MMC)	Wood-Ljungdahl MMC ß-Oxidation	MMC
Complete/ Incomplete oxidizer	Incomplete	Incomplete	Incomplete	Incomplete	Incomplete	Complete	Incomplete
Electron acceptor utilization in pure culture	None	None	None	sulfate, thiosulfate, fumarate	fumarate	sulfate, sulfite, thiosulfate	sulfate, sulfite, thiosulfate, nitrate, O_2, Fe(III)
Substrate utilization in pure culture	crotonate	crotonate	Crotonate	propionate, formate, fumarate, succinate, hydrogen, malate, aspartate, pyruvate	propionate, fumarate, pyruvate, ethanol, lactate	Formate, acetate, propionate, butyrate, valerate, lactate, malate, fumarate, succinate, methanol, ethanol, propanol, butanol, H_2, (up to 50%) CO	propionate, lactate, pyruvate, ethanol, 1-propanol + 1 butanol, H_2

Table 2.4. ***Continues.*** **Physiological characteristics of butyrate and propionate degrading syntrophs and non-syntrophs.** *Syntrophomonas wolfei subsp. wolfei (A), Syntrophus aciditrophicus (B), Syntrophothermus lipocalidus (C), Syntrophobacter fumaroxidans (D), Pelotomaculum thermopropionicum (E), Desulfotomaculum kuznetsovii (F), Desulfobulbus propionicus (G).*

	A	B	C	D	E	F	G
Substrate utilization in co-culture	butyrate, caproate, caprylate, valerate, heptanoate, isoheptanoate	butyrate, benzoate, hexanoate, heptanoate, octanoate, palmitate, stearate, trans-2-pentenoate, trans-2-hexanoate, trans-3-hexanoate, 2-octenoate, methyl esters of butyrate and hexanoate,	Butyrate, Isobutyrate Straight-chain fatty acids from C4 to C10	Propionate	propionate, ethanol, lactate, 1-butanol, ethylene glycol, 1-propanol, 1-pentanol, 1,3-propanediol	None	None
Syntrophic partner used	*M. hungatei* *D. desulfuricans G11* *Methanobacterium bryantii strain MoH* *Methanobrevibacter arboriphilus*	*Methanospirillum hungatei* *D. desulfuricans* G11 in the presence of sulfate	*M. thermoautotrophicum*	*Methanospirillum hungatei* *Methanobacterium formicicum*	*M. Thermoautotro-phicum*	None	None

a Cells stain Gram-negative, but the organism has a Gram-positive cell wall ultrastructure.
b ND: not determined or not reported.

Genes coding for a periplasmic hydrogenase and three extra-cytoplasmic formate dehydrogenases were found in the genome of *S. fumaroxidans* (Müller et al., 2010). Especially the gene Sfum_1273-74 that codes for one of the periplasmic formate dehydrogenase alpha subunits is highly transcribed during syntrophic growth (Worm et al., 2011b) which suggests that succinate oxidation is coupled to formate production and indicates the importance of formate as an electron carrier in syntrophic propionate degradation. Also malate oxidation to oxaloacetate generates two electrons and two protons, which in *S. fumaroxidans* are coupled to NAD^+ reduction by malate dehydrogenase (van Kuijk and Stams, 1996). To couple this to hydrogen production would require a hydrogen partial pressure of 10^{-8} atm that is lower than can be maintained by methanogens (Schink, 1997). The third reaction that generates electrons and protons is the conversion of pyruvate to acetyl-CoA and CO_2 that can be coupled to ferredoxin reduction using the pyruvate:ferredoxin oxidoreductases (Chabriere et al., 1999). Genome analysis suggests that NADH generated from malate oxidation and reduced ferredoxin generated from pyruvate oxidation could be coupled to formate or hydrogen production by confurcating formate dehydrogenases and hydrogenases (Müller et al., 2010). Such a mechanism would use the energy that remains from ferredoxin oxidation with protons to allow the endergonic coupling of NADH oxidation to proton reduction. Formate dehydrogenases from *S. fumaroxidans* were studied for subunit-composition, enzyme activity, cofactor binding and direction of conversion. Formate dehydrogenase 1 contains W, Se, four [2Fe2S], one [4Fe4S] and is a hetero-trimer. Formate dehydrogenase 2 contains W, Se, two [4Fe4S] and is heterodimer. Both enzymes oxidize formate with benzyl viologen and reduce CO_2 with reduced methyl viologen. The purified enzyme was not able to reduce NAD^+ (de Bok et al., 2003). Whether these formate dehydrogenases can confurcate electrons from NADH and reduced ferredoxin to CO_2 reduction, has never been tested.

Syntrophic formate degradation

Genome comparison pointed to the role of formate in syntrophic butyrate and propionate degradation. In the degradation of SCFA, formate and hydrogen play an important role as electron shuttling components. Interestingly syntrophic growth with formate occurs as well. Formate oxidation coupled to hydrogen is endergonic under standard conditions. This is shown by the Gibbs free energy change that is close to zero; 1.3 kJ (**Table 1.1**). However, when formate oxidation is coupled to methane production the conversion is energetically feasible. To share energy between the syntrophic formate oxidizer and the methanogen in such a manner that both organisms gain enough energy to grow, the hydrogen concentrations have to be kept in a low range (between 40 and 100 Pa) (Dolfing et al., 2008). The thermophilic *Moorella* sp. strain AMP and mesophilic *Desulfovibrio desulfuricans* G11 are able to couple formate oxidation to syntrophic growth with methanogens that can only use

hydrogen as electron donor (Dolfing et al., 2008). The electron transfer mechanism that allows syntrophic formate degradation is not known. Possibly an extra-cytoplasmic formate dehydrogenase is coupled to a membrane integrated, cytoplasmic oriented hydrogenase which generates a proton motive force that can be used or ATP synthesis (Dolfing et al., 2008). To what extend and in what types of anaerobic microbial environments syntrophic formate degradation can compete with formate degradation by methanogens is not known.

Phylogeny of short chain fatty acid degraders does not predict syntrophy

Syntrophic methanogenic growth on butyrate is performed by bacteria belonging to the Firmicutes (*Syntrophomonas*, *Syntrophothermus*, *Thermosyntropha* genera) and Deltaproteobacteria (*Syntrophus aciditrophicus*). *Syntrophomonas* is the best represented genus within syntrophic fatty-acid degraders (in terms of available isolates), with 11 species and/or subspecies described thus far (Sousa et al., 2009). Nevertheless, only the genome of *S. wolfei* subsp. *wolfei* has been sequenced (Sieber et al., 2010). Propionate can be syntrophically utilized by *Pelotomaculum*- and *Syntrophobacter* species (Stams et al., 2012). In addition, *Smithella propionica* can degrade propionate in syntrophy with methanogens (Liu et al., 1999). *Syntrophobacter* species can use propionate in syntrophy with hydrogenotrophic methanogens, or alone if sulfate is available in the environment (Plugge et al., 2011). *Pelotomaculum* species do not possess the ability to grow with propionate and sulfate. The genomes of *Syntrophobacter fumaroxidans* and *Pelotomaculum thermopropionicum* are available (Kosaka et al., 2008; Plugge et al., 2012).
Dissimilatory sulfate-reducing bacteria able to use fatty-acids are very diverse. Sulfate-reducing bacteria analysed in the scope of this study are distributed among Deltaproteobacteria and Firmicutes phyla. *Desulfotomaculum* species belong to *Peptococcaceae* family, the same family of the syntrophic *Pelotomaculum* species. Recently, it was shown that the genomes of *D. kuznetsovii* and *P. thermopropionicum* have a high similarity (Visser et al., 2013). The genes involved in propionate metabolism of these two strains were similar, but main differences were found in genes involved in the electron acceptor metabolism. Some *Desulfotomaculum* species – *D. thermobenzoicum* subsp. *thermosyntrophicum* and *D. thermocisternum* – were also shown to grow on propionate in syntrophy with a hydrogenotrophic methanogen (without sulfate) (Nilsen et al., 1996; Plugge et al., 2002).

The ability to grow in syntrophy is either first evolved and then lost or acquired by horizontal gene transfer from a syntroph to a non-syntroph. Multiple horizontal gene transfers of dissimilatory sulfite reductase genes (*dsrAB*) in sulfate-reducing prokaryotes have been suggested by (Klein et al., 2001). These authors found that the topology of a tree based on a large fragment of the *dsrAB* was inconsistent with the corresponding 16S based tree.

Conclusions

Systematic functional profiling of genomes shed light on the question: "what are the key properties that make that a SCFA degrading bacterium is able to grow in syntrophy with methanogens and another not". The presence or absence of extra-cytoplasmic formate dehydrogenases, including their maturation proteins is clearly a difference between syntrophic and non-syntrophic butyrate and/or propionate degraders. Together with transcription and proteomic studies that show an increase of extra-cytoplasmic formate dehydrogenase during syntrophic growth (Worm et al., 2011b; Schmidt et al., 2013), it seems evident that this enzyme is a key factor for syntrophic butyrate and propionate degradation. Moreover, this simultaneously suggests that formate is an important interspecies electron carrier in syntrophic butyrate and propionate degradation. This is supported by the presence of the formate transporter in several butyrate and propionate degrading syntrophs. Further biochemical examination and knock-out experiments of genes involved in formate transport and extra-cytoplasmic formate dehydrogenase activity and maturation would give more insight in the importance of this enzyme complex during syntrophy. Genetic manipulation protocols for SCFA degrading syntrophic bacteria have to be developed. Furthermore, the presence or absence of two domains, both linked to membrane integrated proteins with a currently unknown function in syntrophy, appear to make a difference as well. Both are membrane integrated proteins. One is putatively involved in capsule or biofilm formation and a second in cell division, shape-determination or sporulation. Capsule formation, cell division, shape-determination and sporulation by these bacteria during syntrophic growth could be assessed with microscopic techniques.

Sulfate reducing bacteria such as *Desulfobacterium autotrophicum* HRM2, *Desulfomonile tiedjei* and *Desulfosporosinus meridiei* were never tested for syntrophic growth, but all crucial domains discussed in this review were found in corresponding genomes, which suggests their possible ability to grow in syntrophic association with methanogens. In addition, profiling domains involved in electron transfer mechanisms revealed the important role of the Rnf-complex and the formate transporter in syntrophy, and indicates that DUF224 may have a role in electron transfer in bacteria other than *S. wolfei* as well.

Supporting information

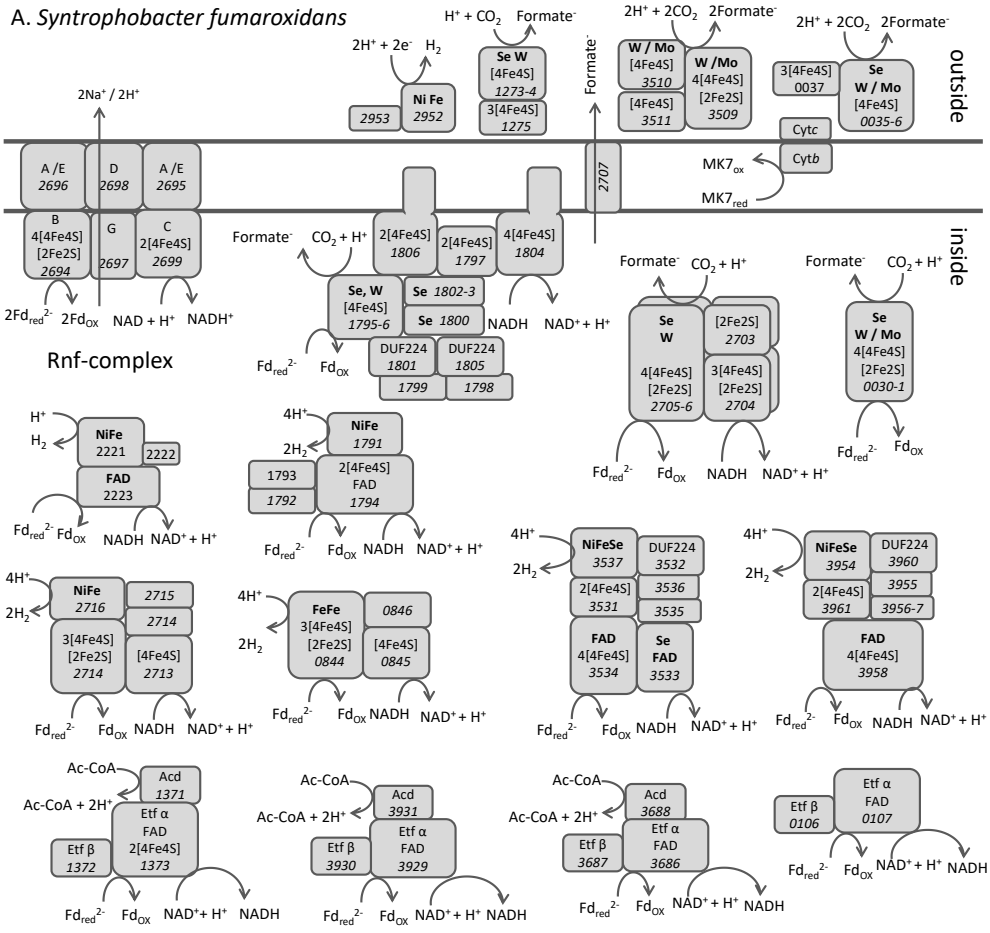

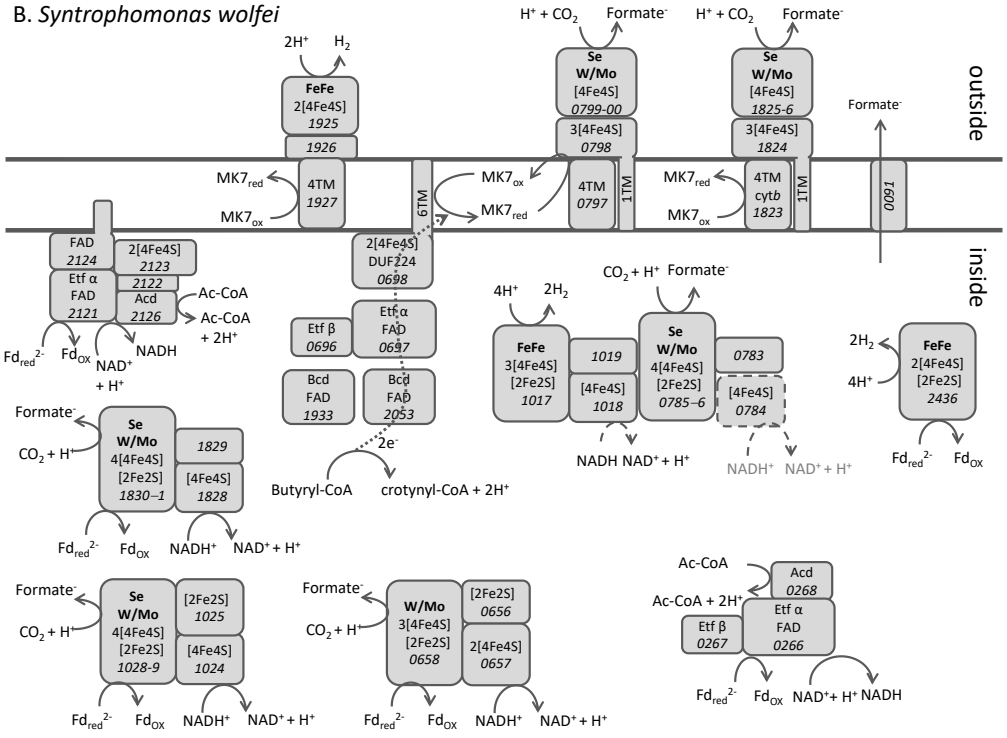
B. Syntrophomonas wolfei
outside
inside
FeFe
2[4Fe4S]
1925
1926
4TM
1927
6TM
2[4Fe4S]
DUF224
0698
Se
W/Mo
[4Fe4S]
0799-00
3[4Fe4S]
0798
4TM
0797
1TM
Se
W/Mo
[4Fe4S]
1825-6
3[4Fe4S]
1824
4TM
cytb
1823
1TM
1691
FAD
2124
2[4Fe4S]
2123
2122
Etf α
FAD
2121
Acd
2126
Etf β
0696
Etf α
FAD
0697
Bcd
FAD
1933
Bcd
FAD
2053
FeFe
3[4Fe4S]
[2Fe2S]
1017
1019
[4Fe4S]
1018
Se
W/Mo
4[4Fe4S]
[2Fe2S]
0785–6
0783
[4Fe4S]
0784
FeFe
2[4Fe4S]
[2Fe2S]
2436
Se
W/Mo
4[4Fe4S]
[2Fe2S]
1830–1
1829
[4Fe4S]
1828
Se
W/Mo
4[4Fe4S]
[2Fe2S]
1028-9
[2Fe2S]
1025
[4Fe4S]
1024
W/Mo
3[4Fe4S]
[2Fe2S]
0658
[2Fe2S]
0656
2[4Fe4S]
0657
Etf β
0267
Acd
0268
Etf α
FAD
0266
Ac-CoA
Ac-CoA + 2H+
Butyryl-CoA
crotonyl-CoA + 2H+
Formate-
CO2 + H+
NADH
NAD+ + H+
Fdred2-
FdOX

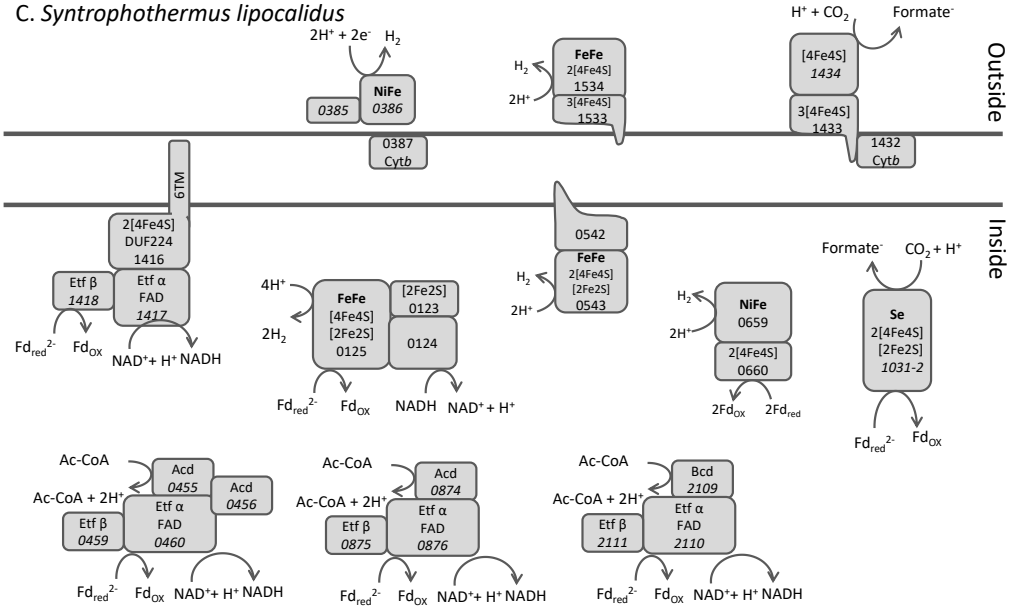
C. Syntrophothermus lipocalidus
Outside
Inside
NiFe
0385
0386
0387
Cytb
FeFe
2[4Fe4S]
1534
3[4Fe4S]
1533
[4Fe4S]
1434
3[4Fe4S]
1433
1432
Cytb
6TM
2[4Fe4S]
DUF224
1416
Etf β
1418
Etf α
FAD
1417
FeFe
[4Fe4S]
[2Fe2S]
0125
[2Fe2S]
0123
0124
0542
FeFe
2[4Fe4S]
[2Fe2S]
0543
NiFe
0659
2[4Fe4S]
0660
Se
2[4Fe4S]
[2Fe2S]
1031-2
Etf β
0459
Etf α
FAD
0460
Acd
0455
Acd
0456
Etf β
0875
Etf α
FAD
0876
Acd
0874
Etf β
2111
Etf α
FAD
2110
Bcd
2109
Ac-CoA
Ac-CoA + 2H+
NADH
NAD+ + H+
Fdred2-
FdOX
2FdOX
2Fdred
Formate-
CO2 + H+

D. *Syntrophus aciditrophicus*

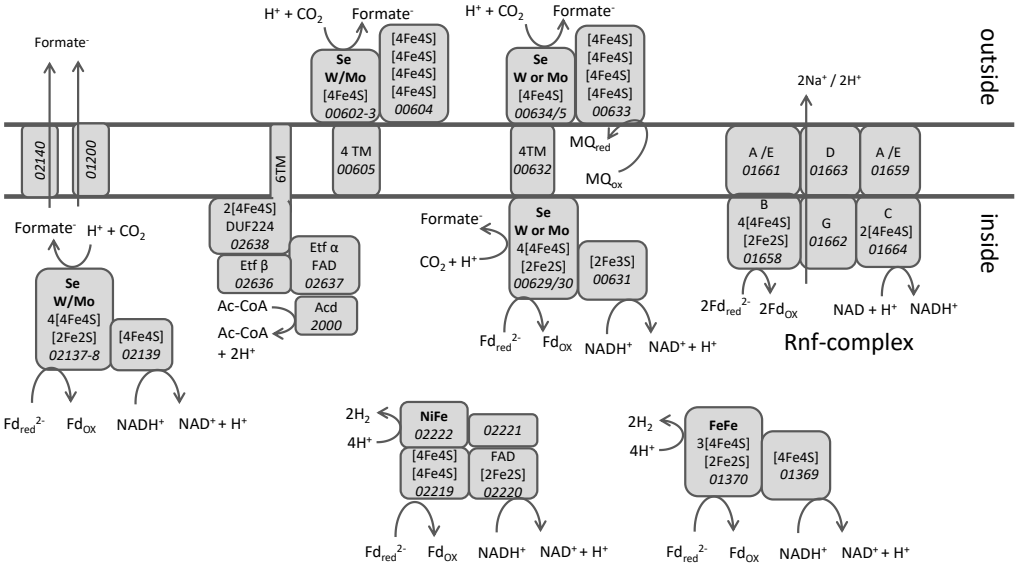

E. *Pelotomaculum thermopropionicum*

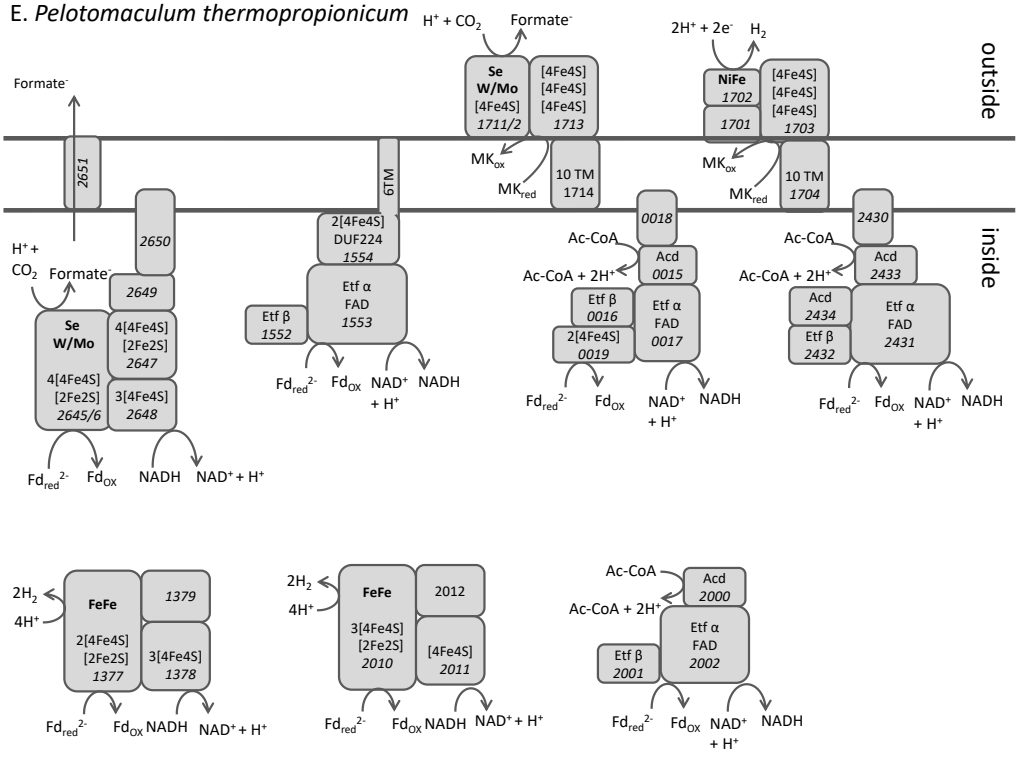

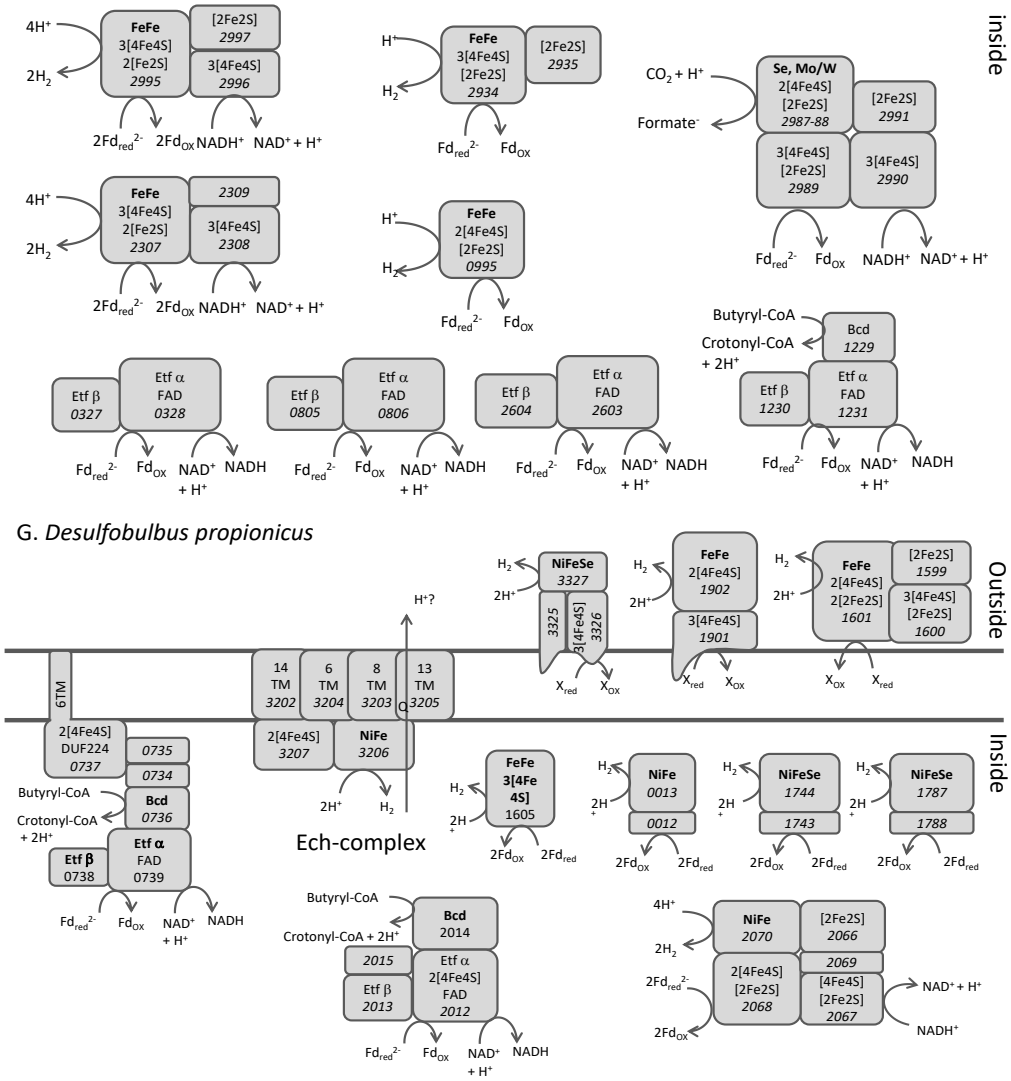

Fig. S1: Energy converting enzyme complexes predicted from the genomes of bacteria that can degrade propionate and butyrate in syntrophic growth with methanogens; *Syntrophobacter fumaroxidans* (A), *Syntrophomonas wolfei* (B), *Syntrophothermus lipocalidus* (C), *Syntrophus aciditrophicus* (D), *Pelotomaculum thermopropionicum* (E), and from those that cannot grow in syntrophic growth with methanogens; *Desulfotomaculum kuznetsovii* (F), and *Desulfobulbus propionicus* (G)

Syntrophy as the microbiological example of Hegel's slave-master dialectics

Chapter 3

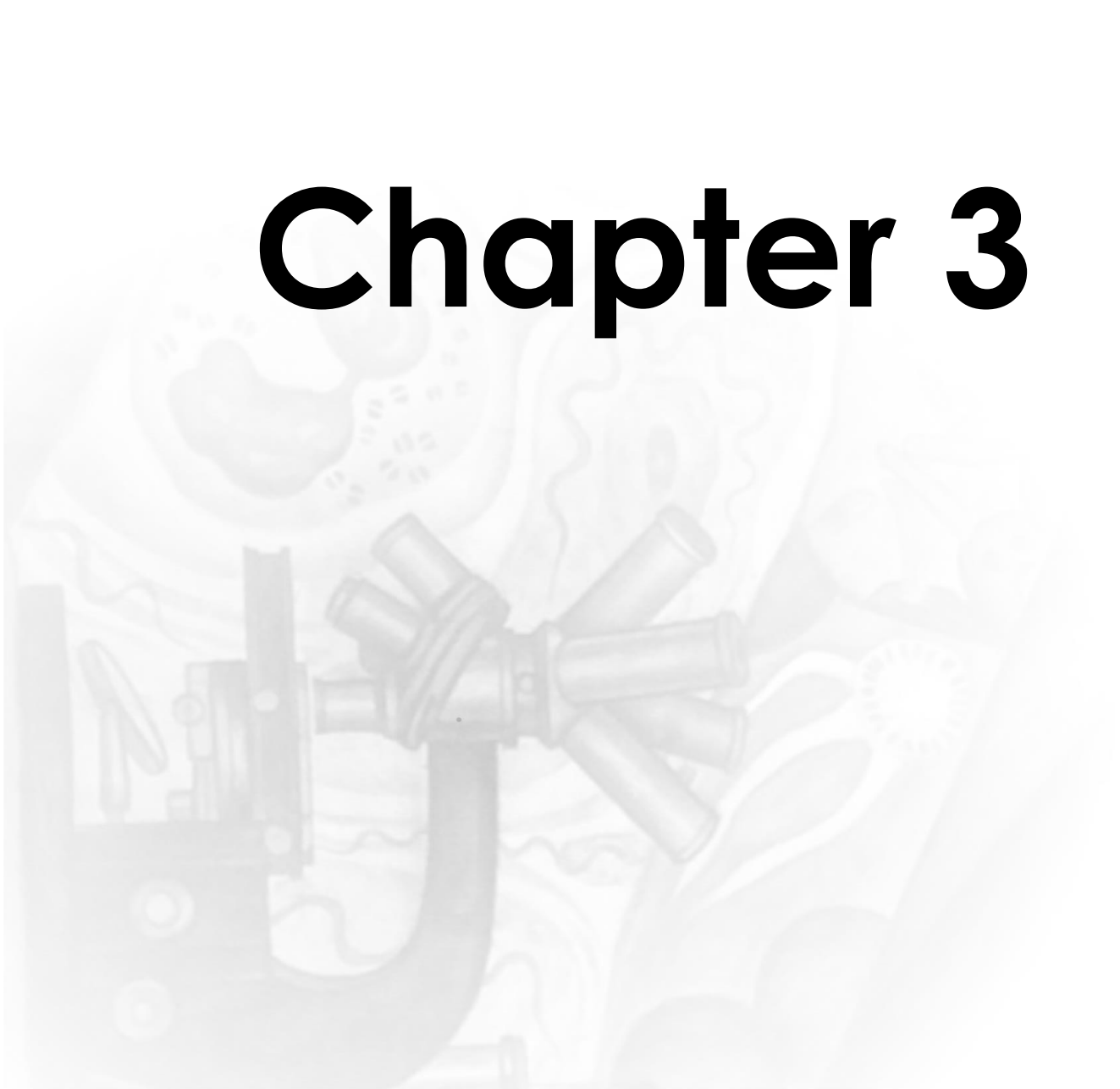

CHAPTER 3

Metabolic flexibility of *Syntrophobacter fumaroxidans*: Syntrophic vs sulfate-reducing lifestyle with propionate as growth substrate

Vicente T. Sedano-Núñez, Alfons J. M. Stams and Caroline M. Plugge

Abstract

Syntrophobacter fumaroxidans is a sulfate-reducing bacterium capable of oxidizing propionate in pure culture coupled to sulfate reduction and in syntrophy with methanogens in the absence of sulfate. The role of *S. fumaroxidans* as a syntroph has been studied, but its metabolic flexibility and adaptation to changing environmental conditions has never been assessed. We hypothesized that the syntrophic metabolism of *S. fumaroxidans* is more efficient than propionate oxidation coupled to sulfate reduction. Perturbations in sulfidogenic pure cultures of *S. fumaroxidans* and in methanogenic cocultures of the bacteria with *Methanospirillum hungatei* were performed. The addition of sulfate to syntrophic cocultures triggered a metabolic shift in *S. fumaroxidans*. Sulfate started to be reduced and the methane production decreased up to 40%. The addition of *M. hungatei* to the sulfidogenic axenic cultures of *S. fumaroxidans* did not lead to an adaptation of *S. fumaroxidans* to a syntrophic lifestyle. Complementary trials showed inhibition of the methanogenic partner at sulfide concentrations present at the moment of the perturbation (above 10 mM). This hampered the metabolic shift of *S. fumaroxidans* towards syntrophy. *Desulfovibrio desulfuricans* G11 was then used as an alternative syntrophic partner that could scavenge H_2 and/or formate from *S. fumaroxidans* while tolerating high levels of sulfide in the medium. Growth of *D. desulfuricans* in the coculture with *S. fumaroxidans* was verified with qPCR. Although growth of *D. desulfuricans* in the coculture was shown, it could not be clearly shown that *S. fumaroxidans* switched its metabolism from sulfidogenesis to syntrophy.

Keywords*:* Syntrophy, sulfate-reducing bacteria, propionate oxidation, metabolic flexibility, methanogens, sulfide inhibition.

Introduction

In anaerobic environments where the amount of inorganic electron acceptors such as nitrate, sulfate, sulfur or oxidized metal ions is low, syntrophic associations between acetogenic bacteria and methanogenic archaea become essential for the complete degradation of organic compounds to methane and CO_2 (Schink and Stams, 2013). In such conditions, degradation of propionate, butyrate and long chain fatty acids is only possible if the products acetate, hydrogen and formate are kept in low concentrations by methanogens (Schink, 1997; Sieber et al., 2012). If the situation changes and sulfate becomes available, sulfate-reducing bacteria (SRB) compete with the methanogens for hydrogen, formate and acetate, but also with entire syntrophic methanogenic communities for substrates like propionate and butyrate (Muyzer and Stams, 2008). While many SRB can grow without sulfate and are engaged in syntrophic associations with methanogens, others lack this ability (Worm et al., 2014). Moreover, some members of generally recognized sulfate-reducing taxonomic groups seem to have lost their ability to respire anaerobically with sulfate (de Bok et al., 2005; Imachi et al., 2006; Plugge et al., 2011).

The metabolic flexibility of SRB to form syntrophic associations despite their ability to reduce sulfate and oxidize fatty acids on their own, enhances their chances of survival when changes in the environment occur and affects the spatial distribution of microbial genera (Carbonero et al., 2014). In general terms, sulfate reduction is favoured over methanogenesis when sufficient sulfate is present (Lovley and Klug, 1983; Muyzer and Stams, 2008). Nevertheless, the growth rates of some SRB indicate a more efficient metabolism when degrading propionate in syntrophy than by reducing sulfate (van Kuijk and Stams, 1995; Wallrabenstein et al., 1995a; Wallrabenstein et al., 1995b; Harmsen et al., 1998). It is important to assess the metabolic flexibility of SRB in fluctuating environments in order to gain knowledge about the dynamics and resilience of microbial communities.

Syntrophobacter fumaroxidans is a propionate-degrading bacterium able to couple propionate oxidation to sulfate reduction. Degradation of propionate coupled to fumarate reduction is also possible (Harmsen et al., 1998). In the absence of inorganic electron acceptors, *S. fumaroxidans* requires an efficient removal of H_2- and formate from the environment, which is usually achieved by growing in syntrophy with H_2 or formate-consuming microorganisms. Although these syntrophic associations are generally described with methanogenic archaea, other H_2 or formate scavengers can function as syntrophic partners (Dong et al., 1994). Sulfidogenic growth of *S. fumaroxidans* has been less studied than its ability to grow syntrophically. Yet it is known that the growth rate of this bacterium with propionate coupled to sulfate reduction is much slower than when grown in syntrophy with methanogenic archaea (van Kuijk and Stams, 1995; Scholten and Conrad, 2000).

Desulfovibrio desulfuricans G11 is a microorganism able to couple the oxidation of lactate, ethanol, formate or H_2 to the reduction of sulfate to sulfide or of nitrate to ammonium (Sheik et al., 2017). In the absence of these electron acceptors, *D. desulfuricans* ferments lactate and alcohols and produces acetate, formate, H_2 and CO_2. Moreover, syntrophic growth on formate with a hydrogenotrophic methanogen has also been reported (Dolfing et al., 2008). However, *D. desulfuricans* is not able to catabolize butyrate, propionate or acetate.

The role of *S. fumaroxidans* as a syntroph has been widely studied and its importance in methanogenic environments documented (McMahon et al., 2001; McMahon et al., 2004; Stams et al., 2012). However, the metabolic flexibility to changes in the environment and the preferred lifestyle of this bacterium requires more investigation. By combining the capacities of *D. desulfuricans* as scavenger of H_2 and formate, and the alternative lifestyles of *S. fumaroxidans* to grow as a sulfate reducer or as a syntroph with methanogenic archaea, we studied the metabolic adaptability of *S. fumaroxidans* to changing environments provoked by different perturbations.

Materials and methods

Organisms and growth conditions

Syntrophobacter fumaroxidans MPOB^T (DSM 10017) was cultivated under anoxic conditions in basal medium as described previously (Stams et al., 1993). Axenic sulfidogenic cultures of *S. fumaroxidans* were grown with 20 mM sodium propionate and 20 mM sodium sulfate. Syntrophic cocultures of *S. fumaroxidans* with the methanogenic archaeon *Methanospirillum hungatei* strain JF1^T (DSM 864) were grown on 30 mM of sodium propionate. Axenic cultures of *M. hungatei* were grown with formate (40 mM) or with hydrogen in the headspace (1.7 atm H_2/CO_2 80:20 vol/vol) and supplemented with 1 mM sodium acetate. *Desulfovibrio desulfuricans* G11 (DSM 7057) was cultured with 40 mM of formate or hydrogen (1.7 atm H_2/CO_2 80:20 vol/vol) as electron donor, and 20 mM sodium sulfate as electron acceptor. Organisms were batch cultured in duplicate or triplicate at 37 °C in 250 ml flasks with 110 ml medium for methanogenic cocultures and 1-liter flasks with 550 ml medium for sulfidogenic cultures. Anaerobic conditions were provided by an 80:20 (vol/vol) gas mixture headspace of N_2/CO_2, or H_2/CO_2 when hydrogen was the electron donor (Plugge, 2005).

For the starvation tests, active cultures of *M. hungatei* growing on H_2/CO_2 or formate were used to inoculate bottles with anaerobic basal medium complemented with vitamins, N_2/CO_2 (80:20 vol/vol) in the gas phase and reducing solution, but without adding any electron donor or carbon source. These bottles were incubated at 37° C and after various periods of starvation the electron donor was added by changing the gas phase to H_2/CO_2 (80:20 vol/vol) or by adding formate (30 mM) to the bottles.

Substrate consumption and product formation were monitored. A similar approach was followed for the starvation test on *Desulfovibrio desulfuricans*, albeit sodium sulfate was added to the basal medium as electron acceptor.

Growth monitoring

Growth was monitored by measuring the optical density at 600 nm (OD600), as well as measuring propionate, sulfate, H_2 or formate consumption and product formation (methane, acetate, and sulfide). Organic acids were measured with a Thermo Scientific Spectrasystem high-performance liquid chromatograph (HPLC) equipped with a Varian Metacarb 67H 300 mm column kept at 45 °C and run with 0.005 mM sulfuric acid as eluent at a flow rate of 0.6 ml min^{-1}. Sulfate concentrations were quantified using a Dionex ICS-1000 ion chromatograph (Dionex) equipped with an IonPac AS22 column and 4.5 mM carbonate/1.4 mM bicarbonate eluent at a flow rate of 1.2 ml min^{-1}. Hydrogen and methane were determined with a CompactGC gas chromatograph (Global Analyser Solutions) with a Molsieve 5A PLOT of 0.53 mm. Hydrogen sulfide was measured by a colorimetric method (Cline, 1969).

Perturbation events

Various perturbation agents were applied to two different growth conditions of *S. fumaroxidans*. For the methanogenic cocultures of *S. fumaroxidans* and *M. hungatei* the perturbations were: the addition of sulfate to the medium (M+Sulf); the addition of sulfate and 20% inoculum of *Desulfovibrio desulfuricans* G11 (M+SulfG11); the addition of sulfate plus the inactivation of the methanogenic partner by adding 1 mM sodium 2-bromoethanesulfonate (BES) (M+SulfBES) and the supply of sulfate and 20% inoculum of active *D. desulfuricans* G11 coupled with the inactivation of the methanogen with BES (M+SulfBESG11). The sulfidogenic axenic cultures of *S. fumaroxidans* were perturbed in the following way: by adding 45% inoculum of active *M. hungatei* in the sulfidogenic culture (S+JF1) or by adding 45% inoculum of active *D. desulfuricans* G11 in the sulfidogenic culture (S+G11). When *M. hungatei* or *D. desulfuricans* G11 were used as perturbation agents, equal amounts of cells grown with H_2/CO_2 or formate were inoculated.

Quantitative PCR

A quantitative PCR (qPCR) analysis was performed in the treatments where *D. desulfuricans* G11 was introduced as part of the perturbations. Two sampling points were established to harvest cells and extract DNA from the biological replicates. The first sampling point took place right after the perturbation event and the second at the end of the experiment. DNA was extracted using the FastDNA® Spin Kit for Soil (MP Biomedicals, Santa Ana, CA) according to the manufacturer's protocol with two 45-second beat beating steps using a FastPrep Instrument (MP Biomedicals). DNA

concentrations were quantified with Qubit® 2.0 Fluorometer (Invitrogen, Carlsbad, CA). Amplifications were done in triplicates in a CFX384 Real-Time PCR Detection System (Bio-Rad Laboratories, Inc., Hercules, CA). The reaction mixture consisted of 5 µl iTaq Universal SYBR Green Supermix (Bio-Rad Laboratories, Inc., Hercules, CA), 0.2 µl reverse primer [50 µM], 0.2 µl forward primer [50 µM], and 2 µl of template DNA [10 ng/µl]. PCR grade water was used to fill up the reaction mixture to 10 µl. Specific 16S rRNA primers designed for *D. desulfuricans* were used DSVspG11 201*f* (5'-ACCTCTGCTTGCATGTTACC-3') and DSVspG11 471*r* (5'-CTGATTAGCACAGTGCGGTTT-3'). The qPCR amplification proceeded as follows: a pre-denaturing step 95 °C (5 min), 40 cycles of 95 °C (30 s), 62 °C (40 s), 72°C (40 s), 80°C (25 s) as optimized by (Junicke et al., 2014). PCR products were checked for specificity by a melting curve analysis (72-95°C) after each amplification step. Triplicate standard curves were obtained with 10-fold serial dilutions ranged from $1x10^8$ to $1x10^1$ copies per µl of 16S rDNA of *D. desulfuricans* G11. The efficiency of the reactions was 100% and the R^2 of the standard curves 0.996. Quantification of specific bacteria was expressed as increase in 16S rRNA gene copies.

Results and discussion

The results of all perturbations applied to methanogenic cocultures and sulfidogenic cultures of *S. fumaroxidans* are summarized in **Table 3.1**. Syntrophic methanogenic cocultures reduced sulfate when this compound was added to the growth medium. However, the adaptation of *S. fumaroxidans* in the methanogenic coculture to a sulfidogenic lifestyle varied along with other factors involved in the different perturbations (**Figure 3.1**). In our analysis, we have compartmentalized this adaptation in two stages, week one and week two after the perturbations took place. Thus, Table 3.1 shows substrate degradation and product formation, measured one and two weeks after the perturbations events.

For the first week after the perturbations, the highest propionate degradation was observed in treatment M+Sulf, where only sulfate was the perturbation agent added to the medium. Although the methanogenic syntrophic lifestyle of *S. fumaroxidans* in this treatment was still important as the levels of methane produced indicate, the amounts of sulfate reduced and sulfide formed seem to indicate that the bacteria channelled more of its reducing equivalents to the reduction sulfate. However, this is not the case as it will be discussed below.

A similar sulfate reduction as in M+Sulf can be noticed in treatment M+SulfBES, where the methanogenic partner was inhibited with BES and no methane was formed. Taking treatment M+SulfBES as a reference, we can extrapolate and infer that an approximate amount of ~9.2 mM of propionate was oxidized in treatment M+Sulf coupled to sulfate reduction, as this was the amount of propionate oxidized in treatment M+SulfBES, where propionate oxidation coupled to methane formation

was inhibited. During propionate degradation reducing equivalents are formed. The reduced forms of electron carriers, such as NADH or reduced ferredoxin need to be re-oxidized to keep propionate degradation going on. *S. fumaroxidans* can couple the re-oxidation of these carriers to proton or CO_2 reduction and form H_2 or formate, respectively, that need to be scavenged by a syntrophic partner; or it can also re-oxidize these equivalents on its own by reducing sulfate and produce sulfide. Theoretically the oxidation of 21 mM of propionate in M+Sulf generates 63 reducing equivalents, which can be used in the formation of 15.8 mM of sulfide and/or methane. Since approximately 7 mM of sulfate was reduced in M+Sulf, the methane formation should be of 8.8 mM, which requires 11.7 mM of propionate. Thus, of the 21 mM of propionate degraded in M+Sulf, approximately 9.2 mM was coupled to sulfate reduction and 11.7 mM to the production of hydrogen and/or formate. Therefore, syntrophy was still the predominant lifestyle of *S. fumaroxidans* despite the availability of sulfate in the medium.

The amount of propionate degraded in treatment M+Sulf shows a highly active *S. fumaroxidans* that efficiently made use of an additional inorganic electron acceptor added to the medium, in this case sulfate. However, it also kept transferring hydrogen and/or formate to the methanogenic partner.

The addition of *D. desulfuricans* as part of the perturbations in treatments M+SulfG11 and M+SulfBESG11 hindered sulfate reduction during the first week, as less sulfate was reduced in comparison to those treatments where G11 was not added. This hampering effect of G11 affects sulfate reduction, but not propionate oxidation. In treatment M+SulfG11, where the methanogen was not inhibited, a high propionate oxidation is observed, most probably by the syntrophic association of *S. fumaroxidans* with *M. hungatei* as the methane produced also indicates. On the other hand, it was not certain at this stage to deduce if sulfate in treatments M+SulfG11 and M+SulfBESG11 was reduced by *D. desulfuricans* or by *S. fumaroxidans*.

For the second week, the substrate consumption and methane production rates diverged from week one as a result of the adaptation of *S. fumaroxidans* to the new environmental conditions. The amount of propionate degraded was less in most of the treatments, with the exception of treatments with M+SulfBESG11. In some cases, the lower amount of propionate oxidized is due to the exhaustion of this substrate during the second week. For instance, in the control treatment and in M+Sulf most of the propionate available was degraded during the first week. Nonetheless, the drop in the methane formation in treatments M+Sulf and M+SulfG11 is remarkable.

Table 3.1. Substrate consumption and product formation by cultures and methanogenic cocultures of *Syntrophobacter fumaroxidans* after diverse perturbation events. Perturbations included addition of sulfate in combination with the inoculation of the methanogen *Methanospirillum hungatei* or the sulfate-reducing bacterium *Desulfovibrio desulfuricans* G11, as well as the inhibition of the methanogenic partner in the cocultures by adding BES.

	Substrates and products concentrations (mmol/l) [a]									
	1st week after perturbation					2nd week after perturbation				
Treatment[b]	Propionate degraded	Sulfate reduced	Acetate formed	CH_4 formed	Sulfide formed	Propionate degraded	Sulfate Reduced	Acetate formed	CH_4 formed	Sulfide formed
Methanogenic cocultures of *S. fumaroxidans* and *Methanospirillum hungatei*										
A) M+Sulf	21.1 ± 0.1	7.9 ± 1.3	16.5 ± 0.6	6.4 ± 0.2	6.8 ± 0.6	7.4 ± 0.8	6.1 ± 0.2	12.4 ± 0.4	0.7 ± 2.3	6.1 ± 0.2
B) M+SulfG11	15.3 ± 0.1	4.4 ± 0.8	8.1 ± 2.8	8.3 ± 3.1	4.1 ± 0.3	11.5 ± 0.2	7.8 ± 0.1	16.8 ± 2.5	0.5 ± 4	7.8 ± 0.1
C) M+SulfBES	9.2 ± 0	7 ± 0	4.2 ± 0	0.8 ± 0	5.6 ± 0.1	8.8 ± 0	6.5 ± 0	11.1 ± 0	-0.8 ± 0.7	6.5 ± 0.1
D) M+SulfBESG11	4.9 ± 1.7	3.6 ± 0.2	1 ±1.3	1.2 ± 0.5	3.6 ± 0.5	8.3 ± 0.1	7.4 ± 0.9	10.4 ± 3.1	-4.6 ± 5.4	7.4 ± 0.9
E) Control	19.9 ± 0.5	0	19 ± 1	16.1 ± 0.2	0 ± 0	10.5 ± 0.4	0	11.3 ± 1.4	8.3 ± 0.8	0 ± 0
Sulfidogenic cultures of *S. fumaroxidans*										
Treatment[c]	Propionate degraded	Sulfate reduced	Acetate formed	CH_4 formed	Sulfide formed	Propionate degraded	Sulfate Reduced	Acetate formed	CH_4 formed	Sulfide formed
F) S+JF1	6.4 ± 0.4	3.7 ± 0.2	5.6 ± 0.2	0.3 ± 01	4.1 ± 0.4	2.3 ± 0.3	3.4 ± 0.4	3.1 ± 0.2	0.1 ± 0	1.4 ± 0.7
G) S+N2JF1	8.9 ± 1	4.6 ± 0.6	9.5 ± 0.3	0.6 ± 0.1	9.0 ± 1.7	N.A.	N.A.	N.A.	N.A.	N.A.
H) S+G11	4.9 ± 0.1	3.3 ± 0.2	4.6 ± 0.3	0 ± 0	4.0 ± 0.6	2.2 ± 0.3	4.0 ± 0.1	2.9 ± 0.2	0 ± 0	-0.4 ± 0.5
I) S+N2G11	8.3	6.5	6.9	0 ± 0	7.6	5.8	5.9	6.2	0 ± 0	3.7

[a] Values are the average of the biological replicates.

[b] For treatments A, C and E 1st week and 2nd week sampling points correspond to 7 and 14 days after perturbations, while for treatments B and D are 5 and 12 days.

[c] 1st week and 2nd week sampling points correspond to 9 and 16 days after perturbation F), for G) and H) is 8 and 15 days and for I) 7 and 14 days after perturbation.

In these treatments, the methanogens might have been inhibited by the high levels of sulfide accumulated in the media after the first week of the perturbations (**Figure 3.1**). Thus, the syntrophic interaction of *M. hungatei* with *S. fumaroxidans* was hampered when the archaeon was not able to scavenge the H_2 and formate produced by the bacterium during propionate oxidation. This toxic effect of sulfide on the methanogen and the combinations with the inhibitory effect of treatments where BES was added allowed us to make some interesting speculations.

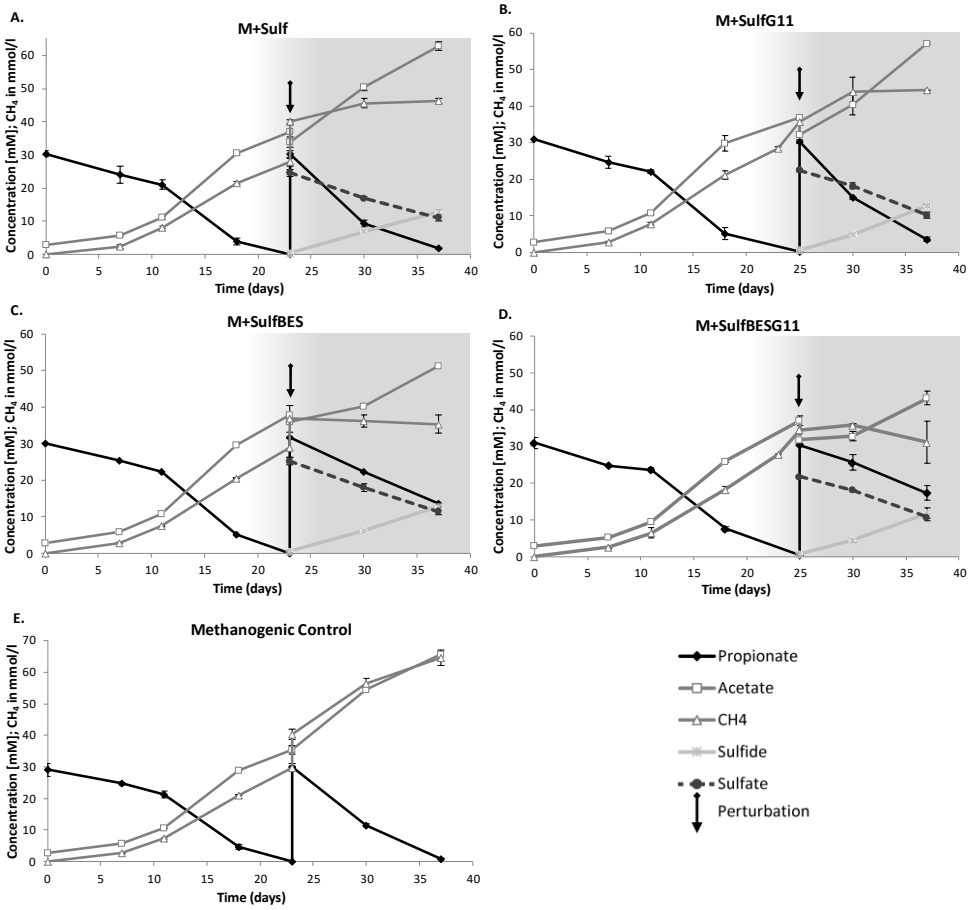

Figure 3.1. Methanogenic cocultures of *S. fumaroxidans* with *M. hungatei* exposed to different perturbation events. (A) Addition of sodium sulfate to the medium. (B) Addition of sulfate and inoculation of active *D. desulfuricans* G11. (C) Inhibition of the methanogenic partner by the addition of 2-bromoethanesulfonate (BES) (D) Inhibition of the methanogenic partner with BES and inoculation of active *D. desulfuricans* G11. (E) Control with a methanogenic coculture of *S. fumaroxidans* with *M. hungatei*.

During the first week M+Sulf and M+SulfBES reduced ~7 mM of sulfate. For the second week, all the treatments, except the control, in average reduced ~7mM of sulfate and the differences in these reductions and in the amounts of propionate oxidized were as follows: M+Sulf, reduced less sulfate of all because it exhausted all the propionate. M+SulfBES had enough propionate but the methanogen was inhibited, and therefore only *S. fumaroxidans* performed sulfidogenesis and consumed similar amounts of propionate and sulfate as in week one. In M+SulfBESG11 more sulfate was reduced than in M+SulfBES, but less propionate oxidation was noticed. These values do not fit the electron recovery calculations where 8.3 mM of propionate would result in a maximum reduction of 6.2 mM of sulfate. The presence of *D. desulfuricans* G11 might have an effect in the differences on sulfate reduction in contrast to when G11 is not present in the medium.

Finally, the highest amount of sulfate reduced and propionate degraded during week two were observed in treatment M+SulfG11. Although here we only observe the formation of traces of methane, we speculate that despite the inhibition of the methanogen by the high concentrations of sulfide in the medium, methane production endures as much as it is possible by the methanogen, while *Syntrophobacter* still couples propionate oxidation to the production of hydrogen and/or formate. Thus, although the methanogen cannot retrieve the hydrogen and formate produced by *Syntrophobacter*, *D. desulfuricans* G11 might take that role and so we observed a higher propionate oxidation and sulfate reduction than when *D. desulfuricans* G11 was not present.

The values presented in Table 3.1 do not always perfectly fit the stoichiometry. In some cases, it is possible that the accumulated methane leaked from the over-pressurized bottles. This is supported by the negative values of methane in treatments M+SulfBES and M+SulfBESG11 in week 2. A table with electron and carbon balance is presented as **Supplementary Material Table S3.1.**

The perturbation in the sulfidogenic cultures of *S. fumaroxidans* took place at the mid-exponential phase (**Figure 3.2**). At this point, sulfide levels were ~10 mM. Although toxicity of hydrogen sulfide is pH dependent and the toxic form (H_2S) is dominant at acidic pH levels (<6), inhibitory effects on anaerobic microorganisms, particularly non-sulfate reducers, are reported already above 3 mM at pH 7 (Lens et al., 1998; Paulo et al., 2015).

The absence of methane production in treatment S+JF1 after the addition of *M. hungatei* indicates that the expected metabolic shift of *S. fumaroxidans* towards a syntrophic lifestyle did not occur (**Figure 3.2.A**). The syntrophic interaction between the bacterium and the methanogen depends on the equilibrium maintained at the pool of metabolites exchanged among these microorganisms. It is not clear whether *S. fumaroxidans* did not provide the hydrogen and formate required by *M. hungatei*,

or the methanogen did not consume such compounds. Considering the high sulfide concentrations in the medium, it is probable that the methanogen was inhibited. To corroborate the inhibitory effect of hydrogen sulfide on *M. hungatei*, pure cultures of the methanogen growing in H_2/CO_2 or formate were tested at different sulfide concentrations (**Figure 3.3**).

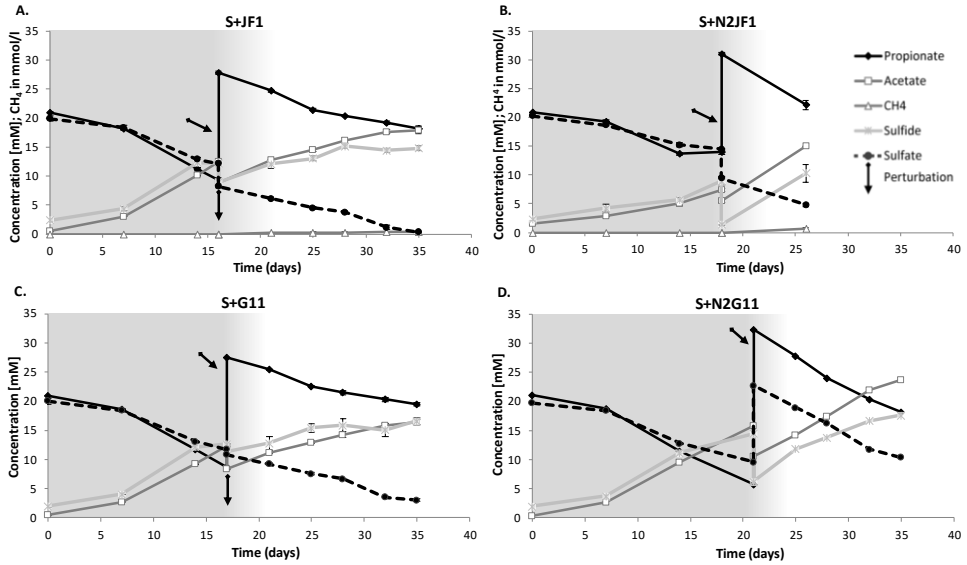

Figure 3.2. Response of sulfate-reducing cultures of *S. fumaroxidans* to the addition of hydrogen- and formate-scavenging microorganisms. (A) Inoculation of active *M. hungatei* at day 16. (B) Inoculation of active *M. hungatei* at day 18 after sulfide was flushed out with N_2. (C) Inoculation of active *D. desulfuricans* G11 at day 17 (D) Inoculation of active *D. desulfuricans* after sulfide was flushed out with N_2 at day 21.

Levels above 4 mM of sulfide had a significant impact on the methane formation and substrate consumption in cultures of *M. hungatei* growing with H_2/CO_2. Cultures growing on formate showed a slightly higher tolerance to sulfide (5 mM), although not high enough to strive at the levels (10 mM) present in the sulfidogenic environment of treatment S+JF1. We tried to decrease the sulfide levels of the sulfidogenic cultures prior the inoculation of the methanogen, by flushing the media in the bottles with N_2 and exchanging the gas phase with N_2/CO_2 on treatment S+N2JF1. Although the sulfide concentration dropped to 1.3 mM and the pH only rose to 7.2, the flushing approach proved ineffective and no methane was detected after the perturbation (**Figure 3.2.B**).

In addition to the sulfide inhibitory effect on the methanogen, the possibility of a delayed metabolic shift of the bacterium was also considered. The growth rate of *S. fumaroxidans* growing on propionate coupled to sulfate reduction is very low (0.024 day^{-1}) (van Kuijk and Stams, 1995) in comparison with syntrophic growth with

propionate (0.17 day^{-1}) (Harmsen et al., 1998). If the adaptation time required by *S. fumaroxidans* to switch its metabolism was longer than the survival time of the methanogen without an available electron donor, the syntrophic association would not take place.

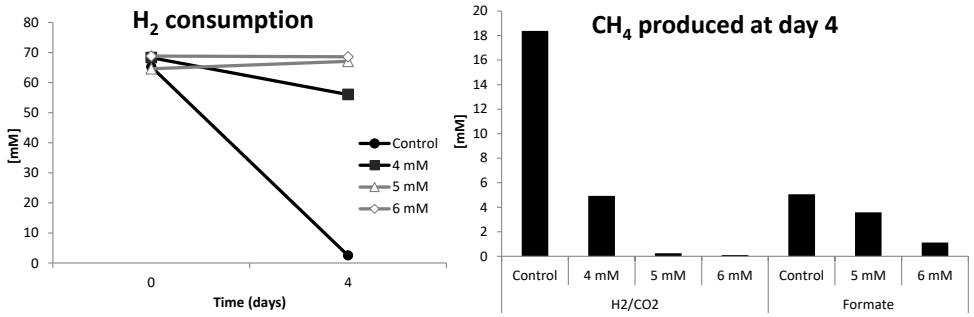

Figure 3.3. Inhibitory effect of sulfide on *Methanospirillum hungatei* strain JF1. Hydrogen consumption by *M. hungatei* cultures growing at different concentrations of sulfide (left). Methane production of *M. hungatei* cultures in H_2/CO_2 or formate under different sulfide concentrations.

To estimate the decay of the syntrophic partner, starvation tests were performed for *M. hungatei*. The archaeon showed to be able to survive for more than 20 days of starvation (**Figure 3.4**). The results showed that at 19 days of starvation (8 days for cultures growing on H_2/CO_2) the viability of the cultures was compromised as the delay in methane production shows in **Figure 3.4**. Nevertheless, we were able to measure methane production in cultures starved up to 39 days.

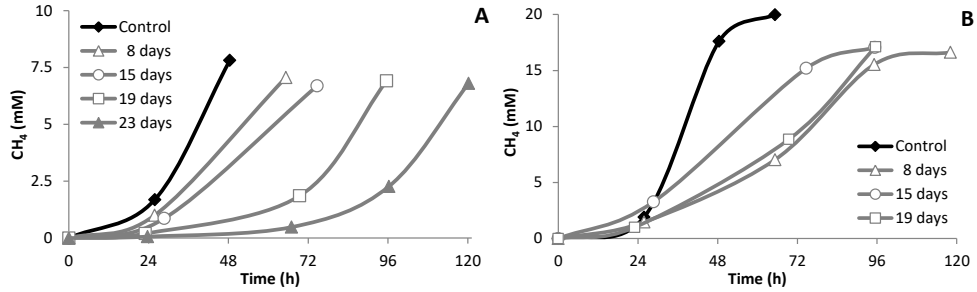

Figure 3.4. Methane production by starved cultures of *M. hungatei*. Starvation days refer to the length of incubation at 37° C without electron donor. Time on x-axis plots the hours after supply of the electron donor: formate [30 mM] in A and H_2/CO_2 in B.

Despite the resilience of the methanogenic partner and the high percentage of inoculum used in the perturbations of the sulfidogenic cultures, the methane detected was not significant and the low detected values (<1 mmol/l) were attributed to decay of the methanogens. A final approach was taken aiming to establish a sulfidogenic syntrophic coculture with *S. fumaroxidans*, which was the addition of

the sulfate reducer, *D. desulfuricans* G11. *D. desulfuricans* G11 has previously been used to obtain a sulfidogenic syntrophic coculture with *Syntrophobacter wolinii* for propionate degradation (Boone and Bryant, 1980).

Data of the substrate consumption and product formation after the perturbations of the sulfidogenic cultures are shown in **Table 3.1**. Despite the absence of methane, indicating that the syntrophic engagement with methanogens did not occur, higher propionate degradation in treatment S+JF1 can be noticed in contrast to S+G11. A possible explanation is that at the moment of the perturbations the sulfide levels were above 10 mM, but when *M. hungatei* was added to the media, the sulfide levels dropped by a dilution effect, whereas when *D. desulfuricans* G11 was added, the sulfide levels were maintained since *D. desulfuricans* G11 was also in a medium high in sulfide **(Figure 3.2)**.,

Sulfate-reducing bacteria generally are assumed to be able to deal with high concentrations of sulfide. However, sulfide inhibition in propionate degradation by *S. wolinii* has been previously reported by (Boone and Bryant, 1980). In that study sulfide concentrations of 5 and 10 mM inhibited propionate degradation by 23 and 51%, respectively. Our results suggest that *S. fumaroxidans* is similarly sensitive to high levels of sulfide. We observed that propionate degradation by *S. fumaroxidans* decreased in those treatments where sulfide levels were kept above 10 mM. The process of flushing out the hydrogen sulfide from the bottles in treatments S+N2JF1 and S+N2G11 favoured propionate degradation coupled to sulfate reduction during the first week after perturbations, in contrast to the lower amounts degraded in the second week where the sulfide levels were once again above 10 mM.

It was not possible to conclude only by analysing the substrates and products dynamics if *S. fumaroxidans* changed its metabolism to couple propionate oxidation to production of hydrogen and/or formate and if *D. desulfuricans* G11 was able to benefit from that change. Therefore, specific primers designed for the 16S rRNA gene of *D. desulfuricans* (Junicke et al., 2014) were used to determine the increase in copy numbers of this bacterium at the end of the experiment after its inoculation during the perturbation events.

The results in **Figure 3.3** show the increase over time in copy numbers per ml culture of the 16S rRNA gene of *D. desulfuricans* G11, which verifies the microscopic observations of growth of the bacterium (Data not shown). It should be noticed that the amount of inoculum used for the perturbation in sulfidogenic cultures was larger than the amount used in the methanogenic cocultures. These results reflect the approach taken in the sulfidogenic perturbations where a higher percentage (45%) of *D. desulfuricans* G11 was added as inoculum during the perturbation.

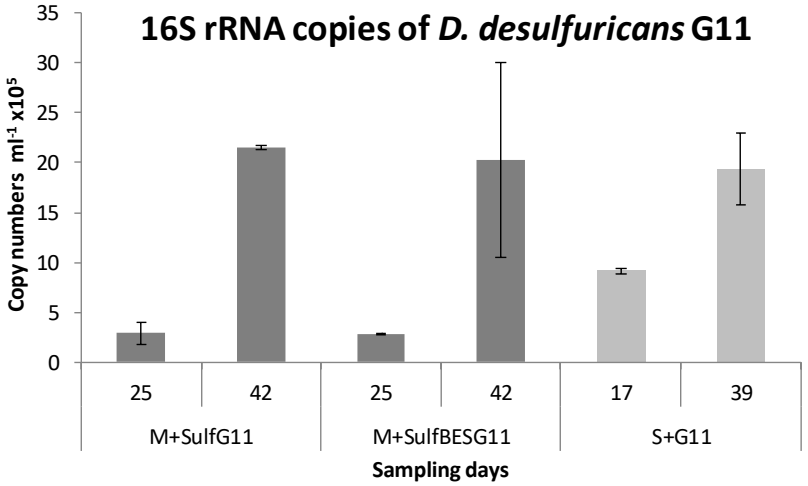

Figure 3.3. 16S rRNA gene abundance of *D. desulfuricans* G11 at the moment of the perturbations and at the end of the experiments. The dark bars show 16S rRNA copy numbers of *D. desulfuricans* G11 in cocultures of *S. fumaroxidans* and *M. hungatei* without (M+SulfG11) and with (M+SulfBESG11) addition of bromoethane sulfonate (BES). Light bars show 16S rRNA copy numbers of *D. desulfuricans* G11 in a sulfidogenic culture of *S. fumaroxidans* at a higher proportion than for the cocultures perturbation.

There is a higher increase in copy numbers of *D. desulfuricans* G11 in the methanogenic cocultures compared to the sulfidogenic culture where G11 barely duplicated its numbers. Propionate oxidation coupled to hydrogen or formate production is endergonic under standard conditions (Equations 1a & 1b **Table 3.2**). To make this conversion energetically feasible, the hydrogen and formate concentrations have to be kept in a very low range (Schink, 1997). In the highly active syntrophic methanogenic cocultures, *S. fumaroxidans* produced formate and hydrogen at high rates while the methanogen kept the levels of those compounds low. Sulfate reducers have a higher affinity for hydrogen than methanogens (Kristjansson et al., 1982; Lovley, 1985). Therefore, once added to the active cocultures, *D. desulfuricans* G11 has competed with the methanogen for hydrogen and formate, which was reflected in the increase in the 16S rRNA gene copy numbers. A similar situation occurred in the isolation of *S. wolinii*, where the authors failed to obtain cocultures of *S. wolinii* with *M. hungatei* and *D. desulfuricans* G11 remained present (Boone and Bryant, 1980). Besides the ability of the sulfate reducer to outcompete the methanogens as a syntrophic partner, the increasing levels of sulfide in M+SulfG11 and the BES added on M+SulfBESG11 also might have contributed to the good proliferation of *D. desulfuricans* G11. Furthermore, syntrophic propionate degradation coupled to sulfidogenesis theoretically yields more energy than when coupled to methane production as can be seen in Equation 1a and 1b of **Table 3.3**.

In the sulfidogenic cultures, *D. desulfuricans* G11 scarcely doubled its numbers after inoculation as part of the perturbation (**Figure 3.3**). Nonetheless, it is interesting that *D. desulfuricans* G11 was able to thrive in this environment. The metabolic activity of *S. fumaroxidans* in sulfidogenic propionate oxidation is very low. Subsequently, a metabolic change, if any, in response to a change in the environment was also expected to be slow. Moreover, as Equation 1a in **Table 3.3** show, such metabolic change is not energetically necessary for *S. fumaroxidans* since propionate oxidation coupled to sulfate reduction yields enough energy for growth without a partner. From Equation 2a and 3a we can deduce that for *D. desulfuricans* G11 it would be beneficial to use the hydrogen and formate produced by *S. fumaroxidans*, but it is intriguing why the latter bacterium would engage in a syntrophic metabolism while having sufficient sulfate to grow independently. Syntrophic degradation of propionate occurs at the limit of what is thermodynamically possible and requires at least one step with reversed electron transport (Worm et al., 2014). To change from sulfidogenic to syntrophic lifestyle a large metabolic shift would be needed in *Syntrophobacter*: hydrogenases, formate dehydrogenases and several confurcating complexes need to be switched on. This may be a long process. But when *D. desulfuricans* G11 is added to an already syntrophic lifestyle it can more easily take over, without much change in the metabolism.

It is still a possibility that the high affinity of *D. desulfuricans* G11 for hydrogen allows this microorganism to scavenge the intermediate hydrogen produced during sulfate reduction by *S. fumaroxidans*. In this case, it would be a parasitic association instead of a syntrophic one. If *S. fumaroxidans* however is genetically driven for syntrophy, a sulfidogenic syntrophic association would be as energetically favourable as a methanogenic one. A genetic predisposition of *S. fumaroxidans* for syntrophy would explain the high proliferation of the alternative hydrogen- and formate-scavenger after perturbations in treatment M+SulfG11 and M+SulfBESG11, as well as the growth of the *Desulfovibrio* in S+G11.

Table 3.3. Gibbs free energy changes of reactions involved in propionate, formate and hydrogen oxidation coupled to reduction of sulfate and methane production.

Equation		Reactions	$\Delta G^{o\prime}$ (kJ/reaction)*
1a	$4CH_3CH_2COO^- + 3SO_4^{2-}$	$\rightarrow 4CH_3COO^- + 4HCO_3^- + H^+ + 3HS^-$	-151.3 kJ
1b	$4CH_3CH_2COO^- + 3H_2O$	$\rightarrow 4CH_3COO^- + HCO_3^- + H^+ + 3CH_4$	-102.4 kJ
2a	$4H_2 + SO_4^{2-} + H^+$	$\rightarrow HS^- + 4H_2O$	-151.9 kJ
2b	$4H_2 + HCO_3^- + H^+$	$\rightarrow CH_4 + 3H_2O$	-135.6 kJ
3a	$4HCOO^- + H^+ + H_2O$	$\rightarrow CH_4 + 3HCO_3^-$	-130.1 kJ
3b	$4HCOO^- + SO_4^{2-} + H^+$	$\rightarrow HS^- + 4HCO_3^-$	-146.7 kJ

* 1 M, pH 7.0, T = 298 K and a partial pressure of gas of 10^5 Pa

Conclusions

The addition of sulfate to syntrophic methanogenic cocultures of *S. fumaroxidans* and *M. hungatei* results in a metabolic shift in *S. fumaroxidans* where sulfidogenesis eventually takes over methanogenesis. Although the metabolic shift to sulfidogenesis was observed soon after the addition of sulfate to the media, methanogenic associations remained dominant until the methanogenic partner was affected and inhibited by sulfide. The metabolic shift of *S. fumaroxidans* to sulfidogenesis was not favoured by the inhibition of the methanogen as the treatments with BES indicate.

The methanogenic cocultures ultimately stopped producing methane due to sulfide toxicity to the methanogen. But it is probable that the syntrophic metabolism of *S. fumaroxidans,* where propionate oxidation is coupled to hydrogen and/or formate production, persisted as the increase of the numbers of *D. desulfuricans* G11 suggests.

The low growth rate of *S. fumaroxidans* in sulfidogenic environments might be attributed to sulfide sensitivity. In environments with sulfide levels above 10 mM, propionate degradation considerably drops in comparison to lower sulfide levels. Thus, the inefficiency of *S. fumaroxidans* to degrade propionate in the presence of sulfate could be related to the sulfide toxicity effect on the bacterium.

Although the thriving of *D. desulfuricans* G11 in coculture with *S. fumaroxidans* in sulfidogenic environments has been verified by qPCR, to know whether *S. fumaroxidans* switched its metabolism from sulfidogenesis to syntrophy still requires further research.

Supplementary material

Table S1.1. Electron and carbon balances of the syntrophic cocultures and sulfidogenic cultures of *Syntrophobacter fumaroxidans* after diverse perturbation events.

Treatments indicating perturbations applied to the cultures	Syntrophic cocultures of *S. fumaroxidans* and *Methanospirillum hungatei*							
	Week 1				Week 2			
	Electron recovery		Carbon balance		Electron recovery		Carbon balance	
	Theoretical	Achieved	Theoretical	Achieved	Theoretical	Achieved	Theoretical	Achieved
M+Sulf	15.8	14.3	36.8	22.9	5.5	6.8	12.9	13.1
	ER %	**90.5**	**CR%**	**62**	**ER %**	**123**	**CR%**	**101.4**
M+SulfG11	11.4	12.4	26.7	16.4	8.6	8.3	20.1	17.3
	ER %	108.2	**CR%**	**61.3**	**ER %**	**96.5**	**CR%**	**86.3**
M+SulfBES	6.9	6.5	16.2	5.0	6.6	6.5	15.5	11.1
	ER %	**93.2**	**CR%**	**31**	**ER %**	**98.4**	**CR%**	**71.6**
M+SulfBESG11	3.7	4.8	8.5	2.1	6.2	7.4	14.5	10.4
	ER %	**131.8**	**CR%**	**25.1**	**ER %**	**119.4**	**CR%**	**71.9**
Control	14.9	16.1	34.8	35.0	7.9	8.3	18.4	19.5
	ER %	107.8	**CR%**	**100.8**	**ER %**	104.8	**CR%**	106.3
Sulfidogenic cultures of *S. fumaroxidans*								
S+JF1	4.81	4.0	11.22	5.91	1.69	1.4	3.94	3.17
	ER %	**83.2**	**CR%**	**52.6**	**ER %**	**82.9**	**CR%**	**80.4**
S+N2JF1	6.67	5.3	15.57	10.18	N.A.	N.A.	N.A.	N.A.
	ER %	**78.9**	**CR%**	**65.4**	N.A.	N.A.	N.A.	N.A.
S+G11	3.71	3.3	8.66	4.57	1.66	4.0	3.88	2.85
	ER %	**88.3**	**CR%**	**52.8**	**ER %**	**243.2**	**CR%**	**73.5**
S+N2G11	6.26	6.5	14.61	6.91	4.35	3.7	10.16	6.24
	ER %	103.3	**CR%**	**47.3**	**ER %**	**85.9**	**CR%**	**61.5**

ER: Electron recovery; CR: Carbon recovery

Mankind has a lot to learn from syntrophy

Chapter 4

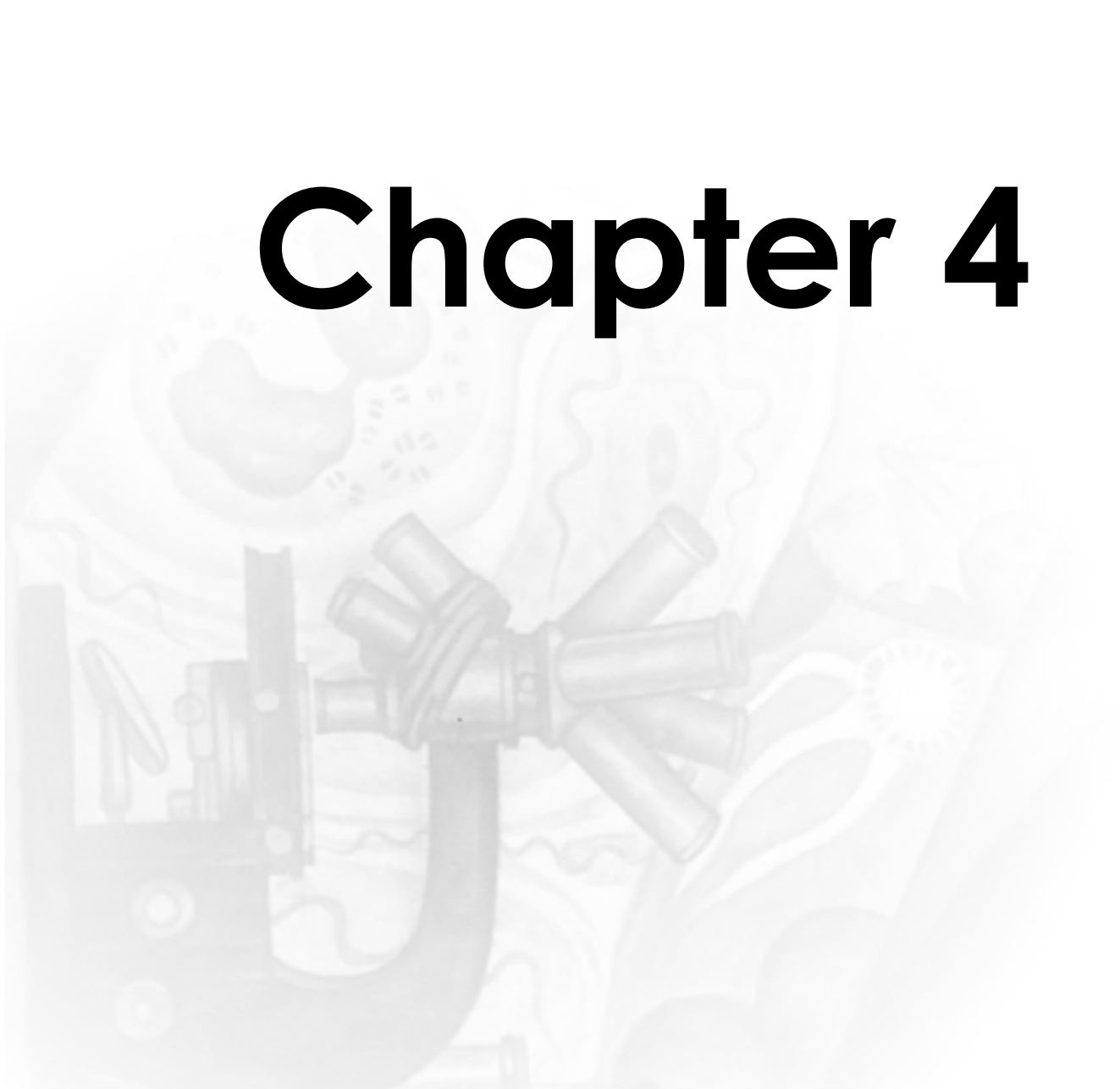

CHAPTER 4

Comparative proteome analysis of propionate degradation by *Syntrophobacter fumaroxidans* in pure culture and in coculture with methanogens

Vicente T. Sedano-Núñez[1], Sjef Boeren[2], Alfons J. M. Stams[1] and Caroline M. Plugge[1]

[1]Laboratory of Microbiology, Wageningen University and Research, The Netherlands

[2]Laboratory of Biochemistry, Wageningen University and Research, The Netherlands

Accepted for publication in Environmental Microbiology

Abstract

Syntrophobacter fumaroxidans is a sulfate-reducing propionate-degrading bacterium that grows in syntrophic interaction with methanogens, but a syntrophic interaction with sulfate-reducing bacteria is also possible. We performed a proteome analysis of *S. fumaroxidans* growing with propionate axenically with sulfate or fumarate, and in syntrophy with *Methanospirillum hungatei*, *Methanobacterium formicicum* or *Desulfovibrio desulfuricans*. Special attention was put on the role of hydrogen and formate in interspecies electron transfer (IET) and energy conservation. Formate dehydrogenase Fdh1 and hydrogenase Hox were the main confurcating enzymes used for energy conservation. In the periplasm, Fdh2 and hydrogenase Hyn play an important role in reverse electron transport associated with succinate oxidation. Periplasmic Fdh3, Fdh4 and Fdh5 were involved in IET. The sulfate reduction pathway was poorly regulated and many enzymes associated with sulfate reduction (Sat, HppA, AprAB, DsrAB and DsrC) were abundant even at conditions where sulfate was not present. Heterodisulfide reductases (Hdr), coupled with flavin oxidoreductase (Flox) or a putative hydrogenase (Mvh-p), were abundant. Hdr/Flox was detected in all conditions while Hdr/Mvh-p was exclusively detected when sulfate was available; these complexes most likely confurcate electrons. Our results suggest that *S. fumaroxidans* mainly used formate for electron release and that different confurcating mechanisms were used in its sulfidogenic metabolism.

Keywords: Syntrophy, sulfate-reducing bacteria, propionate oxidation, interspecies electron transfer, reverse electron transport, hydrogenases, formate dehydrogenases.

Introduction

Syntrophobacter fumaroxidans is a sulfate-reducing deltaproteobacterium able to grow on propionate in syntrophy with methanogens (Harmsen et al., 1998). It can also grow axenically by fermenting fumarate (Stams et al., 1993). To degrade propionate, it requires fumarate or sulfate as electron acceptors, or a H_2- and formate-consuming partner in the absence of an electron acceptor. *S. fumaroxidans* uses the methylmalonyl-CoA (MMC) pathway to degrade propionate to acetate and CO_2 (Plugge et al., 1993). Under standard conditions, propionate oxidation to H_2, formate and acetate is an endergonic process. Reducing equivalents at the redox levels of Fd_{red}, NADH and $FADH_2$, are released in the pyruvate, malate and succinate oxidation steps of the pathway, respectively. To keep the pathway functioning, the reduced electron mediators need to be re-oxidized by reducing protons to H_2 or CO_2 to formate. Consequently, the role of the hydrogen/formate scavenger in the syntrophic association with *S. fumaroxidans* is to maintain H_2 and formate at sufficiently low levels so that propionate degradation becomes energetically feasible (Stams and Dong, 1995). The minimal hydrogen partial pressure (pH_2) that methanogens can maintain is between 1 to 10 Pa (Thauer et al., 2008). This level is not low enough to overcome the most energy-consuming step in the MMC pathway, the oxidation of succinate to fumarate. To couple this step to proton or CO_2 reduction would require a pH_2 of 10^{-10} Pa and a formate concentration below 1 µM (Schink, 1997). Therefore, to drive this reaction, the input of metabolic energy is required. An investment of two-thirds of an ATP via a mechanism known as reverse electron transport (RET) has been suggested by some authors (van Kuijk et al., 1998b; Schink and Stams, 2013).

During RET energy is invested in the form of ATP to generate a proton gradient across the membrane which allows succinate oxidation to proceed (Stams and Plugge, 2009). Membrane-associated proteins, such as ferredoxin:NAD^+ oxidoreductases, cytochromes and periplasmic formate dehydrogenases and hydrogenases, have been reported to be involved in RET (Sieber et al., 2012; Grein et al., 2013). Moreover, novel energy conversion mechanisms have been discovered in anaerobic microorganisms, for instance flavin-based electron bifurcation and its reversal, electron confurcation (Li et al., 2008; Buckel and Thauer, 2013; Schink, 2015). Genome analyses of *S. fumaroxidans* revealed membrane associated proteins, such as a fumarate reductase and a Rnf complex, as well as confurcating hydrogenases and formate dehydrogenases possibly involved in energy conservation mechanisms (Müller et al., 2010; Pereira et al., 2011; Plugge et al., 2012; Worm et al., 2014). Subsequently, transcriptomics studies with *S. fumaroxidans* in syntrophic and axenic cultures showed that a periplasmic formate dehydrogenase (Fdh2) and a hydrogenase (Hyn) play an important role to make the endergonic oxidation of succinate possible (Worm et al., 2011b).

Moreover, it was found that confurcating hydrogenases and confurcating formate dehydrogenases (Hyd1, Hox and Fdh1) are important energy converting enzymes required for propionate degradation (Worm et al., 2011a; Worm et al., 2011b).

In this study, a comparative proteomic analysis of *S. fumaroxidans* was made. Cells grown with propionate coupled to fumarate or sulfate reduction, or in syntrophic associations with *Methanospirillum hungatei* or *Methanobacterium formicicum* were compared. We aim to elucidate the main metabolic differences in lifestyles by identifying the key proteins used by *S. fumaroxidans* in interspecies electron transfer (IET), reverse electron transport (RET), electron confurcating processes and other energy conservation pathways.

In addition to the known syntrophic interactions of *S. fumaroxidans* with methanogens, our study was extended by including the proteomic profiling of *S. fumaroxidans* in coculture with a non-methanogenic partner. *Desulfovibrio desulfuricans* has been studied before in cocultures with *Syntrophobacter wolinii* and *S. fumaroxidans* as a hydrogen- or formate-scavenger in the oxidation of propionate (Boone and Bryant, 1980; Dong et al., 1994; Sheik et al., 2017). However, the nature of the symbiotic interactions of such cocultures was not properly defined. *S. wolinii* and *S. fumaroxidans* are both able to couple propionate oxidation to sulfate reduction instead of proton reduction (Wallrabenstein et al., 1994; van Kuijk and Stams, 1995).

D. desulfuricans is a sulfate reducer that utilizes lactate, ethanol, hydrogen and formate in the presence of sulfate, but not acetate, propionate, butyrate or glucose (McInerney et al., 1979; Sheik et al., 2017). Therefore, a syntrophic relationship with *S. fumaroxidans*, in which hydrogen and formate are produced, would be beneficial for *D. desulfuricans*. Nonetheless, it is intriguing why *Syntrophobacter* would engage in a syntrophic association while having sufficient sulfate to grow independently. By comparing the proteomic profile of *S. fumaroxidans* grown in coculture with *D. desulfuricans* with the proteomic profiles of the other known syntrophic lifestyles, and the sulfidogenic condition, we expect to be able to define the symbiotic relationship of *S. fumaroxidans* with *D. desulfuricans*.

Furthermore, in a syntrophic coculture with *Methanobrevibacter arboriphilus* AZ, *D. desulfuricans* oxidized formate and provided hydrogen to the methanogenic partner (Dolfing et al., 2008). The proteomic analysis of *D. desulfuricans* growing with hydrogen, formate and in coculture with *S. fumaroxidans* will reveal further insight into sulfate-reducing syntrophic cocultures.

Materials and methods

Organisms and growth conditions

Syntrophobacter fumaroxidans was grown in pure culture and in cocultures. *Syntrophobacter fumaroxidans* MPOB^T (DSM 10017) was cultivated under anoxic conditions in basal medium as described previously (Stams et al., 1993). The medium for the pure cultures was supplemented with 20 mM propionate and 60 mM fumarate. Sulfidogenic cultures were grown on 20 mM propionate and 20 mM sulfate. Cocultures of *S. fumaroxidans* with *Methanospirillum hungatei* strain JF1^T (DSM 864) or *Methanobacterium formicicum* MF^T (DSM 1535) were grown with 30 mM of propionate without electron acceptor. A coculture of *S. fumaroxidans* with *Desulfovibrio desulfuricans* G11 (DSM 7057; (Sheik et al., 2017)) was grown with 20 mM propionate and 20 mM sulfate. Axenic cultures of *D. desulfuricans* were grown with 20 mM sulfate and 40 mM formate or hydrogen (1.7 atm H_2/CO_2 80:20 vol/vol). All organisms were batch cultured in triplicate at 37 °C in 1 litre flasks with 550 ml medium under anaerobic conditions provided by a pressurised (172 kPa; 1.7 atm) gas phase of N_2/CO_2 (80:20, vol/vol). Growth was monitored by measuring substrate consumption and product formation (propionate, sulfate, methane, acetate, succinate, malate and/or sulfide). Cells were harvested during mid-exponential growth phase. The cultures for the experiment were inoculated with cells from cultures that adapted to these conditions by transferring them at least five times in media with the respective substrates before the start of the experiment.

Harvesting cells and Percoll gradient centrifugation

Cells were aerobically harvested by centrifugation at 16,000 g for 16 minutes at 4 °C. The pellet was washed twice with TE buffer (10 mM Tris-HCl, pH 7.5; 1 mM EDTA). Only cells from the syntrophic coculture of *S. fumaroxidans* and *M. hungatei* were separated by Percoll gradient centrifugation (Percoll®, Sigma-Aldrich, Missouri, US) as described elsewhere (de Bok et al., 2002a). The separated layers, containing *Syntrophobacter* cells in the upper layer and *Methanospirillum* cells in the lower layer, were collected and subjected to Percoll gradient separation a second time. Cells were then washed twice with 10 mM sodium phosphate buffer (pH 7.5).

Protein extraction and SDS-PAGE

Cells were resuspended in lysis buffer (100 mM Tris-HCl, pH 7.5; 4% w/v SDS; 50 mM dithiothreitol and SIGMAFAST™ Protease Inhibitor Cocktail Tablet (Sigma-Aldrich, Missouri, US)), and passed three times through a French press (French® Type Pressure Cell Disrupter, Stansted Fluid Power, Harlow, UK) at 2 MPa (40K cell). Cell debris and undisrupted cells were removed by centrifugation at 18,000 g for 10 min at 4 °C. The supernatant was collected in Eppendorf™ LoBind Protein Microcentrifuge Tubes and stored at -80 °C. Still in the lysis buffer, proteins were denatured by heating at 95 °C for 5 minutes. Samples were loaded on a 10%

polyacrylamide separation gel (Precise™ Tris-HEPES Gels, Thermo Scientific, Rockford, US) using the Mini-PROTEAN Tetra Cell (Bio-Rad Laboratories B.V, Veenendaal, The Netherlands). The electrophoresis procedure was according to the precast gels manufacturer's instructions. Gels were stained using Coomassie Brilliant Blue (CBB) R-250. Protein concentration was normalized among triplicates and samples in a qualitative way by analysing the gel pictures taken with G:BOX Chemi XT4 (Syngene, Cambridge, UK) and using the software GeneSys version 1.5.5.0 (GeneTools version 4.03.01).

In-gel trypsin digestion

In-gel digestion of proteins and purification of peptides was done following a modified version of a previously described protocol (Rupakula et al., 2013). Disulfide bridges in proteins were reduced by covering the gels with reducing solution (10 mM dithiothreitol, pH 7.6, in 50 mM NH_4HCO_3), and the gels were incubated at 60 °C for 1 h. Alkylation was performed in darkness and shaking (100 rpm) for 1 h by adding 25 ml of iodoacetamide solution (10 mM iodoacetamide in 100 mM Tris-HCl, pH 8.0). Gels were thoroughly rinsed with demineralized water in between steps. Each gel lane was cut into 3 slices, and the slices were cut into approximately 1 mm^3 cubes and transferred to a separate 0.5 ml protein LoBind tube (Eppendorf, Hamburg, Germany). Enzymatic digestion was done with trypsin sequencing grade (Roche, Mannheim, Germany). 100 µl of trypsin solution (5 ng/ µl trypsin in 50 mM NH_4HCO_3) were added to each tube, and incubated 2 hours at 45 °C with gentle shaking. To stop trypsin digestion, trifluoroacetic acid (10 %) was added to the supernatant to lower the pH below 5. The digested protein mixture was purified and concentrated using an in-house made SPE pipette tip (Lu et al., 2011).To recover hydrophobic peptides, 50 µl acetonitrile (vol/vol in 0.1% formic acid) was passed through the column. Finally, the volume was reduced to 20 µl using a SpeedVac concentrator and then adjusted to 50 µl with 0.1% formic acid. Samples were analysed using nLC–MS/MS with a Proxeon EASY nLC and a LTQ-Orbitrap XL mass spectrometer as previously described (Lu et al., 2011).

LC–MS data analysis

The obtained MS/MS spectra were processed with MaxQuant v. 1.5.2.8. Database with the protein sequences of *S. fumaroxidans* was downloaded from UniProt (www.uniprot.org). The protein database of *D. desulfuricans* G11 was the draft genome available in our laboratory. An additional dataset with protein sequences of common contaminants (trypsin, human keratins and bovine serum albumin) was included. False discovery rates (FDR) of less than 1% were set at peptide and protein levels. Modifications for acetylation (Protein N-term), deamidation (N, Q) and oxidation (M) were allowed to be used for protein identification and quantification. All other quantification settings were kept default. Filtering and further bioinformatics and statistical analysis were performed with Perseus v.1.5.3.0. Proteins included in our analysis contain at least two identified peptides of which at

least one is unique and at least one unmodified. Reversed hits and contaminants were filtered out. Protein groups were filtered to require three valid values in at least one experimental group. Label-free quantification (LFQ) intensities (values normalized with respect to the total amount of protein and all of its identified peptides) were used to analyse the abundance of proteins in the fractions and further statistical comparisons among conditions. LFQ intensities were transformed to logarithmic values base 10. Missing values were imputed with random numbers from a normal distribution, the mean and standard deviation of which were chosen to best simulate low abundance values close to noise level (Width: 0.3 and downshift 1.8 times). A multiple-sample test (ANOVA) with permutation based FDR statistics (250 permutations, FDR=0.01 and S0=1) was applied to filter significant proteins. Principal component analyses (PCA) were performed with default settings and without category enrichment in components. Z-score normalization in which the mean of each row (where each row is a protein in triplicate and in different conditions) is subtracted from each value and the result divided by the standard deviation of the row was applied before clustering. Hierarchical clustering of rows, using Euclidean distances, produced a heat map representation of the clustered data matrix. Row clusters were automatically defined (100) and exported to a new matrix. Imputed values were then replaced back to missing values and previously defined clusters were displayed in a new heat map. For *D. desulfuricans* the Z-score and hierarchical clustering was done for columns instead of rows in order to compare the most abundant proteins detected in each condition.

Results

Proteomic overview of S. fumaroxidans and most abundant proteins in all growth conditions

The genome of *S. fumaroxidans* contains 4,098 protein coding genes (Plugge et al., 2012). Our proteomic analysis accurately identified a total of 813 proteins in the five studied conditions. Of these, 84 were designated as proteins with unknown function. 514 proteins were detected in all the studied conditions. This core proteome represented slightly more than 60% of all the detected proteins (**Supporting information, Fig. S4.1.A**). Principal component analysis (PCA) revealed that the protein abundance patterns were reproducible among triplicates of a given growth condition (**Supporting information, Fig. S4.1.B**). Moreover, it shows that protein patterns of *S. fumaroxidans* differ depending on the electron acceptor or syntrophic partner used, clearly separating syntrophic methanogenic conditions from the axenic proteomic profiles. Statistical analysis indicated that 509 proteins significantly differed in at least one condition. This means that 304 proteins were constitutively produced in the five analysed conditions.

Total intensity-based absolute quantification (iBAQ) revealed the most abundant proteins produced in the whole analysis. Most of these proteins were involved in the methylmalonyl-CoA pathway, sulfate reduction, electron transfer or energy conservation. Highly abundant proteins under all five conditions included chaperonins (GroEL & GroES), heat shock proteins and ribosomal proteins. Other abundant proteins had annotated functions involved in protection, signalling, transcription and ferrous ion transport. Rubrerythrins and proteins involved in the biosynthesis of cofactors like iron-molybdenum and molybdopterin were also abundant.

Enzymes of the methylmalonyl CoA pathway

Previous genomic analyses of *S. fumaroxidans* predicted several genes coding for proteins involved in the MMC pathway (Müller et al., 2010; Plugge et al., 2012). Most of these proteins were abundant in our whole-cell proteome analysis. For those predicted proteins that were not detected, paralogous proteins were found in high levels, which suggests that these proteins have a role in the MMC pathway. For instance, the predicted enzymes for propionate activation (Sfum_3926 to Sfum_3934) and for the conversion of acetyl-CoA to acetate (Sfum_0388-0389, Sfum_0745-0746, Sfum_1278 and Sfum_3070) were not detected in the present study. Nevertheless, three sets of proteins were detected for the five conditions: CoA-A (Sfum_0809-0810), CoA-B (Sfum_0811-0812) and CoA-S (Sfum_1132-1134) **(Figure 4.1)**. The amino acid sequences of these proteins indicate a relationship to coenzyme A transferase family I (InterPro IPR004165) and could therefore be involved in propionate activation and/or acetate formation.

As predicted by previous genome studies (Müller et al., 2010; Plugge et al., 2012), the main protein complex responsible for the oxidation of succinate to fumarate was the membrane bound succinate dehydrogenase SdhABC (Sfum_1998-2000), which was abundant in all conditions. During axenic growth on propionate with fumarate, *S. fumaroxidans* converts propionate to succinate. Then, part of the fumarate in this growth condition is oxidized to acetate (Stams et al., 1993). This conversion is energy dependent, producing reducing equivalents during malate oxidation and pyruvate decarboxylation, and is only possible by coupling it to the energy yielding reduction of fumarate to succinate.

The fumarate reductase FrdABEF (Sfum_4092-4095) complex was detected in higher levels during growth with fumarate. With the exception of a few subunits, the FrdABEF complex was not detected in cells grown with methanogens as expected since fumarate reduction only occurs when fumarate is provided. However, the complex was consistently detected in cells where sulfate was available, particularly in the coculture with *D. desulfuricans*.

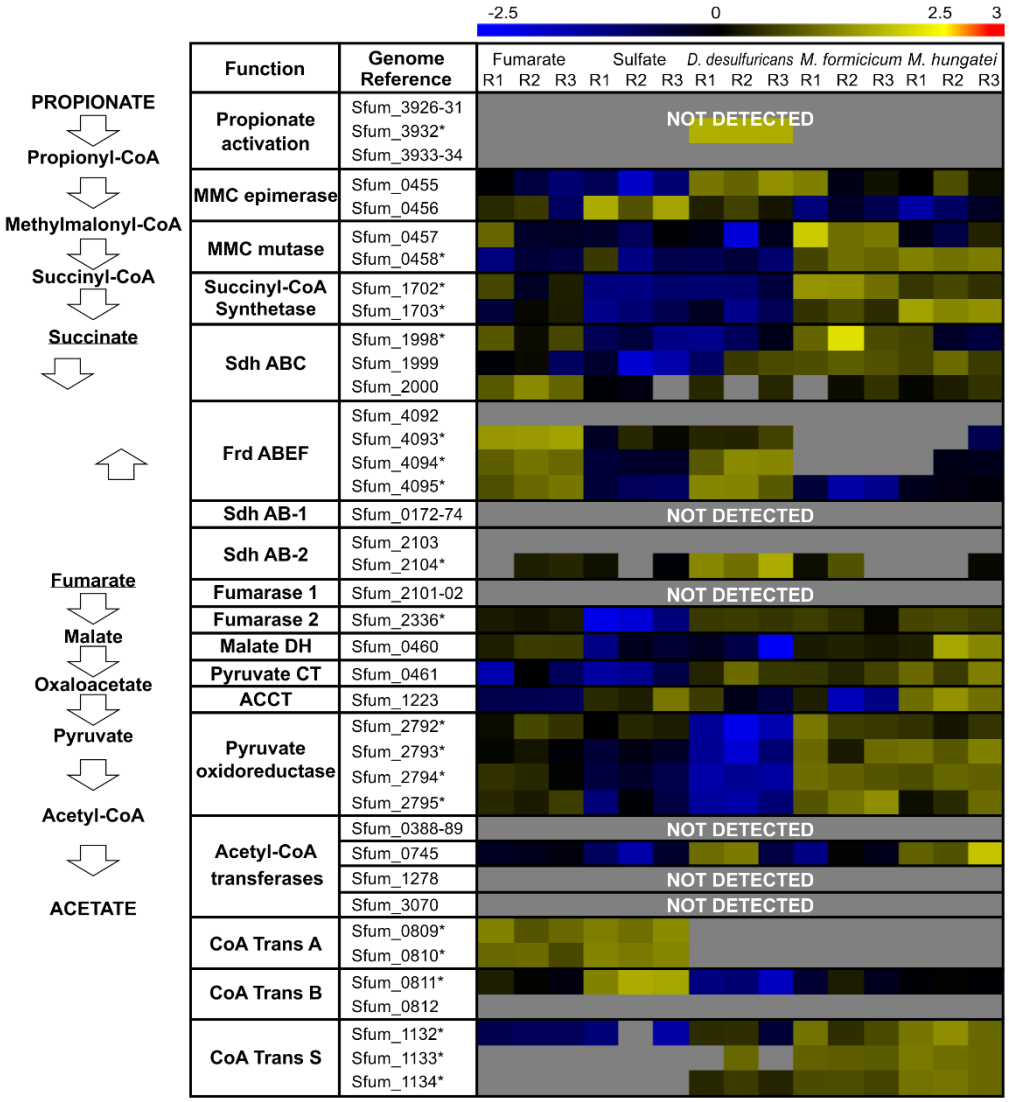

Figure 4.1. Relative expression levels of the proteins used in the methylmalonyl-CoA pathway by *Syntrophobacter fumaroxidans*. Protein abundance levels are shown after Z-score normalization. High relative expression is indicated in yellow and low relative expression is indicated in blue. Grey colour means not detected. In the left side the MMC steps are shown levelled to the associated proteins. The rows in the heat map show the detected proteins in five different growth conditions. The columns show from left to right, in triplicates, the electron acceptor used by *S. fumaroxidans* to couple propionate oxidation: fumarate, sulfate and interspecies compounds transferred to: *Desulfovibrio desulfuricans* G11, *Methanobacterium formicicum* and *Methanospirillum hungatei*. (*) indicates a statistically significant difference in at least one condition. MMC: methylmalonyl-CoA; Sdh: succinate dehydrogenase; Frd: fumarate reductase; DH: dehydrogenase; CT: carboxyltransferase; ACCT: acetyl-CoA carboxyltransferase; CoA Trans: coenzyme A transferase.

In the genome of *S. fumaroxidans* two additional gene clusters show similarity to succinate dehydrogenases SdhAB-1 (Sfum_0172-0174) and SdhAB-2 (Sfum_2103-2104). SdhAB-1 was not detected in our study and only the alpha subunit of SdhAB-2 showed a similar detection profile to FrdABEF. The predicted fumarase in the gene cluster Sfum_2101-02 was not detected in any condition. Instead, a second fumarase from a non-clustered gene (Sfum_2336) was abundant in all conditions. The amino acid sequence of this second fumarase corresponds to the previously isolated and characterized class I fumarase from *S. fumaroxidans* (van Kuijk et al., 1996). Although this protein was abundant in all conditions, lower expression levels were measured in sulfate-reducing cells. Finally, methylmalonyl-CoA mutase (Sfum_0458) and succinyl-CoA synthase (Sfum_1702-1703) were significantly more abundant in syntrophically grown cells, while the pyruvate oxidoreductase (Sfum_2792-2795) showed a lower relative expression during growth with *Desulfovibrio*.

Hydrogenases and formate dehydrogenases involved in electron transfer

The genome of *S. fumaroxidans* indicates the presence of six formate dehydrogenases and eight hydrogenases. Relative abundance levels of the hydrogenases and formate dehydrogenases produced by *S. fumaroxidans* during propionate degradation under different axenic or cocultured conditions are shown in **Figure 4.2**. In this figure can be seen that for most of the detected hydrogenases and formate dehydrogenases, the expression levels measured in syntrophic conditions with methanogens were higher than any of the axenic conditions. Of the two predicted periplasmic hydrogenases, Hyn (Sfum_2952-53) was detected in all conditions albeit more abundant during growth with fumarate and with *D. desulfuricans* G11, while Hyd2 (Sfum_0847-48) was not detected in cells that were grown with sulfate.

Figure 4.2. Relative abundance levels of hydrogenases and formate dehydrogenases in *Syntrophobacter fumaroxidans* during propionate oxidation. Protein abundance levels are shown after Z-score normalization. The detected proteins are shown for five different growth conditions, in triplicates, according to the electron acceptor used by *S. fumaroxidans* to oxidize propionate; from left to right: fumarate, sulfate and interspecies compounds transferred to: *Desulfovibrio desulfuricans* G11, *Methanobacterium formicicum* and *Methanospirillum hungatei*. The colour intensity indicates the degree of protein up- or down regulation where high relative expression is indicated in red and low relative expression is indicated in blue; the grey colour represents not detected. Underlined complex names have been predicted to function as confurcating. Locus tags in bold font indicate the catalytic subunit of the complex. (*) indicates a statistical significant difference in at least one condition.

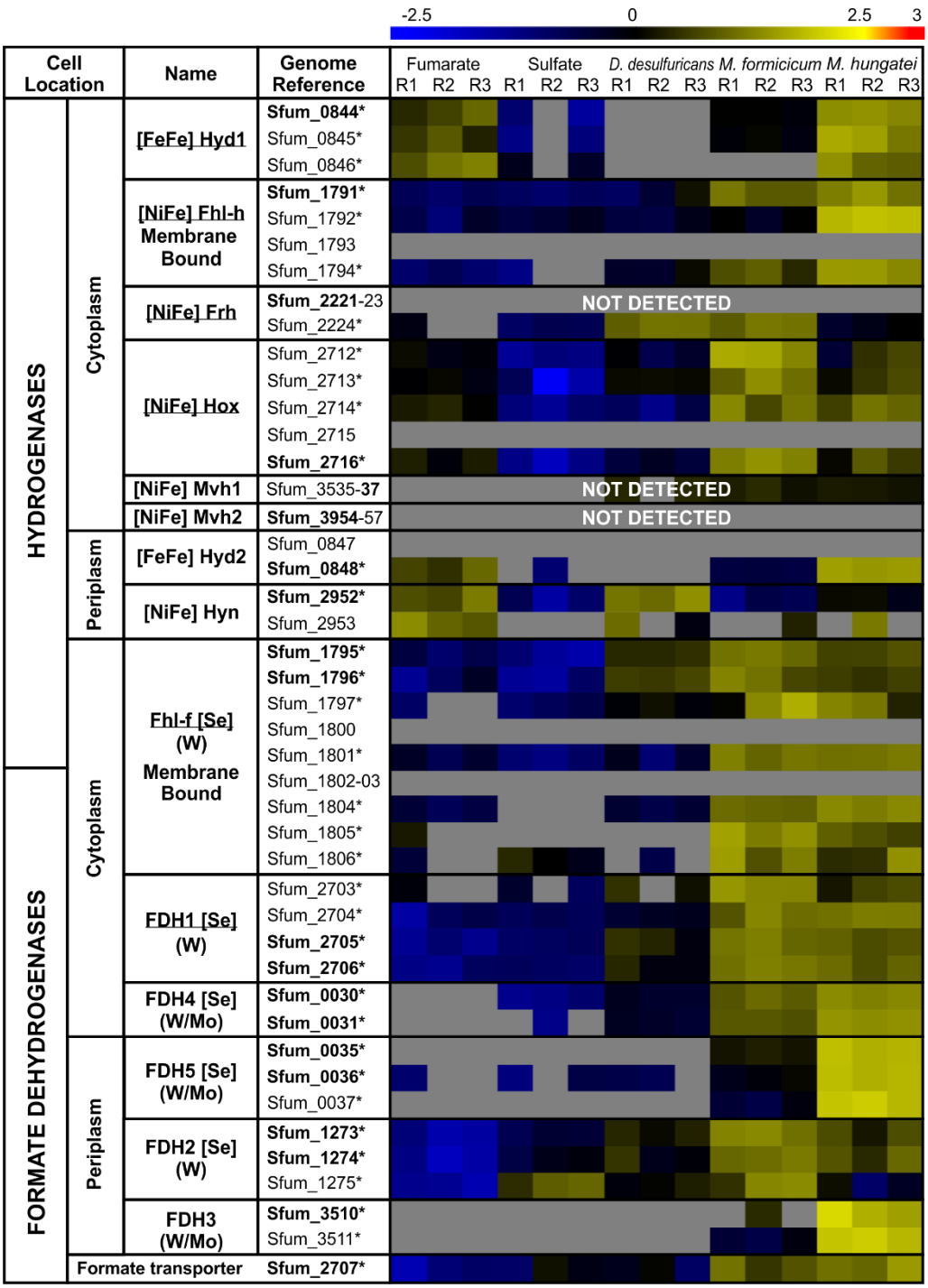
-2.5
0
2.5
3
Cell Location
Name
Genome Reference
Fumarate
Sulfate
D. desulfuricans
M. formicicum
M. hungatei
R1 R2 R3 R1 R2 R3 R1 R2 R3 R1 R2 R3 R1 R2 R3
HYDROGENASES
FORMATE DEHYDROGENASES
Cytoplasm
Periplasm
[FeFe] Hyd1
Sfum_0844*
Sfum_0845*
Sfum_0846*
[NiFe] Fhl-h Membrane Bound
Sfum_1791*
Sfum_1792*
Sfum_1793
Sfum_1794*
[NiFe] Frh
Sfum_2221-23
NOT DETECTED
Sfum_2224*
[NiFe] Hox
Sfum_2712*
Sfum_2713*
Sfum_2714*
Sfum_2715
Sfum_2716*
[NiFe] Mvh1
Sfum_3535-37
NOT DETECTED
[NiFe] Mvh2
Sfum_3954-57
NOT DETECTED
[FeFe] Hyd2
Sfum_0847
Sfum_0848*
[NiFe] Hyn
Sfum_2952*
Sfum_2953
Fhl-f [Se] (W) Membrane Bound
Sfum_1795*
Sfum_1796*
Sfum_1797*
Sfum_1800
Sfum_1801*
Sfum_1802-03
Sfum_1804*
Sfum_1805*
Sfum_1806*
FDH1 [Se] (W)
Sfum_2703*
Sfum_2704*
Sfum_2705*
Sfum_2706*
FDH4 [Se] (W/Mo)
Sfum_0030*
Sfum_0031*
FDH5 [Se] (W/Mo)
Sfum_0035*
Sfum_0036*
Sfum_0037*
FDH2 [Se] (W)
Sfum_1273*
Sfum_1274*
Sfum_1275*
FDH3 (W/Mo)
Sfum_3510*
Sfum_3511*
Formate transporter
Sfum_2707*

S. fumaroxidans has two [NiFe]-hydrogenases (MvhADG) associated with HdrABC clusters (Mvh1, Sfum_3535-3537 and Mvh2, Sfum_3954-3956). None of these proteins, or the neighbouring Hdr, were found in our analysis. For the Frh complex (Sfum_2221-24), only the subunit containing the FAD and NAD^+-binding oxidoreductase domain was detected. Therefore, this protein was classified as not detected. Of the three cytoplasmic hydrogenases detected, Hox (Sfum_2712-16) and Fhl-h (Sfum_1791-94) were present in all conditions. Lastly, Hyd1 (Sfum_0844) was more abundant in syntrophically grown cells and cells grown with propionate and fumarate, but not when sulfate was present.

The three periplasmic formate dehydrogenases (Fdh2, Fdh3 and Fdh5) from *S. fumaroxidans* were abundant during growth in syntrophy with *M. hungatei*. However, for syntrophic growth with *M. formicicum* the detection levels of Fdh5 (Sfum_0035-37) and Fdh3 (Sfum_3509-11) were significantly lower. Fdh3 was not detected in axenic conditions or in the coculture with *D. desulfuricans*, and Fdh5 was scarcely detected in such conditions.

Cytoplasmic Fdh1 (Sfum_2703-06) and periplasmic Fdh2 (Sfum_1273-75) were the most abundant formate dehydrogenases in all conditions. Moreover, significantly higher levels were measured during syntrophic growth**.** The membrane bound Fhl-f (Sfum_1795-1806) was abundant in syntrophically grown cells but showed a lower relative expression during axenic growth. Fdh4 (Sfum_0030-01) had very high relative abundance levels in syntrophic cultures. However, Fdh4 was not detected in the pure culture with fumarate, while only the lowest limits of detection were measured in sulfidogenic growth. The formate transporter (Sfum_2707) was detected in all conditions but more abundant in methanogenic cultures.

Redox proteins involved in dissimilatory sulfate reduction

A set of proteins required for dissimilatory sulfate reduction have previously been predicted in the genome of *S. fumaroxidans* (Pereira et al., 2011). Sulfate adenylyltransferase (Sat), proton-translocating pyrophosphatase (HppA), APS reductase (AprAB), dissimilatory sulfite reductase (DsrAB) and DsrC complexes were among the most abundant proteins in all growth conditions**.** In contrast, neither of the two sulfate transporters (Sfum_0271 & Sfum_0653) predicted in the genome was detected in the analysis. Two periplasmic subunits of the QrcABCD complex (QrcB: Sfum_0610 and QrcC: Sfum_0609) were detected in all conditions and more abundant in syntrophic cultures **(Figure 4.3)**. However, the subunit QrcA (Sfum_0611) a membrane-associated multihaem cytochrome *c*, was not detected. Sfum_4047 is the only other gene in *S. fumaroxidans* genome coding for a membrane-anchored multihaem cytochrome *c*. The product of this gene was also detected in all conditions and more abundant in the cocultures with *M. hungatei* and *D. desulfuricans*.

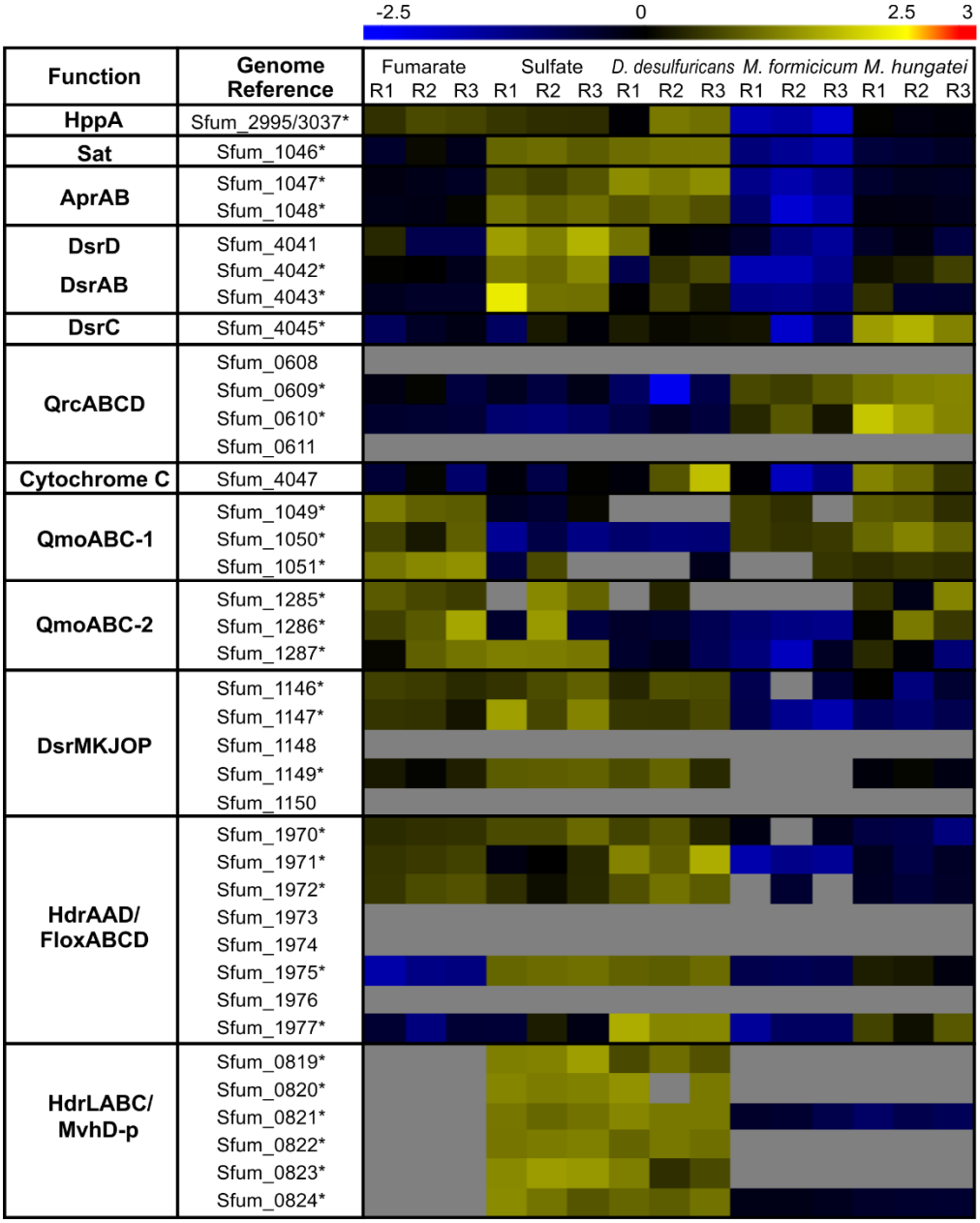

Figure 4.3. Relative abundance levels of proteins involved in sulfate reduction in *Syntrophobacter fumaroxidans*. Abundance levels after shown after Z-score normalization. The columns show in triplicates, the electron acceptor used by *S. fumaroxidans* to couple propionate oxidation, from left to right: fumarate, sulfate and interspecies compounds transferred to: *Desulfovibrio desulfuricans* G11, *Methanobacterium formicicum* and *Methanospirillum hungatei*. High relative expression is indicated in red and low relative expression is indicated in blue. Grey colour means not detected. (*) indicates a statistical significant difference in at least one condition.

The genes coding for the trimeric complex QmoABC (Sfum_1049-1051) are well conserved in all known sulfate-reducing bacteria (SRB) and are commonly located in a *sat-aprAB-qmoABC* cluster (Pereira et al., 2011). Surprisingly, the products of these genes were more abundant in cells grown with fumarate and in syntrophy than in cells grown with sulfate. However, a second QmoABC (Sfum_1285-87) was detected in the proteome in all conditions. This complex was more abundant in cells grown axenically and in the coculture with *M. hungatei*. Similarly, the principal subunits of the DsrMKJOP (Sfum_1146-1150) complex were found in all conditions but more abundant in axenic conditions and in the coculture with *D. desulfuricans*.

Heterodisulfide reductases (Hdr) are enzymes present in methanogens and perform the reduction of CoM-S-S-CoB heterodisulfide to CoM-SH and CoB-SH (Hedderich et al., 2005). Although the substrate of these enzymes CoM-S-S-CoB heterodisulfide has only been found in methanogens, the high number of similar proteins (heterodisulfide reductases-like) in SRB has been emphasized in several genome analyses (McInerney et al., 2007; Strittmatter et al., 2009; Pereira et al., 2011; Grein et al., 2013). Moreover, related enzymes have been purified from other non-methanogenic archaea (Mander et al., 2004). An Hdr was detected in the proteome analysis of *S. wolfei* (Sieber et al., 2015), suggesting that the presence in the genome and production of such an enzyme complex is not dependent of a sulfate-reducing lifestyle, but rather to microorganisms specialized in low energy metabolism. Two of the five predicted heterodisulfide reductases-like enzymes in *S. fumaroxidans* were detected in this study, one associated with a Flox complex Hdr/Flox (Sfum_1970-1977) and the other with a putative methyl viologen hydrogenase Hdr/Mvh-p (Sfum_0819-0824). The Flox section of Hdr/Flox is produced in all conditions. Hdr/Mvh-p was abundant when sulfate was present whereas only the subunits containing FAD/NAD-binding domains were detected in syntrophic cultures. The fifth heterodisulfide reductase-like found in the genome of *S. fumaroxidans* is associated with a pyruvate:Fd oxidoreductase, HdrAL/POR (Sfum_0012-0018); this complex was not detected.

Other proteins involved in energy conservation

The principle of electron bifurcation was originally proposed for a butyryl-CoA dehydrogenase/electron transferring flavoprotein complex (Bcd-Etf) in *Clostridium kluyveri* (Li et al., 2008). Since then three more flavin-containing complexes capable of electron bifurcation in bacteria and archaea have been described: [FeFe]-hydrogenases (Hyd), transhydrogenases (NfnAB) and [NiFe]-hydrogenase/heterodisulfide reductases (MvhADG–HdrABC) (Schut and Adams, 2009; Kaster et al., 2011b; Huang et al., 2012; Buckel and Thauer, 2013).

Although *S. fumaroxidans* is not able to grow on butyrate or crotonate, complexes similar to Bcd/Etf have been predicted from the genome. The acyl-CoA subunit

(Sfum_1371) of one of these complexes was abundant in all conditions, while the Etf subunits (Sfum_1372 and Sfum_1373) were detected in lower levels, and the beta subunit was not detected at all in cells grown in cocultures. A second Etf complex from genes Sfum_0106 and Sfum_0107 was abundant in all conditions at similar levels than the acyl-CoA subunit from gene Sfum_1371. **(Supporting information, Fig. S4.2)** Two additional paralogs coding for Acyl-CoA/Etf complexes were found in the genome (Sfum_3686-88 and Sfum_3929-3931), but not detected in our proteomic analysis. Finally, NfnAB (Sfum_2150-2151), another electron-bifurcating iron-sulfur flavoprotein commonly present in genomic analyses of sulfate reducers was exclusively detected during growth with fumarate.

Proteome generalities of Desulfovibrio desulfuricans

At the time of our analysis, the genome of *Desulfovibrio desulfuricans* G11 was not available from the common databases. Therefore, we used a draft genome available in our laboratory. Currently the genome of *Desulfovibrio desulfuricans* DSM 7057 is freely accessible and counts with 3,020 protein-coding genes (Sheik et al., 2017). Our proteome analysis successfully detected 827 proteins among the three growing conditions. The core proteome of *D. desulfuricans* consists of 344 proteins detected in all studied conditions **(Supporting information, Fig. S4.3.A)**. Only 346 proteins were detected in cells grown in coculture with *S. fumaroxidans*, while the cells growing with hydrogen or formate yielded more than 800 proteins each.

Differences in the proteome composition were explored using principal component analysis (PCA) **(Supporting information, Fig. S4.3.B).** The first principal component (PC1; 88.5% of total variance) clearly separates growth in coculture from axenic growth in formate or hydrogen. However, PC1 did not establish a difference between growth on hydrogen or on formate. The second principal component mainly differentiates the two axenic proteomic profiles, albeit PC2 accounts only for 3.8% of the variability of the data.

Although fewer *D. desulfuricans* proteins were detected in cells grown in coculture with *S. fumaroxidans*, it was possible to recuperate the most abundant proteins in such condition **(Supporting information, Fig. S4.4)**. Among these, we found a periplasmic formate dehydrogenase (FDH3; DsvG11_3108-3110) and a periplasmic [NiFe]-hydrogenase (Hyd2; DsvG11_2079-2080) **(Supporting information, Fig. S4.5)**. A cytoplasmic formate dehydrogenase (FDH1; DsvG11_1734-1736) on the other hand, was detected only in cells grown with formate, while a periplasmic [FeFe]-hydrogenase (Hyd1; DsvG11_0345-0346) was found in both axenic conditions. We predict from our draft genome of *D. desulfuricans* another [NiFe]-hydrogenase with a cytochrome type-b (Hyd3; DsvG11_1724-1726) and a putative confurcating formate dehydrogenase (FDH2; DsvG11_2896-2899), but neither of these enzymes, nor the formate transporter (DsvG11_0600), were detected in the proteomic results.

Other periplasmic and membrane bound proteins were abundant in cells grown in the coculture, for instance cytochrome c552 (DsvG11_0693) and an outer-membrane protein (DsvG11_1704).

Discussion

The majority of the most abundant proteins detected in this study were involved in major processes such as propionate degradation, sulfate reduction, electron transfer, and energy conservation. Other abundant proteins, such as heat-shock proteins, chaperonins, histones and transporters, emphasize the importance of protection, transport and stabilization of diverse macromolecules in the cell. These proteins have previously been reported as highly abundant in several proteomic analyses and identified as common stress-induced molecules required for normal cell growth (Hemmingsen et al., 1988; Lu et al., 2007; Mancuso et al., 2012; Sieber et al., 2015).

Energy-dependent succinate oxidation in MMC

For propionate degradation with fumarate, *S. fumaroxidans* requires a fumarate reductase, whereas to oxidize propionate with sulfate, or in syntrophy, a succinate dehydrogenase is needed. The high levels of the fumarate reductase (FrdABEF) in cells grown with propionate and fumarate reflects the reduction of fumarate in this lifestyle. However, the abundance of this complex in cells growing with sulfate and in coculture with *D. desulfuricans* can only be explained by a reversible performance to succinate oxidation, since no succinate was accumulated in those conditions. Fumarate reductases and succinate dehydrogenases are functionally and structurally related enzymes (Mattevi et al., 1999). The membrane bound SdhABC of *S. fumaroxidans* has previously been purified, characterized and showed activity in both directions, fumarate reduction and succinate oxidation (van Kuijk et al., 1998a). However, FrdABEF has not been purified and as such could not be tested for a reversible activity. Transcription experiments reported that FrdABEF was up-regulated (>2 log ratio) when fumarate was the electron acceptor in contrast with the gene transcription of cells gown in syntrophic cocultures with *M. hungatei* (Worm, 2010). Interestingly in such study FrdABEF was also up-regulated in cells grown with sulfate as the electron acceptor and down-regulated in cells cocultured with *M. formicicum*. Our proteomic study confirms the high expression levels of FrdABEF in propionate plus fumarate cultures. Moreover, FrdABEF was also present in conditions where propionate was oxidized with sulfate and in coculture with *D. desulfuricans*. These results might suggest a reversible function of the fumarate reductase FrdABEF towards succinate oxidation. Nevertheless, although in in-vitro analysis the reversible activity of enzymes is possible, in vivo the enzymes are usually dedicated to one physiological function. Besides *S. fumaroxidans* has a succinate dehydrogenase (SdhABC) for succinate oxidation. A more likely possibility is that fumarate reduction occurred in the sulfidogenic condition. To pull the

oxidation of succinate towards the formation of fumarate, hydrogen and formate, these products have to be efficiently removed. To maintain the levels of fumarate low, the fumarase (Sfum_2336) has to convert fumarate efficiently to malate. This process is very important, and as such fumarase is one of the most abundant proteins in *S. fumaroxidans*. However, cells grown with sulfate show the lowest expression levels of this enzyme (**Figure 4.1**). It might be that if fumarate is not removed efficiently in sulfate-grown cells, the bacteria start to produce FrdABEF.

Hydrogen and formate in IET and RET

During syntrophic growth, *S. fumaroxidans* needs to transfer electrons via hydrogen and/or formate to a syntrophic partner. It has long been speculated that formate plays a more important role than hydrogen as an electron carrier in the syntrophic associations of this bacterium with methanogens (de Bok et al., 2002a; de Bok et al., 2002b). Although slightly higher levels were measured in the formate transporter during syntrophic growth over the axenic conditions, *S. fumaroxidans* must rely on other mechanisms to transfer formate. Three formate dehydrogenases (Fdh2, Fdh3 and Fdh5) contain a twin-arginine translocation (Tat) pathway conserved site, which points to the translocation of these proteins across the cytoplasmic membrane. Fdh3 and Fdh5 were detected only in syntrophically grown cells, while Fdh2 was detected in all conditions, but was more abundant during syntrophic growth. This suggests that periplasmic Fdh3 and Fdh5 are complexes specialized in transferring formate to the syntrophic partner, while Fdh2 is broadly used for energy conservation purposes as part of the reverse electron transport mechanism, possibly coupled to SdhABC or FrdABEF (**Fig. S4.6**).

Among the cytoplasmic formate dehydrogenases, Fdh1 is homologous to the bifurcating [FeFe]-hydrogenase of *Thermotoga maritima* (Schut and Adams, 2009). Furthermore, it contains a conserved site coding for a 51 kDa subunit of a NADH:ubiquinone oxidoreductase which makes this protein a very plausible candidate for a confurcating-type of formate dehydrogenase. Fdh1 was detected in all conditions and higher levels were detected in syntrophic conditions. Similarly, the membrane associated Fhl-f was also detected in all conditions and more abundant in syntrophically grown cells. The ubiquitous detection of Fdh1 and Fhl-f indicates that their role is not restricted to IET, but that these complexes are essential for energy conservation and formate/hydrogen interconversion during propionate degradation. On the other hand, Fdh4 was not detected in cells grown with fumarate, scarcely detected in cells grown with sulfate and highly abundant in methanogenic conditions. This led us to speculate that Fdh4 has an exclusive role in IET. Furthermore, the genes coding for Fdh4 are located upstream in the genome of the periplasmic Fdh5 operon. Considering these observations, we propose that these neighbouring genes coding for cytoplasmic and periplasmic formate dehydrogenases are used mainly for interspecies formate transfer. Thus Fdh3, Fdh4 and Fdh5 seem to form a set of

formate dehydrogenases used by *S. fumaroxidans* to transfer electrons to the syntrophic partner. It is conceivable that these formate dehydrogenases contain a molybdenum catalytic core (Mo-FDH) in contrast to Fdh1 and Fdh2 whose structure has been characterized and were shown to possess only tungsten-containing active sites (W-FDH) (de Bok et al., 2003). Further biochemical analysis of these formate dehydrogenases will give insight of the role of molybdenum in IET mechanisms in methanogenic environments (Plugge et al., 2009; Worm et al., 2011a).

Only five of the eight predicted hydrogenases of *S. fumaroxidans* were detected in the present analysis. Of the two periplasmic hydrogenases, Hyn was more abundant in cells grown with propionate and fumarate and in coculture with *D. desulfuricans*. Hyn has been proposed to be involved in reverse electron transport coupled with FrdABEF for fumarate reduction or SdhABC for succinate oxidation (Worm et al., 2011b). Considering the high levels of Hyn and FrdABEF in the coculture with *D. desulfuricans*, we suggest that indeed Hyn is involved in RET with FrdABEF, whether reducing fumarate in fumarate conditions or reversibly oxidizing succinate in the coculture with *D. desulfuricans* (**Fig. S4.6**).

Of the three cytoplasmic hydrogenases detected, Hox and Fhl-h, which were detected in all conditions, were more abundant in cells grown with the methanogens. Hox is most probably a confurcating hydrogenase involved in energy conservation. The membrane-bound Fhl-h on the other hand, together with Fhl-f might be involved in a cytoplasmic hydrogen-formate interconversion during syntrophic growth to control electron release. Finally, the genes coding for Hyd1 and Hyd2 are adjacent in the genome, the products of these genes are produced only in the presence of fumarate and during syntrophic growth but not when sulfate was available. This might be due to the exclusive use of other confurcating energy-conserving complexes in sulfidogenic conditions that are also coupled to H_2 formation, for instance Mvh-p/Hdr.

Although formate formation seems to prevail in the syntrophic lifestyle of *S. fumaroxidans*, our results indicate that hydrogen, via Hyd1, Hyd2, Hox and Hyn also plays an important role in energy conservation by RET. During growth with fumarate, when IET is not required, these hydrogenases were detected in higher abundance than any of the formate dehydrogenase in such growth condition.

Energy conservation mechanisms in the sulfate-reducing metabolism

All the proteins necessary for sulfate reduction in *S. fumaroxidans* were abundant in this analysis, with the intriguing exception of the sulfate transporters that were not detected. In order to activate sulfate by sulfate adenylyltransferase, sulfate has to be transported into the cell. Therefore, another mechanism for transport of sulfate across the membrane must be used by *S. fumaroxidans*. Several transporters and unknown proteins were among the most abundant proteins in this study, it is

possible that some of them could have played a role in the import of sulfate to the cytoplasm.

The abundance of HppA, Sat, Apr and DsrAB in our proteomic analysis in conditions where sulfate reduction was not observed indicates that the sulfate reduction pathway is not strictly regulated in *S. fumaroxidans*. However, all these enzymes were significantly more abundant in conditions where sulfate was available, indicating sulfidogenic activity in cells grown with sulfate and with *D. desulfuricans*. Similarly, for complexes such as Qmo-2, DsrMKJOP and Hdr/Flox it is possible to observe an up-regulation in axenic conditions and in some cases in coculture with *D. desulfuricans*, while for Qrc and Qmo-1 higher levels are observed in syntrophically grown cells. These observations suggest that the use of these complexes in electron transfer is not constrained to a sulfidogenic lifestyle, and that they could for instance transfer electrons to periplasmic formate dehydrogenases for IET or to the FrdABEF for RET.

Quinone reductase complexes (QrcABCD) are involved in the reduction of the quinone pool in *D. vulgaris* Hildenborough. Furthermore, it was shown that QrcABCD is reduced by periplasmic hydrogenases and formate dehydrogenase via the cytochrome c3 (subunit A of the complex) (Venceslau et al., 2010). Although in *D. vulgaris* the described role of QrcABCD is to reduce menaquinone with electrons gained from hydrogen or formate oxidation during sulfate reduction, we speculate that a reverse process is feasible. In *D. desulfuricans* G20, a mutant lacking the *qrcB* gene was unable to grow with H_2 or formate as electron donor, while it grew similarly as the parent strain with lactate (Li et al., 2009). Moreover, this mutation also inhibited syntrophic growth with a methanogen in lactate (Li et al., 2009). The higher levels of the QrcABCD of *S. fumaroxidans* in cells grown in syntrophy might be explained by its involvement in electron transfer to the periplasmic formate dehydrogenases Fdh3 and Fdh5 **(Figures 4.2 and 4.3)**.

Direct electron transfer from QmoABC to AprAB to facilitate the reduction of sulfate to sulfite has been reported in *Desulfovibrio desulfuricans* (Pires et al., 2003; Pereira, 2008; Duarte et al., 2016). In *Syntrophobacter*, the higher expression levels of the two Qmo complexes in cells grown with fumarate might be due to the use of this membrane bound complex in transferring electrons to FrdABEF for RET. FrdABEF lacks a transmembrane subunit, therefore it has been speculated that it receives electrons from menaquinone via cytochrome b and cytochrome b:quinone oxidoreductases (Müller et al., 2010), however these cytochromes were not detected in our study.

DsrMKJOP is another highly conserved membrane complex in SRB (Rabus et al., 2015). In many Gram-positive SRB only the cytoplasmic-facing DsrMK genes are present, suggesting that this is the minimal functional module (Pereira et al., 2011).

Although in *S. fumaroxidans* the complete gene set of DsrMKJOP is present, only the essential subunits (DsrMK), and the periplasmic DsrO were detected in our proteomic study. In the heat map shown in **Figure 4.3** the expression profile of DsrMKO is similar to that of the Hdr/Flox complex. If Hdr/Flox is used in all conditions to confurcate electrons as will be discussed below, DsrMKO might be involved in electron transfer with this complex.

HdrABC/FloxABCD, a novel NADH dehydrogenase/heterodisulfide reductase widespread in anaerobic bacteria has been proposed to be involved in flavin-based electron bifurcation in *D. vulgaris* Hildenborough (Ramos et al., 2015). The Flox proteins (Sfum_1970-1973) of the Hdr/Flox of *S. fumaroxidans* were constitutively present in all the conditions. Nevertheless, the Hdr-like complex in the Hdr/Flox cluster have a composition different to the canonical HdrABC. For instance, HdrBC is replaced by the cysteine-rich containing HdrD (Sfum_1969), which was not detected in our analysis. Furthermore, two *hdr*A genes are present (Sfum_1974 & Sfum_1977), but only the product of Sfum_1977 was detected. Hdr/Flox could be another confurcating system used by *S. fumaroxidans* to re-oxidize NADH during propionate degradation, and possibly involved in recycling NAD^+ during the partial reduction of fumarate. However, the conformational changes mentioned above might imply functional differences that need to be further investigated.

For the Hdr/Mvh-p complex, the *hdr*ABC genes (Sfum_0819-0821) are next to genes coding for a pyridine nucleotide-disulphide oxidoreductase comprising an HdrL protein (Sfum_0824). HdrL is a large protein containing HdrA and one or two NADH binding domains (Strittmatter et al., 2009; Pereira et al., 2011). An MvhD protein is encoded in Sfum_0823, but the catalytic hydrogenase subunit MvhA is not present. The amino acid sequence of Sfum_0822 indicates a relationship to coenzyme F420 hydrogenase (InterPro, December 2017). However, a BlastP search of the amino acid sequence resulted in significant alignments with sequences of formate dehydrogenases in other SRB. We can only speculate if this Hdr/Mvh-p complex uses hydrogen or formate, but the high detection levels of the complete complex imply an important function in the sulfate-reducing metabolism.

Hdr/Mvh-p was detected only in conditions where sulfate was present, axenically or in the presence of *D. desulfuricans*. The soluble complex MvhADG/HdrABC has been shown to perform flavin-based electron bifurcation in methanogens (Thauer et al., 2008; Kaster et al., 2011b). We speculate that Hdr/Mvh-p is preferred when sulfate is available, over the confurcating hydrogenase Hyd1 which in turn was highly abundant in cells grown with fumarate as electron acceptor and in syntrophy, but not detected when sulfate was in the medium **(Figure 4.2)**. The reason for the preference of Hdr/Mvh under sulfidogenic conditions is unclear. However, it could be related to the substrates used by this complex. The MvhADG/HdrABC in methanogens uses H_2 to reduce ferredoxin and heterodisulfide (Kaster et al., 2011b).

It is possible that the exclusive high levels of Hdr/Mvh-p in our sulfidogenic conditions correspond to the need of reduction of the so called "bacterial heterodisulfide" DsrC (Venceslau et al., 2014).

It has been suggested (Venceslau et al., 2014), that the protein DsrC could serve as a redox hub, linking oxidation of several substrates to sulfate reduction. Our results with *S. fumaroxidans* show DsrC as one of the most abundant proteins present in all conditions and significantly more abundant in syntrophy with *M. hungatei*. The recent discoveries point to the role of DsrC as an electron carrier interacting with DsrAB, DsrMKJOP, Hdr/Flox and Hdr/Mvh, but it could also connect other enzyme complexes like the fumarate reductase FrdABEF in *S. fumaroxidans*, which in turn would also explain the detection of FrdABEF in cells grown with sulfate.

Proteomic profiling of Desulfovibrio desulfuricans

The low amount of *D. desulfuricans* proteins detected from cells grown in coculture with *S. fumaroxidans* can be the result of low biomass in such condition. From microscopic observations we know that the ratio of *S. fumaroxidans* to *D. desulfuricans* was 2:1 (data not shown). Although normalization of the data performed with MaxQuant allowed us to compare the detected proteins with the other growth conditions where more proteins were identified, we rather focused in analysing the most abundant proteins detected in the coculture condition.

The abundance of the periplasmic Hyd2 and periplasmic FDH3 in cells grown with *S. fumaroxidans* indicates that interspecies electron transfer carried by formate and hydrogen was taking place in the coculture. The abundance of the proteins involved in sulfate reduction confirm that *D. desulfuricans* was actively reducing sulfate for which it certainly needed electron donors which could only come from *S. fumaroxidans* in such growth condition. This shows a remarkable metabolic tendency of *S. fumaroxidans* to engage in syntrophic interactions.

Conclusions

This study shows the importance of formate as electron carrier in IET and RET during syntrophic and axenic growth of *Syntrophobacter fumaroxidans*. *S. fumaroxidans* utilizes a specific set of enzymes (Fdh3, Fdh4 and Fdh5) to transfer electrons to the syntrophic partner. Previous isolation and characterization of Fdh1 and Fdh2 have revealed only tungsten-containing active sites (W-FDH). Biochemical analysis of the three above mentioned formate dehydrogenases could provide insight of the role of molybdenum-dependent formate dehydrogenases in syntrophic growth.

Fdh2 and Hyn are the periplasmic enzymes used by *S. fumaroxidans* to recycle hydrogen and formate during RET. While Fdh2 is mainly coupled to Sdh during

succinate oxidation, Hyn seems to be coupled to Frd for fumarate reduction in propionate plus fumarate but also for succinate oxidation in other growth conditions.

Although the sulfate-reducing metabolism is poorly regulated, the abundance of membrane-bound complexes like Qrc, Qmo and DsrMKJOP, consistently found in all conditions, as well as the absence of cytochromes in the present study (only 2 cytochromes detected from 8 predicted in the genome), indicates that those membrane-bound complexes might play a role in the transfer of electrons between cytoplasmic enzymes and the periplasmic formate dehydrogenases and hydrogen dehydrogenases.

Hdr/Mvh-p is the most abundant putatively confurcating system in sulfidogenic conditions, possibly because of its probable connection to DsrC, an electron hub in sulfidogenic metabolism.

The proteomic profiles of both bacteria in the coculture of *S. fumaroxidans* with *D. desulfuricans* gives insight in the metabolic flexibility of *S. fumaroxidans*. Results showed a proteomic profile of *S. fumaroxidans* in which sulfate reduction took place, while energy conservation and IET mechanisms were also used similarly as in the syntrophic associations with methanogens. The proteomic analysis of the partner *D. desulfuricans* confirmed IET via formate and hydrogen carried on by *S. fumaroxidans* in a sulfate rich environment.

Supporting information

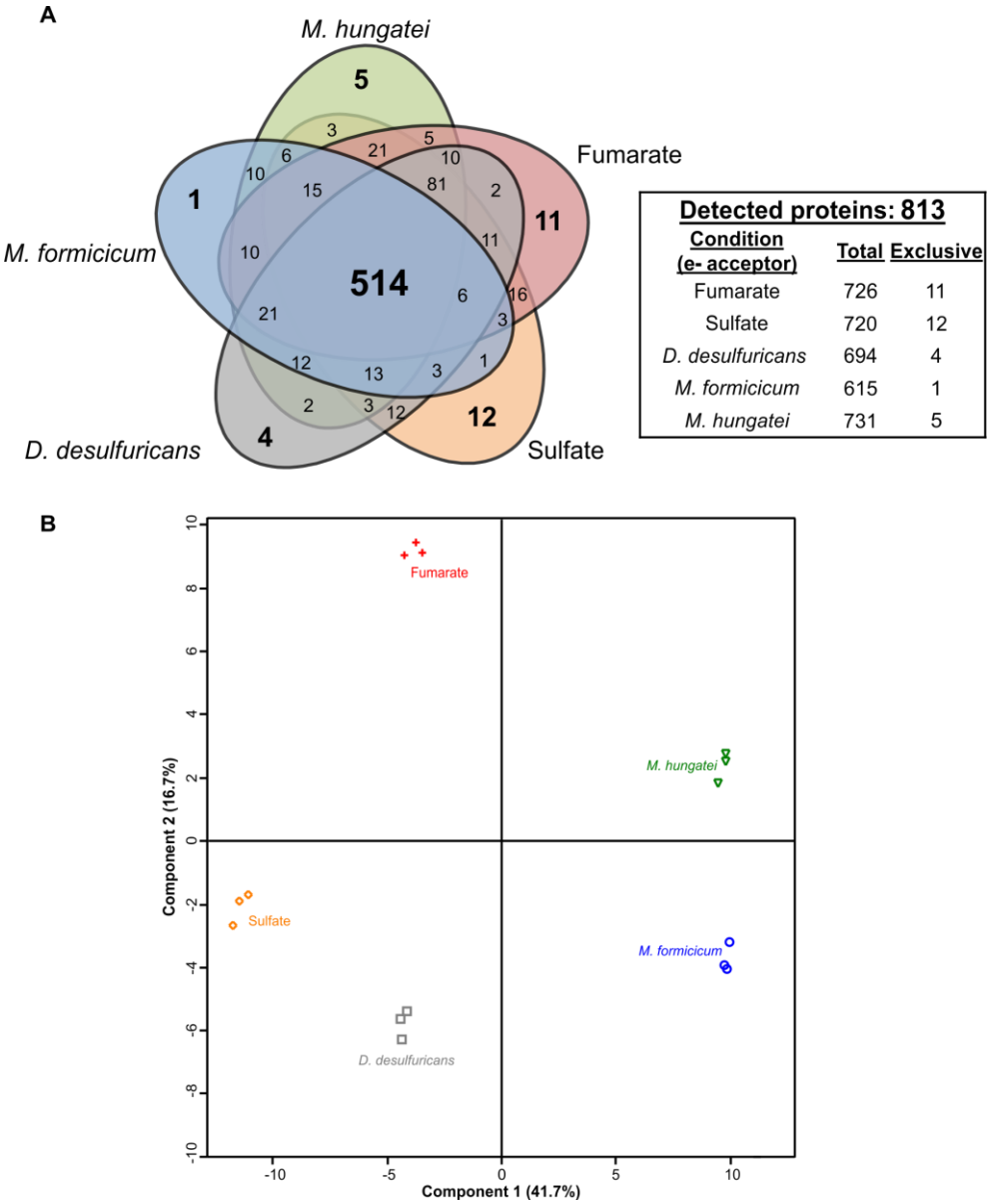

Fig. S4.1. A. Venn diagram of the 813 proteins detected in *Syntrophobacter fumaroxidans* growth on propionate with five different (biological or chemical) electron acceptors. B. Principal Component Analysis performed for *S. fumaroxidans* protein profiles obtained from each triplicate grown under five different conditions. Symbols: Orange diamonds, sulfate reducing; Red crosses, growth with fumarate; Grey squares, in coculture with *Desulfovibrio desulfuricans* in a sulfate rich environment; Green triangles, in syntrophy with *Methanospirillum hungatei*; Blue circles, in syntrophy with *Methanobacterium formicicum*.

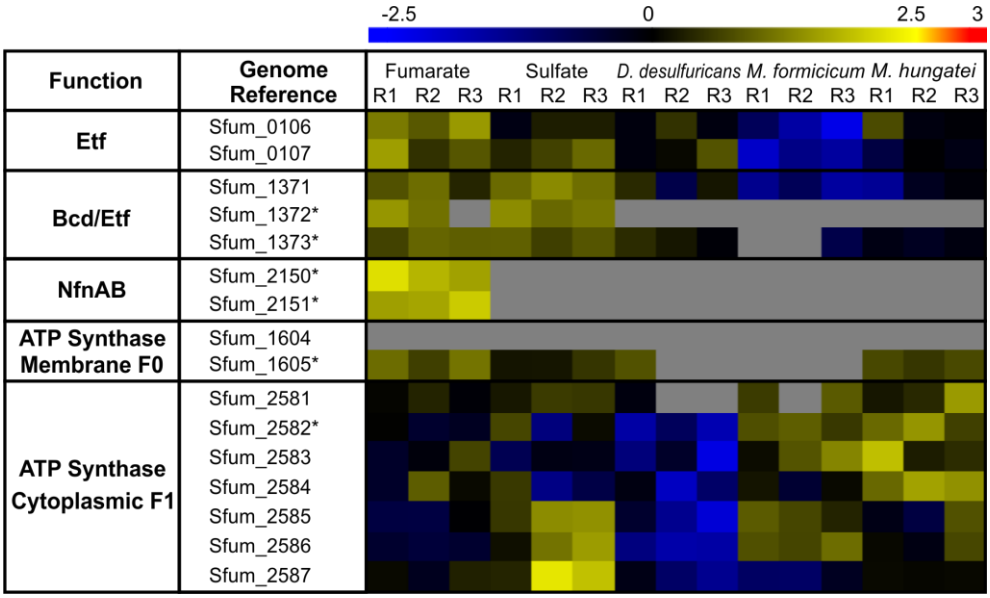

Fig. S4.2. Normalized expression matrix of energy conservation mechanisms predicted for *Syntrophobacter fumaroxidans*. Proteins are shown for five different growth conditions, in triplicates; from left to right: fumarate, sulfate and interspecies compounds transferred to: *Desulfovibrio desulfuricans*, *M. formicicum* and *M. hungatei*. The colour scale illustrates the relative detection level of each protein across the 5 samples; blue (log ratio -2.5) and yellow (log ratio 2.5) indicate lower and higher levels compared to the average level value (in black), respectively. Not detected proteins in a specific condition appear in grey. (*) indicates a statistical significant difference in at least one condition.

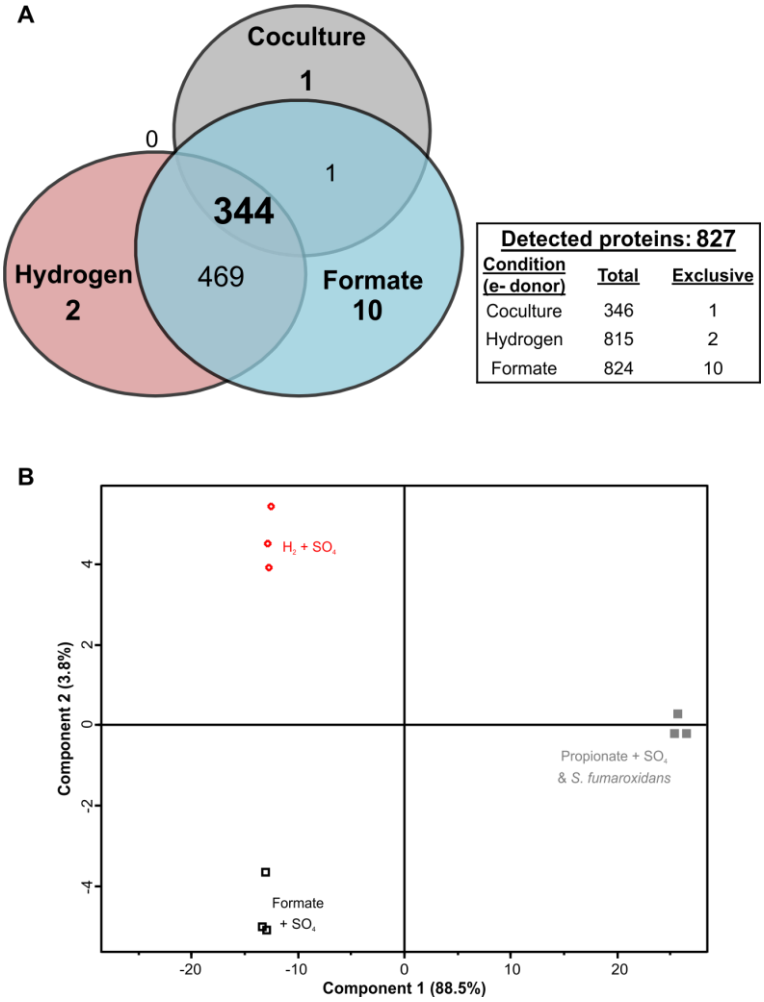

Fig. S4.3. A. Venn diagram of the 827 proteins detected in *Desulfovibrio desulfuricans* growing in sulfate rich medium in coculture with *Syntrophobacter fumaroxidans* or axenically on H_2/CO_2 or formate. B. PCA performed for *D. desulfuricans* protein profiles. Symbols: red diamonds, hydrogenotrophic conditions; black squares, growth with formate and filled grey squares correspond to the cocultured partnership of *D. desulfuricans* with *S. fumaroxidans*.


-3
0
3
4
Formate
Hydrogen
Coculture
R1 R2 R3 R1 R2 R3 R1 R2 R3


-3
0
3
4
Formate
Hydrogen
Coculture
R1 R2 R3 R1 R2 R3 R1 R2 R3
DsvG11_1132 Pirin-like_protein_CC_0481
DsvG11_1036 LigA
DsvG11_0060 Protease_HtpX_homolog
DsvG11_0722 Hypothetical_protein
DsvG11_1468 Nitroreductase
DsvG11_0518 Flavodoxin
DsvG11_1047 Transcription_elongation_factor_GreA
DsvG11_0511 Acetylornithine_aminotransferase
DsvG11_2976 UDP-4-amino-4-deoxy-L-arabinose-oxoglutarate
DsvG11_0257 NADPH_dehydrogenase
DsvG11_2190 UPF0210_protein_Ddes_0622
DsvG11_3042 Phenylacetate-coenzyme_A_ligase
DsvG11_1749 Response_regulator_receiver_domain_protein
DsvG11_2147 Asparagine--tRNA_ligase
DsvG11_0996 Riboflavin_biosynthesis_protein_RibD
DsvG11_1711 Glucose-6-phosphate_isomerase
DsvG11_1340 YicC-like_domain-containing_protein
DsvG11_1772 Phosphoesterase
DsvG11_2997 Periplasmic_binding_protein
DsvG11_2380 Tryptophan_synthase_beta_chain
DsvG11_2003 Elongation_factor_P
DsvG11_0836 Signal_recognition_particle_protein
DsvG11_0140 Alpha-amylase
DsvG11_0720 30S_ribosomal_protein_S15
DsvG11_2989 DNA-directed_RNA_polymerase_sub_omega
DsvG11_1981 Hypothetical_protein
DsvG11_2732 ROS/MUCR_transcriptional_regulator_protein
DsvG11_2118 Aspartate_aminotransferase
DsvG11_0095 EPSP_synthase_3-phosphoshikimate
DsvG11_0145 Family_of_unknown_function_DUF490
DsvG11_0990 3-oxoacyl-[acyl-carrier-protein]_synthase_3
DsvG11_0154 Single-stranded_DNA-binding_protein
DsvG11_0311 Nickel_transport_complex_prot,NikM_subunit
DsvG11_2950 Dihydroorotate_dehydrogenase_B_NAD+,
DsvG11_2621 Hypothetical_protein
DsvG11_1487 Cobyrinic_acid_ac-diamide_synthase
DsvG11_0659 Glycine/sarcosine/betaine_reductase_complex
DsvG11_0121 Ribosomal_protein_L35,_conserved_site
DsvG11_0153 Hypothetical_protein
DsvG11_1613 Flagellar_motor_switch_protein_FliN
DsvG11_2704 Predicted_Rossmann_fold_nucleotide-binding
DsvG11_1420 UspA_domain_protein
DsvG11_1313 Transcription_termination_factor_Rho
DsvG11_0419 UDP-N-acetylmuramoyl-L-alanylDglutamate-2,6
DsvG11_0485 Sulfide_dehydrogenase_subunit_beta
DsvG11_2381 Thymidylate_synthase_ThyX_TS_TSase
DsvG11_2159 ATP-binding_region_ATPase_domain_protein
DsvG11_1029 50S_ribosomal_protein_L13
DsvG11_0023 Aspartate_aminotransferase
DsvG11_0643 Proline--tRNA_ligase
DsvG11_2629 2-hydroxy-3-oxopropionate_reductase
DsvG11_2237 2-nitropropane_dioxygenase_NPD
DsvG11_0167 Tetratricopeptide-like_helical
DsvG11_1578 Pancreas/duodenum_homeobox_protein_1
DsvG11_2267 CheW-like_domain_protein
DsvG11_0594 Hypothetical_protein
DsvG11_0639 Farnesyl_diphosphate_synthase
DsvG11_2335 ATP_phosphoribosyltransferase
DsvG11_1885 Eukaryotic_RNA_Recognition_MotifRRM_profile
DsvG11_1808 Metallo-beta-lactamase_super_protein
DsvG11_0434 6-phosphofructokinase_6
DsvG11_0540 Malonyl_CoA-acyl_carrier_protein_transacylase
DsvG11_1364 Chemotaxis_protein_methyltransferase_2
DsvG11_1459 LigA
DsvG11_1041 Fosforibosylaminoimidazol-succinocarboxamide
DsvG11_0973 Diaminopimelate_decarboxylase
DsvG11_1486 4Fe-4S_ferredoxin_iron-sulfur_binding_domain
DsvG11_0409 Cell_division_protein_FtsZ
DsvG11_2123 50S_ribosomal_protein_L21
DsvG11_1894 Magnesium_and_cobalt_efflux_protein_CorC
DsvG11_0090 Riboflavin_biosynthesis_protein_RibBA
DsvG11_0209 Serine--tRNA_ligase
DsvG11_2935 Bifunctional_protein_FolD
DsvG11_1191 3-isopropylmalate_dehydrogenase
DsvG11_0074 DNA-binding_protein_HU
DsvG11_0962 Ferrous_iron_transport_protein_B
DsvG11_1202 Translation_initiation_factor_IF-1_2
DsvG11_1586 Tungstate_ABC_transporter,_tungstate-binding
DsvG11_0014 Heterodisulfide_reductase,_C_subunit
DsvG11_1190 Diguanylate_cyclase_with_PAS/PAC_sensor
DsvG11_2132 Nitroreductase__protein
DsvG11_0233 Ribosomal_protein_S20
DsvG11_0462 Anti-sigma-28_factor,_FlgM
DsvG11_1444 Hypothetical_protein
DsvG11_2881 ttdA_fumA_fumB:_hydrolyase,_tartrate_alpha
DsvG11_0598 Single_hybrid_motif
DsvG11_2556 Zinc-transporting_ATPase
DsvG11_0152 Biotin/lipoyl_attachment_domain-containing
DsvG11_0818 Hypothetical_protein
DsvG11_2481 Toluene_effluxpump_outermembrane_prot_TtgI
DsvG11_2995 Glutamyl-tRNAGln_amidotransfrse_subunit_A
DsvG11_0440 Cysteine_desulfurase
DsvG11_1013 50S_ribosomal_protein_L7/L12
DsvG11_1081 Hypothetical_protein
DsvG11_1342 Intracellular_protease,_PfpI_
DsvG11_2188 Lysine--tRNA_ligase
DsvG11_0788 Type_I_secretion_outermembrane_protein TolC
DsvG11_0122 50S_ribosomal_protein_L20
DsvG11_0607 Isoleucine--tRNA_ligase
DsvG11_1980 DNA_mismatch_repair_protein_MutS
DsvG11_1876 Penicillin-binding_protein_1A
DsvG11_0151 Acetyl-coenzyme_A_carboxylase_carboxyl
DsvG11_1483 Succinate-semialdehyde_dhydrgnase_[NADP+]
DsvG11_1975 Triosephosphate_isomerase
DsvG11_2239 CTP_synthase
DsvG11_0917 DNA_gyrase_subunit_A
DsvG11_0159 Hdr-like_menaquinol_oxidoreductase_FeS
DsvG11_0330 Flavin_reductase
DsvG11_1776 Glycine_dehydrogenase_[decarboxylating]
DsvG11_3111 Protein_involved_in_formate dehydrogenase
DsvG11_1308 Ribose-phosphate_pyrophosphokinase
DsvG11_2606 6-phosphogluconolactonase
DsvG11_0027 Selenocysteine-specific_elongation_factor
DsvG11_2625 PpkA-related_protein
DsvG11_2313 ATPase-like_protein
DsvG11_1999 Thioredoxin_reductase
DsvG11_0475 Iron-sulfur_cluster-binding_protein
DsvG11_1631 RNA_polymerase_sigma_factor,_region_3/4
DsvG11_2965 ATP_synthase_subunit_delta
DsvG11_2600 ABC_transporter_ATP-binding_protein_uup
DsvG11_2470 Phosphate_acetyltransferase
DsvG11_0010 Iron-sulfur_binding_protein
DsvG11_0535 Peptidyl-prolyl_cis-trans_isomerase_cyp18
DsvG11_1156 UTP--glucose-1-phosphate_uridylyltransferase
DsvG11_1000 Leucine--tRNA_ligase
DsvG11_0129 Transketolase_1
DsvG11_0232 Glycine--tRNA_ligase_beta_subunit
DsvG11_2445 Glutamine--tRNA_ligase
DsvG11_0965 Tryptophan_synthase_beta_chain
DsvG11_1365 HEAT_domain_containing_protein
DsvG11_2463 Alanine--tRNA_ligase
DsvG11_3017 30S_ribosomal_protein_S2
DsvG11_0166 Indolepyruvate_oxidoreductase_subunit_IorA
DsvG11_2710 Nine-heme_cytochrome_c
DsvG11_2386 Extracellular_solute-binding_protein__3
-3
0
3
4
Formate
Hydrogen
Coculture
R1 R2 R3 R1 R2 R3 R1 R2 R3
DsvG11_2028 Pantothenate_synthetase
DsvG11_0936 Glutamine--fructose-6-P_aminotransferase
DsvG11_0503 Single-stranded_nucleicacidbinding_R3Hdomain
DsvG11_0203 Glutamate-pyruvate_aminotransferase_AlaC
DsvG11_0258 Tll1655_protein
DsvG11_2055 30S_ribosomal_protein_S3
DsvG11_1703 Protein_TolB
DsvG11_0410 Cell_division_protein_FtsA
DsvG11_1105 Hydrogenase-4_component_I
DsvG11_0695 NADPH-dependent_FMN_reductase
DsvG11_2567 RNA_polymerase_sigma_factor_RpoD
DsvG11_0202 Homoserine_dehydrogenase
DsvG11_2148 Aspartate-semialdehyde_dehydrogenase
DsvG11_0260 Rhodanese_domain_protein
DsvG11_2599 LigA
DsvG11_0964 Tryptophan_synthase_alpha_chain
DsvG11_2469 Acetate_kinase
DsvG11_1193 3-isopropylmalate_dehydratase_small_subunit
DsvG11_0441 Nitrogen_fixation_protein_NifU
DsvG11_0724 Stomatin-like_protein_2
DsvG11_2450 Glyoxylate_reductase
DsvG11_0838 GMP_synthase_[glutamine-hydrolyzing]
DsvG11_2056 50S_ribosomal_protein_L16
DsvG11_1176 Ribonuclease_Y
DsvG11_2487 Fosforibosylaminoimidazolesuccinocarboxamide
DsvG11_2944 Cytosol_aminopeptidase
DsvG11_1043 Enoyl-[acyl-carrier-prot]_reductase_[NADH]_1
DsvG11_1899 Prokaryotic_integration_host_factor_signature
DsvG11_2892 TATA-binding_protein-associated_factor_MOT1
DsvG11_2480 Efflux_pump_membrane_transporter_BepE
DsvG11_1247 Cysteine_synthase
DsvG11_0147 GTP-binding_protein_TypA/BipA
DsvG11_0865 Ribonucleoside-diphosphate_reductase_NrdZ
DsvG11_0969 Anthranilate_synthase_component_1
DsvG11_2357 2,3-bisphosphoglycerate-independent
DsvG11_0998 6,7-dimethyl-8-ribityllumazine_synthase
DsvG11_1485 UPF0251_protein_HMPREF0179_01225
DsvG11_1309 50S_ribosomal_protein_L25
DsvG11_2895 D-methionine-binding_lipoprotein_MetQ
DsvG11_1859 Hypothetical_protein
DsvG11_2027 S-adenosylmethionine_synthase
DsvG11_0714 Transcription_elongation_protein_NusA
DsvG11_2064 50S_ribosomal_protein_L6
DsvG11_2072 30S_ribosomal_protein_S13
DsvG11_2879 Bacterial_extracellular_solute-binding_protein,
DsvG11_0044 30S_ribosomal_protein_S7
DsvG11_2961 ATP_synthase_F1,_epsilon_subunit
DsvG11_1860 Acetolactate_synthase_large_subunit
DsvG11_0067 NADP_transhydrogenase_subunit_beta
DsvG11_1833 Heavy-metal-associated_domain_profile.
DsvG11_1151 ATP-dependent_zinc_metalloprotease_FtsH
DsvG11_0774 Superoxide_dismutase_[Cu-Zn]_1
DsvG11_1729 Heat_resistant_agglutinin_1
DsvG11_1773 Ribonuclease_E
DsvG11_1741 Substrate-binding_region_of_ABC-type_glycine
DsvG11_2887 NAD-dependent_malic_enzyme
DsvG11_0476 Glucosamine/galactosamine-6-P_isomerase
DsvG11_0083 Branched-chain-amino-acid_aminotransferase
DsvG11_2688 Glutamate-1-semialdehyde_2,1-aminomutase
DsvG11_1888 Preprotein_translocase,_YajC_subunit
DsvG11_2694 50S_ribosomal_protein_L9
DsvG11_2208 Flagellar_filament_33_kDa_core_protein
DsvG11_0687 Prokaryotic_integration_host_factor_signature
DsvG11_1559 Hypothetical_protein
DsvG11_2433 Ribosome-recycling_factor
DsvG11_1679 Bifunctional_purine_biosynthesis_protein_PurH
DsvG11_0036 Outer_membrane_chaperone_Skp_OmpH
DsvG11_0130 Phosphoglycerate_kinase
DsvG11_2603 RutC__protein_y4sK
DsvG11_0137 Leu/Ile/Val-binding_protein_homolog_2
DsvG11_1289 TRM1-like_protein
DsvG11_2907 Adenosylhomocysteinase
DsvG11_1021 Peptidase_M16_inactive_domain_protein
DsvG11_2035 Flagellar_filament_33_kDa_core_protein
DsvG11_1663 Carboxy-terminal-processing_protease
DsvG11_1943 GAF_domain_protein
DsvG11_0484 Sulfide_dehydrogenase_subunit_alpha
DsvG11_0662 Glycine_reductasecomplexcomponent_Bsubunit
DsvG11_1360 Chemotaxis_protein_CheA
DsvG11_1694 Protein_HflK
DsvG11_2066 30S_ribosomal_protein_S5
DsvG11_2075 DNA-directed_RNA_polymerase_subunit_alpha
DsvG11_2048 30S_ribosomal_protein_S10
DsvG11_0660 Thioredoxin_reductase
DsvG11_1010 50S_ribosomal_protein_L11
DsvG11_2222 Outer_membrane_adhesin_like_proteiin
DsvG11_3016 Elongation_factor_Ts
DsvG11_2578 Argininosuccinate_synthase
DsvG11_2074 30S_ribosomal_protein_S4
DsvG11_2050 50S_ribosomal_protein_L4
DsvG11_2021 Dissimilatory_sulfite_reductase_D_DsrD
DsvG11_1927 Glutamate/Asp_periplasmic-binding_protein
DsvG11_0183 Sirohydrochlorin_cobaltochelatase_CbiKP
DsvG11_0992 Phosphopantetheine_attachment_site.
DsvG11_0872 Phosphoribosylformylglycinamidine_cyclo-ligase
DsvG11_0139 Glycosyl_transferase,_group_1_
DsvG11_2184 Periplasmic_nitrate_reductase
DsvG11_2691 Eukaryotic_RNA_Recognition_Motif_RRMprofile
DsvG11_2712 Protein_DVU_0534
DsvG11_1197 Phosphatidylserine_decarboxylase_proenzyme
DsvG11_2951 Fd_reductase-type_FAD_binding_domain
DsvG11_1886 Protein_translocase_subunit_SecF
DsvG11_1673 Tetratricopeptide
DsvG11_1303 Cysteine--tRNA_ligase
DsvG11_1102 4Fe-4S_ferredoxin_iron-sulfur_binding_domain
DsvG11_0539 Arginine--tRNA_ligase
DsvG11_0908 Stage_0_sporulation_protein_J
DsvG11_0547 4-hydroxybenzoate_decarboxylase_subunit_C
DsvG11_0158 Hdr-like_menaquinol_oxidoreductase_Cytochr
DsvG11_1739 Glycine_betaine_transport_ATP-binding_protein
DsvG11_2885 Fumarate_reductase_iron-sulfur_subunit
DsvG11_0346 Periplasmic_[Fe]_hydrogenase_large_subunit
DsvG11_0495 Translation_initiation_factor_IF-2
DsvG11_1715 High-molecular-weight_cytochrome_C
DsvG11_2030 Signaling_protein_YkoW
DsvG11_1419 UIT6__protein
DsvG11_0867 Mitochondrial_small_ribosomal_subunit_Rsm22
DsvG11_1352 Macrolide_export_ATP-binding/permease
DsvG11_1350 Glycosyltransferase_probably_involved_in_cell
DsvG11_1534 Lipopolysaccharide_biosynthesis_protein_RfbH
DsvG11_2550 Hypothetical_protein
DsvG11_0940 Erythronolide_synthase,_modules_3_and_4
DsvG11_2175 3-hydroxyacyl-[acyl-carrier-protein]_dehydratase
DsvG11_0328 6-carboxy-5,6,7,8-tetrahydropterin_synthase
DsvG11_2474 Enterobacterial_TraT_complement_resistance
DsvG11_3038 Flagellar_basal_body-associated_protein_FliL
DsvG11_2850 TolQ_protein
DsvG11_2661 Multidrug_resistance_protein_MdtB
DsvG11_2401 Hypothetical_protein
DsvG11_2125 ATP_synthase_protein_I
DsvG11_1764 Hydrogenase_expression/formation_HypE
DsvG11_1127 Methyltransferase_small_domain_protein


-3
0
3
4
Formate
Hydrogen
Coculture
R1 R2 R3 R1 R2 R3 R1 R2 R3
DsvG11_0342 TPR_repeat
DsvG11_0084 Hydantoinase/oxoprolinase
DsvG11_0190 Cupin_domain_protein
DsvG11_2561 GGDEF_domain-containing_protein
DsvG11_2893 Methionine_import_ATP-binding_protein_MetN
DsvG11_2988 Chaperone_protein_DnaJ
DsvG11_2714 Methyltransferase_type_12
DsvG11_2268 Cytochrome_C_biogenesis_transmembrane
DsvG11_1924 Glutamate/Asp_transport_ATP-binding_protein
DsvG11_1697 Ribonuclease_J_1
DsvG11_0517 Radical_SAM_domain_protein
DsvG11_1063 Molybdenum_cofactor_synthesis domain
DsvG11_2701 Hypothetical_protein
DsvG11_1856 Hypothetical_protein
DsvG11_2535 Zinc_ribbon_domain
DsvG11_2890 GTP_pyrophosphokinase
DsvG11_2730 Adenosylmethionine-8-amino-7-oxononaNoate
DsvG11_2004 DNA_translocase_FtsK
DsvG11_1094 NADH-quinone_oxidoreductase_subunit_D_1
DsvG11_0677 ErfK/YbiS/YcfS/YnhG__protein
DsvG11_0644 4-hydroxy-3-methylbut-2-en-1-yl_diphosphate
DsvG11_0298 Type_I_site-specific_deoxyribonuclease,_HsdR
DsvG11_0556 Cytidylate_kinase
DsvG11_2855 Polymerase/histidinol_phosphatase-like
DsvG11_2811 Flagellar_hook-length_control_protein
DsvG11_2645 2,3-dihydroxybenzoate-AMP_ligase
DsvG11_2538 Protein_of_unknown_function_DUF89
DsvG11_1762 N-acetyl-gamma-glutamyl-phosphate_reductase
DsvG11_1453 Lon_protease
DsvG11_1083 Hypothetical_protein
DsvG11_0982 Molecular_chaperone-like_protein
DsvG11_1059 Signal_recognition_particle_receptor_FtsY
DsvG11_2161 TPR_repeat_protein
DsvG11_1750 Histidine_kinase
DsvG11_0787 Cyclolysin_secretion/processing_ATP-binding
DsvG11_0138 Glycogen_debranching_enzyme
DsvG11_0414 UDP-N-actylglucosamin-N-actylmuramyl-pentpe
DsvG11_2595 Hydrolase,_P-loop
DsvG11_1731 Hypothetical_protein
DsvG11_0491 Precorrin-6Y_C5,15-methyltransferase
DsvG11_1224 Thymidylate_kinase
DsvG11_3021 GntR_bac_regulatory_protein_HTH_signature
DsvG11_1539 Glycosyl_transferases_group_1
DsvG11_2689 Transcriptional_regulators
DsvG11_1835 Glycerol-3-P_dehydrogenase_[NADP+]
DsvG11_2643 Phthiocerol_synthesis_polyketide_synthasetypel
DsvG11_2418 Lipid_A_exportATP-binding/permeaseprotMsbA
DsvG11_1811 ABC-type_Co2+_transport_system,_periplasmic
DsvG11_1637 Endonuclease_III
DsvG11_0858 Polysialic_acid_transport_protein_KpsD
DsvG11_1446 DNA_ligase
DsvG11_1845 o_ant_LIC12162:putativetransferase,LIC12162
DsvG11_0446 Aspartate/ornithinecarbamoyltransferaseAsp/Orn
DsvG11_0942 Capsule_polysaccharide_export_protein_BexD
DsvG11_2570 MutS2_protein
DsvG11_2106 Hypothetical_protein
DsvG11_1916 Flagellar_assembly_protein_FliH
DsvG11_1353 Bifunctional_protein_HtdE
DsvG11_0191 Carbamoyltransferase_hypF2
DsvG11_0207 L-serine_dehydratase
DsvG11_2624 Tetratricopeptide-like_helical
DsvG11_2000 Outer_membrane_protassembly_factor_BamD
DsvG11_0887 OLD__ATP-dependent_endonuclease
DsvG11_2684 Class_III_cytochrome_C_signature
DsvG11_1607 Cytochrome_c_class_I
DsvG11_1171 CsmC-like_protein
DsvG11_1174 Hypothetical_protein
DsvG11_0250 Putative_exonuclease,_RdgC
DsvG11_1921 Phosphoenolpyruvate_synthase
DsvG11_0885 Type_I_site-specific_deoxyribonuclease,_HsdR
DsvG11_1865 Hypothetical_protein
DsvG11_1714 Hypothetical_protein
DsvG11_1357 Rubredoxin-2
DsvG11_0811 Conserved_protein
DsvG11_1246 Chemotaxis_protein_CheV
DsvG11_2238 Phosphoribosylformylglycinamidine_synthase
DsvG11_2260 Transporter,_periplasmic_binding_prot,TRAP-T
DsvG11_2005 Outer_membrane_lipoprotein_carrier_prot_LolA
DsvG11_1074 Serine--pyruvate_aminotransferase
DsvG11_1872 Hypothetical_protein
DsvG11_2815 Stage_II_sporulation_protein
DsvG11_0565 Transcriptional_regulatory_protein_ZraR
DsvG11_1742 Methyl-accepting_chemotaxis_protein
DsvG11_2452 Serine_acetyltransferase,_plasmid
DsvG11_2364 Alkaline_fosfatase_synthesis_sensor_protein
DsvG11_1610 GTPase_Era
DsvG11_1442 ATP-dependent_Clp_protease_ATP-bindingsub
DsvG11_1458 Thiamine_biosynthesis_bifunctional_prot_ThiED
DsvG11_0579 Phosphoheptose_isomerase
DsvG11_2743 Alanine_racemase
DsvG11_2619 17_kDa_surface_antigen
DsvG11_1297 Redoxin_domain_protein
DsvG11_0599 Glutamine_amidotransferase_type_2_domain
DsvG11_0987 Uncharacterized_ACR,_COG1399
DsvG11_1117 Methyltransferase_type_11
DsvG11_1118 TonB-dependent_receptor
DsvG11_1119 Formylmethanofuran_dehydrogenase_subunit_E
DsvG11_0320 GTPase_Der
DsvG11_2980 L-lactate_permease
DsvG11_0989 Phosphate_acyltransferase
DsvG11_1451 ATP-dependent_Clp_protease_proteolytic_sub
DsvG11_3011 Tyrosine--tRNA_ligase
DsvG11_2122 50S_ribosomal_protein_L27
DsvG11_1635 Adenosine_kinase
DsvG11_1413 Fe-only_hydrogenase_maturation_rSAM_protein
DsvG11_0839 tatB;_twin_arginine-targeting_prot_translocase
DsvG11_0033 Adenylyl_cyclase_class-3/4/guanylyl_cyclase
DsvG11_0186 Prokaryotic_membrane_lipoprotein_lipid_atach
DsvG11_2073 30S_ribosomal_protein_S11
DsvG11_0055 8-amino-7-oxononaNoate_synthase
DsvG11_2053 30S_ribosomal_protein_S19
DsvG11_0223 Bifunctional_protein_PyrR
DsvG11_0821 50S_ribosomal_protein_L19
DsvG11_0841 Imidazoleglycerol-phosphate_dehydratase
DsvG11_1326 Hypothetical_protein
DsvG11_1164 Benzoylformate_decarboxylase
DsvG11_0886 DNA_helicase_II
DsvG11_2530 Transporter,_SSS_
DsvG11_0289 Phage_major_capsid_protein,_HK97_
DsvG11_0801 Electron_transport,_RnfABCDGE_typeG
DsvG11_1768 Hypothetical_protein
DsvG11_1482 Dihydroorotase
DsvG11_0918 DNA_gyrase_subunit_B
DsvG11_0860 RmlC-like_cupin_domain
DsvG11_0914 Histidine--tRNA_ligase
DsvG11_0699 3methyl2oxobutanoate_hydroxymethyltransferas
DsvG11_2466 RNA_polymerase-binding_protein_DksA
DsvG11_0663 Glycine_reductase_cmplx_component_B_subun
DsvG11_1748 Hypothetical_protein
DsvG11_2912 Alpha-helical_ferredoxin
DsvG11_1560 Copper-exporting_P-type_ATPase_A
DsvG11_0431 Methionine--tRNA_ligase
DsvG11_0665 Vi_polysacc_biosynthesis_protein_VipB/TviC
DsvG11_2984 Thiazole_synthase
DsvG11_1523 M18__aminopeptidase
DsvG11_2943 Porphyrin_biosynthesis_protein_HemD
DsvG11_1302 Ribose-5-phosphate_isomerase_B
DsvG11_2580 Carbamoyl-phosphate_synthase_small_chain
DsvG11_3104 Nucleoside_triphosphate_pyrofosfohydrolase
DsvG11_2347 NAD_dependent_epimerase/dehydratase
DsvG11_1572 Nickel_responsive_regulator
DsvG11_0878 UDP-N-acetylglucosamine
DsvG11_1474 Cupin_2_conserved_barrel_domain_protein
DsvG11_2865 Tryptophan--tRNA_ligase
DsvG11_2398 UvrABC_system_protein_A
DsvG11_1688 D-alanine--D-alanine_ligase
DsvG11_1760 Soluble_hydrogenase,_small_subunit
DsvG11_1160 Molybdopterin_biosynthesis_MoaE_protein
DsvG11_1682 Glucose-1-phosphate_cytidylyltransferase
DsvG11_1537 Acetolactate_synthase_isozyme_1_large_sub
DsvG11_2620 Trypsin
DsvG11_1870 All-trans-nonaprenyl-diphosphate_synthase
DsvG11_0915 Amidophosphoribosyltransferase_2,_chloroplastic
DsvG11_1137 ATP-dependent_protease_ATPase_sub_HslU
DsvG11_3035 Flagellum_site-determining_protein_YtkH
DsvG11_2957 Elongation_factor_4
DsvG11_2761 Potassium_efflux_system_KefA
DsvG11_2415 Phosphohexose_mutases
DsvG11_1671 Putative_zinc-_or_iron-chelating_domain
DsvG11_2015 DNA_repair_protein_RecN
DsvG11_2422 Flagellar_hook-associated_2_domain_protein
DsvG11_2857 Acting_on_peptide_bonds_Peptidases
DsvG11_2594 Carbohydrate_kinase,_YjeF_related_protein
DsvG11_1412 NA
DsvG11_0925 Transcriptional_regulatory_protein_FlbD
DsvG11_0666 Glycosyltransferase,_group_1__protein
DsvG11_0580 ADP-L-glycero-D-manno-heptose-6-epimerase
DsvG11_0648 GTP-dependent_nucleic_acid-binding_EngD
DsvG11_1611 UPF0001_protein_aq_274
DsvG11_1286 Relaxase/primase-like_fusion_protein
DsvG11_0786 Leukotoxin_secretion_protein_D
DsvG11_0764 Signal-transduction_and_transcriptional-control
DsvG11_0683 Imidazole_glycerol_fosfate_synthase_subunit
DsvG11_0189 Acyl-CoA_synthetase__member2,mitochondrial
DsvG11_0445 Phosphoglycolate_phosphatase
DsvG11_2875 Anaerobic_glycerol-3-fosfate_dehydrogenase
DsvG11_2575 Elongation_factor_G_2
DsvG11_0827 Phosphoenolpyruvate-protein_fosfotransferase
DsvG11_1298 Methionine_synthase
DsvG11_2317 Alkaline_fosfatase_domain-containing_protein
DsvG11_1300 Tetratricopeptide_TPR_2_repeat_protein
DsvG11_0324 High-affinity_branched-chain_aacid_transport
DsvG11_1226 5-nucleotidase_SurE
DsvG11_1915 Flagellar_motor_switch_protein_FliG
DsvG11_1557 Hypothetical_protein
DsvG11_1032 DNA_polymerase_I,_thermostable
DsvG11_0059 Asparagine_synthetase_[glutaminehydrolyzing]1
DsvG11_0144 Surface_antigen_D15
DsvG11_2240 RNA_polymerase_sigma-54_factor
DsvG11_0082 DNA_polymerase_III_subunit_gamma/tau
DsvG11_0533 Ribonuclease_R
DsvG11_2996 Aspartyl/glutamyl-tRNA_amidotransfrse,_C
DsvG11_1168 Hypothetical_protein
DsvG11_2320 Nuclease_SbcCD_subunit_C
DsvG11_0559 Hypothetical_protein
DsvG11_2473 Methyl-accepting_chmtxis_sensory_transducer
DsvG11_1930 HDIG_domain_protein
DsvG11_1873 UPF0272_protein_Moth_2512
DsvG11_0638 1-deoxy-D-xylulose-5-phosphate_synthase
DsvG11_1287 Hypothetical_protein
DsvG11_0005 Hypothetical_protein
DsvG11_0840 Sec-independent_prot_translocase_prot_TatC
DsvG11_0216 Peptide_chain_release_factor_1
DsvG11_2533 Predicted_ATP-dependent_protease
DsvG11_0300 Super_I_DNA_and_RNA_helicases_&_helicase
DsvG11_0835 30S_ribosomal_protein_S16
DsvG11_3023 L-cysteate_sulfo-lyase
DsvG11_1366 Chemotaxis_response_regulator_prot-glutamate
DsvG11_1295 MJ0042__finger-like_protein
DsvG11_0877 Transport-associated
DsvG11_0548 Glutamine-dependent_NAD+_synthetase
DsvG11_0165 Indolepyruvate_oxidoreductase_subunit_iorB
DsvG11_0343 AMIN_domain
DsvG11_2520 Hypothetical_protein
DsvG11_1299 RNA_polymerase_sigma-B_factor
DsvG11_0123 Phenylalanine--tRNA_ligase_alpha_subunit
DsvG11_0975 Amidohydrolase
DsvG11_1832 Copper-exporting_P-type_ATPase_A
DsvG11_0106 Hypothetical_protein
DsvG11_0843 1-5-phosphoribosyl-5-[5-fosforibosylamome
DsvG11_1126 YcaO-domain_protein
DsvG11_0413 UDP-N-acetylmuramate--L-alanine_ligase
DsvG11_2835 Type_III_restriction-modification_system_EcoPI
DsvG11_2938 L-glutamine:2-deoxy-scyllo-inosose
DsvG11_1670 4Fe-4S_Fd-type_iron-sulfur_binding_domain
DsvG11_0990 DSBA_oxidoreductase
DsvG11_1069 Ferrous_iron_transport_protein_B
DsvG11_2534 Porphobilinogen_deaminase
DsvG11_0700 Agmatinase_1
DsvG11_1988 Peptidase_M23
DsvG11_2759 Thiamine-phosphate_synthase
DsvG11_1249 Dihydrolipoyl_dehydrogenase
DsvG11_1528 Tim44_domain_protein
DsvG11_2232 Hypothetical_protein
DsvG11_1850 SirA__protein
DsvG11_1839 4Fe-4S_binding_domain_protein
DsvG11_0033 Acyl_transferase
DsvG11_0897 PE-PGRS__protein
DsvG11_0325 High-affinity_branched-chainaminoacidtransport
DsvG11_1129 Ribosomal_protein_L11_methyltransferase
DsvG11_2476 DNA_topoisomerase_1
DsvG11_2221 Glutamine--tRNA_ligase
DsvG11_1996 Fructose-1,6-bisphosphatase_class_1
DsvG11_1580 Molybdenum_cofactor_synthesis_domainprotein
DsvG11_0051 Multidrug_resistance_efflux_pump-like
DsvG11_1210 Ornithine_carbamoyltransferase
DsvG11_2933 Type_III_pantothenate_kinase
DsvG11_1658 Biosynthetic_arginine_decarboxylase
DsvG11_1173 Bifunctional_protein_GlmU
DsvG11_1234 Pyruvate_ferredoxin/flavodoxin_oxidoreductase
DsvG11_2355 Phenylacetate-coenzyme_A_ligase
DsvG11_2160 Tetratricopeptide_TPR_2_repeat_protein
DsvG11_0669 Threonine_synthase
DsvG11_0228 SurA_N-terminal_domain_protein
DsvG11_0502 Membrane_protein_insertase_YidC
DsvG11_0679 Adenylosuccinate_lyase
DsvG11_2641 Bacitracin_synthase_1
DsvG11_2460 Predicted_Fe-S_oxidoreductases
DsvG11_0204 Methylthioribose-1-phosphate_isomerase
DsvG11_1542 Radical_SAM
DsvG11_0168 Gamma-glutamyl_phosphate_reductase
DsvG11_2416 Xanthan_biosynthesis_protein_XanB
DsvG11_0418 UDPNacetylmuramoyltripeptide-D-alanyl-D-alani
DsvG11_0960 Hypothetical_protein
DsvG11_3107 Formylmethanofuran_dehydrogenase,_sub_E
DsvG11_1790 NAD-dependent_dehydrogenase_subunit
DsvG11_0763 Sulfoacetaldehyde_acetyltransferase
DsvG11_0922 Peptidase_M23
DsvG11_2628 Sulfatase-modifying_factor_1_Flags
DsvG11_1452 ATP-dependent_Clp_protease_ATP-bindingsub
DsvG11_1448 Short-chain_dehydrogenase/reductase_SDR
DsvG11_1361 Response_regulator_receiver_protein

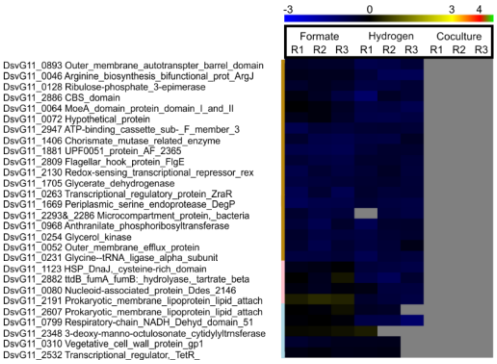

Fig. S4.4. Heat map of hierarchical clustered proteins produced by *Desulfovibrio desulfuricans*. The proteins are shown in a clustered matrix after column Z-score normalization and automatic hierarchical columns clustering. Three growth conditions, in triplicates, are shown according to the electron donor used; from left to right: formate, hydrogen and compounds transferred from *Syntrophobacter fumaroxidans*. The colour scale represents the relative detection level of each protein across the samples; blue log ratio -3, yellow log ratio 3, red log ratio 4 and green log ratio 4.5 indicate lower and higher levels compared to the average level value in black, respectively. The colour intensity indicates the degree of protein up- or down regulation; the grey colour represents not detected.

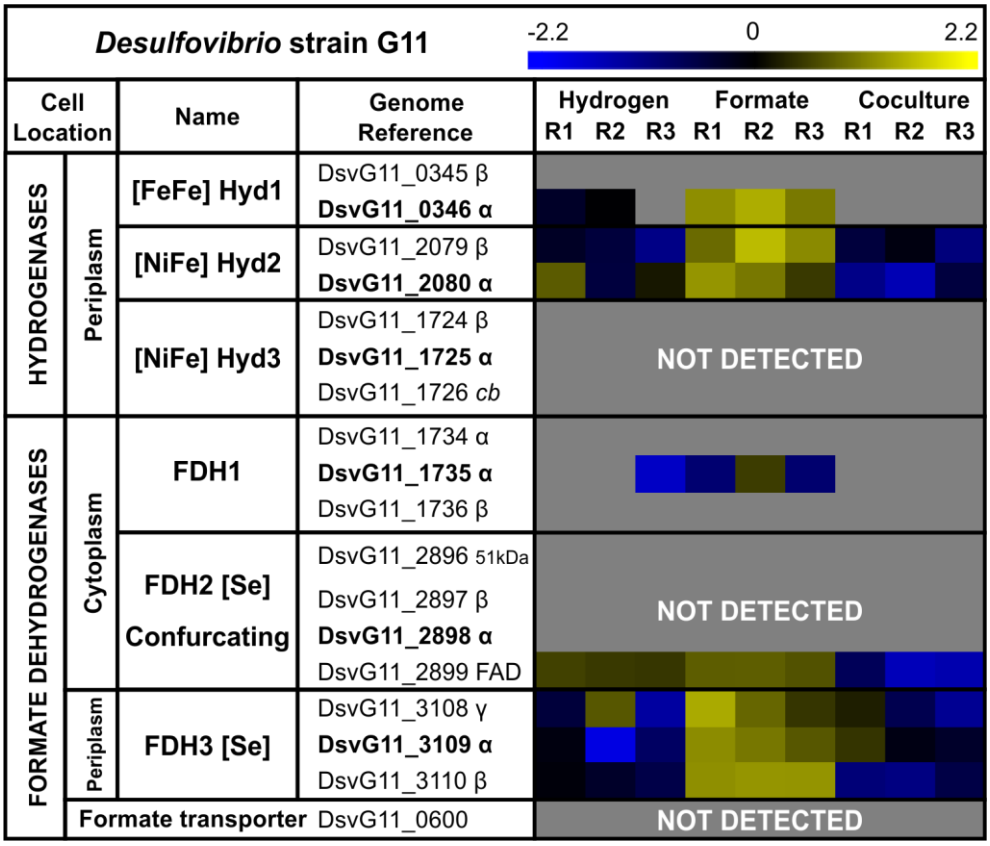

Fig. S4.5. Normalized expression matrix of hydrogenases and formate dehydrogenases of *Desulfovibrio desulfuricans*. The rows in the heat map show proteins levels after row Z-score standardization in three different growth conditions. The columns show from left to right, in triplicates, the electron donor used by *D. desulfuricans*: hydrogen, formate and interspecies compounds transferred from *Syntrophobacter fumaroxidans*. The colour scale indicates the degree of protein down- or up regulation ranging from blue (-2.2 log ratio), to yellow (2.2 log ratio). The colour intensities indicate lower and higher levels compared to the average level 0 value (in black); the grey colour represents not detected. Subunits are indicated after the locus tag.


-2.5
0
2.5
3
Fumarate
Sulfate
D. des
M. form
M. hung
R1 R2 R3 R1 R2 R3 R1 R2 R3 R1 R2 R3 R1 R2 R3
-2.5
0
2.5
3
Fumarate
Sulfate
D. des
M. form
M. hung
R1 R2 R3 R1 R2 R3 R1 R2 R3 R1 R2 R3 R1 R2 R3

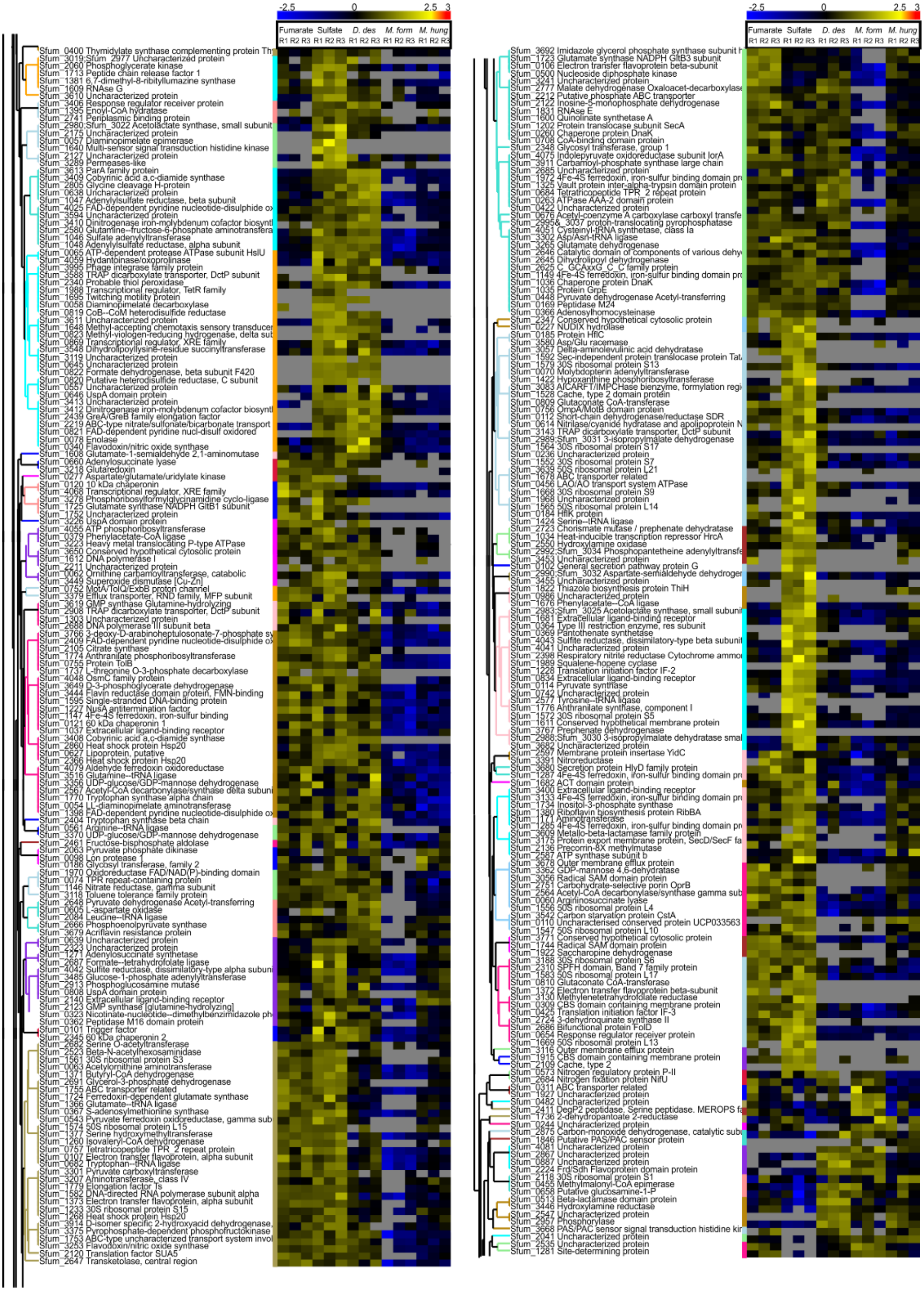
-2.5
0
2.5
3
Fumarate
Sulfate
D. des
M. form
M. hung
R1 R2 R3 R1 R2 R3 R1 R2 R3 R1 R2 R3 R1 R2 R3

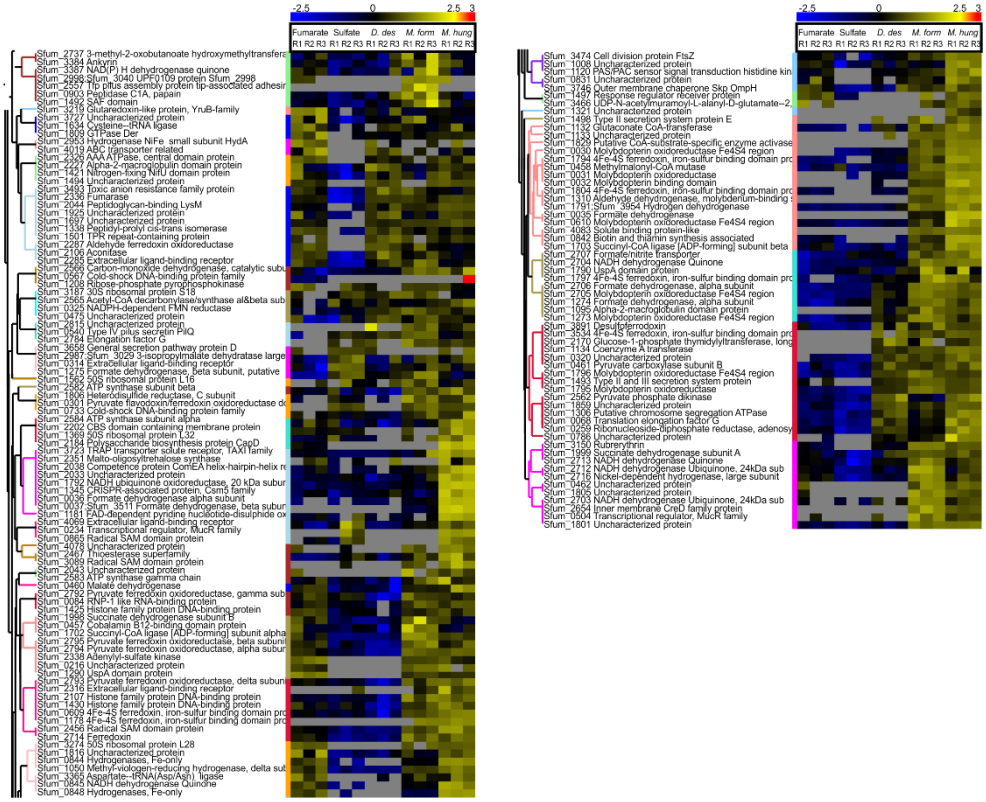

Fig. S4.6. Heat map of hierarchical clustered proteins produced by *Syntrophobacter fumaroxidans* for propionate degradation. The proteins are shown in a clustered matrix after automatic hierarchical cluster of rows from row Z-score normalization values. Proteins appear from left to right, in triplicates, according to the growth conditions defined by the electron acceptor used by *S. fumaroxidans* to oxidize propionate: fumarate, sulfate and interspecies compounds transferred to: *Desulfovibrio desulfuricans*, *Methanobacterium formicicum* and *Methanospirillum hungatei*. The colour scale illustrates the relative detection level of each protein across the samples; blue log ratio -2.5, yellow log ratio 2.5 and red log ratio 3 indicate lower and higher levels compared to the average level value 0 in black. The colour intensity indicates the degree of protein up- or down regulation; the grey colour represents not detected.

Fig. S4.7 Schematic representation of energy converting complexes and proteins involved in sulfate reduction in *Syntrophobacter fumaroxidans* during propionate oxidation.

Proteins not detected
Only detected in growth with sulfate
Abundant in all conditions
Abundant in all conditions but in sulfate
Abundant in syntrophic conditions
Abundant in axenic conditions
Hyd2
FDH3
FDH5
FDH2
Hyn
FDH4
FDH1
Hyd1
Hox
Fumarate
Succinate
SdhABC
FrdABEF
Fhl-h
Fhl-f
Formate
DsrMKJOP
QrcABCD
QmoABC
DsrAB
Hdr:Mvh-p
Hdr:Flox
AprAB
APSk
Sat
APS
Frh
MvhADG/HdrABC I
MvhADG/HdrABC II
Nuo
Ohc
Cyt bd

One need not make it first…

but one must know how to make it!

Chapter 5

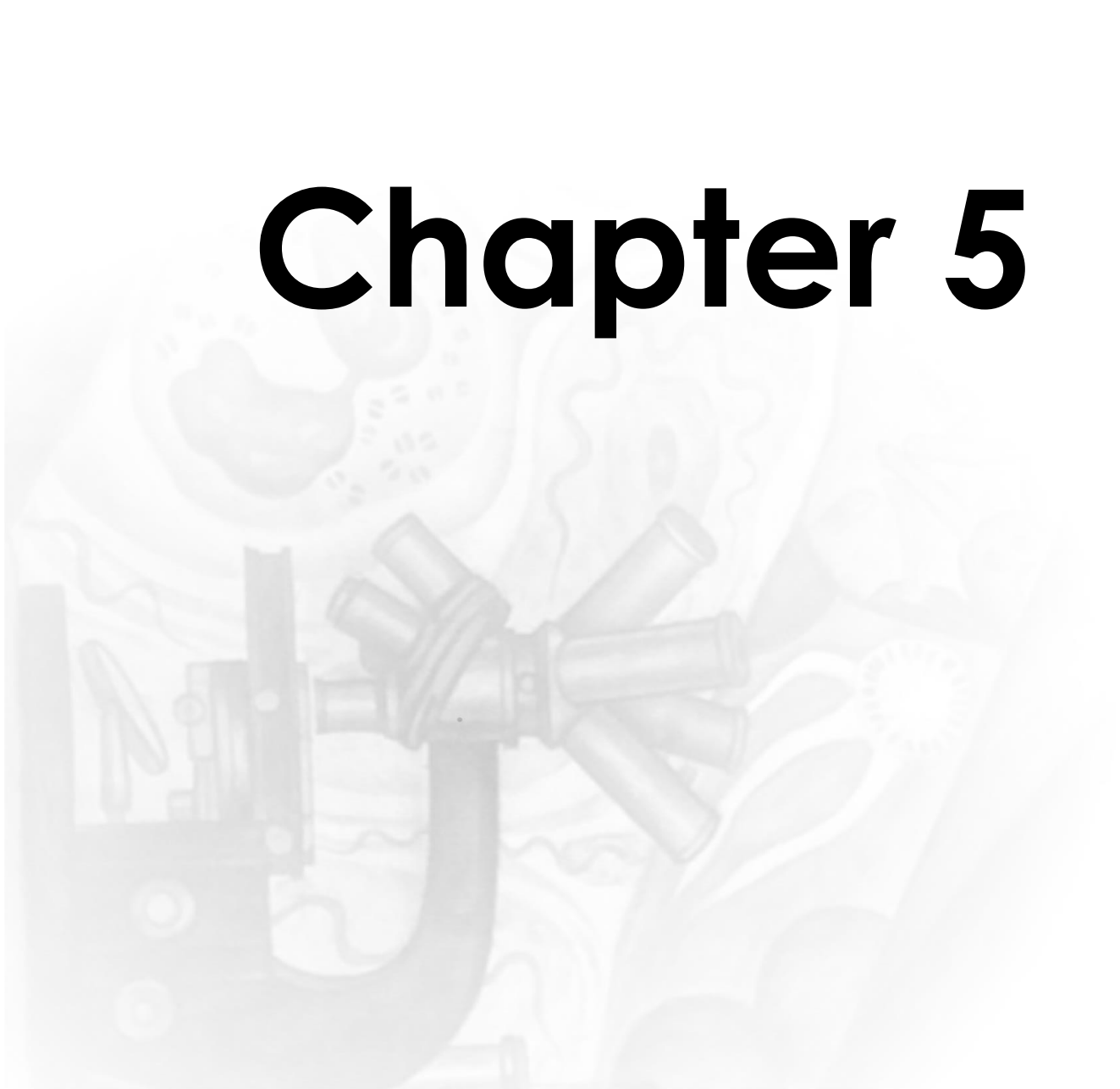

CHAPTER 5

Proteomic analyses of *Methanospirillum hungatei* and *Methanobacterium formicicum* grown in a syntrophic partnership with *Syntrophobacter fumaroxidans* and in pure culture with H_2/CO_2 or formate.

Vicente T. Sedano-Núñez[1], Sjef Boeren[2], Caroline M. Plugge[1] and Alfons J. M. Stams[1]

[1]Laboratory of Microbiology, Wageningen University and Research, The Netherlands

[2]Laboratory of Biochemistry, Wageningen University and Research, The Netherlands

Submitted for publication

Abstract

The hydrogenotrophic methanogens *Methanospirillum hungatei* and *Methanobacterium formicicum* are frequently used as syntrophic partners in methanogenic cocultures. We performed a proteomic analysis of these methanogens grown on H_2/CO_2, formate and in syntrophy with the propionate-degrading bacterium *Syntrophobacter fumaroxidans*. We identified the most abundant proteins used for methane formation and energy conservation, and discussed differences among the cultured conditions and between the methanogens. *M. formicicum* uses a F_{420}-non-reducing hydrogenase (MvhADG) for bifurcation to couple the final methane-producing step catalysed by heterodisulfide reductase (Hdr), to the initial CO_2-reducing step catalysed by formylmethanofuran dehydrogenase (Fmd). *M. hungatei* lacks the MvhAG subunits of the F_{420}-non-reducing hydrogenase MvhADG, instead it employs an F_{420}-reducing hydrogenase (FrhADGB). Moreover, F_{420}-dependent formate dehydrogenases are also used by both methanogens, predominantly in syntrophic growth, for bifurcation. Differential production of enzymes such as Mcr, Mrt and Hdr were found in the methanogenic pathway as well as in diverse extracellular structures such as archaellum and pili. Although both methanogens can grow on hydrogen and formate, the molecular mechanisms analysed in this study, points to the use of hydrogen in *M. formicicum*, and of formate in *M. hungatei*, as electron carriers in their metabolism.

Keywords: Methanogenesis, hydrogen, formate, electron transfer, electron bifurcation, syntrophy, Methanomicrobiales, Methanobacteriales.

Introduction

Hydrogenotrophic methanogens grow by reducing CO_2 with hydrogen to methane. Many hydrogenotrophic methanogens are also able to use formate for growth (Thauer et al., 2008). Methanogens play an essential role in degradation of volatile fatty acids by removing the excess of hydrogen produced by acetogenic bacteria. In the absence of inorganic electron acceptors, the overall anaerobic degradation of fatty acids becomes energetically feasible only at low hydrogen and formate concentrations (Schink, 1997; McInerney et al., 2008; McInerney et al., 2009; Stams and Plugge, 2009). The capacity of the methanogens to keep concentrations of hydrogen and formate very low has been used to obtain syntrophic cocultures with anaerobic acetogenic bacteria degrading butyrate (McInerney et al., 1979), propionate (Boone and Bryant, 1980) and acetate (Zinder and Koch, 1984) among other short and long chain fatty acids (Sousa et al., 2007). Since these methanogenic partners can use both hydrogen and formate, the role of each in interspecies electron transfer (IET) is not clear. The importance of formate as electron carrier in IET was addressed before (Boone et al., 1989), particularly in the syntrophic degradation of propionate (Dong et al., 1994; Dong and Stams, 1995; de Bok et al., 2002b).

In this study, we investigated the metabolism of two hydrogenotrophic methanogens growing in pure culture with formate or H_2/CO_2. Furthermore, we compared the axenic growth of these methanogens to their growth as syntrophic partners of *Syntrophobacter fumaroxidans* strain MPOB^T, a propionate-degrading bacterium. *Methanospirillum hungatei* strain JF1^T is a formate- and hydrogen-utilizing methanogen (Ferry and Wolfe, 1976) and the model partner of *S. fumaroxidans* (Stams et al., 1993). The draft genome of *M. hungatei* has been analysed (Worm et al., 2011b), and its complete genome sequence was described (Gunsalus et al., 2016). *Methanobacterium formicicum* strain MF^T is another hydrogen- and formate-utilizing methanogen (Bryant and Boone, 1987) which also has been used in syntrophic studies with *S. fumaroxidans* (Dong et al., 1994; Worm et al., 2011b) and to obtain defined syntrophic associations with *Pelotomaculum schinkii* (de Bok et al., 2005) and *Syntrophomonas zehnderi* (Sousa et al., 2007). Although the genome of the neotype strain *Methanobacterium formicicum* MF^T and of a strain of rumen origin *M. formicicum* BRM9 are available, their analysis is limited (Kelly et al., 2014; Maus et al., 2014).

Here, we extended the genomic analysis of *M. formicicum* and with a proteomic analysis of both methanogens we studied and compared their metabolism in the three culture conditions. Our aim was to pinpoint the key enzymes that vary between the two electron donors, H_2 and formate, and between axenic and syntrophic growth, as well as to understand the differences between the two methanogens.

Materials and methods

Organisms and growth conditions

Cocultures of *Syntrophobacter fumaroxidans* MPOB^T (DSM 10017) with *Methanospirillum hungatei* JF1^T (DSM 864) or with *Methanobacterium formicicum* MF^T (DSM 1535) were grown with 30 mM of propionate without electron acceptor in anaerobic medium as described previously (Stams et al., 1993). Axenic cultures of *M. hungatei* and *M. formicicum* were grown with 40 mM formate or with hydrogen (1.7 atm H_2/CO_2 80:20 vol/vol) and supplemented with 1 mM of acetate. All microorganisms were batch cultured in triplicate at 37 °C in 1-litre flasks with 550 ml medium under anaerobic conditions provided by a gas phase of 172 kPa (1.7 atm) N_2/CO_2, or H_2/CO_2 (80:20, vol/vol) when hydrogen was required. Cells were harvested during mid-exponential growth phase. The cultures for the experiment were inoculated with cells from cultures that were transferred at least ten times on their respective electron donor before the start of the experiment.

Harvesting cells and Percoll gradient centrifugation

Cells were aerobically harvested by centrifugation at 16,000 g for 16 minutes at 4 °C. The pellet was washed twice with TE buffer (10 mM Tris-HCl, pH 7.5; 1 mM EDTA). Only cells from the syntrophic coculture of *S. fumaroxidans* and *M. hungatei* were separated by Percoll gradient centrifugation (Percoll®, Sigma-Aldrich, MO) as described elsewhere (de Bok et al., 2002a). The separated layers, containing *Syntrophobacter* cells in the upper layer and *Methanospirillum* cells in the lower layer, were collected and subjected to Percoll gradient separation a second time. Cells were then washed twice with 10 mM sodium phosphate buffer (pH 7.5).

Protein extraction and SDS-PAGE

Cells were resuspended in lysis buffer (100 mM Tris-HCl, pH 7.5; 4% w/v SDS; 50 mM dithiothreitol and SIGMAFAST™ Protease Inhibitor Cocktail Tablet (Sigma-Aldrich, MO)), and passed three times through a French press (French® Type Pressure Cell Disrupter, Stansted Fluid Power, Harlow, UK) at 2 MPa (40K cell). Cell debris and undisrupted cells were removed by centrifugation at 18,000 g for 10 min at 4 °C. The supernatant was collected in Eppendorf™ LoBind Protein Microcentrifuge Tubes and stored at -80 °C. Still in the lysis buffer, proteins were denatured by heating at 95 °C for 5 minutes. Samples were loaded on a 10% polyacrylamide separation gel (25201, Precise™ Tris-HEPES Gels, Thermo Scientific, Rockford, US) using the Mini-PROTEAN Tetra Cell (Bio-Rad Laboratories B.V, Veenendaal, The Netherlands). The electrophoresis procedure was according to the precast gels manufacturer's instructions. Gels were stained using Coomassie Brilliant Blue (CBB) R-250. Protein concentration was normalized among triplicates

and samples in a qualitative way by analysing the gel pictures taken with G:BOX Chemi XT4 (Syngene, Cambridge, UK) and using the software GeneSys version 1.5.5.0 (GeneTools version 4.03.01).

In-gel trypsin digestion

In-gel digestion of proteins and purification of peptides was done following a modified version of a previously described protocol (Rupakula et al., 2013). Disulfide bridges in proteins were reduced by covering the gels with reducing solution (10 mM dithiothreitol, pH 7.6, in 50 mM NH_4HCO_3), and the gels were incubated at 60 °C for 1 h. Alkylation was performed in darkness and shaking (100 rpm) for 1 h by adding 25 ml of iodoacetamide solution (10 mM iodoacetamide in 100 mM Tris-HCl, pH 8.0). Gels were thoroughly rinsed with demineralized water in between steps. Each gel lane was cut into 3 slices, and the slices were cut into approximately 1 mm^3 cubes and transferred to a separate 0.5 ml protein LoBind tube (Eppendorf, Hamburg, Germany). Enzymatic digestion was done with trypsin sequencing grade (Roche, Mannheim, Germany). 100 µl of trypsin solution (5 ng/ µl trypsin in 50 mM NH_4HCO_3) were added to each tube, and incubated 2 hours at 45 °C with gentle shaking. To stop trypsin digestion, trifluoroacetic acid (10 %) was added to the supernatant to lower the pH below 5. The digested protein mixture was purified and concentrated using an in-house made SPE pipette tip (Lu et al., 2011).To recover hydrophobic peptides, 50 µl acetonitrile (vol/vol in 0.1% formic acid) was passed through the column. Finally, the volume was reduced to 20 µl using a SpeedVac concentrator and then adjusted to 50 µl with 0.1% formic acid. Samples were analysed using nLC–MS/MS with a Proxeon EASY nLC and a LTQ-Orbitrap XL mass spectrometer as previously described (Lu et al., 2011).

LC–MS data analysis

The obtained MS/MS spectra were processed with MaxQuant v. 1.5.2.8. Databases with the protein sequences of the organisms involved in the study were downloaded from UniProt (www.uniprot.org). An additional dataset with protein sequences of common contaminants (trypsin, human keratins and bovine serum albumin) was included. False discovery rates (FDR) of less than 1% were set at peptide and protein levels. Modifications for acetylation (Protein N-term), deamidation (N, Q) and oxidation (M) were allowed to be used for protein identification and quantification. All other quantification settings were kept default. Filtering and further bioinformatics and statistical analysis were performed with Perseus v.1.5.3.0. Proteins included in our analysis contain at least two identified peptides of which at least one is unique and at least one unmodified. Reversed hits and contaminants were filtered out. Protein groups were filtered to require three valid values in at least one experimental group. Label-free quantification (LFQ) intensities (values normalized with respect to the total amount of protein and all its identified peptides)

were used to analyse the abundance of proteins in the fractions and further statistical comparisons among conditions. LFQ intensities were transformed to logarithmic values base 10. Missing values were imputed with random numbers from a normal distribution, the mean and standard deviation of which were chosen to best simulate low abundance values close to noise level (Width: 0.3 and downshift 1.8 times). A multiple-sample test (ANOVA) with permutation based FDR statistics (250 permutations, FDR=0.01 and S0=1) was applied to filter significant proteins. PCA were performed with default settings and without category enrichment in components. Z-score normalization in which the mean of each row (where each row is a protein in triplicate and in different conditions) is subtracted from each value and the result divided by the standard deviation of the row was applied before clustering. Hierarchical clustering of rows, using Euclidean distances, produced a heat map representation of the clustered data matrix. Row clusters were automatically defined and exported to a new matrix. Imputed values were then replaced back to missing values and previously defined clusters were displayed in a new heat map.

Genome analysis of Methanobacterium formicicum

Amino acid sequences of protein coding genes for methanogenesis and energy conservation in *M. hungatei* were obtained from the Integrated Microbial Genomes (IMG) system in DOE-Joined Genome Institute (Version 4.560 Mar. 2016). Such sequences were used to retrieve similar functional genes in the genome of *M. formicicum* using the BLAST (Altschul et al., 1990) service of the IMG website. The locus tags assigned to the genes of *M. formicicum* in UniProt are referred to as DSM1535_xxxx, where the x indicate the gene numbers. For practical purposes in this study we refer to the locus tag of *M. formicicum* as Mfor_xxxx. Amino acid sequences obtained from the best hits were then analysed with InterProScan 5 (version 5RC7, 27th January 2014) to corroborate the presence of key functional domain profiles. TMHMM Server v. 2.0 (Krogh et al., 2001) was used to identify transmembrane helices and the Tat P 1.0 Server of CBS was used to predict twin-arginine translocation (Tat) motifs (Bendtsen et al., 2005).

Results and discussion

Proteomic profiles and most abundant proteins

The genome of *M. hungatei* predicts 3,239 protein-coding genes (Gunsalus et al., 2016). Our proteome analysis detected 825 proteins, of which 149 proteins are without known function. The core proteome of *M. hungatei* consisted of 625 proteins which were detected in all studied conditions. 186 proteins were detected only in the axenic conditions, namely formate- and hydrogen-grown cells, but not in syntrophically grown cells **(Supporting information, Fig. S5.1.A)**. The number of

proteins detected in the syntrophic growth condition, only 631, was substantially lower than the amount obtained in the hydrogen and formate conditions with more than 800 proteins each. Considering that the protein extraction was equally successful, and the protein concentration analysed was the same for all studied conditions, this difference in the number of proteins detected was unexpected. This may indicate a more constrained metabolism when the methanogen grows in syntrophy and is limited by the efficiency of the bacterial partner to provide hydrogen, formate and possibly other compounds. The few exclusive proteins for each condition were without predicted function.

The genome of *M. formicicum* has only 2,409 protein-coding genes (Maus et al., 2014). Our study resulted in the detection of 716 proteins of which 117 are with unknown function. The core proteome comprises 574 proteins present in all conditions. 137 proteins were exclusively detected in cells grown with hydrogen or formate, but not in syntrophically grown cells. **(Supporting information, Fig. S5.1.B)**. Similarly, as in *M. hungatei*, the number of proteins obtained from syntrophically grown cells (576) was lower than that obtained from pure cultures. A lower number of proteins detected in syntrophically grown cells indicate, for both methanogens, that during syntrophic growth a restricted set of proteins are produced to perform methanogenesis.

Principal component analysis (PCA) was used to determine the protein abundance variation of the samples according to the different electron donors used for growth: hydrogen, formate or compounds derived from *S. fumaroxidans* **(Figure 5.1)**. For both methanogens, the first principal component (PC1; ~76% of total variance) clearly separates the proteomic profiles of the syntrophic conditions from those in axenic growth. However, PC1 does not establish a difference between growth on hydrogen or on formate for any of the methanogens. The second principal component in *M. hungatei* (PC2; 7% of total variance) differentiates the three growth conditions. However, for *M. formicicum*, PC2 does not differentiate between growth with formate and the syntrophically grown cells, with the notable exception of one triplicate of the latter. Nevertheless, PC2 accounts for only 6.3% of the variability of the data.

Methanogenesis pathway

All the proteins previously predicted to be involved in the production of methane from hydrogen + CO_2 and formate by *M. hungatei* (Gunsalus et al., 2016) were abundant in our study. For *M. formicicum,* we performed our own genomic analysis to manually reconstruct the methanogenic pathway and verified the production of the predicted proteins with the proteomic results.

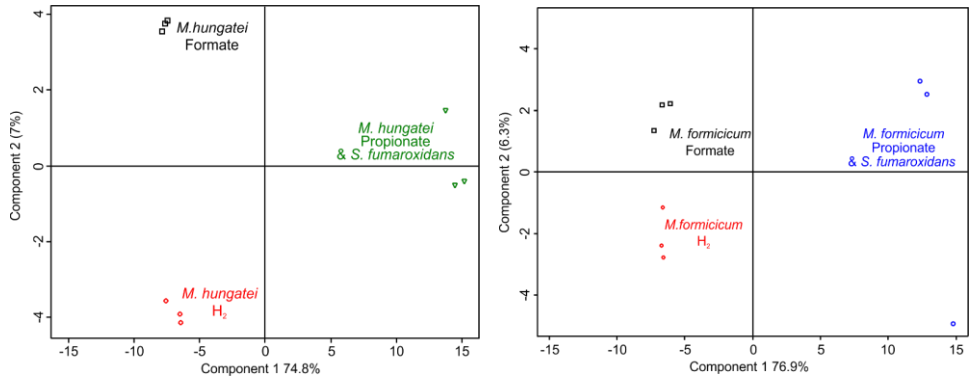

Figure 5.1. Principal Component Analysis performed for *Methanospirillum hungatei* (left) and *Methanobacterium formicicum* (right) proteins produced in three growth conditions. Symbols: red diamonds, hydrogenotrophic conditions; black squares, growth with formate; Green triangles and blue circles correspond to the cocultured partnership of *M. hungatei* and *M. formicicum* respectively with *Syntrophobacter fumaroxidans*.

The first step in methanogenesis from CO_2 is catalysed by a formylmethanofuran dehydrogenase. Two isoenzymes have been found in methanogens, a tungsten-containing isoenzyme (Fwd) and a molybdenum-containing isoenzyme (Fmd) (Thauer, 1998). Both isoenzymes present in the thermophilic methanogen *Methanothermobacter marburgensis* strain Marburg have been purified and studied further (Hochheimer et al., 1995; Hochheimer et al., 1996; Hochheimer et al., 1998). Moreover, genomic and amino acid sequence comparisons have shown that the catalytic subunits of molybdenum isoenzymes (*fmdB*), such as the one from *Methanosarcina barkeri*, are more closely related to the molybdenum isoenzymes than to the tungsten isoenzymes from *M. marburgensis* or *Methanothermobacter wolfeii* (Vorholt et al., 1997). We compared the amino acid sequences of the three catalytic subunits found in *M. hungatei* (*mhun_1983*, *mhun_1988, mhun_1994*) and the one found in *M. formicicum* (Mfor_1495) to all the known *fmdB* and *fwdB* sequences used in the analysis of (Vorholt et al., 1997). All the sequences of the catalytic subunits of *M. hungatei* and *M. formicicum* are less than 45% identical to the molybdenum *fmdB* from *M. barkeri*, *M. marburgensis* and *M. wolfeii*. In contrast, the identities to the tungsten *fwdB* from *M. marburgensis, M. wolfeii, Methanocaldococcus jannaschii* and *Methanopyrus kandleri* were in all cases above 45%. Although it has been implied that the tungsten isoenzyme FwdB prevails in thermophilic and hyperthermophilic methanogens (Hochheimer et al., 1998), a tungsten FwdB is presumably present in the mesophilic *Methanosarcina acetivorans* and *M. barkeri* (Matschiavelli and Rother, 2015). Therefore, it is possible that *M. hungatei* and *M. formicicum* contain the tungsten isoforms of formylmethanofuran dehydrogenase.

Of the three sets of formylmethanofuran dehydrogenases (Fmd/Fwd) in *M. hungatei*, the enzyme encoded in Mhun_1981-1984 was predominant in all the analysed conditions. The Fmd/Fwd encoded in Mhun_1987-1994 was not detected and only the major subunits of the third Fmd/Fwd (Mhun_2106-2112) were detected in our analysis **(Figure 5.2)**. For *M. formicicum* only one Fmd/Fwd was found encoded in the genome (Mfor_1492-1497) and its proteins were constitutively detected in our analysis. Other minor subunits such as Fmd/Fwd-E, Fmd/Fwd-F and Fmd/Fwd-G were found elsewhere encoded in the genome (Mfor_1518 & 1521, Mfor_1527 and Mfor_1528 respectively) and abundant in the proteome. Interestingly, subunit Fmd/Fwd-F contains a polyferredoxin that is believed to be the ferredoxin that mediates electron transfer to Fwd/Fmd after bifurcation from the complex Hdr/Mvh (Hochheimer et al., 1995; Costa et al., 2010). Therefore, the production of these kind of proteins might be related to the transfer of electrons in the metabolic processes.

Of the three methenyl-tetrahydromethanopterin (methenyl-H4MPT) cyclohydrolases (Mch) predicted in the genome of *M. hungatei*, Mch2 (Mhun_0444) was the most abundant and detected in all conditions, while Mch1 (Mhun_0022) was only detected in axenic conditions and Mch3 (Mhun_2384) was not detected at all. In *M. formicicum*, two formylmethanofuran-H4MPT formyltransferases (Ftr1: Mfor_1101 and Ftr2: Mfor_2022) were detected in all conditions, although Ftr1 was significantly more abundant than Ftr2.

Methylene-H4MPT dehydrogenase (Mtd) and methylene-H4MPT reductase (Mer) were detected in high levels in both methanogens. In *M. hungatei* these enzymes were significantly more abundant in syntrophically grown cells while in *M. formicicum* they were constitutively produced at the studied conditions. Mtd and Mer play an important role in re-oxidation of cofactor F_{420}, and, excluding a couple of histones, were the most abundant proteins together with methyl-coenzyme M reductase (Mcr) in both methanogens.

M. formicicum contains two isoenzymes of methyl-CoM reductase: isoenzyme I (McrABG) encoded by the transcription of *McrAGCDB* and isoenzyme II (MrtABG) encoded by *MrtAGDB* **(Figure 5.2)**. Mcr (Mfor_0905-0909) was detected in significantly higher levels in syntrophically grown cells. Mrt (Mfor_1092-1095) on the other hand was not detected in syntrophic conditions, but very high levels were found in axenically grown cells.The transcription of *Mcr* and *Mrt* is dependent on the growth phase and substrate availability. While *Mrt* is mainly transcribed in the early exponential phase, *Mcr* is preferably expressed in the late exponential growth phase (Bonacker et al., 1992; Morgan et al., 1997). We harvested our cells during mid-log phase, so we can only speculate whether the absence of Mrt in syntrophically grown cells with *S. fumaroxidans* corresponds to a slight difference in the time of harvest or to the limited supply of hydrogen or formate during syntrophic conditions.

In both methanogens subunit McrC of methyl-CoM reductase was not detected, while McrD and MrtD were detected in lower levels than the rest of the methyl-CoM reductase subunits. The function of these subunits is not known, although a role in the activation of the enzyme and in posttranslational modifications, respectively, has been proposed (Prakash et al., 2014; Zheng et al., 2016).

Finally, the membrane-bound H4MPT S-methyltransferase (Mtr) and the soluble heterodisulfide reductase (Hdr) were consistently detected in both methanogens grown at the different conditions. Nevertheless, subunit HdrA (Mhun_1838) in *M. hungatei* was significantly more abundant in syntrophically grown cells. The catalytic site of the heterodisulfide reductase is located in subunit HdrB (Mhun_1837), but HdrA contains the FAD-binding domain and four [4Fe-4S] clusters that allegedly make this subunit the site where electron bifurcation takes place (Hedderich et al., 1994; Hamann et al., 2007). In the genome of most methanogens, HdrA is non-adjacent to HdrBC, consistent with the possible use of HdrA in other complexes besides Hdr (Hedderich et al., 1994; Kaster et al., 2011a). In *M. hungatei* HdrA is adjacent to HdrBC, but in *M. formicicum* not. In fact, two genes coding for the HdrA subunit are scattered in the genome in positions Mfor_1232 (*hdrA1*) and Mfor_2055 (*hdrA2*), while *hdrBC* are in Mfor_0471-72. Although the HdrA1 of *M. formicicum* was equally abundant in all conditions, its levels were significantly higher than the HdrBC complementary subunits. Moreover, HdrA2 was detected only in axenically grown cells. These results in both methanogens suggest that HdrA is used in bifurcating mechanisms of energy conservation in association with other complexes besides HdrBC. Remarkably, in the genome of *M. hungatei* next to *hdrABC* the subunit Fwd/Fmd-F is encoded in Mhun_1835 (*fwd/fmdF*), which as mentioned before is thought to function as an electron carrier between Hdr and Fwd/Fmd. FwdF was abundant in all growing conditions of *M. hungatei*.

Figure 5.2. Protein expression heat map of the of the proteins used in methanogenic pathways of *Methanospirillum hungatei* JF1 (left) and *Methanobacterium* MFOR (right). The rows in the heat map show proteins levels after Z-score standardization in three different growth conditions. The columns show from left to right, in triplicates, the electron donor used by the microorganisms to produce methane: formate, hydrogen and interspecies compounds transferred from *Syntrophobacter fumaroxidans*. The colour scale indicates the degree of protein down- or up regulation ranging from blue (-2.5 log ratio), to yellow (2.5 log ratio). The colour intensities indicate lower and higher levels compared to the average level 0 value (in black); the grey colour represents not detected. Fwd/Fmd: formylmethanofuran dehydrogenase; Ftr: formylmethanofuran-H4MPT formyltransferase; Mch: methenyl-H4MPT cyclohydrolase; Mtd: methylene-H4MPT dehydrogenase; Mer: methylene-H4MPT reductase; Mtr: membrane bound H4MPT S-methyltransferase; Mcr & Mrt: methyl-CoM reductase isoenzyme I & II respectively; Hdr: heterodisulfide reductase; and Mvh: F_{420}-non-reducing hydrogenase. (*) indicates a statistically significant difference in at least one condition. Subunits are indicated after the locus tag.

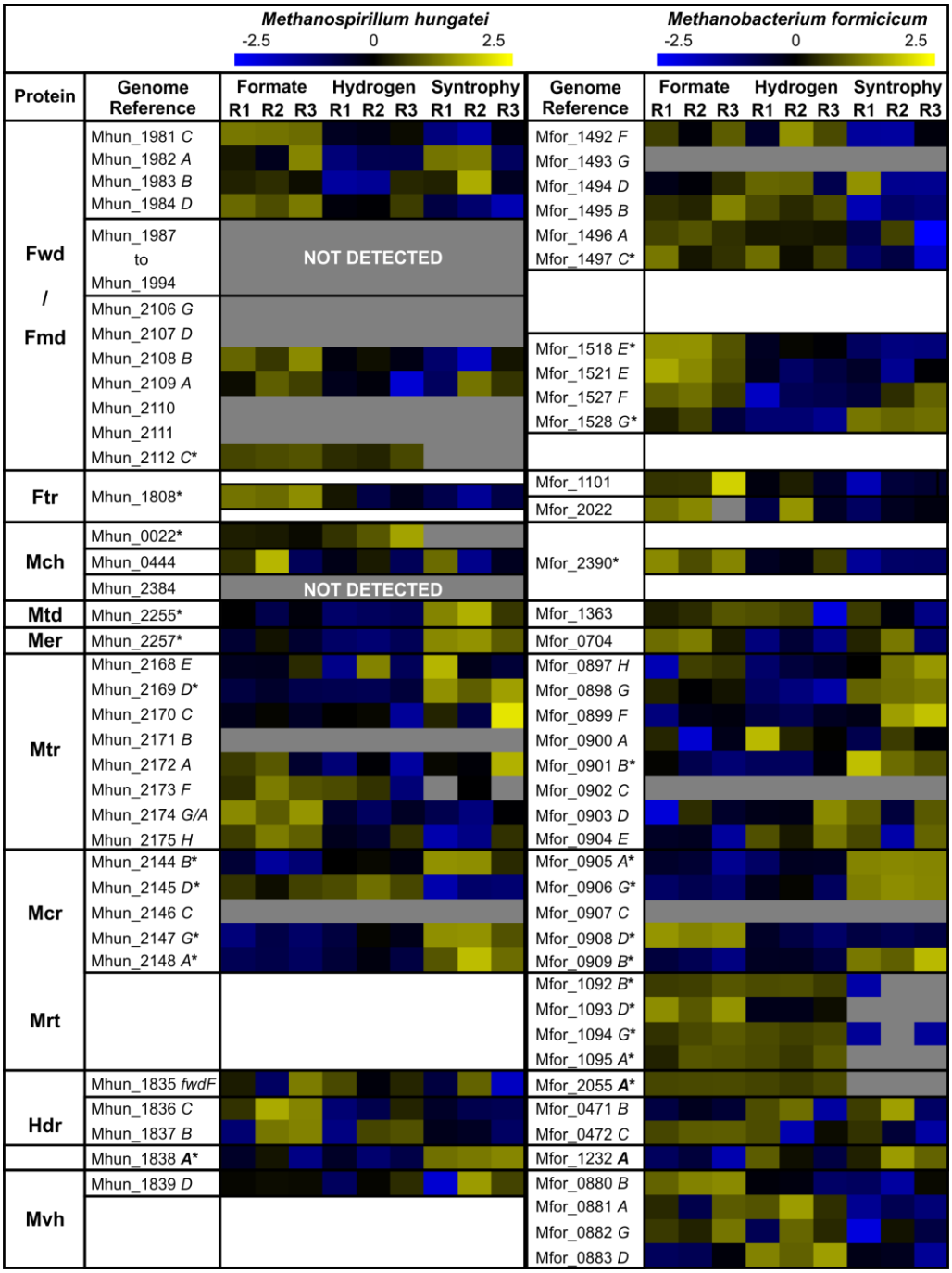
Methanospirillum hungatei
-2.5
0
2.5
Methanobacterium formicicum
-2.5
0
2.5
Protein
Genome Reference
Formate R1 R2 R3
Hydrogen R1 R2 R3
Syntrophy R1 R2 R3
Genome Reference
Formate R1 R2 R3
Hydrogen R1 R2 R3
Syntrophy R1 R2 R3
Fwd / Fmd
Mhun_1981 C
Mhun_1982 A
Mhun_1983 B
Mhun_1984 D
Mhun_1987 to Mhun_1994
NOT DETECTED
Mhun_2106 G
Mhun_2107 D
Mhun_2108 B
Mhun_2109 A
Mhun_2110
Mhun_2111
Mhun_2112 C*
Mfor_1492 F
Mfor_1493 G
Mfor_1494 D
Mfor_1495 B
Mfor_1496 A
Mfor_1497 C*
Mfor_1518 E*
Mfor_1521 E
Mfor_1527 F
Mfor_1528 G*
Ftr
Mhun_1808*
Mfor_1101
Mfor_2022
Mch
Mhun_0022*
Mhun_0444
Mhun_2384
NOT DETECTED
Mfor_2390*
Mtd
Mhun_2255*
Mfor_1363
Mer
Mhun_2257*
Mfor_0704
Mtr
Mhun_2168 E
Mhun_2169 D*
Mhun_2170 C
Mhun_2171 B
Mhun_2172 A
Mhun_2173 F
Mhun_2174 G/A
Mhun_2175 H
Mfor_0897 H
Mfor_0898 G
Mfor_0899 F
Mfor_0900 A
Mfor_0901 B*
Mfor_0902 C
Mfor_0903 D
Mfor_0904 E
Mcr
Mhun_2144 B*
Mhun_2145 D*
Mhun_2146 C
Mhun_2147 G*
Mhun_2148 A*
Mfor_0905 A*
Mfor_0906 G*
Mfor_0907 C
Mfor_0908 D*
Mfor_0909 B*
Mrt
Mfor_1092 B*
Mfor_1093 D*
Mfor_1094 G*
Mfor_1095 A*
Hdr
Mhun_1835 fwdF
Mhun_1836 C
Mhun_1837 B
Mfor_2055 A*
Mfor_0471 B
Mfor_0472 C
Mhun_1838 A*
Mfor_1232 A
Mvh
Mhun_1839 D
Mfor_0880 B
Mfor_0881 A
Mfor_0882 G
Mfor_0883 D

Role of formate and hydrogen in methanogenesis

Insight into the mechanism by which methanogens oxidize hydrogen or formate is important from the perspective of the use of these compounds as electron carriers in the metabolic processes and for energy conservation. In hydrogenotrophic methanogens like *M. hungatei* and *M. formicicum* formate and hydrogen are the electron donors that generate reduced ferredoxin and cofactor F_{420} that are used in diverse steps of the methanogenic pathway **(Supporting information, Fig. S5.3 & S5.4)**. There are indications that hydrogen is formed when methanogens grow on CO and formate (Costa et al., 2013a; Diender et al., 2016). The need of hydrogen to start methanogenesis from CO_2 can be explained by its role in the so called Wolfe cycle (Thauer, 2012), a flavin-based electron bifurcation mechanism that links the initial reduction of CO_2 by Fwd/Fmd with a multi-complex formed by HdrABC and an F_{420}-non-reducing hydrogenase (MvhADG) (Setzke et al., 1994; Stojanowic et al., 2003; Hedderich et al., 2005). However, many members of the Methanomicrobiales lack the genes coding for MvhA and MvhG (Thauer et al., 2010). That is the case for *M. hungatei*, where only *mvhD* (Mhun_1839) is found in the genome adjacent to *hdrABC* (**Figure 5.2**). MvhD was abundant in all growing conditions of *M. hungatei*.

It has been suggested that the subunits FrhAG of a coenzyme F_{420}-dependent [NiFe]-hydrogenase (FrhADGB) are used instead of MvhAG to form a functional complex with the MvhD subunit and HdrABC (Anderson et al., 2009; Kaster et al., 2011a). Indeed, the FrhADGB of *M. hungatei* (Mhun_2329-2332) was abundant in all conditions and the most abundant hydrogenase in this methanogen **(Figure 5.3)**. *M. formicicum* on the other hand, is a member of Methanobacteriales and contains a complete MvhADGB (Mfor_0880-0883) which was also abundant in all conditions. Therefore, it is possible that MvhADGB in *M. formicicum* and FrhADGB in *M. hungatei* are the enzymes involved in the multi-subunit bifurcating complex that with HdrABC couples the exergonic reduction of CoM-S-S-CoB to the unfavourable reduction of ferredoxin with H_2 (Kaster et al., 2011b).

Figure 5.3. Normalized expression matrix of hydrogenases and formate dehydrogenases of *Methanospirillum hungatei* JF1 (left) and *Methanobacterium formicicum* MFOR (right). Protein abundance levels are shown after Z-score normalization. The detected proteins are shown for three different growth conditions. The columns show from left to right, in triplicates, the electron donor used by the microorganisms: formate, hydrogen and interspecies compounds from *Syntrophobacter fumaroxidans*. (*****) marks a statistically significant difference in at least one condition. The colour intensity indicates the degree of protein up- or down regulation compared to the average level value in black; the grey colour is used for not detected proteins.

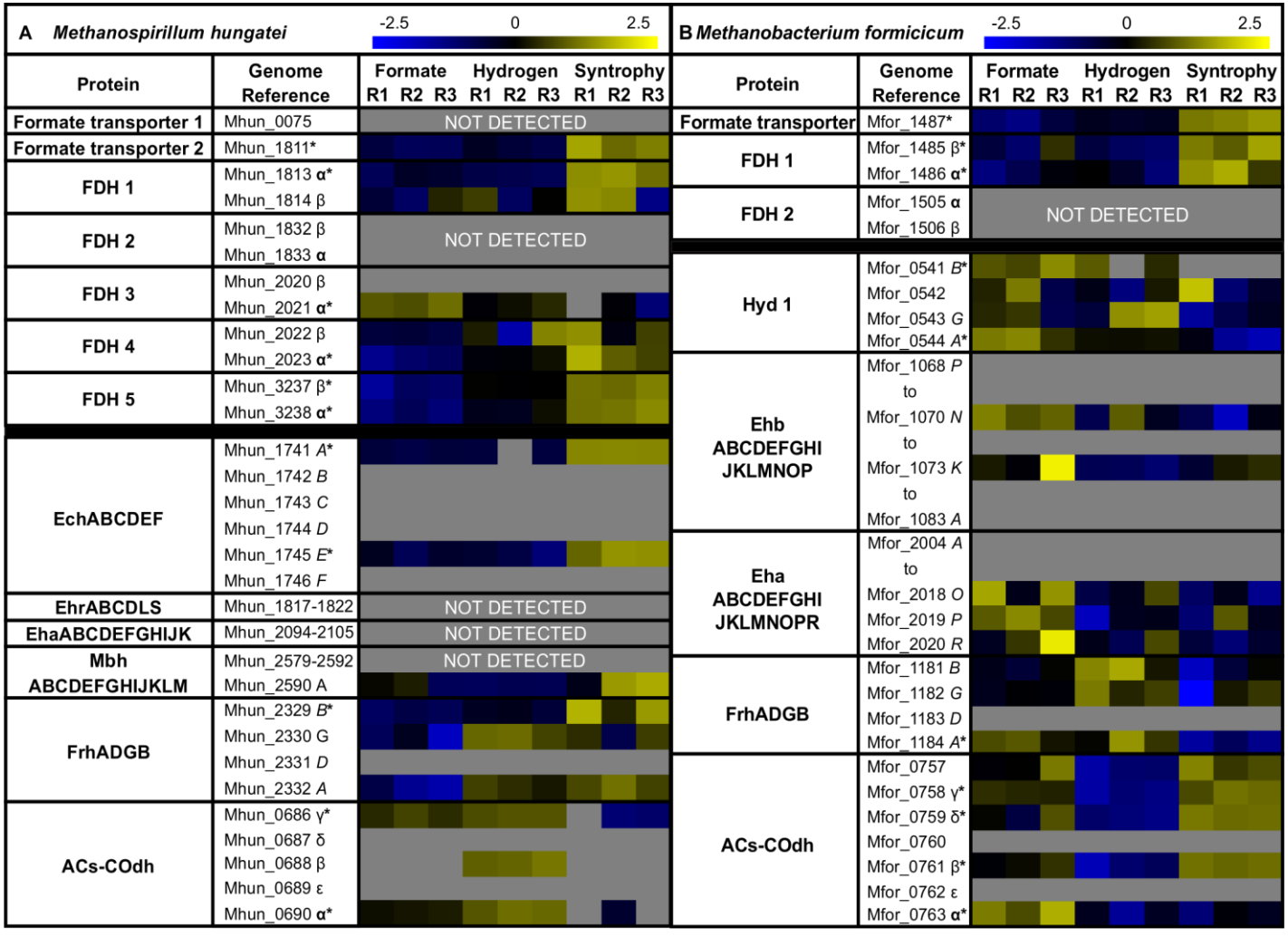
A Methanospirillum hungatei
-2.5
0
2.5
Protein
Genome Reference
Formate R1 R2 R3
Hydrogen R1 R2 R3
Syntrophy R1 R2 R3
Formate transporter 1
Mhun_0075
NOT DETECTED
Formate transporter 2
Mhun_1811*
FDH 1
Mhun_1813 α*
Mhun_1814 β
FDH 2
Mhun_1832 β
Mhun_1833 α
NOT DETECTED
FDH 3
Mhun_2020 β
Mhun_2021 α*
FDH 4
Mhun_2022 β
Mhun_2023 α*
FDH 5
Mhun_3237 β*
Mhun_3238 α*
EchABCDEF
Mhun_1741 A*
Mhun_1742 B
Mhun_1743 C
Mhun_1744 D
Mhun_1745 E*
Mhun_1746 F
EhrABCDLS
Mhun_1817-1822
NOT DETECTED
EhaABCDEFGHIJK
Mhun_2094-2105
NOT DETECTED
Mbh ABCDEFGHIJKLM
Mhun_2579-2592
NOT DETECTED
Mhun_2590 A
FrhADGB
Mhun_2329 B*
Mhun_2330 G
Mhun_2331 D
Mhun_2332 A
ACs-COdh
Mhun_0686 γ*
Mhun_0687 δ
Mhun_0688 β
Mhun_0689 ε
Mhun_0690 α*
B Methanobacterium formicicum
-2.5
0
2.5
Protein
Genome Reference
Formate R1 R2 R3
Hydrogen R1 R2 R3
Syntrophy R1 R2 R3
Formate transporter
Mfor_1487*
FDH 1
Mfor_1485 β*
Mfor_1486 α*
FDH 2
Mfor_1505 α
Mfor_1506 β
NOT DETECTED
Hyd 1
Mfor_0541 B*
Mfor_0542
Mfor_0543 G
Mfor_0544 A*
Ehb ABCDEFGHI JKLMNOP
Mfor_1068 P
to
Mfor_1070 N
to
Mfor_1073 K
to
Mfor_1083 A
Eha ABCDEFGHI JKLMNOPR
Mfor_2004 A
to
Mfor_2018 O
Mfor_2019 P
Mfor_2020 R
FrhADGB
Mfor_1181 B
Mfor_1182 G
Mfor_1183 D
Mfor_1184 A*
ACs-COdh
Mfor_0757
Mfor_0758 γ*
Mfor_0759 δ*
Mfor_0760
Mfor_0761 β*
Mfor_0762 ε
Mfor_0763 α*

During growth on formate electrons may flow from formate to Hdr using an F_{420}-reducing formate dehydrogenase instead of the F_{420}-reducing hydrogenase (Costa et al., 2010). For this reason, H_2 is not required as intermediate in methanogenesis from formate (Lupa et al., 2008).

In *M. formicicum* only *fdh1* (Mfor_1485-1486) codes for cofactor F_{420} binding domains. Fdh1 was detected in all conditions in *M. formicicum*, and significantly more abundant in syntrophically grown cells. Fdh2 was not detected in any growth conditions in our study. The amino acid sequence of this enzyme, *fdh2* (Mfor_1505-1506), does not predict cofactor F_{420} binding domains. In the case of *M. hungatei*, the five formate dehydrogenases present in its genome are nearly identical (Gunsalus et al., 2016), and all of them contain cofactor F_{420} binding motives in their amino acid sequences. Therefore, all of them could in theory be used in the Wolfe cycle, although Fdh1 (Mhun_1813-1814) was the most abundant formate dehydrogenase in all conditions and significantly more abundant in syntrophically grown cells.

When methanogens use formate as substrate, it is first imported inside the cell by the formate transporter, then it is oxidized by a formate dehydrogenase to generate reduced cofactor F_{420} ($F_{420}H_2$) which is required in several steps of methanogenesis. In the genome of both methanogens genes coding for Fdh1 (Mhun_1813-1814 & Mfor_1485-1486) are adjacent to their formate transporter coding gene (Mhun_1811 & Mfor_1487). These formate transporters and formate dehydrogenases were among the most abundant proteins detected in both methanogens. Therefore, the Fdh1 in each methanogen, is most probably the main formate dehydrogenase used to generate $F_{420}H_2$ necessary for the intermediate reduction steps in methanogenesis performed by Mtd and Mer. Moreover, significantly higher levels of the formate transporter and the associated Fdh1 were detected in syntrophically grown cells of both methanogens in comparison with axenic conditions. This indicates that formate was an important compound provided from *Syntrophobacter fumaroxidans*.

In *M. hungatei*, Fdh2 (Mhun_1832-1833) was not detected. Interestingly, Fdh3 (Mhun_2020-2021) was the only formate dehydrogenase that was significantly more abundant in formate-grown cells. Thus, it might be that it has a similar function as Fdh1. Fdh4 (Mhun_2022-2023) and Fdh5 (Mhun_3237-3238) were more abundant in syntrophically grown cells. Fdh5 was the second most abundant formate dehydrogenase after Fdh1 and followed by Fdh4. We suggest that Fdh4 and Fdh5 associate with HdrA, which is also more abundant in syntrophic cultures, to form bifurcating protein complexes for energy conservation at energy-limited conditions such as during syntrophic growth.

Of the five hydrogenases predicted from the genome of *M. hungatei*, only two were detected in our proteome study, Frh and Ech. Although not all the subunits of the energy-conserving hydrogenase (Ech) were detected, the most important parts

corresponding to the catalytic subunit (EchE: Mhun_1745) and the major membrane integrated subunit (EchA: Mhun_1741) were detected. Consequently, the complex was considered functional. This was not the case for the membrane-bound hydrogenase, where only the alpha-subunit of the complex (MbhA: Mhun_2590) was detected in low levels. However, in previous transcriptomic studies the transcription levels of this complex were higher than those of Ech in all tested conditions (Worm et al., 2011b). Furthermore, our results contrary to the transcriptomics study show a significant higher abundance of Ech in syntrophic conditions. Although an important anaplerotic role of energy-converting hydrogenase Eha in hydrogenotrophic methanogens was proposed (Lie et al., 2012), this membrane-bound complex was not detected in the present study and it was not considered in the previous transcriptomic study.

In contrast to *M. hungatei*, all the hydrogenases found in the genome of *M. formicicum* were detected in our analysis. Although only few subunits of the multimeric energy-converting hydrogenases Eha and Ehb were detected, these corresponded to the active sites of the complexes. Therefore, we categorized the enzymes as being produced. In *M. formicicum*, also Frh was the most abundant hydrogenase in all studied conditions, excluding Mvh which has been discussed above. The relative abundance of all the hydrogenases remains constant among the studied conditions, and only the alpha-subunits of the Hyd1 and Frh showed a significant increase in cells that were grown axenically. Also, in both axenic conditions MvhADGB is the most abundant energy conservation protein, and only in syntrophically grown cells the Fdh1 and the formate transporter were more abundant than MvhADGB**.**

In a previous transcriptomic analysis, no main differences in the transcriptional levels of hydrogenases or formate dehydrogenases of *M. hungatei* were observed between cells grown syntrophically or grown with hydrogen or formate (Worm et al., 2011b). It has been documented that the propionate degradation rate of *S. fumaroxidans* in coculture with *M. formicicum* was lower than that in the coculture with *M. hungatei*, and that this might be related to the Km values of the formate dehydrogenases of the methanogenic partners as well as their formate threshold values (Dong et al., 1994).

A proteomic study of propionate degradation by *S. fumaroxidans* in axenic conditions and in syntrophy with *M. hungatei* and *M. formicicum* (Sedano-Nunez et al., unpublished), revealed that formate is the preferred carrier by the bacterium in the interspecies electron transfer to the syntrophic partner. The present study indicates that *M. hungatei* mainly uses formate dehydrogenases in its methanogenic metabolism, while most of its multiple hydrogenases seemingly are not used, or at least were not detected in our study. In contrast, *M. formicicum* relies on its

hydrogenases regardless the electron donor available, which in the syntrophic association with *S. fumaroxidans* it is likely formate.

Carbon assimilation, autotrophy in M. formicicum vs acetate dependence in M. hungatei

Hydrogenotrophic methanogens can assimilate carbon via acetyl-CoA generated from methyl-H4MPT. The reductive acetyl-CoA pathway includes a reduction of CO_2 to CO, which is subsequently combined with methyl-H4MPT and CoA-SH to form acetyl-CoA. The key enzyme that performs these reactions is therefore referred to as CO dehydrogenase-acetyl-CoA synthase (ACs-COdh) (Berg et al., 2010). Both *M. hungatei* and *M. formicicum* encode in their genome ACs-COdh (Mhun_0686-0690 and Mfor_0757-0763, respectively). The role of ACs-COdh in *M. hungatei* is unknown since the archaeon, despite having the necessary genes to fix carbon, needs to acquire acetate supplied in the medium as the major supply for cell carbon (Ferry and Wolfe, 1977). As can be seen in **Figure 5.3** the ACs-COdh of *M. hungatei* was scarcely detected. It might be argued that ACs-COdh was not produced by *M. hungatei* since acetate was supplemented in the medium. However, the same medium supplied with acetate was used to grow *M. formicicum*, in which high levels of detection of the ACs-COdh complex in all conditions indicates a role in assimilatory metabolism. The epsilon subunit of the complex and the COdh maturation protein (Mfor_0760) were not detected in any condition. Interestingly these subunits have been found in higher abundance in *M. marburgensis* when performing CO-oxidation (Diender et al., 2016). Since in our study CO oxidation does not take place, these subunits were absent in the proteome.

Other abundant proteins in all growth conditions

The total intensity-based absolute quantification (iBAQ) was used to rank the most abundant proteins produced in all growth conditions. Proteins associated with protection, transport and stabilization of other proteins and macromolecules are commonly abundant in several microbial proteomic studies (Ishihama et al., 2008; Moriya, 2015). This is also the case for our proteomic analysis of *M. hungatei* and *M. formicicum*.

In *M. hungatei*, among the most abundant proteins was an uncharacterized protein (Mhun_2513) containing a domain of unknown function DUF3821 (IPR024277). This domain is largely confined to sequences from Methanomicrobiales and found in putative lipases, but the function is still unknown (InterPro, 5RC7, 27th January 2014). Two other proteins (Mhun_1218 & Mhun_3140) that are related to the formation of archaeal pili and archaeal flagella were also among the most abundant proteins in all the studied conditions of *M. hungatei*. Previous genomic analysis predicted the presence of a basal body structure in the *flhGFHIJ* (Mhun_0101-0105)

gene cluster in *M. hungatei* (Gunsalus et al., 2016). However, only one subunit of the flhGFHIJ complex was detected at low levels in our study (**Figure 5.4**).

The extracellular filament structure formerly called archaeal flagellum is now referred to as archaellum (Jarrell and Albers, 2012). In addition to motility, the archaella are involved in cellular adhesion, biofilm formation and symbiotic interactions such as cell-cell contact (Bellack et al., 2011; Jarrell et al., 2011). Of the three genes coding for the archaella filaments in *M. hungatei*, only the product of Mhun_3140 was detected. This protein was among the most abundant in all conditions, and not only in syntrophic grown cells, therefore a role of cell-cell interaction with the syntrophic partner is not likely, although motility or other type of adhesion are still feasible traits. The atomic model of this specific archaellum protein indicates that archaella exhibit similarities to both bacterial flagella and bacterial type IV pili (Poweleit et al., 2016).

Besides the archaella structures, the genome of *M. hungatei* reveals the presence of 12 genes coding for Archaeal type IV pili. Archaeal pili also play important roles in surface adhesion and they could also play a role to establish cell to cell interactions with the syntrophic partner (Esquivel et al., 2013). Although these appendages have never been observed by electron microscopy, the product of one of these paralogs (Mhun_1218) was the fourth most abundant protein in *M. hungatei*, and it was consistently present in the three studied conditions. Interestingly, the other four paralogs (Mhun_0296-0299) were detected at high levels in cells grown axenically but were not detected in syntrophically grown cells. Lastly two more paralogs (Mhun_0310-0311) were retrieved in all conditions, but these were significantly more abundant in axenic conditions **(Figure 5.4)**. These results indicate that the function of these archaeal pili, as in the case of the archaella, is not dependent on syntrophic associations, but they might still be linked to cell-cell interactions among the methanogens themselves.

Other proteins that could be involved in regulating cell adhesion are surface layer proteins (SLP or S-layer proteins). In *Methanosarcina mazei* and *M. acetivorans* SLP's are thought to regulate cell adhesion and it was found that beta-propeller, PKD, and beta-helix domains account for the complete architecture of numerous SLPs in those methanogens (Jing et al., 2002). Many hypothetical proteins containing these domains were found in the genome of *M. hungatei* (Mhun_2440-42; Mhun_0417-0426). Moreover, several of those proteins ranked high in the total iBAQ values.

In contrast, in the genome of *M. formicicum* there are no genes coding for proteins containing PKD, beta-helix or beta-propeller domains. This seems reasonable since, with the exception of *Methanothermus fervidus*, there are no reports of the presence of an S-layer in the other known members of the Methanobacteriales (Albers and

Meyer, 2011). In this order a polymer similar to bacterial peptidoglycan, known as pseudomurein, is the predominant compound in the cell wall (Steenbakkers et al., 2006; Visweswaran et al., 2011).

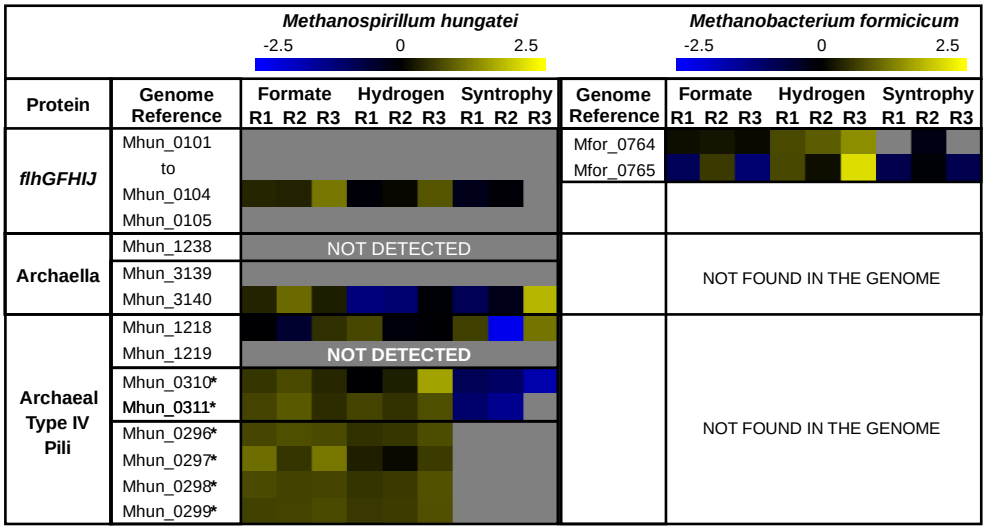

Figure 5.4. Normalized expression matrix of proteins involved in cell-surface structures of *Methanospirillum hungatei* and *Methanospirillum formicicum*. The rows in the heat map show the detected proteins after Z-score standardization in three different growth conditions. The columns show from left to right, in triplicates, the electron donor used by the microorganisms: formate, hydrogen and interspecies compounds from *Syntrophobacter fumaroxidans*. (*) marks a statistically significant difference in at least one condition. The colour intensity indicates the degree of protein up- or down regulation compared to the average level value in black; the grey colour is used for not detected proteins

Conclusions

The higher abundance of the formate transporter and Fdh1 in syntrophically grown cells of *M. hungatei* and *M. formicicum* strongly indicates that interspecies electron transfer via formate occurred during syntrophic growth with *Syntrophobacter fumaroxidans* and that this bacterium mainly produces formate in the conversion of propionate.

M. formicicum uses a F_{420}-non-reducing hydrogenase (MvhADG) for bifurcation in the Wolfe cycle while *M. hungatei* employs a F_{420}-reducing hydrogenase (FrhADGB). In syntrophic growth, a F_{420}-dependent formate dehydrogenase is used in both methanogens for electron bifurcation.

We also propose that in *M. hungatei*, Fdh4 and/or Fdh5 can form a bifurcating complex with HdrA independent of the Wolfe cycle and that these complexes are necessary at energy-limited growth conditions, such as during syntrophic growth.

Moreover, we speculate that *M. hungatei* uses formate in its metabolic processes regardless whether hydrogen or formate is the substrate. This consideration is based on the number of formate dehydrogenase genes present in its genome and the abundance of formate dehydrogenases even when hydrogen is the substrate, whereas many available hydrogenases were not abundant in our studied conditions. The higher abundance of Mtd and Mer in syntrophically grown cells in *M. hungatei*, fits with the abundance of cofactor F_{420} depending formate dehydrogenases Fdh1, Fdh4 and Fdh5 also more abundant in *M. hungatei* cells grown with *S. fumaroxidans*.

In *M. formicicum* on the other hand, for reduction of CO_2 to methane seems to preferentially use hydrogen as electron carrier since all the hydrogenases in catabolic (Mvh, Frh and Hyd1) and anabolic reactions (EhA and EhB) were equally abundant in cells grown with hydrogen, formate or in syntrophy with *S. fumaroxidans*. Still the use of formate remains important in some conditions such as syntrophic growth with *S. fumaroxidans*.

Supporting information

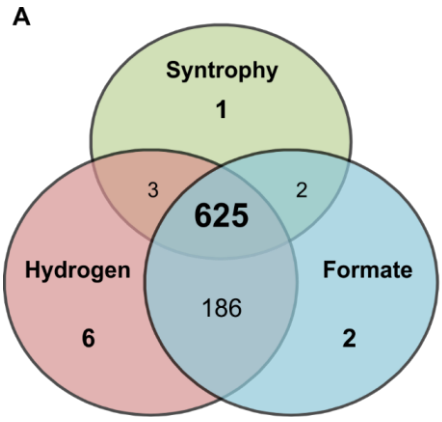

Detected proteins: 825		
Condition (e- donor)	Total	Exclusive
Syntrophy	631	1
Hydrogen	820	6
Formate	815	2

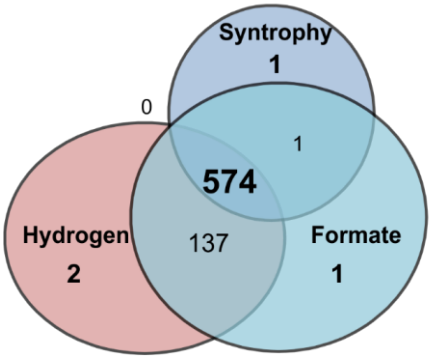

Detected proteins: 716		
Condition (e- donor)	Total	Exclusive
Syntrophy	576	1
Hydrogen	713	2
Formate	713	1

Fig. S5.1. Venn diagrams of the proteomic profiles of *Methanospirillum hungatei* (A) and *Methanobacterium formicicum* (B) growing syntrophically with *Syntrophobacter fumaroxidans* and axenically on H_2/CO_2 or formate.


-2.5
0
2.5
Formate
Hydrogen
Syntrophy
R1 R2 R3 R1 R2 R3 R1 R2 R3
Mhun_0138 Uncharacterized protein
Mhun_3053 Thiol-driven fumarate reductase, flavoprotein subu
Mhun_2527 GMP synthase [glutamine-hydrolyzing] subunit B
Mhun_1206 Fructose-1,6-bisphosphatase class 1
Mhun_1829 Uncharacterized protein
Mhun_0521 ABC transporter tungsten-binding protein
Mhun_2702 Uncharacterized protein
Mhun_2022 Formate dehydrogenase, beta subunit F420
Mhun_1556 Uncharacterized protein
Mhun_2600 Glucose-6-phosphate isomerase
Mhun_0112 CheC, inhibitor of MCP methylation
Mhun_0842 Putative nickel-responsive regulator
Mhun_0804 DNA-directed RNA polymerase subunit
Mhun_0912 Peptidase M42
Mhun_1136 Glycerol-1-phosphate dehydrogenase [NADP+]
Mhun_2426 PKD
Mhun_2992 Pyruvate flavodoxin/ferredoxin oxidoreductase-like
Mhun_0049 DNA-directed RNA polymerase subunit H
Mhun_1160 UvrABC system protein A
Mhun_1011 DNA topoisomerase 1
Mhun_0990 Methyl-accepting chemotaxis sensory transducer
Mhun_0649 Nitroreductase
Mhun_1861 CRISPR-associated helicase, Cas3 family
Mhun_2455 RNA-binding region RNP-1 RNA recognition motif
Mhun_2292 Homoserine dehydrogenase
Mhun_0779 L-glutamine synthetase
Mhun_2277 Bifunctional NADPH-hydrate repair enzyme Nnr
Mhun_1816 DEAD/DEAH box helicase-like protein
Mhun_0069 Uncharacterized protein
Mhun_1835 Formylmethanofuran dehydrogenase, subunit F
Mhun_0558 Tryptophan synthase beta chain
Mhun_1083 Uncharacterized protein
Mhun_2159 Dinitrogenase iron-molybdenum cofactor biosynthe
Mhun_3084 NAD-dependent epimerase/dehydratase
Mhun_0354 Methyl-accepting chemotaxis sensory transducer
Mhun_2109 Formylmethanofuran dehydrogenase, subunit A
Mhun_1465 Pyrophosphate-dependent phosphofructokinase
Mhun_1148 Beta-ribofuranosylaminobenzene 5-phosphate syn
Mhun_0068 Uncharacterized protein
Mhun_0449 UPF0285 protein Mhun_0449
Mhun_1349 Multi-sensor signal transduction histidine kinase
Mhun_2674 Uncharacterized protein
Mhun_2669 Methyl-accepting chemotaxis sensory transducer
Mhun_1481 Multi-sensor signal transduction histidine kinase
Mhun_0951;Mhun_1641;Mhun_1648 Methyl-accepting chemot
Mhun_0039 Alanine--tRNA ligase
Mhun_0617 PBS lyase HEAT-like repeat
Mhun_0110 CheA signal transduction histidine kinases
Mhun_2944 Methyl-accepting chemotaxis sensory transducer
Mhun_1753 Uncharacterized protein
Mhun_1514 Helicase-like protein
Mhun_0729 Metal dependent phosphohydrolase
Mhun_1061 Phosphoribosylformylglycinamidine synthase subu
Mhun_2801 Uncharacterized protein
Mhun_0962 Uncharacterized protein
Mhun_2360 2-isopropylmalate synthase
Mhun_2254 Uncharacterized protein
Mhun_1983 Formylmethanofuran dehydrogenase, subunit B
Mhun_1038 Proteasome-activating nucleotidase
Mhun_1077 Putative ATP-dependent Lon protease
Mhun_0813 Radical SAM
Mhun_1769 V-type ATP synthase beta chain 3
Mhun_1814 Formate dehydrogenase, beta subunit F420
Mhun_3170 Type II secretion system protein E
Mhun_2610 Phosphoenolpyruvate synthase
Mhun_1982 Formylmethanofuran dehydrogenase, subunit A
Mhun_2336 DNA-directed RNA polymerase, subunit L
Mhun_2499 PKD
Mhun_2737 Uncharacterized protein
Mhun_1289 ATPase AAA-2
Mhun_1471 CoA-binding protein
Mhun_3166 Putative PAS/PAC sensor protein
Mhun_1242 Acetolactate synthase
Mhun_0745 Metal dependent phosphohydrolase
Mhun_1422 Methyl-accepting chemotaxis sensory transducer
Mhun_2555 Uncharacterized protein
Mhun_1048;Mhun_0324;Mhun_1933 Multi-sensor signal transd
Mhun_3167 Multi-sensor signal transduction histidine kinase
Mhun_2988 Metallophosphoesterase
Mhun_1777 4Fe-4S ferredoxin, iron-sulfur binding protein
Mhun_0536 ATPase, E1-E2 type
Mhun_1141 Pyruvate phosphate dikinase
Mhun_1184 V-type ATP synthase beta chain 1
Mhun_1693 Predicted aconitase subunit 1
Mhun_1311 Rubrerythrin
Mhun_1580 Uncharacterized protein
Mhun_1271 4Fe-4S ferredoxin, iron-sulfur binding protein
Mhun_2528 CTP synthase
Mhun_2689 Cache sensor signal transduction histidine kinase
Mhun_1692 Peptidase U34, dipeptidase
Mhun_2332 Coenzyme F420-reducing hydrogenase, alpha sub
Mhun_2859 Oligosaccharyl transferase, STT3 subunit
Mhun_2433 Catalase-peroxidase
Mhun_1272 Carbon-monoxide dehydrogenase, catalytic subun
Mhun_0947 Peptidase S8 and S53, subtilisin, kexin, sedolisin
Mhun_0566 CoA-binding protein
Mhun_0681;Mhun_1356 Methyl-accepting chemotaxis sensory
Mhun_2367 Short-chain dehydrogenase/reductase SDR
Mhun_1828 Uncharacterized protein
Mhun_2144 Methyl-coenzyme M reductase, beta subunit
Mhun_2147 Methyl-coenzyme M reductase, gamma subunit
Mhun_2023 Formate dehydrogenase, alpha subunit F420
Mhun_1243 Putative R-citramalate synthase CimA
Mhun_1294 Signal transduction histidine kinase-like protein
Mhun_0099 TPR repeat
Mhun_2415 Peptidase S1 and S6, chymotrypsin/Hap
Mhun_3238 Formate dehydrogenase, alpha subunit F420
Mhun_3237 Formate dehydrogenase, beta subunit F420
Mhun_0347 Methyl-accepting chemotaxis sensory transducer
Mhun_1203 Alpha-glucan phosphorylase
Mhun_1797 3-isopropylmalate dehydrogenase
Mhun_2270 Uncharacterized membrane protein required for N-
Mhun_2759 Uncharacterized protein
Mhun_1495 Aspartate-semialdehyde dehydrogenase
Mhun_2366 Uncharacterized protein
Mhun_2329 Coenzyme F420-reducing hydrogenase, beta subu
Mhun_1561 Acetyl-CoA hydrolase/transferase
Mhun_2189 Hydroxylamine reductase
Mhun_1634 Uncharacterized protein
Mhun_2590 Membrane bound hydrogenase subunit mbhL
Mhun_1807 Rubrerythrin
Mhun_0958 Uncharacterized protein
Mhun_1177 V-type H+-transporting ATPase subunit E
Mhun_2257 5,10-methylenetetrahydromethanopterin reductase
Mhun_1378 CRISPR-associated protein, Cse4 family
Mhun_0139 Dihydroxy-acid dehydratase
Mhun_0528 Uncharacterized protein
Mhun_3190 Pyruvate carboxylase subunit A
Mhun_2970 FO synthase subunit 2
Mhun_2105 Membrane-bound hydrogenase subunit ehaO
Mhun_0822 Uncharacterized protein
Mhun_1042 Uncharacterized protein
Mhun_2255 F420-dependent methylenetetrahydromethanopter
Mhun_1492 4-hydroxy-tetrahydrodipicolinate synthase
Mhun_1644 Transcriptional regulator, ArsR family
Mhun_0451 Pyruvate ferredoxin oxidoreductase, delta subunit
Mhun_3001 PEGA
Mhun_1838 CoB--CoM heterodisulfide reductase subunit A
Mhun_2069 Methyl-accepting chemotaxis sensory transducer v
Mhun_2169 Tetrahydromethanopterin S-methyltransferase sub
Mhun_1813 Formate dehydrogenase, alpha subunit F420
Mhun_1741 Ech hydrogenase subunit A
Mhun_1811 Formate/nitrite transporter
Mhun_2462 Glyceraldehyde-3-phosphate dehydrogenase
Mhun_0453 Pyruvate ferredoxin oxidoreductase, beta subunit
Mhun_0781 Archaeal glutamate synthase [NADPH]
Mhun_1745 Ech hydrogenase subunit E
Mhun_2319 Adenylosuccinate synthetase
Mhun_2513 Uncharacterized protein
Mhun_2311 ABC transporter related protein
Mhun_2700 Uncharacterized protein
Mhun_0450 Pyruvate ferredoxin oxidoreductase, gamma subu
Mhun_0949 TPR repeat
Mhun_2148 Methyl-coenzyme M reductase, alpha subunit
Mhun_2551 Methyl-accepting chemotaxis sensory transducer v
Mhun_1245 Ketol-acid reductoisomerase
Mhun_3126 PKD
-2.5
0
2.5
Formate
Hydrogen
Syntrophy
R1 R2 R3 R1 R2 R3 R1 R2 R3
Mhun_0452 Pyruvate ferredoxin oxidoreductase, alpha subunit
Mhun_2092 Putative PAS/PAC sensor protein
Mhun_1244 Uncharacterized protein
Mhun_0797 Uncharacterized protein
Mhun_1178 V-type ATP synthase subunit I
Mhun_3140 Flagellin
Mhun_2172 Tetrahydromethanopterin S-methyltransferase subu
Mhun_1027 Triosephosphate isomerase
Mhun_1770 V-type ATP synthase alpha chain 3
Mhun_0437 Uncharacterized protein
Mhun_2170 Tetrahydromethanopterin S-methyltransferase subu
Mhun_0095 Succinyl-CoA synthetase ADP-forming beta subuni
Mhun_2168 Tetrahydromethanopterin S-methyltransferase subu
Mhun_0426 PKD
Mhun_1555 Transglutaminase-like protein
Mhun_3181 tRNA-splicing ligase RtcB
Mhun_0346 Peptidase S9B, dipeptidylpeptidase IV-like protein
Mhun_1447 PT repeat
Mhun_1183 V-type ATP synthase alpha chain 1
Mhun_3022 Signal recognition particle receptor FtsY
Mhun_1837 CoB--CoM heterodisulfide reductase subunit B
Mhun_1834 Formylmethanofuran dehydrogenase, subunit G
Mhun_1827 Uncharacterized protein
Mhun_1767 UspA
Mhun_1733 tRNA intron endonuclease
Mhun_1706 Response regulator receiver domain protein CheY-
Mhun_0293 ABC-type metal ion transport system periplasmic c
Mhun_1602 30S ribosomal protein S28e
Mhun_2104 Membrane-bound hydrogenase subunit ehaN
Mhun_2870 50S ribosomal protein L40e
Mhun_2498 PKD
Mhun_3227 N-acetyl-gamma-glutamyl-phosphate reductase
Mhun_0423 PKD
Mhun_1218 Uncharacterized protein
Mhun_2271 Uncharacterized protein
Mhun_1164 PKD
Mhun_0597 PKD
Mhun_0486 Peptidase S8 and S53, subtilisin, kexin, sedolisin
Mhun_0420 PKD
Mhun_0421 PKD
Mhun_1614 SPFH domain, Band 7 family protein
Mhun_2609 Uncharacterized protein
Mhun_2867 30S ribosomal protein S27ae
Mhun_0424 PKD
Mhun_1929 Beta-lactamase
Mhun_0425 PKD
Mhun_1948 Uncharacterized protein
Mhun_2393 2-oxoacid:acceptor oxidoreductase, delta subunit,
Mhun_1825 TrkA-C
Mhun_1035 2-amino-3,7-dideoxy-D-threo-hept-6-ulosonate syn
Mhun_0627 Small GTP-binding protein domain
Mhun_0422 PKD
Mhun_0493 Response regulator receiver sensor signal transdu
Mhun_0432 Uncharacterized protein
Mhun_2562 Glutamyl-tRNA reductase
Mhun_2475 L-aspartate aminotransferase apoenzyme / phosph
Mhun_1534 Uncharacterized protein
Mhun_2474 N5-carboxyaminoimidazole ribonucleotide mutase
Mhun_2442 PKD
Mhun_1334 Molybdenum ABC transporter, periplasmic molybda
Mhun_1466 Fructose-bisphosphate aldolase
Mhun_3230 Acetylglutamate kinase
Mhun_3118 Methyltransferase type 12
Mhun_2898 50S ribosomal protein L18e
Mhun_2761 Uncharacterized protein
Mhun_2557 Uncharacterized protein
Mhun_2288 Prefoldin subunit beta
Mhun_1105 SSU ribosomal protein S6P modification protein
Mhun_1459 Aminotransferase
Mhun_0116 Argininosuccinate synthase
Mhun_1944 Peptidase S8 and S53, subtilisin, kexin, sedolisin
Mhun_2849 SufBD
Mhun_1156 DNA polymerase
Mhun_2531 Histidinol dehydrogenase
Mhun_3060 50S ribosomal protein L37e
Mhun_2945 Aminoglycoside phosphotransferase
Mhun_2262 AMP phosphorylase
Mhun_0551 UvrD/REP helicase
Mhun_0975 Ribose-phosphate pyrophosphokinase
Mhun_3032 IMP cyclohydrolase
Mhun_2450 AMP-dependent synthetase and ligase
Mhun_1971 Uncharacterized protein
Mhun_1839;Mhun_1842 F420-non-reducing hydrogenase subu
Mhun_1609 ABC transporter related protein
Mhun_0058 Uncharacterized protein
Mhun_1513 Uncharacterized protein
Mhun_3174 Reduced coenzyme F420:NADP oxidoreductase
Mhun_0727 Uncharacterized protein
Mhun_3087 Uncharacterized protein
Mhun_2617 Uncharacterized protein
Mhun_1284 Uncharacterized protein
Mhun_2080 Exonuclease SbcC
Mhun_2395 Pyruvate flavodoxin/ferredoxin oxidoreductase-like
Mhun_1060 AIR synthase related protein
Mhun_1925 CheW protein
Mhun_1303 UPF0182 protein Mhun_1303
Mhun_1544 Dipeptidyl aminopeptidase/acylaminoacyl-peptidas
Mhun_2693 PAS/PAC sensor signal transduction histidine kinas
Mhun_1762 V-type ATP synthase subunit E 2
Mhun_0331 Methyl-accepting chemotaxis sensory transducer
Mhun_0630 Pyruvate oxidase
Mhun_0499 Methyl-accepting chemotaxis sensory transducer w
Mhun_1119 tRNA-archaeosine synthase
Mhun_0622 4Fe-4S ferredoxin, iron-sulfur binding protein
Mhun_2324 2,3-bisphosphoglycerate-dependent phosphoglyce
Mhun_2438 Carboxylyase-related protein
Mhun_0149 Uncharacterized protein
Mhun_2299 Uncharacterized protein
Mhun_2930 Uncharacterized protein
Mhun_1424 Uncharacterized protein
Mhun_1722 Putative PAS/PAC sensor protein
Mhun_2746;Mhun_2748 Uncharacterized protein
Mhun_1836 CoB--CoM heterodisulfide reductase subunit C
Mhun_1055 Chaperonin Cpn10
Mhun_0148 Putative PAS/PAC sensor protein
Mhun_0668 Cobalamin Vitamin B12 biosynthesis CbiX protein
Mhun_3005 Uncharacterized protein
Mhun_1181 V-type ATP synthase subunit C
Mhun_2174 Tetrahydromethanopterin S-methyltransferase, sub
Mhun_3189 Pyruvate carboxylase subunit B
Mhun_0165 Archaeal histone
Mhun_0790 Phosphoribosyl-ATP pyrophosphatase
Mhun_0568 TATA-box-binding protein
Mhun_1780 Uncharacterized protein
Mhun_0224 Fmn-binding protein
Mhun_3025 tRNA pseudouridine synthase Pus10
Mhun_2396 Thiamine pyrophosphate enzyme-like TPP-binding
Mhun_0911 Aminotransferase
Mhun_0931 Uncharacterized protein
Mhun_0728 Uncharacterized protein
Mhun_3049 Glutaredoxin
Mhun_2307 CoA enzyme activase
Mhun_3054 Aspartokinase
Mhun_2497 PKD
Mhun_0936 Uncharacterized protein
Mhun_1204 Uncharacterized protein
Mhun_0444 Methenyltetrahydromethanopterin cyclohydrolase
Mhun_0648 Peptidase S8 and S53, subtilisin, kexin, sedolisin
Mhun_3057 Uncharacterized protein
Mhun_1339 Uncharacterized protein
Mhun_0532 Uncharacterized protein
Mhun_0032 Amino acid ABC transporter substrate-binding prote
Mhun_0489 von Willebrand factor, type A
Mhun_2458 Archaeal histone
Mhun_0919 Archaeal histone
Mhun_0972 Chaperonin Cpn60/TCP-1
Mhun_0104 Type II secretion system protein E
Mhun_0576 Archaeal histone
Mhun_0611 PRC-barrel
Mhun_0097 Uncharacterized protein
Mhun_1984 Formylmethanofuran dehydrogenase, subunit D
Mhun_2441 PKD
Mhun_0306;Mhun_0047;Mhun_2057;Mhun_2058 Uncharacteri
Mhun_0955 Tetratricopeptide TPR_2


-2.5
0
2.5
Formate
Hydrogen
Syntrophy
R1 R2 R3 R1 R2 R3 R1 R2 R3
Mhun_3004 3-hydroxy-3-methylglutaryl coenzyme A reductase
Mhun_2897 50S ribosomal protein L13
Mhun_0976 Lon-B peptidase, Serine peptidase, MEROPS fam
Mhun_1932 Uncharacterized protein
Mhun_2481 Transcription initiation factor IIB
Mhun_0496 APHP
Mhun_2473 Aminotransferase
Mhun_2335 Translation initiation factor 2 subunit beta
Mhun_0642 Putative PAS/PAC sensor protein
Mhun_1163 PKD
Mhun_2918 Histidine--tRNA ligase
Mhun_2619 Nucleotidyl transferase
Mhun_2126 DegT/DnrJ/EryC1/StrS aminotransferase
Mhun_1241 Acetolactate synthase, small subunit
Mhun_1128 Translation initiation factor 2 subunit alpha AeIF-2a
Mhun_0741 Uncharacterized protein
Mhun_0089 Fumarase alpha subunit
Mhun_0092 2-oxoglutarate ferredoxin oxidoreductase, alpha su
Mhun_2637 Putative PAS/PAC sensor protein
Mhun_0646 Transcriptional regulator, MarR family
Mhun_1120 tRNA-guanine15 transglycosylase
Mhun_2175 Tetrahydromethanopterin S-methyltransferase, sub
Mhun_1981 Formylmethanofuran dehydrogenase, subunit C
Mhun_2106 Formylmethanofuran dehydrogenase, subunit B
Mhun_2938 PRC-barrel
Mhun_0045 Glutamate synthase NADPH GltB2 subunit
Mhun_1491 30S ribosomal protein S17e
Mhun_2484 Hydrogenase accessory protein HypB
Mhun_2406 Uncharacterized protein
Mhun_0592 AMP-dependent synthetase and ligase
Mhun_1721 Acetyl-coenzyme A synthetase
Mhun_2173 Tetrahydromethanopterin S-methyltransferase, sub
Mhun_3235 Anti-sigma-factor antagonist STAS domain protein
Mhun_0527 Uncharacterized protein
Mhun_0932 GHMP kinase
Mhun_2968 Putative PAS/PAC sensor protein
Mhun_0052 DNA-directed RNA polymerase
Mhun_2811 Ribonucleoside-triphosphate reductase, anaerobic
Mhun_1081 Uncharacterized protein
Mhun_0970 PKD
Mhun_0550 ATP-dependent nuclease subunit B-like protein
Mhun_0593 TATA-box-binding protein
Mhun_3096 GCN5-related N-acetyltransferase
Mhun_2717 Uncharacterized protein
Mhun_2604 Uncharacterized protein
Mhun_2176 Cysteine--tRNA ligase
Mhun_1493 4-hydroxy-tetrahydrodipicolinate reductase
Mhun_1623 Amino acid-binding ACT
Mhun_1604 Nucleoside diphosphate kinase
Mhun_0606 Isoleucine--tRNA ligase
Mhun_0846 Proteasome subunit beta
Mhun_2334 GTP cyclohydrolase MptA
Mhun_1973 Nitrite and sulphite reductase 4Fe-4S region
Mhun_1078 Uncharacterized protein
Mhun_1592 Elongation factor 1-alpha
Mhun_2122 NDP-hexose 3-C-methyltransferase TylCIII
Mhun_2625 Methionine--tRNA ligase
Mhun_2229 Adenylate kinase
Mhun_1894 Uncharacterized protein
Mhun_2021 Formate dehydrogenase, alpha subunit F420
Mhun_2414 V-type H+-translocating pyrophosphatase
Mhun_0088 50S ribosomal protein L10e
Mhun_2032 Methyl-accepting chemotaxis sensory transducer v
Mhun_2854 Nucleotidyl transferase
Mhun_2050 ATP phosphoribosyltransferase
Mhun_0174 Phosphoenolpyruvate carboxylase
Mhun_0978 Peptidase U62, modulator of DNA gyrase
Mhun_2053 Peptidase S8 and S53, subtilisin, kexin, sedolisin
Mhun_2994 TPR repeat
Mhun_3052 Thiol-driven fumarate reductase, iron-sulfur protein
Mhun_2526 Acetylornithine aminotransferase
Mhun_0556 6-phosphofructokinase
Mhun_0672 Branched chain amino acid aminotransferase apoe
Mhun_2339 Methionine aminopeptidase
Mhun_3080 NAD-dependent epimerase/dehydratase
Mhun_3184 Biotin--acetyl-CoA-carboxylase ligase
Mhun_2258 Cell division GTPase-like protein
Mhun_1113 Ornithine carbamoyltransferase
Mhun_1067 Uncharacterized protein
Mhun_0057 Uncharacterized protein
Mhun_0356 RNA-binding region RNP-1 RNA recognition motif
Mhun_0109 Chemotaxis response regulator protein-glutamate
Mhun_2156 Uncharacterized protein
Mhun_0651 Uncharacterized protein
Mhun_1791 Tryptophan synthase alpha chain
Mhun_2409 Pentapeptide repeat
Mhun_0923 S-adenosylmethionine synthase
Mhun_1957 Methyl-accepting chemotaxis sensory transducer
Mhun_1566 RNA-binding region RNP-1 RNA recognition motif
Mhun_2625 Tetratricopeptide TPR_2
Mhun_0977 Peptidase U62, modulator of DNA gyrase
Mhun_0667 Uncharacterized protein
Mhun_0179 Heat shock protein 70
Mhun_0310 Uncharacterized protein
Mhun_1197 Phosphoglucomutase/phosphomannomutase alpha
Mhun_2921 Uncharacterized protein
Mhun_2861 Translation initiation factor 2 subunit gamma AeIF-
Mhun_2118 NAD-dependent epimerase/dehydratase
Mhun_1803 50S ribosomal protein L24e
Mhun_1942 Beta-lactamase-like protein
Mhun_2893 Enolase 3
Mhun_2181 O-acetylhomoserine sulfhydrolase
Mhun_0022 Bifunctional protein FolD
Mhun_1554 Beta-lactamase-like protein
Mhun_1787 Anthranilate phosphoribosyltransferase
Mhun_3200 Glycosyl transferase, family 2
Mhun_2851 Uncharacterized protein
Mhun_1808 Formylmethanofuran--tetrahydromethanopterin for
Mhun_1165 V-type ATP synthase subunit D
Mhun_1056 60 kDa chaperonin
Mhun_0495 Methyl-accepting chemotaxis sensory transducer
Mhun_0352 Acetyl-coenzyme A synthetase
Mhun_0332 ATPase, E1-E2 type
Mhun_0128 Protein GrpE
Mhun_0225 Uncharacterized protein
Mhun_3033 Uncharacterized protein
Mhun_0660 Cell division protein FtsZ
Mhun_1166 Peptidyl-prolyl cis-trans isomerase
Mhun_0127 Chaperone protein DnaJ
Mhun_0052 Glutamyl-tRNAGln amidotransferase subunit E
Mhun_0795 Beta-lactamase-like protein
Mhun_2345 Uncharacterized protein
Mhun_1846 Multi-sensor signal transduction histidine kinase
Mhun_0015 Methyl-accepting chemotaxis sensory transducer
Mhun_0023 Serine hydroxymethyltransferase
Mhun_0824 Adenylosuccinate lyase
Mhun_1732 Tryptophanyl-tRNA synthetase
Mhun_2353 Quinolinate synthetase A
Mhun_2361 3-isopropylmalate dehydratase large subunit
Mhun_2924 Uncharacterized protein
Mhun_0515 Uncharacterized protein
Mhun_1007 Threonine--tRNA ligase
Mhun_3063 D-3-phosphoglycerate dehydrogenase
Mhun_2942 Diaminopimelate decarboxylase
Mhun_2336 AAA ATPase, central region
Mhun_0044 Ferritin and Dps
Mhun_1117 Sulfide dehydrogenase Flavoprotein subunit SudA
Mhun_0497 Uncharacterized protein
Mhun_0916 Replication factor C large subunit
Mhun_2075 ThiJ/PfpI
Mhun_2471 ORC1-type DNA replication protein
Mhun_3039 Response regulator receiver sensor signal transdu
Mhun_2596 Putative PAS/PAC sensor protein
Mhun_2284 LSU ribosomal protein L37AE
Mhun_1935 Putative ribose 1,5-bisphosphate isomerase
Mhun_0690 Acetyl-CoA decarbonylase/synthase complex subu
Mhun_1345 Uncharacterized protein
Mhun_2837 Arginine--tRNA ligase
Mhun_3043 Endothelin-converting enzyme, Metallo peptidase,
Mhun_1781 Uncharacterized protein
Mhun_1175 Methyl-accepting chemotaxis sensory transducer
Mhun_3045 TPR repeat
Mhun_2698 Uncharacterized protein
Mhun_0821 Uncharacterized protein
Mhun_2074 Clostripain
-2.5
0
2.5
Formate
Hydrogen
Syntrophy
R1 R2 R3 R1 R2 R3 R1 R2 R3
Mhun_2074 Clostripain
Mhun_0053 DNA-directed RNA polymerase subunit A
Mhun_2606 Tetratricopeptide TPR_2
Mhun_2157 Small GTP-binding protein domain
Mhun_2440 PKD
Mhun_2428 Uncharacterized protein
Mhun_1779 LemA
Mhun_1943 Multi-sensor signal transduction histidine kinase
Mhun_0093 2-oxoglutarate ferredoxin oxidoreductase, beta sub
Mhun_2231 50S ribosomal protein L15
Mhun_2213 Cysteine desulfurase IscS
Mhun_1485 Uncharacterized protein
Mhun_1750 ATPase
Mhun_2598 Uncharacterized protein
Mhun_2279 50S ribosomal protein L15e
Mhun_1456 Peptidase S8 and S53, subtilisin, kexin, sedolisin
Mhun_2051 Phosphoribosyl-AMP cyclohydrolase
Mhun_3197 Uncharacterized protein
Mhun_3176 Protein-export membrane protein SecD
Mhun_2112 Formylmethanofuran dehydrogenase, subunit C
Mhun_0217 UbiE/COQ5 methyltransferase
Mhun_1307 Protease HtpX homolog
Mhun_2316 Diaminopimelate epimerase
Mhun_2296 Elongation factor Tu, domain 2
Mhun_1628 Bifunctional enzyme Fae/Hps
Mhun_1010 Geranylgeranylglyceryl phosphate synthase
Mhun_1182 V-type ATP synthase subunit F
Mhun_0311 Uncharacterized protein
Mhun_3027 DNA-directed RNA polymerase, subunit F
Mhun_3090 Polysaccharide biosynthesis protein CapD
Mhun_1826 Uncharacterized protein
Mhun_2463 Tyrosine--tRNA ligase
Mhun_3129;Mhun_3127;Mhun_3128 Uncharacterized protein
Mhun_3021 Prefoldin subunit alpha
Mhun_2508 30S ribosomal protein S3Ae
Mhun_2318 TPR repeat
Mhun_1130 50S ribosomal protein L44e
Mhun_1696 Uncharacterized protein
Mhun_2479 Peptidase S8 and S53, subtilisin, kexin, sedolisin
Mhun_1595 Uncharacterized protein
Mhun_0542 UspA
Mhun_1022 Uncharacterized protein
Mhun_2115 Uncharacterized protein
Mhun_2986 Putative PAS/PAC sensor protein
Mhun_2446 Aspartate--tRNAAsp/Asn ligase
Mhun_1785 Anthranilate synthase, component I
Mhun_0935 Hydrogenase expression/formation protein HypE
Mhun_0084 Argininosuccinate lyase
Mhun_0462 Pyridoxamine 5-phosphate oxidase-related, FMN-
Mhun_2399 CheW protein
Mhun_0994 Replication factor C small subunit
Mhun_2010 Molybdenum ABC transporter, periplasmic molybd
Mhun_2907 Putative signal-transduction protein with CBS dom
Mhun_2836 Peptide chain release factor subunit 1
Mhun_2554 Uncharacterized conserved protein UCP033563
Mhun_1135 UPF0179 protein Mhun_1135
Mhun_0003 CheW protein
Mhun_0131 Ferritin and Dps
Mhun_0096 Succinyl-CoA ligase [ADP-forming] subunit alpha
Mhun_2249 30S ribosomal protein S19
Mhun_3085 Uncharacterized protein
Mhun_2734 Peroxiredoxin
Mhun_0554 Uncharacterized protein
Mhun_1253 FO synthase subunit 1
Mhun_0463 Putative signal transduction histidine kinase
Mhun_2243 50S ribosomal protein L14
Mhun_2943 LL-diaminopimelate aminotransferase apoenzyme
Mhun_2363 3-isopropylmalate dehydrogenase
Mhun_2858 NAD-dependent epimerase/dehydratase
Mhun_2145 Methyl-coenzyme M reductase, protein D
Mhun_3028 Uncharacterized protein
Mhun_2485 30S ribosomal protein S8e
Mhun_2253 50S ribosomal protein L3
Mhun_0050 DNA-directed RNA polymerase, subunit B
Mhun_1440 Putative PAS/PAC sensor protein
Mhun_3026 50S ribosomal protein L21e
Mhun_2239 30S ribosomal protein S14 type Z
Mhun_2164 Dimerogenase iron--molybdenum cofactor biosynthe
Mhun_1205 Small nuclear ribonucleoprotein, LSM family
Mhun_1606 Tetratricopeptide TPR_2
Mhun_2488 30S ribosomal protein S6e
Mhun_2233 30S ribosomal protein S5
Mhun_1036;Mhun_3083 2-amino-3,7-dideoxy-D-threo-hept-6-u
Mhun_1037 Transcriptional regulator, XRE family
Mhun_2902 30S ribosomal protein S13
Mhun_2132 GDP-mannose 4,6-dehydratase
Mhun_0657 50S ribosomal protein L11
Mhun_0024 Asparagine deamidase
Mhun_0656 50S ribosomal protein L1
Mhun_2626 Valine--tRNA ligase
Mhun_0666 Acyl-CoA decarbonylase/synthase gamma subun
Mhun_2236 LSU ribosomal protein L32E
Mhun_2250 50S ribosomal protein L2
Mhun_2362 3-isopropylmalate dehydratase, small subunit
Mhun_0847 Putative signal transduction protein with CBS dom
Mhun_1863 CRISPR-associated protein Csc2
Mhun_2922 ATPase, PilT family
Mhun_0024 Uncharacterized protein
Mhun_0601 ATPase associated with various cellular activities,
Mhun_1180 V-type ATP synthase subunit E 1
Mhun_0996 TPR repeat
Mhun_2886 Geranylgeranyl-diphosphate synthase / farnesyl-di
Mhun_2735 Alkylphosphonate uptake core
Mhun_1593 30S ribosomal protein S10
Mhun_2205 ABC transporter, substrate-binding protein, aliphati
Mhun_2340 Peptidase M24
Mhun_2124 Glycosyl transferase, group 1
Mhun_0973 PurE-like protein
Mhun_1249 LipA
Mhun_2572 Uncharacterized protein
Mhun_0938 Uncharacterized protein
Mhun_2142 DegT/DnrJ/EryC1/StrS aminotransferase
Mhun_2247 30S ribosomal protein S3
Mhun_2573 Uncharacterized protein
Mhun_2839 O-phosphoserine--tRNACys ligase
Mhun_1547 Uncharacterized protein
Mhun_0655 50S ribosomal protein L10
Mhun_0825 Dihydroneopterin aldolase
Mhun_2113 UDP-glucose 6-dehydrogenase
Mhun_0081 Uncharacterized protein
Mhun_2394 Pyruvate ferredoxin oxidoreductase, gamma subun
Mhun_0769 S-layer domain-like protein
Mhun_1051 Uridylate kinase
Mhun_0535 Uncharacterized protein
Mhun_1717 Phosphoesterase, RecJ-like protein
Mhun_2923 Leucine--tRNA ligase
Mhun_2852 Phosphoglucomutase/phosphomannomutase alph
Mhun_0956 Adenosylhomocysteinase
Mhun_2828 Elongation factor 2
Mhun_2762 PKD
Mhun_1343 Ferrous iron transport protein B
Mhun_2489 Protein translation factor IF-2
Mhun_2900 30S ribosomal protein S11
Mhun_0083 Glutamyl-tRNAGln amidotransferase subunit D
Mhun_2274 Nascent polypeptide-associated complex protein
Mhun_0658 Transcription elongation factor Spt5
Mhun_2896 30S ribosomal protein S9
Mhun_2063 Uncharacterized protein
Mhun_0565 Uncharacterized protein
Mhun_1956 Uncharacterized protein
Mhun_2217 Hydroxyethylthiazole kinase
Mhun_2863 DNA-directed RNA polymerase, subunit E
Mhun_2359 Pyruvate ferredoxin/flavodoxin oxidoreductase
Mhun_0051 DNA-directed RNA polymerase
Mhun_0292 Cobalamin synthase CobN subunit
Mhun_2358 Indolepyruvate oxidoreductase subunit IorA
Mhun_0621 Carbonic anhydrase Gamma family Znll-dependen
Mhun_2283 Uncharacterized protein
Mhun_2797 Transcription factor E
Mhun_1627 AMP-dependent synthetase and ligase
Mhun_1949 Uncharacterized protein
Mhun_2632 Inosine-5-monophosphate dehydrogenase
Mhun_1624 Phenylacetate-CoA ligase
Mhun_0190 ABC transporter related protein
Mhun_0218 Extracellular solute-binding protein, family 5
Mhun_3141 Tetratricopeptide TPR_2
Mhun_2724 5-Nucleotidase-like protein

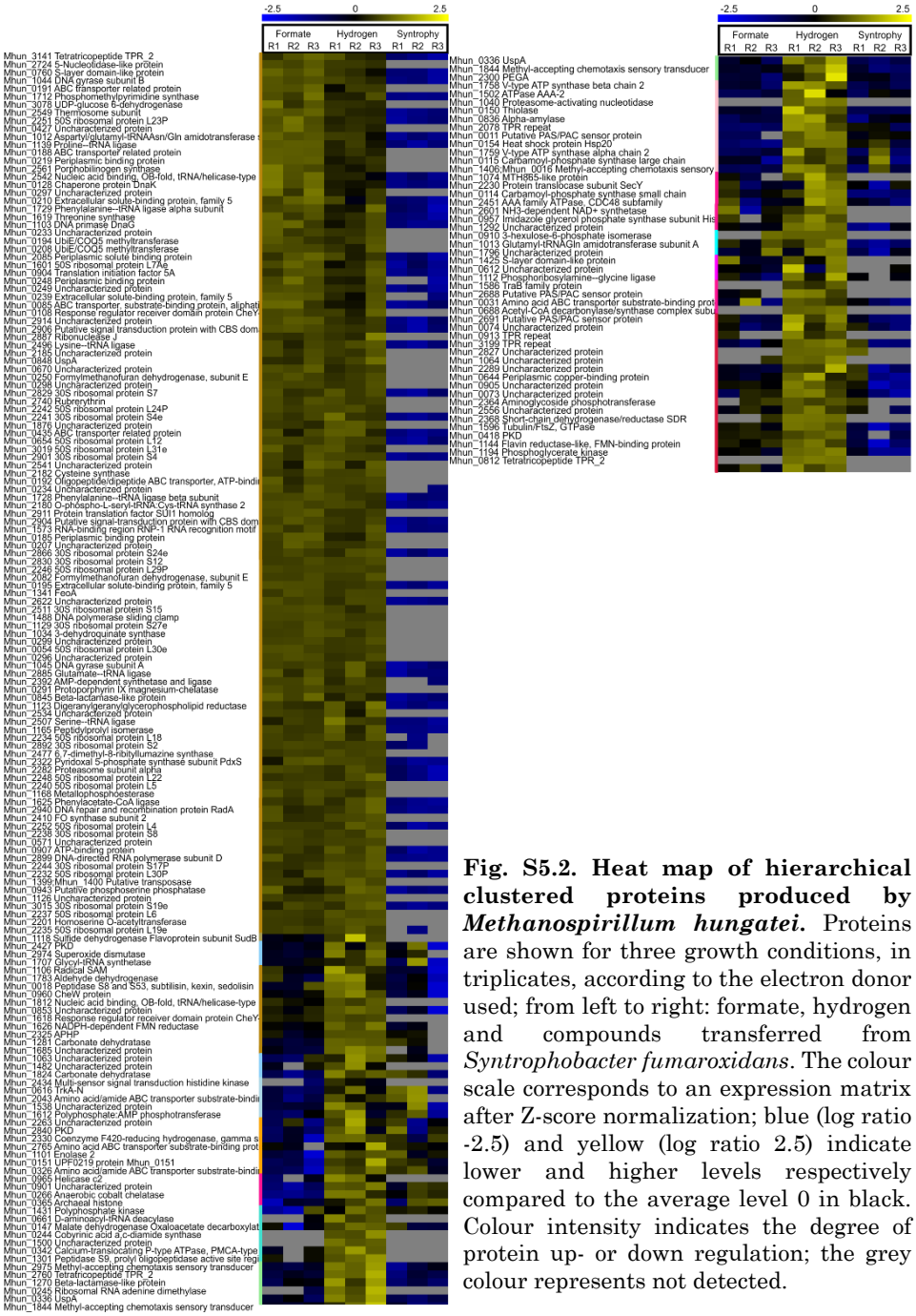

Fig. S5.2. Heat map of hierarchical clustered proteins produced by *Methanospirillum hungatei*. Proteins are shown for three growth conditions, in triplicates, according to the electron donor used; from left to right: formate, hydrogen and compounds transferred from *Syntrophobacter fumaroxidans*. The colour scale corresponds to an expression matrix after Z-score normalization; blue (log ratio -2.5) and yellow (log ratio 2.5) indicate lower and higher levels respectively compared to the average level 0 in black. Colour intensity indicates the degree of protein up- or down regulation; the grey colour represents not detected.


-2.5
0
2.5
Formate
Hydrogen
Syntrophy
R1 R2 R3 R1 R2 R3 R1 R2 R3
Mfor_0601 Archaeal histone A1
Mfor_0472 CoB-CoM heterodisulfide reductase iron-sulfur subu
Mfor_0015 Uncharacterized protein
Mfor_0174 TATA-box-binding protein
Mfor_2177 Histone acetyltransferase
Mfor_0132 O-phospho-L-seryl-tRNA:Cys-tRNA synthase
Mfor_1197 DNA polymerase sliding clamp
Mfor_0734 4Fe-4S ferredoxin
Mfor_1073 4Fe-4S ferredoxin
Mfor_0709 Sirohydrochlorin cobaltochelatase
Mfor_0542 Uncharacterized protein
Mfor_0536 Uncharacterized protein
Mfor_1919 Uncharacterized protein
Mfor_0904 Tetrahydromethanopterin S-methyltransferase subu
Mfor_2256 Uncharacterized protein
Mfor_1876 Uncharacterized protein
Mfor_0574 F420-dependent NADP reductase
Mfor_0903 Tetrahydromethanopterin S-methyltransferase subu
Mfor_0940 Archaeoflavoprotein AfpA
Mfor_1734 Peroxiredoxin
Mfor_0635 Uncharacterized protein
Mfor_0575 3-hexulose-6-phosphate isomerase HxlB2
Mfor_1889 Uncharacterized protein
Mfor_1558 2-oxoacid:acceptor oxidoreductase subunit alpha
Mfor_2241 Uncharacterized protein
Mfor_1471 Carbonic anhydrase
Mfor_1527 Formylmethanofuran dehydrogenase subunit FwdF
Mfor_0130 Glyceraldehyde-3-phosphate dehydrogenase
Mfor_1631 Tetrahydromethanopterin S-methyltransferase subu
Mfor_0922 TRAM domain-containing protein
Mfor_1735 Ferritin
Mfor_0730 Pyruvate synthase subunit PorC
Mfor_0786 UPF0145 protein BRM9_0823
Mfor_0079 CRISPR-associated negative autoregulator, DevR f
Mfor_0988 Pyridoxamine 5-phosphate oxidase family protein
Mfor_0633 Uncharacterized protein
Mfor_0580 Archaeal histone B
Mfor_2186 Uncharacterized protein
Mfor_0789 tRNAIle2 2-agmatinylcytidine synthetase TiaS
Mfor_0898 Tetrahydromethanopterin S-methyltransferase subu
Mfor_1528 4Fe-4S ferredoxin iron-sulfur binding domain-contai
Mfor_1665 Superoxide reductase
Mfor_2159 Redox-active disulfide protein
Mfor_0851 Peptidase C14 caspase catalytic subunit p20
Mfor_1292 Uncharacterized protein
Mfor_2298 Uncharacterized protein
Mfor_0759 Acetyl-CoA decarbonylase/synthase complex subuni
Mfor_1048 Uncharacterized protein
Mfor_0761 Acetyl-CoA decarbonylase/synthase complex subun
Mfor_0757 4Fe-4S ferredoxin
Mfor_0758 Acetyl-CoA decarbonylase/synthase complex subun
Mfor_0326 Protein translation factor SUI1 homolog
Mfor_1485 Formate dehydrogenase subunit beta
Mfor_1232 CoB--CoM heterodisulfide reductase subunit A HdrA
Mfor_1834 Type III restriction protein res subunit
Mfor_2252 Choloylglycine hydrolase
Mfor_1236 Uncharacterized protein
Mfor_1551 Uncharacterized protein
Mfor_1975 Uncharacterized protein
Mfor_1464 Uncharacterized protein
Mfor_0857 Uncharacterized protein
Mfor_1142 Flavodoxin
Mfor_0918 Uncharacterized protein
Mfor_1330 Uncharacterized protein
Mfor_1487 Probable formate transporter
Mfor_1486 Formate dehydrogenase subunit alpha
Mfor_0187 Uncharacterized protein
Mfor_0022 Uncharacterized protein
Mfor_0081 CRISPR-associated nuclease/helicase Cas3
Mfor_2070 Uncharacterized protein
Mfor_0371 Uncharacterized protein
Mfor_0506 Uncharacterized protein
Mfor_2150 Putative secreted protein
Mfor_0909 Methyl-coenzyme M reductase I subunit beta
Mfor_0905 Methyl-coenzyme M reductase alpha subunit McrA
Mfor_0906 Methyl-coenzyme M reductase I subunit gamma
Mfor_1230 Replication factor-A domain-containing protein
Mfor_0617 Uncharacterized protein
Mfor_0901 Tetrahydromethanopterin S-methyltransferase subu
Mfor_0533 Roadblock/LC7 domain-containing protein
Mfor_0710 Uncharacterized protein
Mfor_1794 Uncharacterized protein
Mfor_2192 Uncharacterized protein
Mfor_0897 Tetrahydromethanopterin S-methyltransferase subu
Mfor_0899 Tetrahydromethanopterin S-methyltransferase subu
Mfor_2151 Aspartate-semialdehyde dehydrogenase
Mfor_0465 Uncharacterized protein
Mfor_1965 Uncharacterized protein
Mfor_0817 Daunorubicin resistance ABC transporter ATPase su
Mfor_2152 4-hydroxy-tetrahydrodipicolinate reductase
Mfor_0732 Pyruvate synthase subunit PorA
Mfor_0704 5,10-methylenetetrahydromethanopterin reductase
Mfor_1277 Formylmethanofuran dehydrogenase subunit E
Mfor_0198 Anthranilate synthase component 1
Mfor_2019 4Fe-4S ferredoxin
Mfor_2417 CBS domain-containing protein
Mfor_2040 Cysteine desulfurase IscS
Mfor_0877 Uncharacterized protein
Mfor_1730 Uncharacterized protein
Mfor_2081 Uncharacterized protein
Mfor_0345 Uncharacterized protein
Mfor_1669 Uncharacterized protein
Mfor_0167 ATPase
Mfor_2245 Uncharacterized protein
Mfor_0878 Putative secreted protein
Mfor_1386 PAS/PAC sensor protein
Mfor_2393 Pyridoxamine 5-phosphate oxidase family protein
Mfor_1409 O-phosphoserine--tRNACys ligase
Mfor_0738 Phosphate-specific transport system accessory prot
Mfor_1343 Acetolactate synthase
Mfor_0471 CoB--CoM heterodisulfide reductase subunit B HdrB
Mfor_0312 50S ribosomal protein L15
Mfor_1840 DNA/RNA helicase
Mfor_1786 Uncharacterized protein
Mfor_1821 Protease
Mfor_1844 Uncharacterized protein
Mfor_2178 Deoxyribose-phosphate aldolase
Mfor_1592 Uncharacterized protein
Mfor_0765 Type II secretion system protein E GspE
Mfor_0543 Methyl viologen-reducing hydrogenase gamma subu
Mfor_1529 Molybdenum-pterin binding protein Mop1
Mfor_0674 MCM family protein
Mfor_1784 Uncharacterized protein
Mfor_0881 F420-non-reducing hydrogenase subunit A
Mfor_1067 Uncharacterized protein
Mfor_1570 Hydroxylamine reductase
Mfor_0546 Replication factor C small subunit
Mfor_0611 Fructose 1,6-bisphosphatase Fbp
Mfor_2343 Putative membrane protein
Mfor_2183 Putative membrane protein
Mfor_1264 ATP-dependent DNA helicase
Mfor_1453 Imidazole glycerol phosphate synthase subunit HisF
Mfor_1013 Catalase-peroxidase
Mfor_1385 2-isopropylmalate synthase LeuA
Mfor_2305 Cupin
Mfor_1255 Rubrerythrin
-2.5
0
2.5
Formate
Hydrogen
Syntrophy
R1 R2 R3 R1 R2 R3 R1 R2 R3
Mfor_2305 Cupin
Mfor_1255 Rubrerythrin
Mfor_2090 Uncharacterized protein
Mfor_0825 Methyl-coenzyme M reductase component A2 AtwA
Mfor_1099 Bifunctional NADPH-hydrate repair enzyme Nnr
Mfor_1050 Formamidopyrimidine-DNA glycosylase
Mfor_0900 Tetrahydromethanopterin S-methyltransferase subu
Mfor_0075 Uridylate kinase
Mfor_0529 Site-determining protein
Mfor_0883 F420-non-reducing hydrogenase iron-sulfur subunit
Mfor_1104 SPFH domain/Band 7 family protein
Mfor_2227 Oxidoreductase MW2403
Mfor_2201 UDP-N-acetylglucosamine 2-epimerase
Mfor_1683 N-acetyl-gamma-glutamyl-phosphate reductase
Mfor_0244 Vl polysaccharide biosynthesis protein
Mfor_1538 Phosphomethylpyrimidine synthase
Mfor_2121 Glutamine synthetase GlnA1
Mfor_1181 Coenzyme F420 hydrogenase subunit beta
Mfor_1822 Uncharacterized protein
Mfor_1715 Uncharacterized protein
Mfor_1543 DNA ligase
Mfor_1206 Signal recognition particle 54 kDa protein
Mfor_1677 Phenylalanine--tRNA ligase beta subunit
Mfor_2226 4Fe-4S ferredoxin iron-sulfur binding domain-contai
Mfor_0735 Formate hydrogenlyase, iron-sulfur subunit 2
Mfor_1370 Imidazoleglycerol-phosphate dehydratase
Mfor_1316 UPF0147 protein BRM9_2384
Mfor_2043 Pyridoxamine 5-phosphate oxidase-like FMN-bindin
Mfor_1070 Energy-converting hydrogenase B subunit N EhbN
Mfor_1389 PQQ repeat-containing cell surface protein
Mfor_1577 Methanogenesis marker protein 9
Mfor_2115 Triphosphoribosyl-dephospho-CoA protein
Mfor_0300 DNA-directed RNA polymerase subunit D
Mfor_0935 Archaeal glutamate synthase [NADPH]
Mfor_1304 Cyclophilin type peptidyl-prolyl cis-trans isomerase
Mfor_2144 Rhodanese domain-containing protein
Mfor_1335 Putative branched-chain-amino-acid aminotransfera
Mfor_0731 Pyruvate ferredoxin oxidoreductase delta subunit P
Mfor_0880 Polyferredoxin protein MvhB
Mfor_1521 Formylmethanofuran dehydrogenase, subunit E reg
Mfor_0056 Uncharacterized protein
Mfor_0908 Methyl-coenzyme M reductase D subunit McrD
Mfor_0150 CBS domain-containing membrane protein
Mfor_1342 Putative acetolactate synthase small subunit
Mfor_2386 Carboxymuconolactone decarboxylase family prote
Mfor_1363 F420-dependent methylenetetrahydromethanopteri
Mfor_0102 Adenine deaminase
Mfor_1176 Uncharacterized protein
Mfor_1344 Phosphoribosylamine--glycine ligase
Mfor_1681 Protein-export membrane protein SecF
Mfor_0532 Uncharacterized protein
Mfor_0741 Phosphate import ATP-binding protein PstB
Mfor_0595 Argininosuccinate lyase
Mfor_2181 Archaeal histone A2
Mfor_2163 ATP-dependent DNA helicase Hel308
Mfor_1680 Protein-export membrane protein SecD
Mfor_2022 Formylmethanofuran-tetrahydromethanopterin form
Mfor_0335 Uncharacterized protein
Mfor_0824 UPF0251 protein BRM9_0861
Mfor_0518 ACT domain-containing protein
Mfor_1355 Cell division ATPase MinD1
Mfor_1490 Molybdopterin-guanine dinucleotide biosynthesis pr
Mfor_1741 Methyl-coenzyme M reductase component A2 AtwA
Mfor_0696 DNA-binding protein MutS2
Mfor_0004 Uncharacterized protein
Mfor_0308 50S ribosomal protein L34e
Mfor_1555 Ketoisovalerate ferredoxin oxidoreductase gamma s
Mfor_0074 Uncharacterized protein
Mfor_0328 30S ribosomal protein S3
Mfor_NotFound 50S ribosomal protein L37e
Mfor_2459 50S ribosomal protein L12
Mfor_0547 Replication factor C large subunit
Mfor_2309 Phosphoribosylformylglycinamidine synthase subun
Mfor_1848 Putative transcriptional regulator
Mfor_2449 ABC transporter ATP-binding protein
Mfor_2025 CBS domain-containing protein
Mfor_0781 PRC-barrel domain-containing protein
Mfor_0127 KH domain-containing protein
Mfor_0590 DNA-directed RNA polymerase
Mfor_2102 Sensory transduction histidine kinase
Mfor_2377 Exosome subunit
Mfor_2176 PRC-barrel domain-containing protein
Mfor_1733 Superoxide dismutase
Mfor_0620 Glutamine amidotransferase
Mfor_0273 Family 2 glycosyl transferase
Mfor_0377 Uncharacterized protein
Mfor_0622 Coenzyme F420 hydrogenase
Mfor_1956 2-amino-3,7-dideoxy-D-threo-hept-6-ulosonate synt
Mfor_2400 Putative hydrogenase nickel incorporation protein H
Mfor_0658 50S ribosomal protein L31e
Mfor_2439 Universal stress protein UspA5
Mfor_2103 Response regulator receiver protein
Mfor_2042 O-acetylhomoserine Thiol-lyase
Mfor_0301 30S ribosomal protein S11
Mfor_0306 Ribosomal protein L14e Rpl14e
Mfor_1997 Uncharacterized protein
Mfor_1326 30S ribosomal protein S15
Mfor_1846 SMC domain-containing protein
Mfor_0057 Demethylmenaquinone methyltransferase
Mfor_2208 Uncharacterized protein
Mfor_2410 DEAD-box ATP-dependent RNA helicase CshA
Mfor_2378 Proteasome subunit alpha
Mfor_2424 Cell wall biosynthesis protein Mur ligase family
Mfor_0278 Uncharacterized protein
Mfor_0733 Pyruvate ferredoxin oxidoreductase beta subunit Po
Mfor_0939 AsnC family transcriptional regulator
Mfor_1542 Histidine kinase/response regulator hybrid protein
Mfor_0763 Acetyl-CoA decarbonylase/synthase complex subuni
Mfor_0803 Uncharacterized protein
Mfor_1842 Adenine specific DNA methylase Mod
Mfor_0795 V-type ATP synthase subunit I
Mfor_1524 ABC transporter substrate-binding protein
Mfor_0200 Indole-3-glycerol phosphate synthase
Mfor_0604 Aspartate transaminase
Mfor_0882 F420-non-reducing hydrogenase subunit G
Mfor_2023 PfkB domain-containing protein
Mfor_1038 CBS domain-containing protein
Mfor_1957 3-dehydroquinate synthase
Mfor_2153 4-hydroxy-tetrahydrodipicolinate synthase
Mfor_1097 Digeranylgeranylglycerophospholipid reductase
Mfor_0009 Peptidase U62 modulator of DNA gyrase
Mfor_0343 Uncharacterized protein
Mfor_0091 Peptide chain release factor subunit 1
Mfor_2311 Uroporphyrinogen-III C-methyltransferase
Mfor_1504 Extracellular solute-binding protein
Mfor_0145 Uncharacterized protein
Mfor_0563 3-hydroxy-3-methylglutaryl coenzyme A reductase
Mfor_1766 tRNA-guanine15 transglycosylase
Mfor_0782 Probable L-aspartate dehydrogenase
Mfor_1182 Coenzyme F420 hydrogenase gamma subunit FrhG
Mfor_2096 Circadian clock protein KaiC
Mfor_2396 Uncharacterized protein
Mfor_2074 Homoserine dehydrogenase
Mfor_1301 Uncharacterized protein
Mfor_0118 Putative R-citramalate synthase CimA
Mfor_0645 ORC1-type DNA replication protein

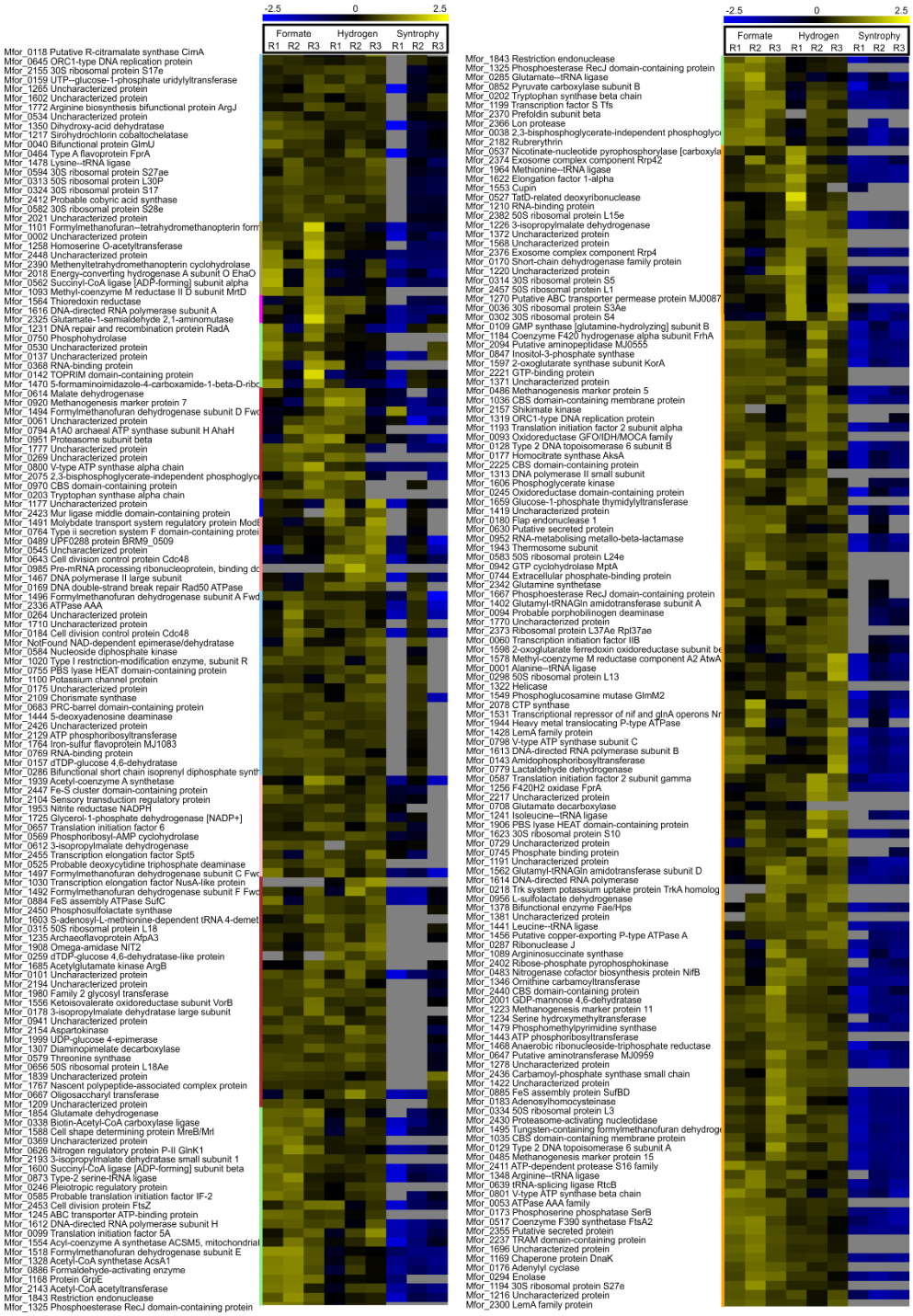
-2.5
0
2.5
Formate
Hydrogen
Syntrophy
R1 R2 R3 R1 R2 R3 R1 R2 R3
Mfor_0118 Putative R-citramalate synthase CimA
Mfor_0645 ORC1-type DNA replication protein
Mfor_2155 30S ribosomal protein S17e
Mfor_0159 UTP--glucose-1-phosphate uridylyltransferase
Mfor_1265 Uncharacterized protein
Mfor_1602 Uncharacterized protein
Mfor_1772 Arginine biosynthesis bifunctional protein ArgJ
Mfor_0534 Uncharacterized protein
Mfor_1350 Dihydroxy-acid dehydratase
Mfor_1217 Sirohydrochlorin cobaltochelatase
Mfor_0040 Bifunctional protein GlmU
Mfor_0464 Type A flavoprotein FprA
Mfor_1478 Lysine--tRNA ligase
Mfor_0594 30S ribosomal protein S27ae
Mfor_0313 50S ribosomal protein L30P
Mfor_0324 30S ribosomal protein S17
Mfor_2412 Probable cobyric acid synthase
Mfor_0582 30S ribosomal protein S28e
Mfor_2021 Uncharacterized protein
Mfor_1101 Formylmethanofuran--tetrahydromethanopterin form
Mfor_0002 Uncharacterized protein
Mfor_1258 Homoserine O-acetyltransferase
Mfor_2448 Uncharacterized protein
Mfor_2390 Methenyltetrahydromethanopterin cyclohydrolase
Mfor_2018 Energy-converting hydrogenase A subunit O EhaO
Mfor_0562 Succinyl-CoA ligase [ADP-forming] subunit alpha
Mfor_1093 Methyl-coenzyme M reductase II D subunit MrtD
Mfor_1564 Thioredoxin reductase
Mfor_1616 DNA-directed RNA polymerase subunit A
Mfor_2325 Glutamate-1-semialdehyde 2,1-aminomutase
Mfor_1231 DNA repair and recombination protein RadA
Mfor_0750 Phosphohydrolase
Mfor_0530 Uncharacterized protein
Mfor_0137 Uncharacterized protein
Mfor_0368 RNA-binding protein
Mfor_0142 TOPRIM domain-containing protein
Mfor_1470 5-formaminoimidazole-4-carboxamide-1-beta-D-ribo
Mfor_0614 Malate dehydrogenase
Mfor_0920 Methanogenesis marker protein 7
Mfor_1494 Formylmethanofuran dehydrogenase subunit D Fwc
Mfor_0061 Uncharacterized protein
Mfor_0794 A1A0 archaeal ATP synthase subunit H AhaH
Mfor_0951 Proteasome subunit beta
Mfor_1777 Uncharacterized protein
Mfor_0269 Uncharacterized protein
Mfor_0800 V-type ATP synthase alpha chain
Mfor_2075 2,3-bisphosphoglycerate-independent phosphoglyc
Mfor_0970 CBS domain-containing protein
Mfor_0203 Tryptophan synthase alpha chain
Mfor_1177 Uncharacterized protein
Mfor_2423 Mur ligase middle domain-containing protein
Mfor_1491 Molybdate transport system regulatory protein ModE
Mfor_0764 Type II secretion system F domain-containing protei
Mfor_0489 UPF0288 protein BRM9_0509
Mfor_0545 Uncharacterized protein
Mfor_0643 Cell division control protein Cdc48
Mfor_0985 Pre-mRNA processing ribonucleoprotein, binding do
Mfor_1467 DNA polymerase II large subunit
Mfor_0169 DNA double-strand break repair Rad50 ATPase
Mfor_1496 Formylmethanofuran dehydrogenase subunit A Fwd
Mfor_2336 ATPase AAA
Mfor_0264 Uncharacterized protein
Mfor_1710 Uncharacterized protein
Mfor_0184 Cell division control protein Cdc48
Mfor_NotFound NAD-dependent epimerase/dehydratase
Mfor_0584 Nucleoside diphosphate kinase
Mfor_1020 Type I restriction-modification enzyme, subunit R
Mfor_0755 PBS lyase HEAT domain-containing protein
Mfor_1100 Potassium channel protein
Mfor_0175 Uncharacterized protein
Mfor_2109 Chorismate synthase
Mfor_0683 PRC-barrel domain-containing protein
Mfor_1444 5-deoxyadenosine deaminase
Mfor_2426 Uncharacterized protein
Mfor_2129 ATP phosphoribosyltransferase
Mfor_1764 Iron-sulfur flavoprotein MJ1083
Mfor_0769 RNA-binding protein
Mfor_0157 dTDP-glucose 4,6-dehydratase
Mfor_0286 Bifunctional short chain isoprenyl diphosphate synth
Mfor_1939 Acetyl-coenzyme A synthetase
Mfor_2447 Fe-S cluster domain-containing protein
Mfor_2104 Sensory transduction regulatory protein
Mfor_1953 Nitrite reductase NADPH
Mfor_1725 Glycerol-1-phosphate dehydrogenase [NADP+]
Mfor_0657 Translation initiation factor 6
Mfor_0569 Phosphoribosyl-AMP cyclohydrolase
Mfor_0612 3-isopropylmalate dehydrogenase
Mfor_2455 Transcription elongation factor Spt5
Mfor_0525 Probable deoxycytidine triphosphate deaminase
Mfor_1497 Formylmethanofuran dehydrogenase subunit C Fwc
Mfor_1030 Transcription elongation factor NusA-like protein
Mfor_1492 Formylmethanofuran dehydrogenase subunit F Fwc
Mfor_0884 FeS assembly ATPase SufC
Mfor_2450 Phosphosulfolactate synthase
Mfor_1603 S-adenosyl-L-methionine-dependent tRNA 4-demet
Mfor_0315 50S ribosomal protein L18
Mfor_1235 Archaeoflavoprotein AfpA3
Mfor_1908 Omega-amidase NIT2
Mfor_0259 dTDP-glucose 4,6-dehydratase-like protein
Mfor_1685 Acetylglutamate kinase ArgB
Mfor_0101 Uncharacterized protein
Mfor_2194 Uncharacterized protein
Mfor_1980 Family 2 glycosyl transferase
Mfor_1556 Ketoisovalerate oxidoreductase subunit VorB
Mfor_0178 3-isopropylmalate dehydratase large subunit
Mfor_0941 Uncharacterized protein
Mfor_2154 Aspartokinase
Mfor_1999 UDP-glucose 4-epimerase
Mfor_1307 Diaminopimelate decarboxylase
Mfor_0579 Threonine synthase
Mfor_0656 50S ribosomal protein L18Ae
Mfor_1839 Uncharacterized protein
Mfor_1767 Nascent polypeptide-associated complex protein
Mfor_0667 Oligosaccharyl transferase
Mfor_1209 Uncharacterized protein
Mfor_1854 Glutamate dehydrogenase
Mfor_0338 Biotin-Acetyl-CoA carboxylase ligase
Mfor_1588 Cell shape determining protein MreB/Mrl
Mfor_0369 Uncharacterized protein
Mfor_0626 Nitrogen regulatory protein P-II GlnK1
Mfor_2193 3-isopropylmalate dehydratase small subunit 1
Mfor_1600 Succinyl-CoA ligase [ADP-forming] subunit beta
Mfor_0873 Type-2 serine-tRNA ligase
Mfor_0246 Pleiotropic regulatory protein
Mfor_0585 Probable translation initiation factor IF-2
Mfor_2453 Cell division protein FtsZ
Mfor_1245 ABC transporter ATP-binding protein
Mfor_1612 DNA-directed RNA polymerase subunit H
Mfor_0099 Translation initiation factor 5A
Mfor_1554 Acyl-coenzyme A synthetase ACSM5, mitochondrial
Mfor_1518 Formylmethanofuran dehydrogenase subunit E
Mfor_1328 Acetyl-CoA synthetase AcsA1
Mfor_0886 Formaldehyde-activating enzyme
Mfor_1168 Protein GrpE
Mfor_2143 Acetyl-CoA acetyltransferase
Mfor_1843 Restriction endonuclease
Mfor_1325 Phosphoesterase RecJ domain-containing protein
-2.5
0
2.5
Formate
Hydrogen
Syntrophy
R1 R2 R3 R1 R2 R3 R1 R2 R3
Mfor_1843 Restriction endonuclease
Mfor_1325 Phosphoesterase RecJ domain-containing protein
Mfor_0285 Glutamate--tRNA ligase
Mfor_0852 Pyruvate carboxylase subunit B
Mfor_0202 Tryptophan synthase beta chain
Mfor_1199 Transcription factor S Tfs
Mfor_2370 Prefoldin subunit beta
Mfor_2366 Lon protease
Mfor_0038 2,3-bisphosphoglycerate-independent phosphoglyc
Mfor_2182 Rubrerythrin
Mfor_0537 Nicotinate-nucleotide pyrophosphorylase [carboxyla
Mfor_2374 Exosome complex component Rrp42
Mfor_1964 Methionine--tRNA ligase
Mfor_1622 Elongation factor 1-alpha
Mfor_1553 Cupin
Mfor_0527 TatD-related deoxyribonuclease
Mfor_1210 RNA-binding protein
Mfor_2382 50S ribosomal protein L15e
Mfor_1226 3-isopropylmalate dehydrogenase
Mfor_1372 Uncharacterized protein
Mfor_1568 Uncharacterized protein
Mfor_2376 Exosome complex component Rrp4
Mfor_0170 Short-chain dehydrogenase family protein
Mfor_1220 Uncharacterized protein
Mfor_0314 30S ribosomal protein S5
Mfor_2457 50S ribosomal protein L1
Mfor_1270 Putative ABC transporter permease protein MJ0087
Mfor_0036 30S ribosomal protein S3Ae
Mfor_0302 30S ribosomal protein S4
Mfor_0109 GMP synthase [glutamine-hydrolyzing] subunit B
Mfor_1184 Coenzyme F420 hydrogenase alpha subunit FrhA
Mfor_2094 Putative aminopeptidase MJ0555
Mfor_0847 Inositol-3-phosphate synthase
Mfor_1597 2-oxoglutarate synthase subunit KorA
Mfor_2221 GTP-binding protein
Mfor_1371 Uncharacterized protein
Mfor_0486 Methanogenesis marker protein 5
Mfor_1036 CBS domain-containing membrane protein
Mfor_2157 Shikimate kinase
Mfor_1319 ORC1-type DNA replication protein
Mfor_1193 Translation initiation factor 2 subunit alpha
Mfor_0093 Oxidoreductase GFO/IDH/MOCA family
Mfor_0128 Type 2 DNA topoisomerase 6 subunit B
Mfor_0177 Homocitrate synthase AksA
Mfor_2225 CBS domain-containing protein
Mfor_1313 DNA polymerase II small subunit
Mfor_1606 Phosphoglycerate kinase
Mfor_0245 Oxidoreductase domain-containing protein
Mfor_1659 Glucose-1-phosphate thymidylyltransferase
Mfor_1419 Uncharacterized protein
Mfor_0180 Flap endonuclease 1
Mfor_0630 Putative secreted protein
Mfor_0952 RNA-metabolising metallo-beta-lactamase
Mfor_1943 Thermosome subunit
Mfor_0583 50S ribosomal protein L24e
Mfor_0942 GTP cyclohydrolase MptA
Mfor_0744 Extracellular phosphate-binding protein
Mfor_2342 Glutamine synthetase
Mfor_1667 Phosphoesterase RecJ domain-containing protein
Mfor_1402 Glutamyl-tRNAGln amidotransferase subunit A
Mfor_0094 Probable porphobilinogen deaminase
Mfor_1770 Uncharacterized protein
Mfor_2373 Ribosomal protein L37Ae Rpl37ae
Mfor_0060 Transcription initiation factor IIB
Mfor_1598 2-oxoglutarate ferredoxin oxidoreductase subunit be
Mfor_1578 Methyl-coenzyme M reductase component A2 AtwA
Mfor_0001 Alanine--tRNA ligase
Mfor_0298 50S ribosomal protein L13
Mfor_1322 Helicase
Mfor_1549 Phosphoglucosamine mutase GlmM2
Mfor_2078 CTP synthase
Mfor_1531 Transcriptional repressor of nif and glnA operons Nr
Mfor_1944 Heavy metal translocating P-type ATPase
Mfor_1428 LemA family protein
Mfor_0798 V-type ATP synthase subunit C
Mfor_1613 DNA-directed RNA polymerase subunit B
Mfor_0143 Amidophosphoribosyltransferase
Mfor_0779 Lactaldehyde dehydrogenase
Mfor_0587 Translation initiation factor 2 subunit gamma
Mfor_1256 F420H2 oxidase FprA
Mfor_2217 Uncharacterized protein
Mfor_0708 Glutamate decarboxylase
Mfor_1241 Isoleucine--tRNA ligase
Mfor_1906 PBS lyase HEAT domain-containing protein
Mfor_1623 30S ribosomal protein S10
Mfor_0729 Uncharacterized protein
Mfor_0745 Phosphate binding protein
Mfor_1191 Uncharacterized protein
Mfor_1562 Glutamyl-tRNAGln amidotransferase subunit D
Mfor_1614 DNA-directed RNA polymerase
Mfor_0218 Trk system potassium uptake protein TrkA homolog
Mfor_0956 L-sulfolactate dehydrogenase
Mfor_1378 Bifunctional enzyme Fae/Hps
Mfor_1381 Uncharacterized protein
Mfor_1441 Leucine--tRNA ligase
Mfor_1456 Putative copper-exporting P-type ATPase A
Mfor_0287 Ribonuclease J
Mfor_1089 Argininosuccinate synthase
Mfor_2402 Ribose-phosphate pyrophosphokinase
Mfor_0483 Nitrogenase cofactor biosynthesis protein NifB
Mfor_1346 Ornithine carbamoyltransferase
Mfor_2440 CBS domain-containing protein
Mfor_2001 GDP-mannose 4,6-dehydratase
Mfor_1223 Methanogenesis marker protein 11
Mfor_1234 Serine hydroxymethyltransferase
Mfor_1479 Phosphomethylpyrimidine synthase
Mfor_1443 ATP phosphoribosyltransferase
Mfor_1468 Anaerobic ribonucleoside-triphosphate reductase
Mfor_0647 Putative aminotransferase MJ0959
Mfor_1278 Uncharacterized protein
Mfor_2436 Carbamoyl-phosphate synthase small chain
Mfor_1422 Uncharacterized protein
Mfor_0885 FeS assembly protein SufBD
Mfor_0183 Adenosylhomocysteinase
Mfor_0334 50S ribosomal protein L3
Mfor_2430 Proteasome-activating nucleotidase
Mfor_1495 Tungsten-containing formylmethanofuran dehydrog
Mfor_1035 CBS domain-containing membrane protein
Mfor_0129 Type 2 DNA topoisomerase 6 subunit A
Mfor_0485 Methanogenesis marker protein 15
Mfor_2411 ATP-dependent protease S16 family
Mfor_1348 Arginine--tRNA ligase
Mfor_0639 tRNA-splicing ligase RtcB
Mfor_0801 V-type ATP synthase beta chain
Mfor_0053 ATPase AAA family
Mfor_0173 Phosphoserine phosphatase SerB
Mfor_0517 Coenzyme F390 synthetase FtsA2
Mfor_2355 Putative secreted protein
Mfor_2237 TRAM domain-containing protein
Mfor_1696 Uncharacterized protein
Mfor_1169 Chaperone protein DnaK
Mfor_0176 Adenylyl cyclase
Mfor_0294 Enolase
Mfor_1194 30S ribosomal protein S27e
Mfor_1216 Uncharacterized protein
Mfor_2300 LemA family protein

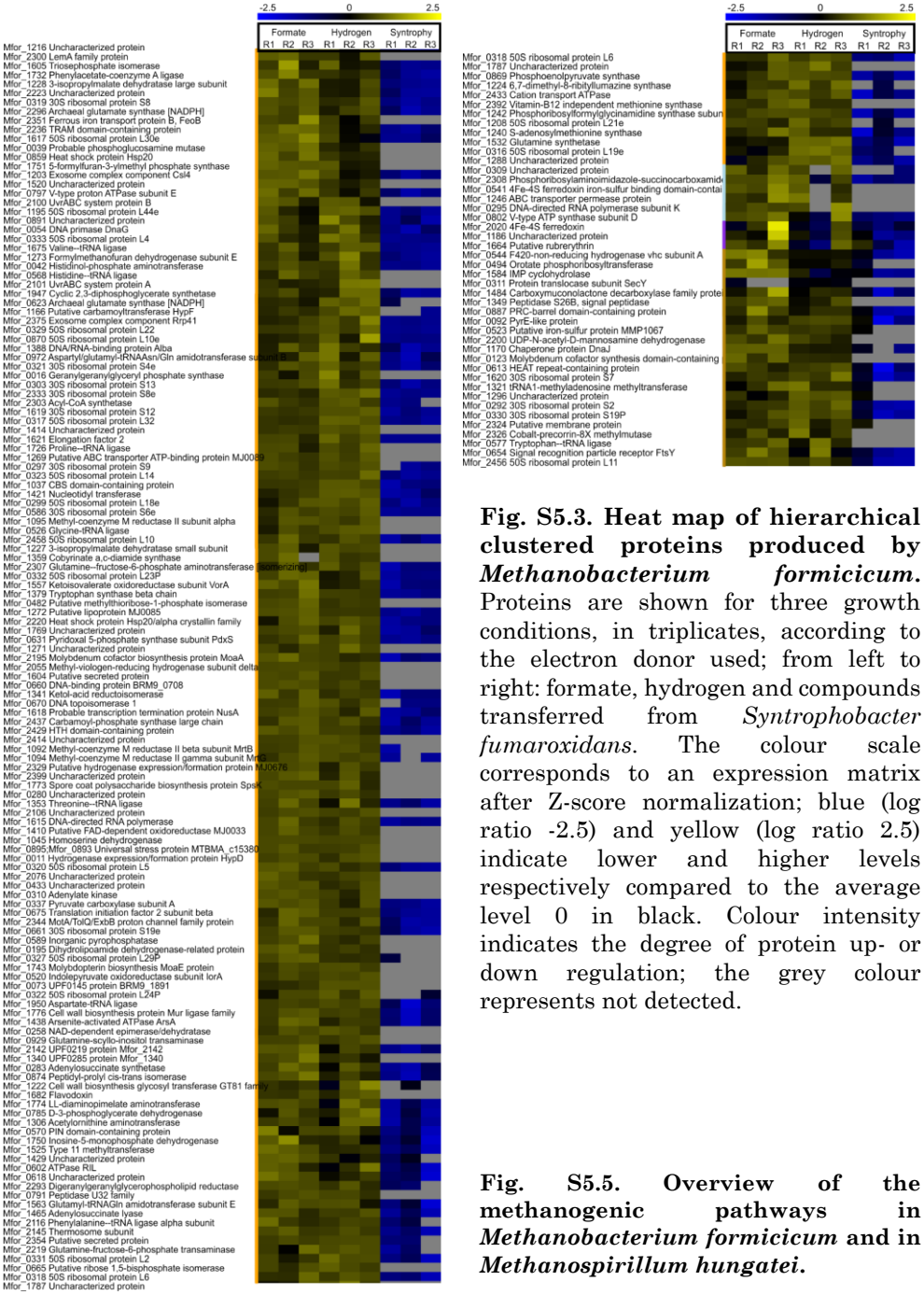

Fig. S5.3. Heat map of hierarchical clustered proteins produced by *Methanobacterium formicicum*. Proteins are shown for three growth conditions, in triplicates, according to the electron donor used; from left to right: formate, hydrogen and compounds transferred from *Syntrophobacter fumaroxidans*. The colour scale corresponds to an expression matrix after Z-score normalization; blue (log ratio -2.5) and yellow (log ratio 2.5) indicate lower and higher levels respectively compared to the average level 0 in black. Colour intensity indicates the degree of protein up- or down regulation; the grey colour represents not detected.

Fig. S5.5. Overview of the methanogenic pathways in *Methanobacterium formicicum* and in *Methanospirillum hungatei*.

Methanospirillum hungatei JF1

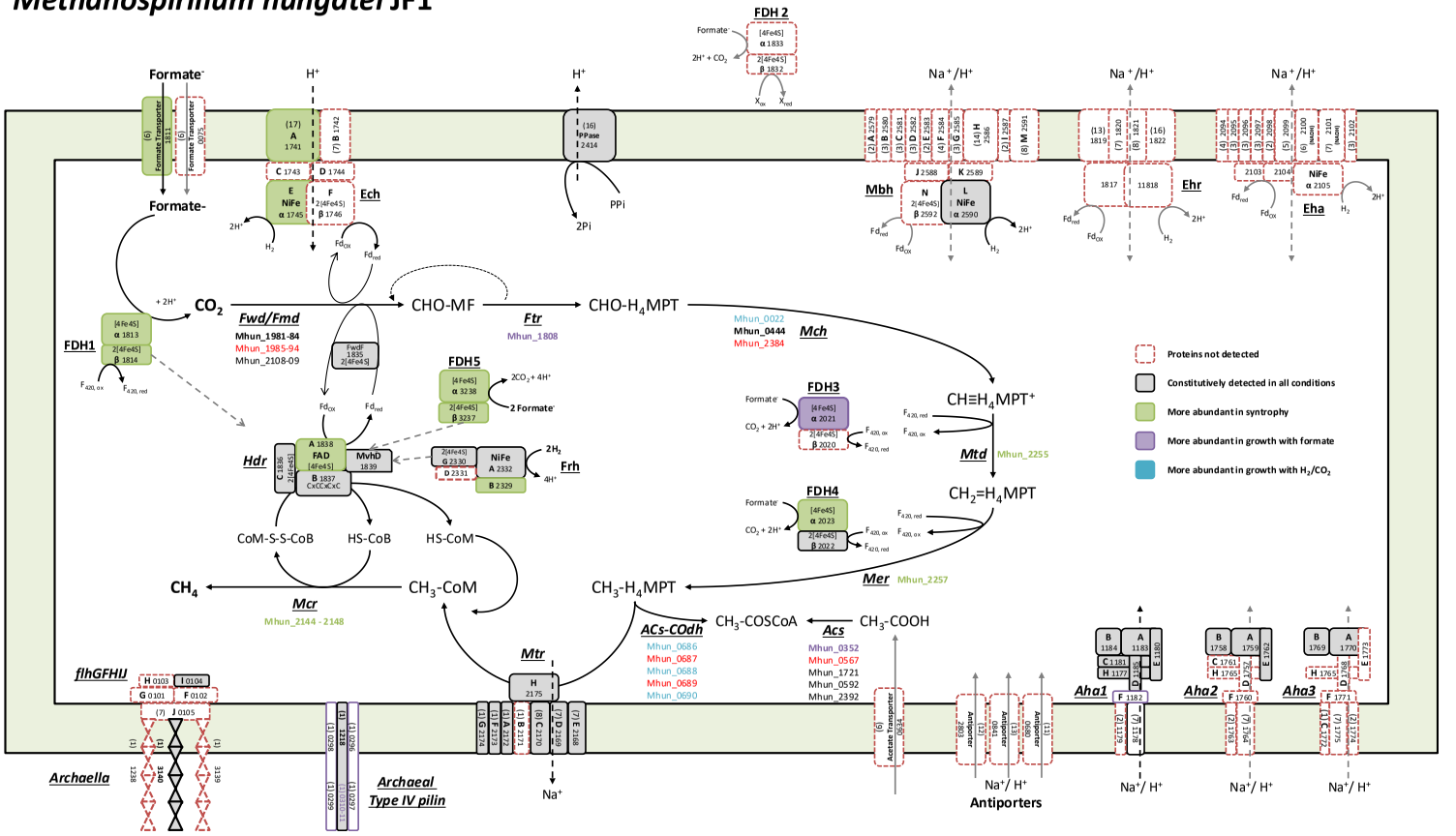

Methanobacterium formicicum DSM1535

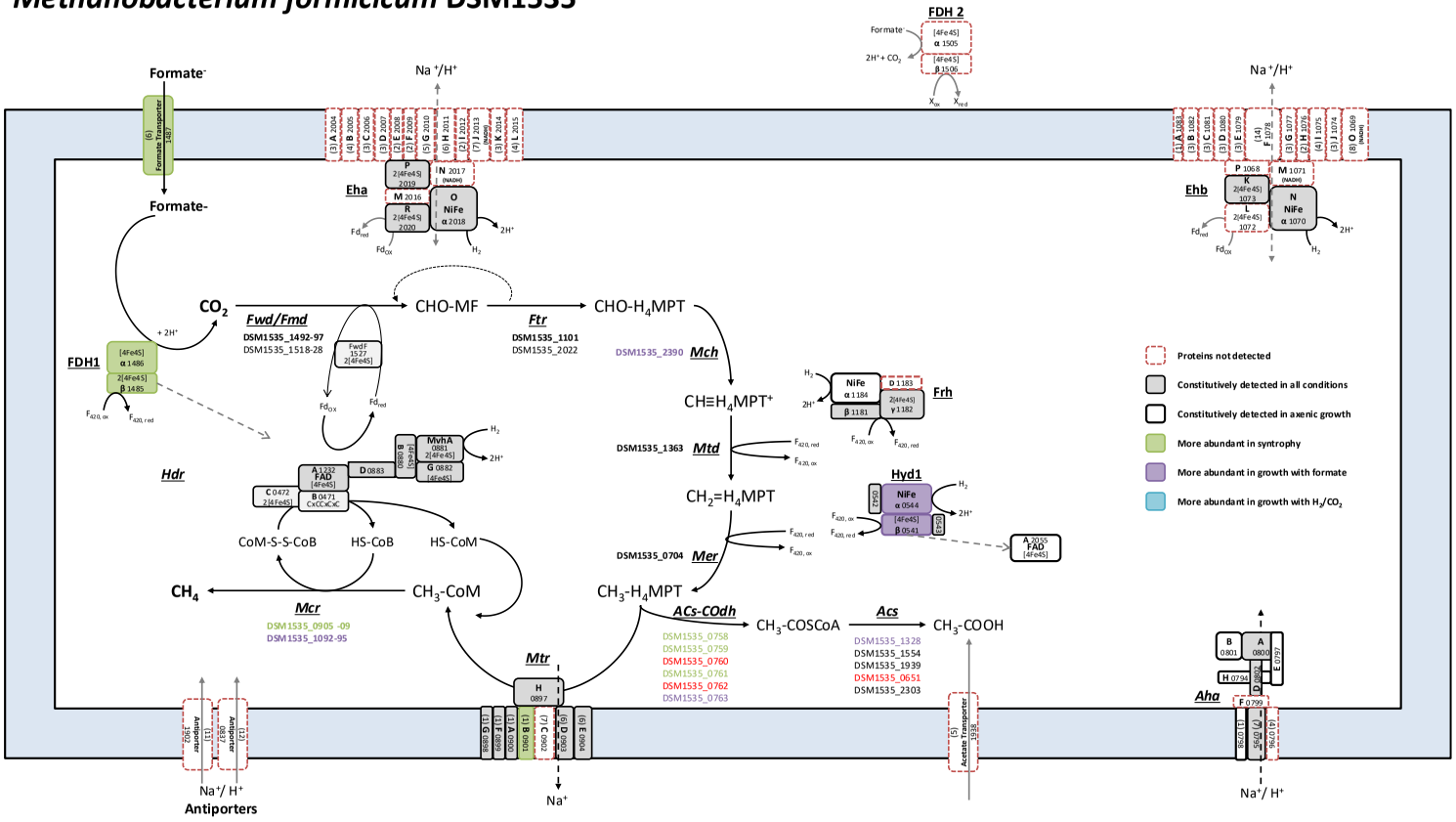

"Genome sequencing has changed taxonomy"

Richard Dawkins

Chapter 6

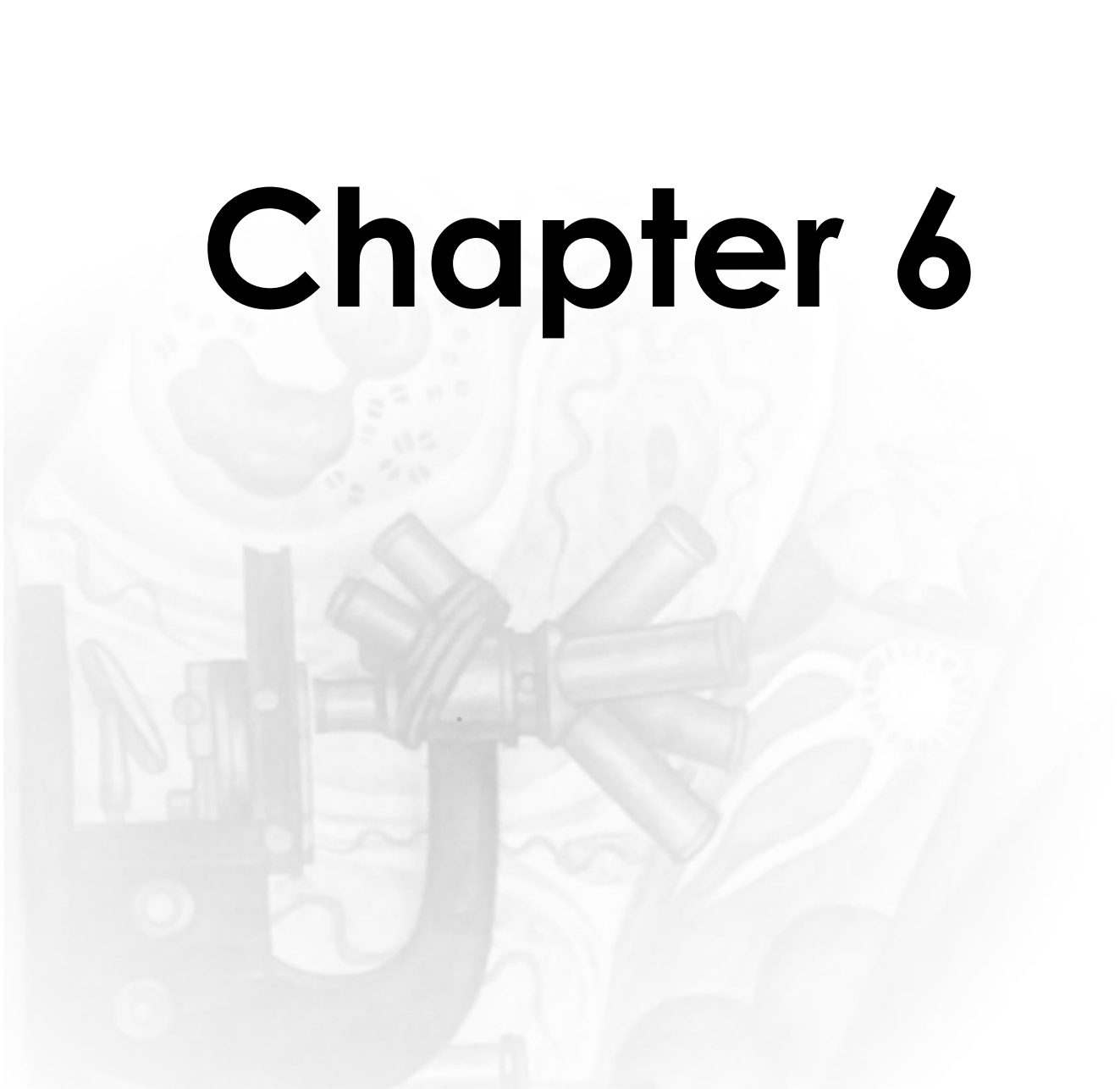

CHAPTER 6

Microbial community analysis and performance of a mesophilic anaerobic membrane bioreactor treating pot ale

Sedano-Núñez V.T.[1], Van der Zee F.P.[2], Ollier J.[3], Stams A.J.M.[1] and Plugge C.M.[1]

[1]Laboratory of Microbiology, Wageningen University and Research, The Netherlands

[2]Biothane Systems Intl/Veolia Water Solutions & Technologies, Delft, The Netherlands

[3]Air Liquide, Grenoble, France.

In preparation for publication

Abstract

In this study we evaluated start-up, performance and robustness to high loading tests of an anaerobic membrane bioreactor (AnMBR). A 10-liter, completely stirred anaerobic bioreactor in combination with an ultrafiltration cross flow module was operated at 37 °C for 242 days. The reactor was fed with pot ale from a whiskey distillery in Scotland. High loading tests (HLT) via short time increases of volumetric loading rate (VLR) were applied to assess the robustness of the biomass and monitor biological and biochemical responses to such disturbances. The reactor was rather robust in performance and recovered from 2 and 3-fold increases in VLR for up to 6 hours. Hydrogen concentrations were constantly measured and showed an increase in response to the HLT in parallel to the increase of total-VFA in the permeate. Population dynamics in the reactor was monitored by Illumina MiSeq sequencing. The presence of microorganisms of all metabolic groups illustrates the importance of a balanced and diverse biomass to have a robust and stable methanogenic reactor. The relative abundance of families of proteolytic bacteria was high, while hydrogenotrophic methanogens, such as *Methanobacteriaceae*, dominated the methanogenic community in the reactor. The putative methanogenic lineage of unassigned WCHA1-57 became dominant at the end of the experiment, but it was unassigned *Woesearchaeota* that dominated the archaeal community for most part of the experiment. An interaction between proteolysis, amino acid degradation and syntrophic methanogenesis was proposed among members of *Porphyromonadaceae*, unassigned *Cloacimonetes* and methanogenic archaea.

Keywords: Anaerobic digestion, microbial community, volumetric loading rate disturbance, hydrogen concentration.

Introduction

Anaerobic membrane bioreactors (AnMBR) have emerged in the last decades as one of the innovative options to treat wastewaters from food processing, paper, pharmaceutical, landfill and textile industries (Aquino et al., 2006; Yang et al., 2006; Le-Clech, 2010). The reported advantages of AnMBR over conventional wastewater treatment systems are: high biomass retention, excellent effluent quality, low sludge production, a small footprint and high net energy production (Liao et al., 2006; Wan et al., 2011). Although biofouling (He et al., 2005; Dereli et al., 2014) and disruption of flocs (Stroot et al., 2001; Padmasiri et al., 2007) are some of the main challenges in the application of AnMBR, other factors also affect the treatment performance and stability of the reactor. These include operational conditions such as temperature, hydraulic retention time (HRT) and organic loading rate (OLR) (Skouteris et al., 2012; Lin et al., 2013; Ozgun et al., 2013).

The sludge composition, or more specifically the structure and functionality of the microbial communities in the bioreactor are essential for good performance of anaerobic digestion (AD) (Carballa et al., 2015; Lucas et al., 2015). Methanogenic communities of bacteria and archaea play an indispensable role in the complete conversion of organic material to methane and carbon dioxide (Stams et al., 2012). An imbalance among acidogenesis, fermentation and methanogenesis will generally lead to accumulation of volatile fatty acids (VFA) and in some cases to a complete collapse of the system. Ammonia inhibition, acidification, and foaming, especially at high organic loading rates are causing these instabilities (Guo et al., 2014; Li et al., 2015). Several studies have addressed the link between OLR disturbances and the microbial communities (Belostotskiy et al., 2015; Li et al., 2016). Exploration of the microbial community composition in anaerobic digesters is important as it increases our understanding of the different processes occurring in the reactor.

Pot ale is the main liquid by-product of whiskey distilleries (Melamane et al., 2007; Graham et al., 2012). Large volumes of pot ale are generated during production of whiskey; for every litre of alcohol, 8 – 15 litres of pot ale are produced (Mohana et al., 2009). Distillery spent wash is considered a high-strength wastewater with a very high chemical and biochemical oxygen demand (COD and BOD) and with low pH (Acharya et al., 2008). These characteristics and the large quantities of pot ale generated annually, have attracted interest in using this by-product for biogas production in anaerobic digesters (Tokuda et al., 1998; Goodwin et al., 2001; Barrena et al., 2017).

The particular composition of pot ale rich in protein, phosphorous and organic acids requires a robust system that can endure the variations in the composition of the feed, as well as the high levels of VFA and ammonia, without limiting the biogas production in the system. Ammonia, above certain concentration thresholds, can

have an inhibitory effect on methanogens (Vidal et al., 2000; Ariunbaatar et al., 2015). Ammonia levels between 50 and 200 $mg \cdot l^{-1}$ stimulate methanogens (McCarthy, 1964), but free ammonia concentrations higher than 300 $mg \cdot l^{-1}$ have shown severe anaerobic treatment inhibition in mesophilic conditions, presumably by inhibiting the methanogens (Omil, 1995). Ammonia toxicity levels are highly dependent on pH and temperature since the cause of toxicity is the un-ionized form of ammonia (free ammonia) which is the dominant form at high pH and temperatures (Vidal et al., 2000; Rajagopal et al., 2013; Yenigun and Demirel, 2013). Several studies indicate that hydrogenotrophic methanogens (from the orders *Methanomicrobiales*, *Methanococcales*, *Methanocellales*, *Methanobacteriales* and *Methanopyrales*) are more tolerant to the ammonia toxicity than acetoclastic methanogens (from the orders *Methanosarcinaceae* and *Methanosaetaceae*), regardless the temperature of the experimental conditions (Koster and Lettinga, 1984; Angelidaki and Ahring, 1993; Calli et al., 2005; Zhang et al., 2014; Wang et al., 2016).

The inhibitory effect of VFA on hydrolysis and methanogenesis is difficult to evaluate due to interactions between VFA concentrations and pH (Azman et al., 2015). High VFA concentrations can lead to a drop in pH values, and eventual toxic conditions in bioreactors. However, in highly buffered systems, the pH changes can be small, therefore, independently from pH, VFA are usually tracked for process monitoring (Murto et al., 2004; Siegert and Banks, 2005). Researchers are not in agreement over which VFA is the best indicator for impending reactor failure: acetic acid, propionic acid, i-butyric, i-valeric or the ratio of propionic to acetic acid (Marchaim and Krause, 1993; Boe et al., 2008; Franke-Whittle et al., 2014).

Besides ammonia and VFA, other compounds which are known to cause toxic or have inhibitory effects in biogas reactors and affect methanogenesis are hydrogen sulfide, as well as hydrogen and heavy metals (Guwy et al., 1997; Franke-Whittle et al., 2014; Paulo et al., 2015). Many hydrogen-producing reactions are thermodynamically unfavourable unless the partial pressure of hydrogen is kept low (Thauer et al., 1977; Schink, 1997; Kleerebezem and Stams, 2000). Therefore, hydrogen consuming methanogens play an indispensable role in maintaining hydrogen levels low in syntrophic communities with bacteria (Stams et al., 2012). Thus, an increase in hydrogen might be useful to predict disturbances between fermentative processes and methanogenesis (Conrad, 1999; Junicke et al., 2015). The use of hydrogen concentrations as a performance monitor for anaerobic digestion has been addressed before with inconsistent conclusions (Mosey and Fernandes, 1989; Kidby and Nedwell, 1991; Cord-Ruwisch et al., 1997).

This study analysed microbial diversity, process parameters and performance during the start-up and stable operation of a mesophilic AnMBR treating pot ale, as well as the robustness of the bioreactor and the stability of biomass composition to

overloading events. Moreover, we investigated if hydrogen concentrations can be used as an early warning indicator of process instability.

Materials and methods

Operation of the membrane bioreactor

A pilot-scale anaerobic membrane bioreactor with a working liquid volume of 10 litres was continuously fed and operated for 242 days. The continuous flow stirred-tank reactor (CSTR) was inoculated with crushed and sieved granular anaerobic sludge (~10 g VSS l^{-1}) taken from a full-scale Biobed® EGSB reactor treating fermentation industry wastewater. 1 litre of sludge was added to the reactor and mixed with 5 g $\cdot l^{-1}$ $NaHCO_3$ up to the final working volume. The reactor was fed with pot ale and maintained at a constant temperature of 37 °C. The pH was kept at 7.3 ± 0.2 by dosing 2 M NaOH when necessary (**Supporting information, Fig. S6.1**).

The feed, obtained from a whiskey distillery in Scotland, was kept at a controlled temperature of 4°C and magnetic stirring before entering the CSTR. The composition of the feed is listed in **Supporting information, Table S6.1**. Undiluted pot ale was fed for the first 120 days; after that, the feeding continued with tap water diluted pot ale (1:1 vol/vol) until the end of the experiment.

An ultrafiltration cross flow module composed of a tubular polyvinylidene fluoride membrane (80 cm length, 5.2 mm inner diameter and 30 nm pore size) separated the biomass from the effluent. Volatile fatty acids (VFA) in the permeate were quantified daily using a Varian 3900 gas chromatograph (Agilent, Santa Clara, CA) equipped with a silica column (25 m and 0.53 mm internal diameter) and a flame ionization detector. Samples of feed and sludge were centrifuged (5 min, 10,000 x g) and passed through 0.45 µm cellulose filters prior to their quantification.

The biogas production of the CSTR was measured with a wet tipping biogas meter and its composition was monitored continuously via the online Agilent 490 micro gas chromatograph (Agilent, Santa Clara, CA) equipped with two channels (Molsieve 5A column for H_2; PPQ 10m column for CH_4 and CO_2; thermal conductivity detector; Argon and Helium were used as carrier gases).

Volumetric loading rates (VLR) varied during the experiment. By gradually increasing the feed flow during the start-up stage of the reactor an optimum VLR was established at 5 ± 0.8 g $\cdot$COD $\cdot l^{-1} \cdot day^{-1}$ after day 140. The hydraulic retention time (HRT) was kept at 10 days. **Table 6.1** summarizes the operational conditions of the reactor, the different stages of functioning and the stages when the high load tests took place.

High load tests (HLT) were applied to the reactor by increasing the VLR for short defined periods of time. The first overload test was done at day 149 in which the VLR was increased from 4 to 10 g·COD·l^{-1}·day^{-1} for 4 hours. An increase up to 11 g·COD·l^{-1}·day^{-1} of the VLR was applied for the second HLT for 6 hours on day 156. The third high load test (day 184) increased the VLR levels from 6 to 9.5 and then up to 12.5 g·COD·l^{-1}·day^{-1} over a period of 6 hours. During the HLT experiments, H_2 concentrations of the biogas were measured online with the gas chromatographer every 12 minutes. Permeate samples for VFA analysis were collected every 30 minutes.

Multiple physicochemical and biological parameters were regularly analysed in the feed, sludge and permeate to monitor the operational status of the AnMBR (TCOD, T(S)S, V(S)S, TKN, SKN, Total-P, ortho-P, VFA, anions, cations, etc.). Moreover, sludge samples were taken along the different stages of operation to perform chemical and microbiological analysis. For the 1st HLT, the sludge was extracted from the reactor one day before the experiments (day 148). This was done to allow the pressure on the AnMBR to stabilize and have an H_2 baseline measurement with the GC as constant as possible before the increase in the VLR. Subsequent sludge samples were taken a day after the 1st HLT (day 150) and after the 3rd HLT (day 184).

Specific acetoclastic methanogenic activity (SAMA) assays were carried on using Oxitop® equipment (WTW, Weilheim, Germany). 300 ml bottles were filled with 49.4 ml of sludge from the reactor and mixed with 0.6 ml sodium acetate (250 g·COD·l^{-1}). The initial F/M-ratio was 0.17 g·COD·g·VSS^{-1}. Anaerobic conditions were provided by flushing bottles with N_2/CO_2 mixture (70:30, vol/vol). The bottles were placed in shakers at 37 °C. Biogas and methane production was calculated by measuring the pressure increase in the bottles every 20 minutes by Oxitop® heads. The analyses were performed in duplicates and two consecutive feeds with sodium acetate were applied in each replicate.

Total Kjeldahl Nitrogen (TKN) was determined with Simplified TKN Kit™ (Hach Company, Loveland, CO). COD was measured with Hach Lange Kits™ (Hach Company, Loveland, CO).

Table 6.1. Operational conditions for 242 days of an anaerobic membrane bioreactor operated at 37 °C and HRT of 10 days.				
Stage	**Operation time(days)**	**Feed details**	**VLR ($g \cdot COD \cdot l^{-1} \cdot d^{-1}$)**	**Notes**
0	1	Undiluted Pot Ale	1.2	Inoculation
I Start-up	2 – 120		1.2 – 8.5	Unstable performance characterised by permeate T-VFA peaks >10 meq $\cdot l^{-1}$
II Detox	121 – 140	Tap water Diluted Pot Ale (1:1) & $NaHCO_3$	3 - 5.4	Accumulated VFA after ammonia inhibition were flushed away
III Stable operation	141 – 148	Tap water Diluted Pot Ale (1:1 vol. /vol.)	3.8 – 5	VFA in the permeate: <5 meq $\cdot l^{-1}$
IV 1st HLT	149 - 155		10	High Load Tests (HLT) and recovery of the bioreactor
			4.1	
V 2nd HLT	156 - 183		11	
			4.1 – 6.1	
VI 3rd HLT	184 - 218		12.5	
			4.8 - 5.2	
VII Stable operation	219- 242		5.5– 8.4	Stable performance

Microbial community analyses by next generation 16S rRNA amplicon sequencing

Sludge samples (~50 ml) were collected during 16 sampling points (**Figure 6.1**). Samples were kept at -80 °C prior to genomic DNA extraction. Samples were washed with PBS solution with 0.5 mM EDTA twice to remove humic acids and other contaminants that could have an inhibitory effect on DNA extraction and PCR reactions. Genomic DNA was extracted from the sixteen samples with technical duplicates using the FastDNA® Spin Kit for Soil (MP Biomedicals, Santa Ana, CA) according to the manufacturer's protocol with additional two 45-second beat beating steps with a FastPrep Instrument (MP Biomedicals). Concentrations and quality of the obtained DNA were determined with a Nanodrop® (ND-1000) spectrophotometer (Nanodrop Technologies, Wilmington, DE). Extracted DNA from selected samples was used for bacterial and archaeal community analyses. The amplification of bacterial and archaeal 16S rRNA gene fragments was done using a 2-step PCR protocol. The first PCR amplification of bacterial 16S rRNA gene fragments was done using a set of primers composed by the 27F-DegS (5′-GTT[TC]GAT[TC][AC]TGGCTCAG-3′) (Van den Bogert et al., 2011; van den Bogert et al., 2013) and an equimolar mix of two reverse primers; 338R-I and 338-R-II (5′-

GC[AT]GCC[AT]CCCGTAGG[TA]GT-3′) (Daims et al., 1999). For the archaeal 16S rRNA gene amplification primers 518F (5′-CAGC[AC]GCCGCGGTAA-3′) (Wang and Qian, 2009) and 905R (5′-CCCGCCAATTCCTTTAAGTTTC-3′) (Kvist et al., 2007) were used. PCR amplifications were carried out using 500 nM of each forward and reverse primer (Biolegio BV, Nijmegen, The Netherlands), 1 unit of Phusion Hot Start DNA polymerase (Thermo Scientific, USA), 10 µl of 5x HF-buffer, 200 µM dNTP mix and 1 µl DNA template. PCR grade water was used to fill up the reaction mixture to 50 µl. The PCR amplification proceeded as follows: a pre-denaturing step of 99 °C for 30 s, 25 cycles of denaturing at 98 °C (10 s), annealing at 56 °C for bacterial and 60 °C for archaeal (20 s), extension at 72°C (20 s) and a final extension at 72°C (10 min). After positive amplifications, technical duplicates were pooled and prepared for the second PCR amplification. This second step was performed to extend 8 nt barcodes to the amplicons, as described previously (Hamady et al., 2008). Barcoded amplification was performed using 5 µl of the first PCR product, 500 nM of each forward and reverse primer (Biolegio BV, Nijmegen, The Netherlands), 2 units of Phusion Hot Start DNA polymerase (Thermo Scientific, Waltham, MA), 20 µl of 5x HF-buffer, 200 µM dNTP mix, and filling up the reaction mixture to 100 µl with nuclease free water. The second PCR program was as follows: the 98 °C pre-denaturing step for 30 s, five cycles of 98 °C (10 s), 52° C (20 s), 72 °C (20 s) and 72 °C (10 min). Barcoded PCR products were cleaned using the HighPrep™ PCR clean-up system (MagBio Genomics Inc., Gaithersburg, MD). DNA was quantified using Qubit® 2.0 Fluorometer (Thermo Fisher Scientific, MA). After the second PCR, barcoded samples were pooled in equimolar quantities to create a library. Archaeal and bacterial libraries were purified a second time and sent to GATC Biotech (Konstanz, Germany) for sequencing on the Illumina MiSeq platform.

Sequencing data analysis

16S rRNA gene sequencing data was analysed using NG-Tax, an in-house pipeline (Ramiro-Garcia et al., 2016). Paired-end libraries were filtered to contain only read pairs with perfectly matching barcodes, and those barcodes were used to demultiplex reads by sample. Resulting reads were separated by sample using the affiliated barcodes. Taxonomy affiliation was done with the SILVA 16S rRNA reference database by using an open reference approach as described by (Quast et al., 2013). The minimum threshold that an operational taxonomic unit (OTU) needs to be present compared to the whole database, the percentage identity threshold for the blastn and the percentage for the error correction were settled in default values, 0.1, 100 and 98.5, respectively. Quantitative Insights into Microbial Ecology (QIIME) v1.2 (Caporaso et al., 2010) was used to define microbial compositions based on the described pipeline.

Filtering, subsetting and diversity analyses of the microbial communities were performed using the phyloseq R package for reproducible interactive analysis and

graphics of microbiome census data (McMurdie and Holmes, 2013). All non-bacterial and unassigned OTUs were removed from the bacterial samples, as well as all non-archaeal and unassigned OTUs were removed from the archaeal samples prior to any downstream analysis. Samples with <2,500 reads were also removed. The read counts of the merged technical replicates were normalized using the CSS method from metagenomeSeq package v1.11 (Paulson et al., 2013) in R v.3.3.2 (Team, 2016).

Results and discussion

Start-up period of the reactor

During the start-up period of the reactor, diverse operational problems such as membrane blockage and fouling, gas leakage and pump failures occurred throughout the first 60 days of operation. In addition, change in composition of the pot ale, supplied by the whiskey distillery, caused problems during the start-up period. A gradual increase in the Total Kjeldahl Nitrogen (TKN) levels in the pot ale from 1.5 $g \cdot l^{-1}$ at the beginning of the operation of the reactor up to 4.9 $g \cdot l^{-1}$, around day 110 to 120, resulted in VFA accumulation to levels above 20 $meq \cdot l^{-1}$ (**Supporting information, Fig. S2**).

The operational variations in the distillery industry results in a highly variable composition of pot ale. High levels of protein, lactic acid and yeast cells that sink in the bottom of the whiskey fermenters are commonly reported in pot ale studies (Goodwin and Stuart, 1994; Graham et al., 2012; Barrena et al., 2017). Protein breakdown occurs during anaerobic digestion which leads to the build-up of ammonia. Therefore, as the levels of TKN in the feed and in the reactor increased, ammonia inhibition of methanogens might have occurred in the AnMBR.

When hydrogen stops being consumed by methanogens it accumulates and syntrophic interactions are disrupted, but also some non-syntrophic fermentative reactions cannot occur anymore, such as lactate and ethanol conversion to acetate (Giovannini et al., 2016). The increase in H_2 levels (above 100 ppm) and VFA accumulation (mainly composed of acetate) observed between day 116 and 136 are an indication of a disruption between hydrogen-producing and hydrogenotrophic microbial communities, most probably caused by the high levels of ammonia in the reactor. **Figure 6.1** shows the reactor performance along the 242 days of operation. Repeated VFA accumulation peaks can be noticed at the beginning of the start-up period and principally when the reactor was affected by ammonia toxicity.

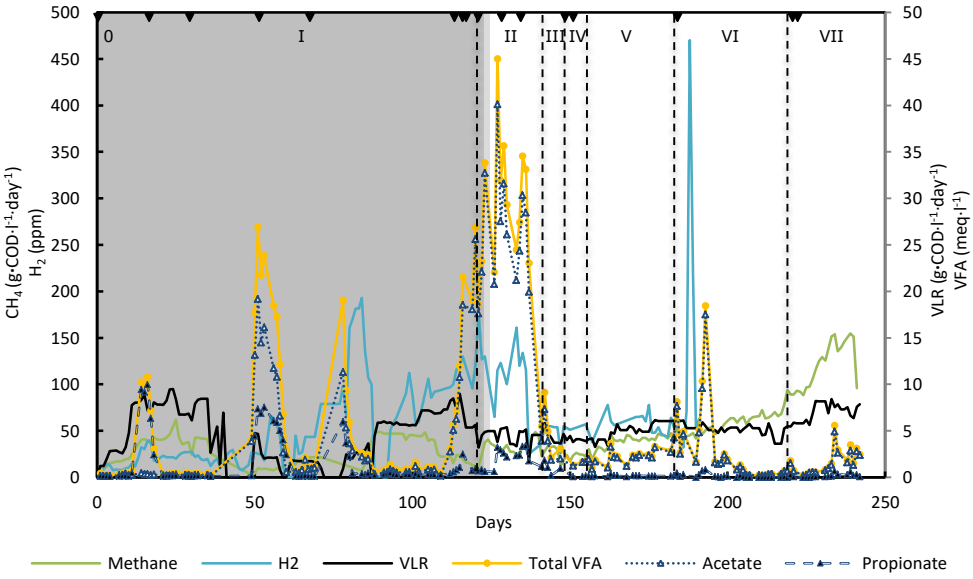

Figure 6.1. Performance of the AnMBR operated at 37 °C for 242 days. Volumetric loading rate (VLR), total volatile fatty acids (VFA), acetate, propionate, methane and H_2 are plotted. The dark area indicates undiluted and white area diluted pot ale dosing. Triangles marks (▼) at the top of the plot show the sampling points for the microbiological analyses. Reactor stages are divided by dotted lines and signalled with roman numbers.

It has been reported that total ammonia (TAN) and free ammonia (FAN) concentrations above 3 g·NH_4^+-N·l^{-1} and 0.15 g·NH_3-N·l^{-1}, respectively, have an obvious inhibitory effect on methanogenesis and lower the potential methane yield in anaerobic digesters (Wang et al., 2015; Tian et al., 2017). A study has shown that syntrophic acetate oxidation coupled with hydrogenotrophic methanogenesis is the dominant pathway in digesters with high ammonia levels (2.8–4.57 g·NH_4^+-N·l^{-1}), while acetoclastic methanogenesis dominate at low ammonia (<1.21 g·NH_4^+-N·l^{-1}) (Fotidis et al., 2013).

To reverse the ammonia inhibitory effect on methanogens, the pot ale was diluted with tap water to maintain the TKN levels lower than 2.5 g·l^{-1}. Additionally, the bioreactor was fed with a $NaHCO_3$ solution on day 137 to flush away the accumulated VFA. These actions were effective, and a stable performance of the reactor was finally achieved with VFA levels <5 meq·l^{-1} in the permeate and ~50 ppm of H_2 in the biogas at day 140. Once the AnMBR was stable a maximum capacity of the reactor was settled at ~5 g·COD·l^{-1}·day^{-1}.

High load tests period

Once the pot ale fed to the reactor was diluted and the reactor stabilized, overloading experiments were carried out to assess the robustness and evaluate the response of the reactor to drastic increases of VLR. In **Figure 6.2** we can observe in detail the H_2 and VFA responses to the high load tests. The first high load test (HLT) was done at day 149 when the system was performing stable at an aimed VLR of 4 g·COD·l^{-1}·day^{-1}. For four hours the VLR was increased to 10 g·COD·l^{-1}·day^{-1}. Total-VFA and H_2 levels increased in response to this overloading event. Four hours after, when the load was set back to 4 g·COD·l^{-1}·day^{-1}, the H_2 concentration decreased to normal levels of ~55 ppm rapidly after it reached a maximum of 70.5 ppm. Total-VFA concentrations of the permeate increased from 1.6 to 5.7 meq·l^{-1} and took longer to decrease to normal levels of < 1.5 meq·l^{-1}. Acetate was the main component in the increase of Total-VFA.

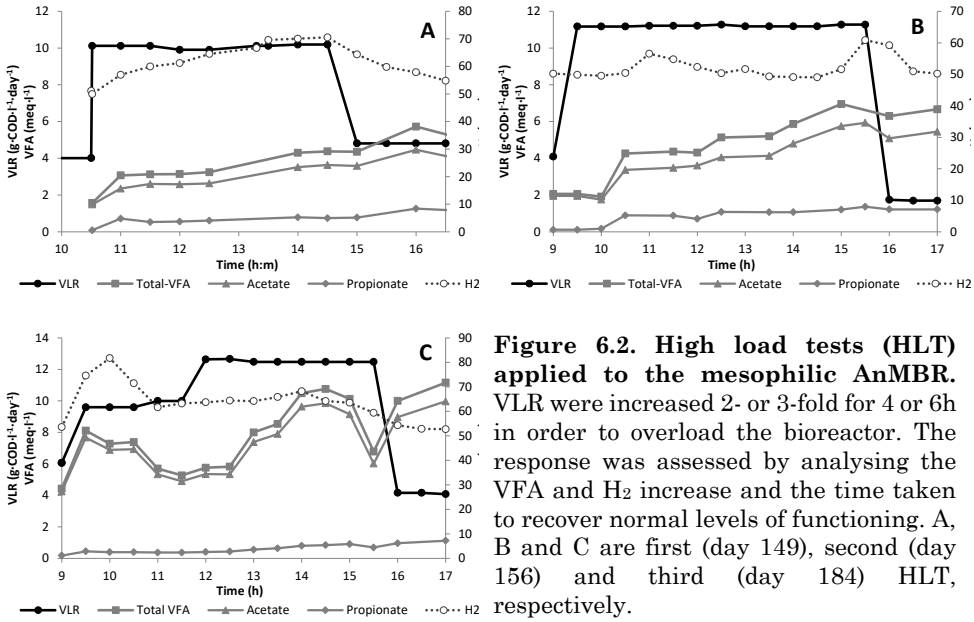

Figure 6.2. High load tests (HLT) applied to the mesophilic AnMBR. VLR were increased 2- or 3-fold for 4 or 6h in order to overload the bioreactor. The response was assessed by analysing the VFA and H_2 increase and the time taken to recover normal levels of functioning. A, B and C are first (day 149), second (day 156) and third (day 184) HLT, respectively.

The effect of the first high load test in the performance of the bioreactor was mild. No significant differences were found in the specific acetoclastic methanogenic activities before and after the HLT (**Table 6.2**). A second HLT was done by increasing the VLR further, up to 11 g·COD·l^{-1}·day^{-1} on day 156 for a longer period (6 hours). This time, the H_2 levels only reached a maximum of 60.9 ppm and rapidly recovered when the VLR was decreased. Total-VFA reached 7 meq·l^{-1}, although the initial values were 2.1 meq·l^{-1}. The main accumulated fatty acid was acetate up to 5.9 meq·l^{-1}, whereas propionate increased only to 1.4 meq·l^{-1}.

As the reactor proved to be robust to the short term HLT, the potential of the reactor to operate in a higher VLR for a longer period was explored after day 160. Starting with 4 g·COD·l^{-1}·day^{-1} the VLR was gradually increased to 6 g·COD·l^{-1}·day^{-1} in a period of 10 days (days 160-170).

On day 184, a third HLT was carried for 6 hours with an escalated VLR increase (**Figure 6.2.C**). After an hour of the HLT, H_2 concentration reached 81.7 ppm. However, it decreased to levels of ~68 ppm as in the previous HLTs. Total-VFA accumulation, mainly composed of acetate, reached higher levels (11.2 meq·l^{-1}) as the load test was higher this time.

Although the reactor was normally recovering to the last HLT and the H_2 and VFA levels were dropping back to normal, another setback occurred when pot ale had to be replaced with vinasse due to issues with the delivery of pot ale from the distillery in Scotland. Vinasse was used to feed the reactor for 4 days (days 186-190). Vinasse had also been used in day 77 due to lack of pot ale, but only for a day. The change of feed resulted in VFA accumulation up to 18.5 meq·l^{-1} and a peak on H_2 concentration up to 470 ppm. The reactor stopped, and it was restarted with pot ale as feed and a VLR of 5 g·COD·l^{-1}·day^{-1}. During the last month of the experiment, VLR was gradually increased to 8 g·COD·l^{-1}·day^{-1}, while the VFA remained at low acceptable levels (2.5 - 3 meq·l^{-1}). The reactor proved to have the capacity to recover despite these different disturbances.

Performance of the reactor

The specific acetoclastic methanogenic activity was tested on sludge samples from the bioreactor one day before and one or two days after the HLTs (**Table 6.2**). No significant differences were found between the measurements before and after HLTs, and obtained values fell within normal range for anaerobic sludge (0.1-1 g·COD·g^{-1}·VSS·d^{-1}) (Fang et al., 1994; Regueiro et al., 2012). The performance of the AnMBR resulted in a COD removal of 97.1% (±2.4%), with a biogas production rate of 27±3 l·d^{-1}, composed of 60% CH_4 (±3.1%).

Table 6.2. Specific acetoclastic methanogenic activity (SAMA) tests before and after high loading tests (HLT)

HLT	SAMA Test Before HLT*		SAMA Test After HLT*	
	1st feed	2nd feed	1st feed	2nd feed
1st HLT (day 149)	0.26 (±0.04)	0.24 (±0.01)	0.28 (±0.01)	0.22 (±0.01)
2nd HLT (day 156)	0.27 (±0.01)	0.23 (±0.01)	0.31 (±0.05)	0.26 (±0.01)
3rd HLT (day 184)	0.14 (±0.0)	0.12 (±0.01)	0.11 (±0.01)	0.12 (±0.0)

*Values in g·COD/g^{-1}·VSS·d^{-1}

Acetate and propionate were the main fatty acids accumulated when the reactor faced disturbances in its performance. Some studies report that acetic and butyric acid concentrations of 2,400 and 1,800 mg $\cdot l^{-1}$, respectively, had no significant impact on the activity of methanogens while a propionic acid concentration of 900 mg $\cdot l^{-1}$ resulted in inhibition of methanogens and decreased bacterial numbers(Wang et al., 2009). Others proposed that acetic acid levels higher than 800 mg $\cdot l^{-1}$ or a propionic to acetic acid ratio larger than 1.4 predict digester failure (Buyukkamaci and Filibeli, 2004; Romsaiyud et al., 2009).

During the start-up stage of our reactor, three peaks of total-VFA exceeding 800 mg $\cdot l^{-1}$ could be seen when the reactor was fed with undiluted pot ale (day 16, 50-57 and 78) (**Figure 6.1**). For the first of these peaks propionate was the main component with a propionic to acetic acid ratio of 37. For the other two peaks propionate still contributed to >35% of the total-VFA, however more acetate (1,150 mg $\cdot l^{-1}$ on day 51 and 680 mg $\cdot l^{-1}$ on day 78) than propionate (543 mg $\cdot l^{-1}$ on day 51 and 444 mg $\cdot l^{-1}$ on day 78) was accumulated. Similarly, acetate was the main VFA accumulated during the period with ammonia inhibition (days 115-139), and after the bioreactor was fed with diluted pot ale, while the propionate share remained ~10% of the total-VFA. In digesters treating high-strength waste with high ammonia content, ammonia inhibition will be the primary process controlling factor, but different systems will have their own levels of VFAs that can be considered 'normal' for the reactor (Angelidaki et al., 1993). Thus, it is not possible to indicate the state of an anaerobic process based only on VFA levels.

During the provoked disturbances in our AnMBR via the HLT, but also in the period with high ammonia concentrations and during the changes of feed to vinasse, the H_2 concentrations varied significantly, in some cases after VFA accumulation events (day 81), in some other in parallel with the disturbance of the AnMBR (days 115-139) and in some others prior the collapse of the reactor (day 188) (**Figure 6.1**). In our study, the ease of on-line H_2 concentration measurements and its rapid response to perturbations in the performance of the AnMBR supports the use of this parameter as an early warning indicator of process instability.

Microbial community analysis

The sequencing of the 16S rRNA bacterial and archaeal genes resulted in an average of 300,108 reads for bacteria and 47,019 reads for the archaea. However, wrongly assigned OTUs were present at domain level. After filtering out the wrongly assigned OTUs, the number of reads per sample ranged from 60,914 to 561,911 for bacteria and 4,767 to 114,533 for archaea. These reads were assigned to eighteen bacterial phyla, thirty classes, twenty-seven orders and forty-four families. For the archaeal reads, four phyla, five classes, five orders and nine families were correctly assigned (**Supplementary Table 6.3**).

Bacterial community dynamics

The relative abundances of the assigned OTUs at family level are presented in **Figure 6.3**. Families with at least 1% relative abundance in a sample are presented in the plot. In the inoculum *Porphyromonadaceae* (28%), *Syntrophaceae* (26%), *Anaerolineaceae* (15%) and *Bacteroidaceae* (12%) were the dominant families.

Members of the *Porphyromonadaceae* produce VFA from the degradation of complex carbohydrates, proteins and peptides (Ziganshin et al., 2011). For instance, *Proteiniphilum acetatigenes* (Chen and Dong, 2005), *Petrimonas sulfuriphila* (Grabowski et al., 2005), *Paludibacter propionicigenes* (Ueki et al., 2006), *Proteiniphilum saccharofermentans*, *Petrimonas mucosa* and *Fermentimonas caenicola* (Hahnke et al., 2015; Hahnke et al., 2016) are all acetate or/and propionate producing bacteria, many isolated from mesophilic laboratory-scale biogas reactors. Therefore, this bacterial family is predicted to be involved in hydrolysis and acidogenesis during AD of the pot ale. *Porphyromonadaceae* remained abundant for great part of the start-up stage, reaching up to 50% of relative abundance at day 66. The thriving of this family fits with its description as proteolytic bacteria and members of this family might have taken advantage of the high availability of peptide constituents of the pot ale for acidogenesis. After the feed was changed to diluted pot ale (day 121) the relative abundance of this family gradually decreased to only 2%. A decrease in the supply of proteinaceous compounds might have limited growth of this family; however, although diluted, pot ale is still high in protein, so other compounds might have had an influence. At the end of the experiment the relative abundance *of Porphyromonadaceae* increased again to 24%, possibly promoted by the feeding of the reactor with vinasse at days 186-190.

The relative abundance of *Syntrophaceae* quickly dropped from 26% in the inoculum to levels less than 2% during the start-up stage and it was not detected when the reactor reached a stable performance at day 140. For *Anaerolineaceae*, the relative abundance gradually decreased during the start-up period to remain within 2-3% during the HLTs stage while *Bacteroidaceae* disappeared from the sludge after the first days of operation of the AnMBR.

For unassigned *Bacteroidia* and unassigned *Bacteroidetes* the relative abundance increased up to 23% and 11%, respectively, during the stable performance of the bioreactor (days 134-150). According to (De Vrieze et al., 2015) *Bacteroidetes* might be dominant in digesters operating at mesophilic conditions and under low VFA levels. After the start-up stage of the bioreactor and once the VFA concentrations were stabilized to remain lower than 200 $mg \cdot l^{-1}$, the relative abundance of the *Bacteroidetes* became significant (day 127). At the end of the experiment the relative abundance reached 46%.

The relative abundance of *Comamonadaceae* in the bioreactor during the start-up stage, and the period with high ammonia levels, reached 28% on day 150. Members of the *Comamonadaceae* family are aerobic bacteria known for their denitrifying activity in aerobic treatment systems (Khan et al., 2002; Sadaie et al., 2007). Nevertheless, several species, such as *Comamonas koreensis*, have been characterized as facultatively anaerobic (Chang et al., 2002; Peng et al., 2013). A study in an alternating aerobic/anaerobic reactor indicates a role of this family in biological phosphorus and phosphate removal (Ge et al., 2015). The average nitrate measured in the pot ale fed to the reactor was only 15 mg $\cdot l^{-1}$, while higher phosphorus concentrations were reported in the feed (P_{total} 603±74 mg $\cdot l^{-1}$, **Supporting information, Table S6.1**). Lower concentrations of total phosphorus than in the feed were measured in the permeate, mainly in form of orthophosphate (**Supporting information, Figure S6.2**). Therefore, the function of *Comamonadaceae* in our AnMBR could be of a polyphosphate accumulating organism (PAO), but as more members of this family are being isolated and characterized, other biological roles should be keep in mind for consideration (Subhash et al., 2016; Xie et al., 2016).

The information available of the *Lentimicrobiaceae* family is limited to a recently isolated anaerobic bacterium *Lentimicrobium saccharophilum* (Sun et al., 2016). This bacterium was isolated from methanogenic granular sludge in a full-scale mesophilic UASB reactor treating high-strength starch-based organic wastewater. *L. saccharophilum* grows on a narrow range of carbohydrates and the major fermentative end products from glucose were acetate, malate, propionate, formate and hydrogen. Our results show an increase of the relative abundance of *Lentimicrobiaceae* during the start-up stage of the experiment and until the ammonia reached toxic levels. When diluted pot ale was fed into the reactor *Lentimicrobiaceae* disappeared from bacterial community.

The unassigned *Cloacimonetes* was enriched during the start-up stage and remained important throughout the different stages of the AnMBR. During the stable performance of the bioreactor it accounted for a 20% of relative abundance, and this percentage increased to 39% at day 184 after the HLTs. Previously known as WWE1 (Rinke et al., 2013), uncultured members of *Cloacimonetes* have been linked to interactions with syntrophic methanogenic consortia (Lykidis et al., 2011; Wu et al., 2013). The authors proposed a role for uncultivated *Cloacimonetes* taxa in additional syntrophic interactions beyond the standard H_2-producing syntroph–methanogen partnership that may serve to improve community stability. Another study proposed that *Candidatus* Cloacamonas acidaminovorans, an amino acid fermenter, is a syntrophic bacterium present in many anaerobic digesters (Pelletier et al., 2008). Moreover, (Nobu et al., 2015) found out that *Atribacteria* and *Cloacimonetes* may perform syntrophic propionate metabolism in a methanogenic bioreactor and speculate that chaining syntrophic interactions (secondary syntrophy) and substrate exchange may facilitate proteinaceous detritus metabolism.

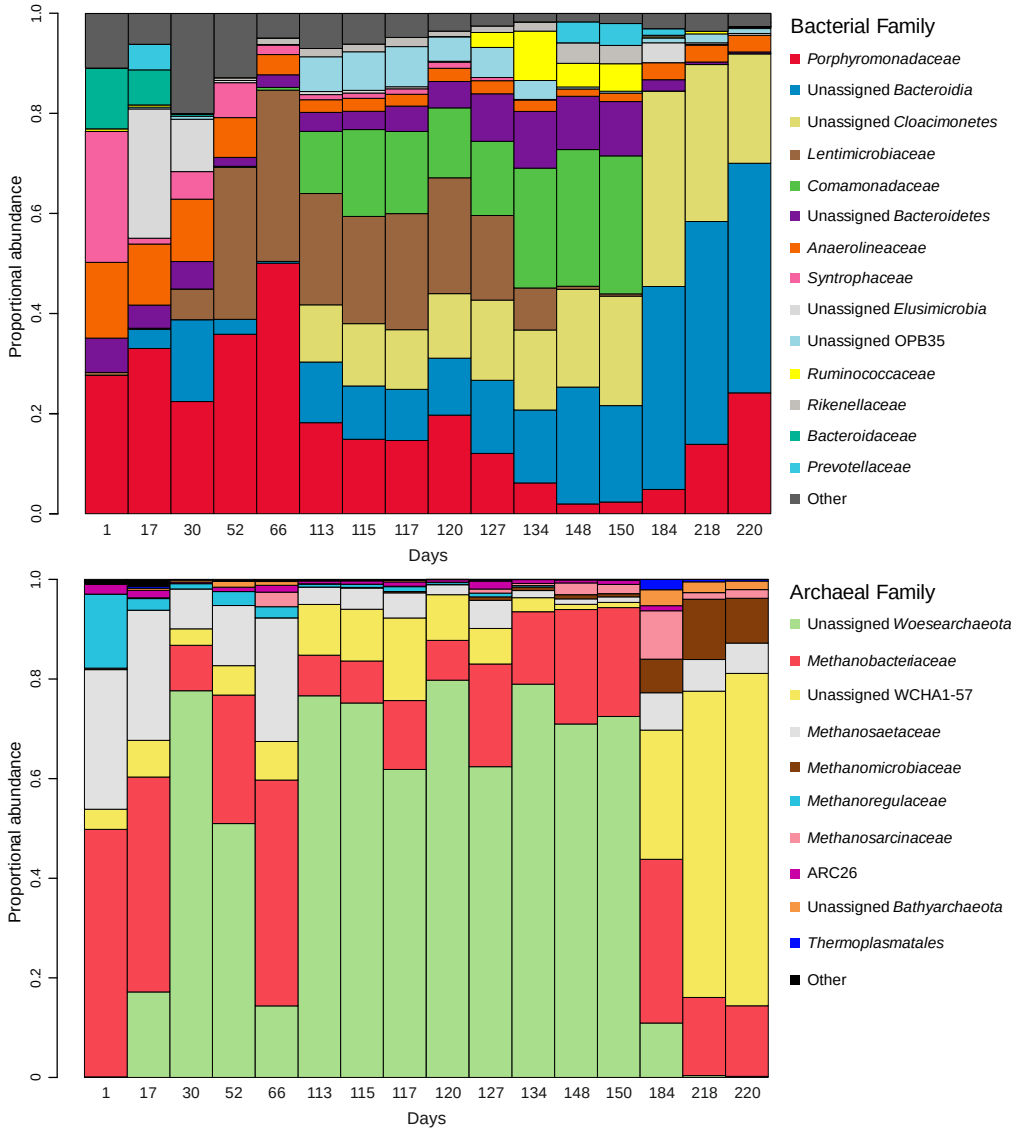

Figure 6.3. Bacterial (a) and archaeal (b) community dynamics in the AnMBR. Phylogenetic annotation at family level with abundance >1% in at least one sample. Unassigned was used to indicate groups that could not be classified at family level. "Other" integrates the remaining families with less than 1% of relative abundance.

In this context, but bringing back the discussion to *Porphyromonadaceae* family, a proteolytic strain isolated from granular sludge of a UASB reactor treating brewery wastewater, *Proteiniphilum acetatigenes,* accelerated the propionate-degradation rate of a methanogenic propionate-degrading syntrophic coculture (Chen and Dong, 2005). Therefore, it is interesting to speculate about the role of *Porphyromonadaceae* and unassigned *Cloacimonetes* in our AnMBR, since an interaction between

proteolysis, amino acid degradation and syntrophic methanogenesis is highly probable in the AD of pot ale.

Syntrophic acetate oxidation (SAO) is the predominant pathway for methane production in anaerobic digestion processes high in ammonia and volatile fatty acids (Schnürer et al., 1999). Therefore, the lack of *Clostridia* was unexpected since many SAO members belong to this class. For instance, *Thermacetogenium phaeum*, *Tepidanaerobacter acetatoxydans*, *Clostridium ultunense* and *Syntrophaceticus schinkii*. Nevertheless, recent studies have shown that syntrophic acetate oxidizers are phylogenetically diverse and not restricted to *Clostridia* only (Müller et al., 2016; Westerholm et al., 2016). For instance, *Spirochaetes* have been associated with syntrophic acetate oxidation (Lee et al., 2015).

Archaeal community dynamics

The inoculum sludge showed a dominance of hydrogenotrophic methanogens with a relative abundance of 50% of *Methanobacteriaceae* and 15% of *Methanoregulaceae*. The acetoclastic methanogens were represented by Methanosaetaceae (28%). *Methanobacteriaceae* persisted as the most important methanogenic family, occasionally the relative abundance dropped to less than 10% during the start-up stage, but levels between 21 and 33% were common during the stable operation of the AnMBR. *Methanoregulaceae* on the other hand quickly disappeared during the start-up stage and it was not detected during the stable operation of the reactor.

The relative abundance of *Methanosaetaceae* significantly decreased after the start-up stage. Acetoclastic methanogens are more susceptible to ammonia inhibition than hydrogenotrophic methanogens, therefore the high levels of ammonia during the start-up stage might have contributed to reduce the abundance of *Methanosaetaceae*. During stable operation (days 134-150) the relative abundance of *Methanosaetaceae* did not surpass the 1%, while only 6 – 8% was reached after day 184.

The unassigned *Woesearchaeota* became relevant soon after the beginning of operation of the reactor on day 17, and dominated the archaeal community since day 30 with relative abundance levels generally >70%. *Woesearchaeota* has been mostly reported in saline habitats and sediments, but it has also been detected in sludge (Ortiz-Alvarez and Casamayor, 2016). Recent single-cell genome re-construction analyses in members of *Woesearchaeota* showed small genomes sizes and the lack of core biosynthetic pathways, suggesting that these archaea may have a symbiotic or parasitic lifestyle (Castelle et al., 2015). Although the information available from *Woesearchaeota* is limited, genomic analysis of members of this group (Castelle et al., 2015) allow us to suggest that the role of unassigned *Woesearchaeota* in our bioreactor is of a fermentative and hydrogen-producing archaeon.

The relative abundance of unassigned WCHA1-57 increases during the start-up stage from 4% in the inoculum to 17% on day 117. After a significant decrease of the relative abundance to only 1% on day 150, the relative abundance of unassigned WCHA1-57 increases to dominates the archaeal community at the last stage of operation of the reactor. The uncultured archaeal group WCHA1-57 (also called WSA2 or ARC I) may represent a new order of hydrogenotrophic methanogens that contributes to methane production in anaerobic digesters (Saito et al., 2015).

Similar to our results, WCHA1-57 and *Methanobacterium* were the dominant methanogens in a pilot-scale AnMBR operated at extremely short HRT (Mei et al., 2017). Moreover, WCHA1-57 has been reported as the predominant archaeal component (>70%) in anaerobic digesters treating municipal sewage sludge (Chouari et al., 2005).

Interestingly, the relative abundances of unassigned WCHA1-57 and unassigned *Woesearchaeota*, are contrasting along the operational stages of the AnMBR. When the relative abundance of *Woesearchaeota* are >70%, the relative abundance of unassigned WCHA1-57 does not exceed the 10%; and only when the relative abundance of unassigned *Woesearchaeota* drops to <11%, unassigned WCHA1-57 take over as the dominant OTU in the archaeal community (>60%). We can only speculate if these groups of archaea endure competition for some common substrates. Nevertheless, we have suggested some lines above a hydrogen-producing role of unassigned *Woesearchaeota* and a hydrogenotrophic role of unassigned WCHA1-57, therefore other factors influencing the antagonism between these groups should be considered.

The effect of HLT to microbial community change

There is an important shift of the archaeal and bacterial community between days 66 and 113, as well as between days 150 and 184. The performance of the reactor indicates that on day 78 the total-VFA values accumulated up to 19 meq $\cdot l^{-1}$ (**Figure 6.1**). During the start-up period several operational problems occurred, in this case on day 77 the reactor was fed with vinasse as the pot ale from the distillery was not available. The increase in VFA and the shift in the microbial community seem to be related to this event.

Between days 150 and 184, another important shift in the bacterial and archaeal communities took place. This coincides with the period in which the high load experiments were performed (days 149 and 156). After the third HLT, the relative abundance of *Methanomicrobiaceae* increased to important levels (12%). Also, the relative abundance of *Methanosaeta* increased from 1% before the HLTs to 6 – 8% during the last stage of operation. Among bacteria, unassigned *Bacteroidia* and

unassigned *Cloacimonetes* co-dominated the bacterial community in the reactor after the HLTs.

Conclusions

The reactor showed excellent performance with regard to COD removal and effluent quality. Moreover, it proved to be a robust system able to cope with the short high loading levels in the VLR during the HLTs and in a longer term in the last month of operation. The microbial population was able to withstand changes in hydrogen concentrations and total-VFA accumulation, with some groups of microorganisms taking over other groups while maintaining an overall good performance of the reactor.

Hydrogenotrophic methanogens dominated the methanogenic community in the reactor. Considering that pot ale is a protein rich feed, it seems plausible that acetoclastic microorganisms were inhibited by the high levels of ammonia. Not only the relative abundance of acetoclastic methanogens was low, but also the lack of *Clostridia*, which includes many SAO members, was unexpected. Therefore, other acetoclastic microorganisms, yet unknown, may have had a role in acetate degradation which is important in high ammonia anaerobic digestion processes.

The detection of members of all metabolic groups in the anaerobic degradation chain (hydrolytic, fermentative, syntrophic, acetogenic and methanogenic) illustrates the importance of a balanced and diverse biomass to have a robust and stable methanogenic reactor. Furthermore, the high relative abundance of uncultured groups of bacteria and archaea shows the potential for exploring the functions of novel uncultured microorganisms.

The monitoring of hydrogen concentrations in the biogas might be insufficient as a stand-alone control variable for anaerobic digestion, but its rapid response and ease of on-line measurement supports its use in digester control along with other liquid phase parameters to be measured on-line, for instance VFA or dissolved H_2.

Acknowledgments

This research was supported by the Dutch Technology Foundation (STW) (project 11603), which is part of the Netherlands Organization for Scientific Research (NWO), and which is partly funded by the Ministry of Economic Affairs. Research of AJMS is supported by the European Research Council (ERC grant 323009) and the Gravitation grant (024.002.002) of the Netherlands Ministry of Education, Culture and Science.

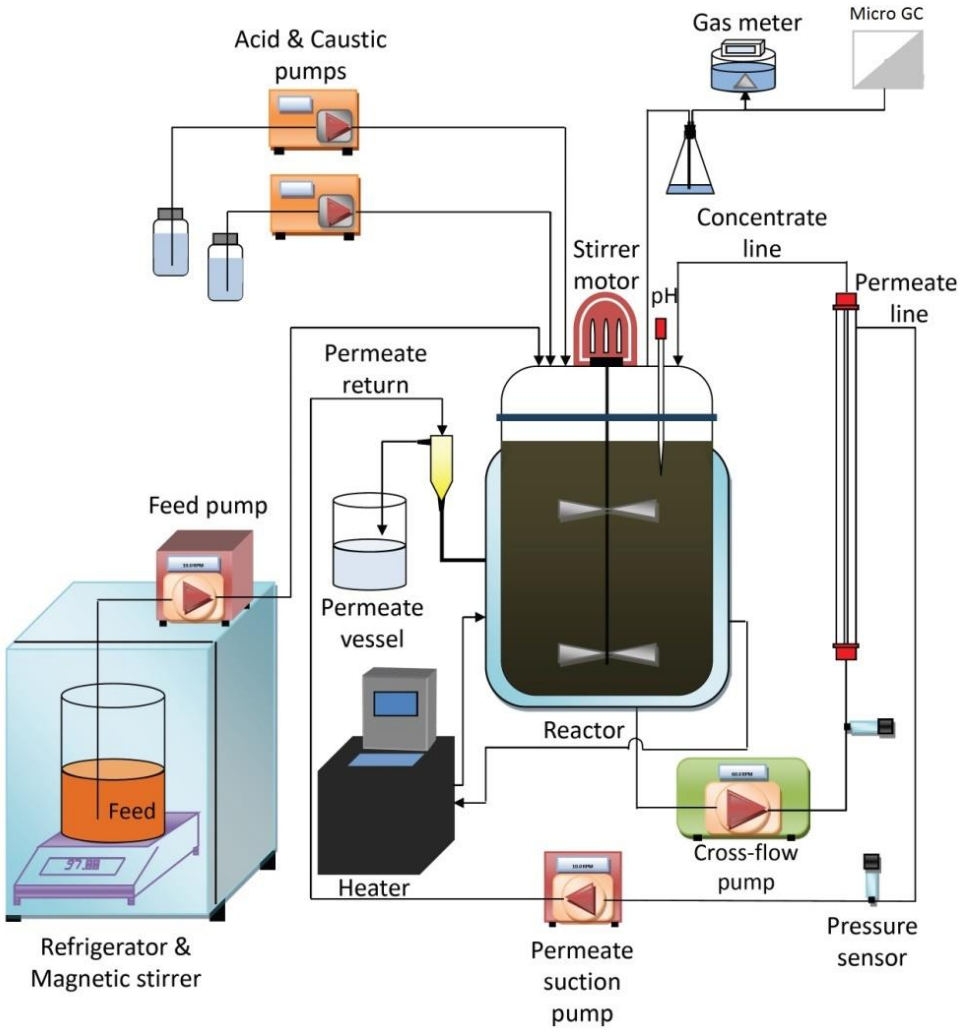

Fig. S6.1. Lab-scale reactor set-up schematic representation. Modified from (Dereli et al., 2015)

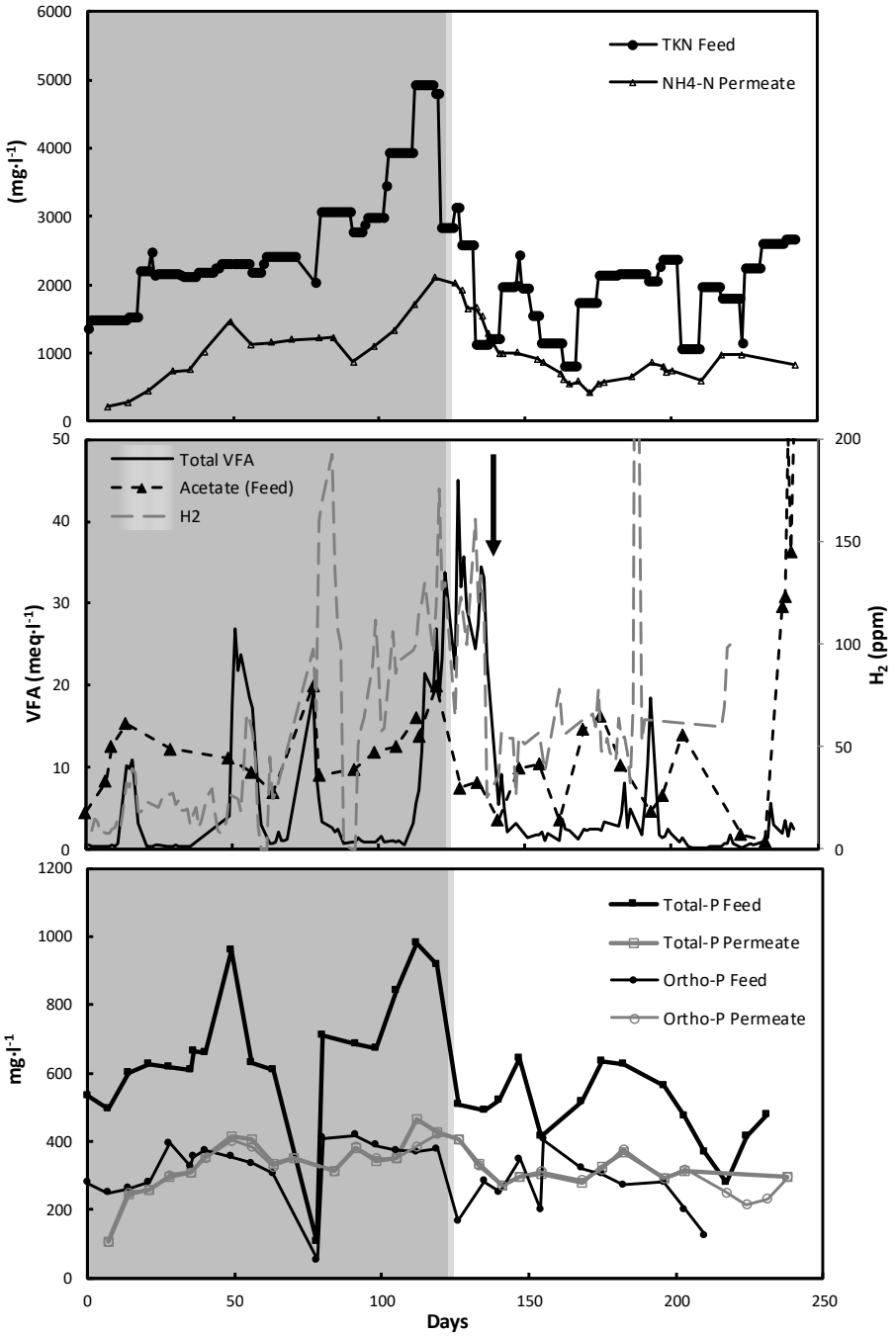

Fig. S6.2. TKN, VFA, H_2 and P concentrations in the pot ale (feed), permeate and biogas. The grey area indicates the period when undiluted pot ale was used. The black arrow marks the point when the reactor was fed with $NaHCO_3$ to wash away the high VFA levels.

Table S6.1. General composition of the pot ale.			
Parameters	**Values (mg·l^{-1})**	**Parameters**	**Values (mg·l^{-1})**
Total COD	62,241 ± 7,572	Ammonium (NH_4)	80 ± 9
Soluble COD	52,336 ± 4,926	Sulfate	163 ±53
Total Solids (TS)	54,540 ± 12,090	Chlorides	383 ± 15
Volatile Solids (VS)	50,659 ± 11,718	Calcium	76 ± 77
Total Suspended Solids (TSS)	24,638 ± 11,022	Magnesium	165 ± 62
Volatile Suspended Solids (VSS)	23,238 ± 10,327	Potassium	1036 ± 57
Total phosphorous (P_{total})	603 ± 74	Sodium	33 ± 14
Phosphate (PO_4)	352 ± 44	Copper	1.5 ± 0.8
Total Kjeldahl Nitrogen (TKN)	2,170 ± 581	pH	4 ± 0.4
Soluble Kjeldahl Nitrogen (SKN)	1,158 ± 93		

Table S6.2. Number of reads per sample obtained by NGS analysis.

Reactor Stage	Sample[1]	Bacterial			Archaeal		
		Total	Filtered[2]	Merged[3]	Total	Filtered[2]	Merged[3]
0	A_1	242444	236424	666511	**4803**	**4767**	18575
	A_2	442591	430087		13858	13808	
I	B_1	249235	238637	800548	14076	9801	44836
	B_2	**616068**	**561911**		41312	35035	
	C_1	337600	314388	607939	**171263**	**114533**	190710
	C_2	321540	293551		112787	76177	
	D_1	498373	493030	652482	9600	9300	33321
	D_2	161738	159452		25828	24021	
	E_1	204733	198876	481556	17211	16543	27420
	E_2	289208	282680		11576	10877	
	F_1	200737	192240	426786	25103	21514	104299
	F_2	240690	234546		94523	82785	
	G_1	425210	412879	547029	35266	30002	76621
	G_2	137928	134150		50872	46619	
	H_1	221170	210949	593192	30994	28982	99382
	H_2	397467	382243		73216	70400	
	I_1	355596	340924	613384	50728	48494	92826
	I_2	284037	272460		46220	44332	
II	J_1	189576	180899	280942	30211	28697	70925
	J_2	104329	100043		44209	42228	
	K_1	154978	149089	451624	12627	11391	66098
	K_2	314081	302535		60200	54707	
III	L_1	91558	90680	507354	70502	66119	141484
	L_2	425552	416674		80774	75365	
IV	M_1	427718	417505	703964	88254	84630	111166
	M_2	290848	286459		28163	26536	
V	N_1	347177	333540	795027	11951	9948	26796
	N_2	488748	461487		18107	16848	
VI	O_1	**61409**	**60914**	263916	20949	17919	40967
	O_2	205644	203002		31738	23048	
VII	P_1	416891	413673	869154	60005	46886	143985
	P_2	458567	455481		117672	97099	
Average		**300107**	**289419**	**578838**	**47019**	**40294**	**80588**

[1] Biological samples with technical replicates were sequenced.
[2] Reads after filtering out wrongly assigned OTUs at domain level.
[3] Sum of the technical replicates reads

Table S6.3. Taxonomic assignations of the reads obtained by NGS analysis.

BACTERIA

PHYLUM	CLASS	ORDER	FAMILY	GENUS
Actinobacteria	*Actinobacteria*	*Acholeplasmatales*	*Acholeplasmataceae*	*Acinetobacter*
Aminicenantes	*Anaerolineae*	*Anaerolineales*	*Alcaligenaceae*	*Alcaligenes*
Bacteroidetes	*Bacilli*	*Bacillales*	*Anaerolineaceae*	*Geobacter*
Caldiserica	*Bacteroidetes*	*Bacteroidales*	*Anaerolineaceae*	*Lactobacillus*
Chlorobi	*Bacteroidia*	*Bacteroidia*	*Bacteroidaceae*	*Leuconostoc*
Chloroflexi	*Betaproteobacteria*	*Burkholderiales*	*Campylobacteraceae*	*Longilinea*
Cloacimonetes	BSA1B-03	*Caldisericales*	CAP-aah99b04	*Macellibacteroides*
Elusimicrobia	*Caldisericia*	*Campylobacterales*	*Christensenellaceae*	*Mesotoga*
Firmicutes	*Candidatus*	*Chlorobiales*	*Clostridiales*	*Prevotella*
Ignavibacteriae	*Chlorobia*	*Clostridiales*	*Comamonadaceae*	*Proteiniphilum*
Microgenomates	*Cloacimonetes*	*Desulfuromonadales*	*Erysipelotrichaceae*	*Pseudomonas*
Nitrospirae	*Clostridia*	*Erysipelotrichales*	*Eubacteriaceae*	*Romboutsia*
Proteobacteria	*Deltaproteobacteria*	*Ignavibacteriales*	*Geobacteraceae*	*Syntrophobacter*
Spirochaetae	*Elusimicrobia*	*Kosmotogales*	*Helicobacteraceae*	Uncultured
Synergistetes	*Epsilonproteobacteria*	*Lactobacillales*	*Ignavibacteriaceae*	
Tenericutes	*Erysipelotrichia*	*Methylophilales*	*Kosmotogaceae*	
Thermotogae	*Gammaproteobacteria*	NB1-n	*Lachnospiraceae*	
Verrucomicrobia	*Ignavibacteria*	*Nitrospirales*	*Lactobacillaceae*	
	LD1-PB3	*Petrotogales*	*Lentimicrobiaceae*	
	LNR	*Propionibacteriales*	*Leuconostocaceae*	
	Mollicutes	*Pseudomonadales*	M2PB4-65	
	Nitrospira	*Sphingobacteriales*	*Marinilabiaceae*	
	OPB35	*Spirochaetales*	*Methylophilaceae*	
	Sphingobacteriia	*Synergistales*	*Moraxellaceae*	
	Spirochaetes	*Syntrophobacterales*	*Nitrospiraceae*	
	Synergistia	*Thermoanaerobacterale*	OPB56	
	Thermotogae	Uncultured	*Peptostreptococcaceae*	
	W27		*Petrotogaceae*	
	W5		PHOS-HE36	
	Uncultured		*Planococcaceae*	
			Porphyromonadaceae	
			Prevotellaceae	
			Prolixibacteraceae	
			Propionibacteriaceae	
			Pseudomonadaceae	
			Rikenellaceae	
			Ruminococcaceae	
			Spirochaetaceae	
			ST-12K33	
			Synergistaceae	
			Syntrophaceae	
			Syntrophobacteraceae	
			WCHB1-02	
			Uncultured	

ARCHAEA

PHYLUM	CLASS	ORDER	FAMILY	GENUS
Bathyarchaeota	*Methanobacteria*	*Methanobacteriales*	ARC26	*Methanobacterium*
Euryarchaeota	*Methanomicrobia*	*Methanomicrobiales*	GOM	*Methanoculleus*
Woesearchaeota	*Thermoplasmata*	*Methanosarcinales*	*Methanobacteriaceae*	*Methanolinea*
WSA2	WCHA1-57	*Thermoplasmatales*	*Methanomicrobiaceae*	*Methanomethylovorans*
	Uncultured	Uncultured	*Methanoregulaceae*	*Methanosaeta*
			Methanosaetaceae	*Methanosarcina*
			Methanosarcinaceae	*Methanospirillum*
			Methanospirillaceae	Uncultured
			Thermoplasmatales	

"There is only certainty with respect to the past, and with respect to the future, the certainty of death"

Erich Fromm

Chapter 7

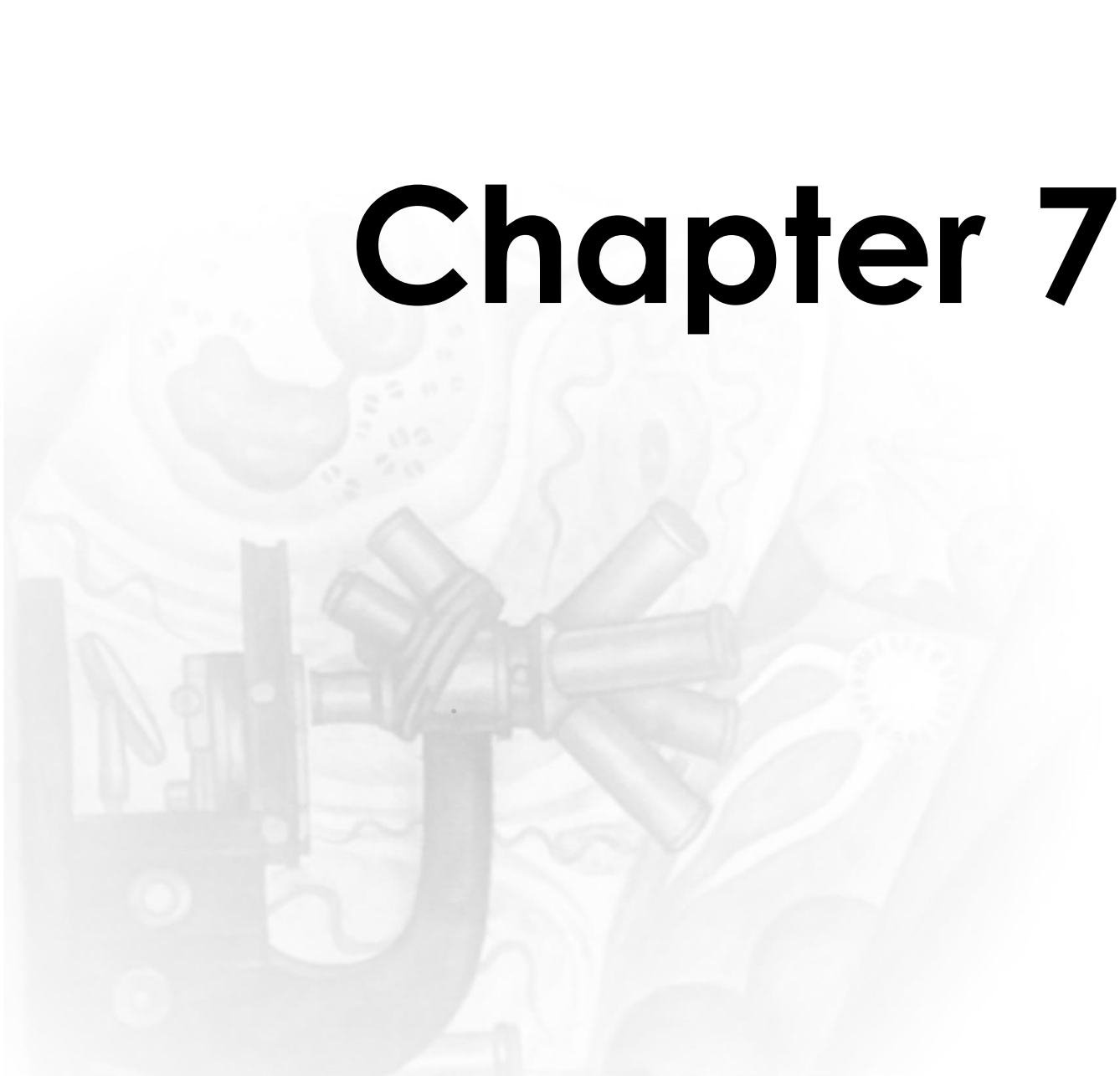

CHAPTER 7

GENERAL DISCUSSION

Phenotypically distinct microorganisms may form obligate syntrophic interactions because they are metabolically dependent on each other in certain conditions (Schink, 1997; McInerney et al., 2008; Stams and Plugge, 2009; Morris et al., 2013). The low energy yield associated with fatty acid degradative pathways can only be conserved by some microorganisms via specialized biochemical mechanisms. Despite the ecological importance of the syntrophic interactions, our understanding of the molecular basis of syntrophic lifestyle remains limited. A better understanding of how microorganisms cope with energetic constraints is important to provide new insights into methane production, waste treatment, and to engineer biotechnological processes or to design synthetic enzymes for the catalysis of energetically unfavourable reactions.

The research presented in this thesis focussed on the molecular mechanisms used by *Syntrophobacter fumaroxidans*, a propionate-oxidizing bacterium, and its methanogenic partners *Methanospirillum hungatei* and *Methanobacterium formicicum*. An emphasis was put on the interspecies electron transfer (IET) and the importance of formate as an interspecies electron carrier in syntrophic propionate degradation. In addition, alternative energy conservation mechanisms and their role in sulfate reduction and methanogenesis are discussed. Genome and proteome analyses revealed a detailed description of propionate degradation by *Syntrophobacter fumaroxidans* (**Chapter 4**) as well as of the methanogenic metabolism of two hydrogenotrophic methanogens, *Methanospirillum hungatei* and *Methanobacterium formicicum*, grown in syntrophic association and in pure cultures (**Chapter 5**).

In **Chapter 2** the occurrence of genetic markers for syntrophic growth on butyrate and propionate were explored in the genomes of short chain fatty acid degraders known to engage in syntrophy with methanogens. The domain-based functional profiling analyses shows that the presence of periplasmic formate dehydrogenases and their maturation proteins FdhE in the genome of syntrophs is a difference with the non-syntrophic butyrate and propionate degraders.

A previous genome comparison study of syntrophic bacteria reports that confurcating hydrogenases and membrane-associated reverse electron transport (RET) complexes are present in syntrophs and that they play a critical role in syntrophy (Sieber et al., 2012). The analyses presented in **Chapter 2** confirms the importance of membrane associated RET complexes, like the Rnf or Ech complexes. However, the presence of confurcating hydrogenases in non-syntrophic bacteria, like *Desulfotomaculum kuznetsovii* and *Desulfobulbus propionicus*, indicates that these complexes are not exclusive for syntrophs and can also be important in energy conservation in non-syntrophic bacteria. The analysis of Sieber and co-workers was restricted to genomes of syntrophs whereas the analysis in **Chapter 2** of this thesis also included genomes of non-syntrophic sulfate-reducing bacteria (SRB). However, not many of those SRB

have been tested for syntrophic butyrate or propionate degradation. Only *Desulfotomaculum kuznetsovii* and *Desulfobulbus propionicus* are validated non-syntrophic bacteria. To strengthen the importance of the analysis, more butyrate- and propionate-degrading SRB should be tested for syntrophic capability.

Moreover, the combination of more than one molecular mechanism as a characteristic of syntrophs was not completely explored in Chapter 2. For instance, it has been proposed that the proton-translocating pyrophosphatase (HppA) in SRB has a role in energy conservation by proton translocation and hydrolysis of pyrophosphate (Cypionka, 1995; Baltscheffsky et al., 1999). A reverse use of this transmembrane protein to conserve energy could be feasible (Serrano et al., 2007). The HppA, in contrast with Rnf, was ubiquitously present in all the analysed syntrophic microorganisms in **Chapter 2**, even in the non-sulfate reducers such as *Syntrophomonas wolfei*. It can be argued, as in the case of the confurcating hydrogenases, that although HppA is not present in *D. propionicus,* it is present in the genome of the non-syntroph *D. kuznetsovii*, therefore HppA is not a genetic marker for syntrophic growth. However, if we hypothesise that syntrophs need both: complexes for RET, such as HppA or Rnf, and complexes that facilitate IET, we observed that neither of the validated non-syntrophic bacteria fulfils both conditions. Although the genome of *D. kuznetsovii* revealed the presence of HppA, it lacks periplasmic formate dehydrogenases and periplasmic hydrogenases (Visser et al., 2013). Whereas, *D. propionicus* despite having genes coding for periplasmic hydrogenases, lacks proton translocating mechanisms like Rnf or HppA. Therefore, butyrate- and propionate-degrading bacteria must need both RET and IET mechanisms to be able to grow in syntrophy.

Although the genes suspected to be exclusive in syntrophic microorganisms correspond to those coding for energy metabolism, other protein domains putatively involved in the formation of spatial structures such as capsule or biofilm (IPR019079) and cell-shape determination (IPR018365) were also highlighted to be important for syntrophic growth. Numerous studies have found genes involved in the formation of spatial structures such as biofilm, granule formation and flagella and pili synthesis, to be important for syntrophic interactions (Kato and Watanabe, 2010; Summers et al., 2010; Krumholz et al., 2015). However, many biofilm formation and flagellar proteins are also produced during axenic growth (Nadell et al., 2009; Clark et al., 2012). Although cellular aggregation and the structure of a mixed community might facilitate the exchange of metabolites between cells (Ishii et al., 2005; Shimoyama et al., 2009; Brileya et al., 2014), these are not essential attributes in the formation and maintenance of syntrophy, as the interspecies electron transfer.

It is presented in **Chapter 2** that phylogeny does not predict syntrophy, nonetheless other potential genomic markers for syntrophy have been investigated. Recently, a genetic polymorphism has been described where only a specific genotype of

Desulfovibrio vulgaris is able to engage in syntrophy with *Methanococcus maripaludis* (Grosskopf et al., 2016). Interestingly, the reported genetic alterations in the syntrophic genotype are not related to interspecies electron transfer but involved in RET during lactate oxidation. One mutation affects the enzymes that catalyse lactate uptake and the conversion of pyruvate, while the second mutation is affecting the H^+/Na^+ ion-translocating subunit of a membrane-bound dehydrogenase. The authors proposed that the identified polymorphism in the latter gene increases the number of ions which can translocate over the membrane per number of hydrogen produced. Thereby, the cell can use the membrane gradient as a form of cellular energy to invest in lactate oxidation (Grosskopf et al., 2016). This hypothesis reinforces the importance of proton translocating mechanisms in syntrophic bacteria. Furthermore, it glances at the differential capacities of proton translocating mechanisms present in syntrophic bacteria, to transport protons more efficiently than in non-syntrophic bacteria. A similar energy conservation concept has been proposed before by hypothesising that the smallest quantum of energy that can be transported via electron transfer phosphorylation by the ATP synthase is lower in syntrophs than in non-syntrophic bacteria (Worm, 2010).

The maximum number of protons that have to be translocated across the membrane for ATP synthesis, or hydrolysis in RET, is determined by the number of c-subunits in the membrane integrated F_0 region of the ATP synthase (Nakanishi-Matsui and Futai, 2006). With one full rotation of the ATP synthase complex, each of the three catalytic ß subunits in the F_1 region synthesizes/hydrolyses one ATP molecule, and each of the c-subunits in F_0 transports one proton. (Nakanishi-Matsui et al., 2010; Soga et al., 2017). Among the bacteria analysed in **Chapter 2**, syntrophs contain smaller ATP synthase c-subunits than sulfate reducers. Thus, in principle, the membrane integrated rotor in syntrophs may contain more c-subunits. A higher number of protons translocated per ATP hydrolysed would result in an increase of the smallest quantum of biologically conservable energy. Therefore, a c-subunit to ATP synthase ratio would give insight in the minimum amount of energy that can be conserved by syntrophs. Yet, this ratio is not known for the analysed bacteria in chapter 2. The size of the c-subunits discussed above are only predictions based on the amino acid sequences available in their genome. Biochemical and further proteomic analysis of ATP synthases are necessary to reinforce this hypothesis. Unfortunately, in the proteomic analysis in chapter 4 the c-subunit was not detected in any of the growth conditions.

Chapter 3 focused on the metabolic flexibility of *S. fumaroxidans* to grow in syntrophy with *M. hungatei* or *D. desulfuricans* in a sulfate-rich medium. In general, sulfate reduction is favoured over methanogenesis when sufficient sulfate is present (Lovley and Klug, 1983; Muyzer and Stams, 2008). Our results showed sulfate

reduction by *S. fumaroxidans*, but propionate oxidation coupled to hydrogen and formate production also occurred at enough levels to sustain *D. desulfuricans* growth.

In this thesis, the capacity of sulfate reducers to grow in syntrophy has been discussed (**Chapter 2 & 3**). Several comparative transcriptomic analyses have been performed to find out the key genetic elements for syntrophy by considering the metabolic flexibility of SRB (Walker et al., 2009; Plugge et al., 2010; Plugge et al., 2011). However, in those studies sulfate was added to syntrophic cocultures to assess the change in gene expression. **Chapter 3** also included a perturbation in sulfate-reducing cultures towards syntrophic conditions by adding a hydrogen/formate scavenging microorganism. Syntrophic cocultures have been obtained before by adding an hydrogen scavenger (Boone and Bryant, 1980), however in our experimental approach the addition of the syntrophic partner did not involve a limitation of sulfate and the levels of sulfide were high. The study in **Chapter 3** might have given different results if sulfate would have been limited. In the study of (Grosskopf et al., 2016), cultures of clones of *D. vulgaris* prone to engage in syntrophy produced more hydrogen during lactate oxidation compared to those clones with a non-syntrophic genotype. Nevertheless, this hydrogen accumulation was observed only when sulfate was not provided or when it was limited at 50% (30 mM lactate and 7.5mM SO_4^{2-}).

The sulfate-reducing capacities of members of *Syntrophobacteracea* have been shown in sulfate-perturbed methanogenic environments (Liu and Conrad, 2017). Yet, the growth rate of *S. fumaroxidans* with propionate and sulfate is much slower than when grown in syntrophy with methanogens (van Kuijk and Stams, 1995; Scholten and Conrad, 2000). The slow growth rates as sulfate reducers, or even the lack of ability to respire sulfate, of some members of *Syntrophobacterales*, such as *Smithella spp.* and *Syntrophus spp.*, has led to the speculation that these bacteria might be losing the ability for sulfate respiration after dealing with low concentrations of sulfate in methanogenic environments (Plugge et al., 2011). Moreover, evolutionary experiments support these theories. It has been shown that the mutations that cause the specialization for syntrophy, result in detriment of sulfate-reducing capacities in cocultures of *D. vulgaris* and *M. maripaludis* (Hillesland and Stahl, 2010; Hillesland et al., 2014). In **Chapter 3** we assessed how prone *S. fumaroxidans* is to grow in syntrophy despite the availability of enough sulfate to grow on its own, thus indirectly estimating the hypothetical loss of sulfate-reducing capacities of our model bacterium. It is remarkable that even in a sulfate-rich medium *S. fumaroxidans* maintained a syntrophic relationship with a hydrogen/formate scavenger. In **Chapter 4** it was observed that most of the enzymes required for sulfate reduction were present in all growth conditions. Therefore, the prevalence of propionate oxidation coupled to proton and CO_2 reduction in sulfate-rich medium also points to

the fact that the molecular mechanisms for energy conservation available in *S. fumaroxidans* genome, are ubiquitously produced.

Nevertheless, the ubiquitous production by *S. fumaroxidans* of proteins involved in sulfate reduction and in hydrogen and formate production, might be an advantageous trait. Recently, an evolutionary experiment in cocultures of *D. vulgaris* and *M. maripaludis* was done with fluctuating availability of sulfate (Turkarslan et al., 2017). Results showed that when sulfate availability fluctuated too frequently in an environment with excess lactate and the abundance of methanogens, the gene regulation in *D. vulgaris* to shift repeatedly between sulfate-reducing and syntrophic physiologies drove the cultures to collapse. It was concluded that transcription regulation can be detrimental in a rapidly fluctuating environment.

Biochemical, genomic and transcriptomic analysis of *Syntrophobacter fumaroxidans* has been performed (de Bok et al., 2002b; Müller et al., 2010; Worm et al., 2011b; Plugge et al., 2012). **Chapter 4** widened our knowledge of the molecular mechanisms for energy conservation used by *S. fumaroxidans* during propionate degradation under different growth conditions. The importance of formate as interspecies electron carrier in *S. fumaroxidans* has been demonstrated before in cocultures with *M. hungatei* (de Bok et al., 2002a). Our results furthermore identified a set of three formate dehydrogenases (Fdh3, Fdh4 and Fdh5) that transfer electrons to the syntrophic partner. Two formate dehydrogenases (Fdh1 and Fdh2) have been purified from *S. fumaroxidans* (de Bok et al., 2003). Both enzymes were produced in fumarate-grown cells as well as in cells grown syntrophically on propionate with *M. hungatei*. Our proteomic results showed that Fdh1 and Fdh2 are the main formate dehydrogenases ubiquitously produced in propionate-degrading cultures, which is in agreement with the study of de Bok for the syntrophically grown cells with *M. hungatei* and suggest a similar production of these two enzymes during fumarate fermentation.

Purification of *S. fumaroxidans* Fdh1 and Fdh2 showed that both enzymes are tungsten (W) containing (de Bok et al., 2003). A following study revealed that growth in the presence of W led to an increase in total FDH activity relative to growth with molybdenum (Mo), either in coculture with *M. hungatei* or in axenic growth with propionate and fumarate (Plugge et al., 2009). The presence of both trace elements (W and Mo) on the other hand decreased total FDH activity in propionate and fumarate-grown cultures, which suggested an antagonistic effect of Mo in W-containing FDH. Remarkably, such effect was not observed for cells grown in coculture, which indicated the involvement of other FDHs than those known at the time of the study which were only the W-containing Fdh1 and Fdh2. Our proteomic results revealed that Fdh3, Fdh4 and Fdh5 are the formate dehydrogenase involved in IET. Moreover, these FDHs most probably contain Mo and can incorporate W, as the increase in total FDH activity with cocultured cells grown in the presence of W

suggests. However, this assumption must be verified by purifying and characterizing the enzymes.

Enzyme activity studies dependent on the presence, absence or combination of W and Mo in the medium have been performed before in the model microorganisms studied in this thesis. In *S. fumaroxidans* the antagonistic effect of Mo in the W-FDHs has been discussed (Plugge et al., 2009). While for *M. hungatei* an antagonistic effect of Mo in the total FDH activity was observed in cells of this methanogen, which suggests that at least one of its FDHs (most probably W-containing) cannot incorporate Mo. The enzyme assays in *M. hungatei* cells grown with H_2/CO_2 or in coculture with *S. fumaroxidans* showed a higher total FDH activity when W and Mo were available in the growth medium than when only W was provided (Plugge et al., 2009). However, for formate grown cells the total FDH activity decreased with Mo presence in contrast to only-W supplemented medium. The proteomic analysis in chapter 5 showed that Fdh3 in *M. hungatei* is the only FDH that was more abundant in cells grown with formate than in cells grown with H_2/CO_2 or in coculture with *S. fumaroxidans*. Thus, we speculated that Fdh3 of *M. hungatei* might not be able to incorporate Mo, in contrast to the other W-FDHs.

In *M. formicicum* no antagonistic effect of W was reported, but this methanogen was not able to synthetize an active FDH during growth with W and lack of Mo (May et al., 1988). **Chapter 5** revealed that the only FDH detected at the studied conditions of *M. formicicum* was Fdh1. Therefore, it is possible that this FDH is a Mo-containing enzyme. A better understanding of the implications of the metal content of FDHs, and other pterin enzymes such as formylmethanofuran dehydrogenases, in the interactions within methanogenic microbial communities might contribute to the optimization of metal dosage in anaerobic methanogenic bioreactors.

Regulatory mechanisms to express isoenzymes with different functions, under different conditions, with different cell locations, or incorporating different metals in the active site often allow the use of different pathways for energy conservation and adaptation to environmental constrains, such as substrate or metal availability (da Silva et al., 2013). For instance, enzymatic studies in *D. vulgaris* Hildenborough showed that a W-FDH is the main FDH in hydrogenotrophic conditions while the Mo-FDH was the most important FDH during growth with formate (da Silva et al., 2011). A following study with deletion mutants for the two main FDH detected in *D. vulgaris* provided the first direct evidence for the involvement of formate cycling during growth with lactate coupled to sulfate reduction (da Silva et al., 2013). In *S. fumaroxidans* the periplasmic Fdh2 might fulfil such role during growth with sulfate as showed in **Chapter 4**, besides the hydrogen cycling with Hyn.

In **Chapter 6**, the performance and robustness to high loading tests of an anaerobic membrane bioreactor (AnMBR) were evaluated. The population analysis showed the presence of members of all metabolic groups of the anaerobic degradation chain which was essential for the robustness and stability of the reactor. The diversity of the microbial population permitted to some groups of microorganisms to take over other groups when changes in hydrogen concentrations and total-VFA accumulation were observed in the bioreactor. The abundance of uncharacterized microorganisms from known phyla and candidate phyla without cultivated representatives, shows the importance and urge for the isolation of novel uncultured microorganisms that permit us to investigate their functions in complex microbial communities.

Moreover, the results presented in **Chapter 6** showed that the hydrogen concentrations can be used in digester control along with other liquid phase parameters to be measured on-line, for instance VFA or dissolved H_2.

The importance of hydrogenases and formate dehydrogenases in the interactions of microorganisms present in methane producing environments has been discussed. But it is noteworthy to mention that there is an increasing interest in investigating the reversible biochemical processes of hydrogen and formate production, as well as the interconversion of these compounds for purposes of energy storage (Pereira, 2013). The developing of biocatalysts to produce reduced carbon compounds from CO_2 has been proposed and investigated in the last decade (Reda et al., 2008; Mourato et al., 2017). CO_2 removal from the atmosphere as a mean of relieving global warming while producing fuels or chemical feedstocks is an attractive possibility (El-Zahab et al., 2008; Yadav et al., 2012; Sakai et al., 2017) Moreover, the potential use of microorganisms as biocatalysts for H_2 production from formate is currently in the spotlight for a future H_2-based economy (Hambourger et al., 2008; Martins et al., 2015; Martins et al., 2016).

Thus, after decades of research, the enzymes that catalyse two of the simplest redox reactions in nature remain to be intensively studied and are strong candidates to facilitate new types of fuel cells and other technological developments in a post-oil society.

Future research

- Biochemical and structural analysis of Fdh3, Fdh4 and Fdh5 of *S. fumaroxidans* is important as it could provide insight into the importance of molybdenum-dependent formate dehydrogenases during syntrophic growth.

- Sulfate-reducing bacteria such as *Desulfobacterium autotrophicum*, *Desulfomonile tiedjei* and *Desulfosporosinus meridiei* were never tested for syntrophic growth, but all crucial domains discussed in chapter 2 were found in the corresponding genomes, which suggests their possible ability to grow in syntrophic associations. Therefore, these bacteria should be tested for syntrophic growth. We attempted to establish a methanogenic syntrophic coculture by inoculating active *M. hungatei* in a lactate-grown culture of *D. autotrophicum*, but this was not successful. It is probable that the methanogen did not endure the high levels of sulfide in the medium. We suggest testing the above mentioned SRB for syntrophic growth with other sulfide resistant bacteria such as *Desulfovibrio desulfuricans*.

- The effect of short term overloading events in the microbial population of the AnMBR will be better evaluated by an RNA-based next generation sequencing which will allow to reveal the effect on the activity of specific microbial communities.

- Experimental evolution studies with slow-growing microorganisms such as *S. fumaroxidans* might be challenging, but the long term transferring of this bacterium growing under different conditions might be useful to evaluate in-lab evolution (Hillesland and Stahl, 2010). A genetic comparison of de novo genome sequences of *S. fumaroxidans* cultures after several generations under different propionate-degrading conditions might lead to the detection of specific mutations that will help to understand the sulfate-reducing, syntrophic and fumarate respiratory genotype of this model bacterium.

- A phenomenon where only some subunits of multimeric enzymes seem to be produced in a modular way was frequently observed in the proteomic analyses discussed in this thesis. The molecular analysis of genes and proteins in this thesis showed that another level of molecular interactions shall be considered for discussion. Protein subunits and protein domains should be investigated as the building blocks that ultimately define the protein roles in the metabolism (Grein et al., 2013).

- Hdr/Mvh-p is the most abundant putatively confurcating system during sulfate-reducing growth of *S. fumaroxidans*. This putative Hdr of *S. fumaroxidans* should be purified, its activity assessed and its role in sulfate reduction studied.

- Recently a classification system and web tool for the structural and functional analysis of hydrogenases has been developed (Søndergaard et al., 2016). The tool predictions for metal content, function and location of those hydrogenases present in *S. fumaroxidans*, *M. hungatei* and *M. formicicum* were correctly assigned in agreement with the roles suggested in this thesis. We suggest that the development of a similar web tool for an easy and faster analysis of formate dehydrogenases will be helpful to investigate the metabolism of syntrophic and sulfate-reducing bacteria.

- The metabolites exchanged during syntrophy are not exclusively restricted to electron transfer. The proteomic profiles of *M. hungatei* and *M. formicicum* showed that during syntrophic growth only a restricted set of proteins is produced compared to axenic growth on H_2/CO_2 or formate. Some biosynthetic pathways, such as biosynthesis of aromatic amino acids might not have been expressed during syntrophic growth in these methanogens. In this context, secondary syntrophy, where complementarity of amino acid metabolism takes place (Nobu et al., 2015), should be considered and further investigated in methanogenic communities.

REFERENCES

Acharya, B.K., Mohana, S., and Madamwar, D. (2008). Anaerobic treatment of distillery spent wash - a study on upflow anaerobic fixed film bioreactor. *Bioresource Technology* 99**,** 4621-4626.

Albers, S.V., and Meyer, B.H. (2011). The archaeal cell envelope. *Nature Reviews Microbiology* 9**,** 414-426.

Altschul, S.F., Gish, W., Miller, W., Myers, E.W., and Lipman, D.J. (1990). Basic local alignment search tool. *Journal of Molecular Biology* 215**,** 403-410.

Anderson, I., Ulrich, L.E., Lupa, B., Susanti, D., Porat, I., Hooper, S.D., Lykidis, A., Sieprawska-Lupa, M., Dharmarajan, L., Goltsman, E., Lapidus, A., Saunders, E., Han, C., Land, M., Lucas, S., Mukhopadhyay, B., Whitman, W.B., Woese, C., Bristow, J., and Kyrpides, N. (2009). Genomic characterization of Methanomicrobiales reveals three classes of methanogens. *PLoS One* 4**,** e5797.

Angelidaki, I., and Ahring, B.K. (1993). Thermophilic anaerobic digestion of livestock waste: the effect of ammonia. *Applied Microbiology and Biotechnology* 38**,** 560-564.

Angelidaki, I., Ellegaard, L., and Ahring, B.K. (1993). A mathematical model for dynamic simulation of anaerobic digestion of complex substrates: focusing on ammonia inhibition. *Biotechnology and Bioengineering* 42**,** 159-166.

Aquino, S.F., Hu, A.Y., Akram, A., and Stuckey, D.C. (2006). Characterization of dissolved compounds in submerged anaerobic membrane bioreactors (SAMBRs). *Journal of Chemical Technology and Biotechnology* 81**,** 1894-1904.

Ariunbaatar, J., Scotto Di Perta, E., Panico, A., Frunzo, L., Esposito, G., Lens, P.N., and Pirozzi, F. (2015). Effect of ammoniacal nitrogen on one-stage and two-stage anaerobic digestion of food waste. *Waste Management* 38**,** 388-398.

Azman, S., Khadem, A.F., Van Lier, J.B., Zeeman, G., and Plugge, C.M. (2015). Presence and role of anaerobic hydrolytic microbes in conversion of lignocellulosic biomass for biogas production. *Critical Reviews in Environmental Science and Technology* 45**,** 2523-2564.

Baltazar, C.S.A., Marques, M.C., Soares, C.M., Delacey, A.M., Pereira, I.a.C., and Matias, P.M. (2011). Nickel-Iron-Selenium Hydrogenases - An Overview. *European Journal of Inorganic Chemistry* 2011**,** 948-962.

Baltscheffsky, M., Schultz, A., and Baltscheffsky, H. (1999). H^+-PPases: a tightly membrane-bound family. *FEBS Letters* 457**,** 527-533.

Barrena, R., Traub, J.E., Gil, C.R., Goodwin, J.a.S., Harper, A.J., Willoughby, N.A., Sanchez, A., and Aspray, T.J. (2017). Batch anaerobic digestion of deproteinated malt whisky pot ale using different source inocula. *Waste Management*.

Bassegoda, A., Madden, C., Wakerley, D.W., Reisner, E., and Hirst, J. (2014). Reversible interconversion of CO_2 and formate by a molybdenum-containing formate dehydrogenase. *Journal of the American Chemical Society* 136**,** 15473-15476.

Beaty, P.S., and Mcinerney, M.J. (1990). Nutritional features of *Syntrophomonas wolfei*. *Applied and Environmental Microbiology* 56**,** 3223-3224.

Bellack, A., Huber, H., Rachel, R., Wanner, G., and Wirth, R. (2011). *Methanocaldococcus villosus* sp. nov., a heavily flagellated archaeon that adheres to surfaces and forms cell-cell contacts. *International Journal of Systematic and Evolutionary Microbiology* 61**,** 1239-1245.

Belostotskiy, D.E., Ziganshina, E.E., Siniagina, M., Boulygina, E.A., Miluykov, V.A., and Ziganshin, A.M. (2015). Impact of the substrate loading regime and phosphoric acid supplementation on performance of biogas reactors and microbial community dynamics during anaerobic digestion of chicken wastes. *Bioresource Technology* 193**,** 42-52.

Bendtsen, J.D., Nielsen, H., Widdick, D., Palmer, T., and Brunak, S. (2005). Prediction of twin-arginine signal peptides. *BMC Bioinformatics* 6.

Berg, I.A., Kockelkorn, D., Ramos-Vera, W.H., Say, R.F., Zarzycki, J., Hugler, M., Alber, B.E., and Fuchs, G. (2010). Autotrophic carbon fixation in archaea. *Nature Reviews Microbiology* 8**,** 447-460.

Berggren, G., Adamska, A., Lambertz, C., Simmons, T.R., Esselborn, J., Atta, M., Gambarelli, S., Mouesca, J.M., Reijerse, E., Lubitz, W., Happe, T., Artero, V., and Fontecave, M. (2013). Biomimetic assembly and activation of [FeFe]-hydrogenases. *Nature* 499**,** 66-69.

Biegel, E., Schmidt, S., Gonzalez, J.M., and Müller, V. (2011). Biochemistry, evolution and physiological function of the Rnf complex, a novel ion-motive electron transport complex in prokaryotes. *Cellular and molecular life sciences* 68**,** 613-634.

Blank, C.E. (2009). Not so old Archaea - the antiquity of biogeochemical processes in the archaeal domain of life. *Geobiology* 7**,** 495-514.

Boe, K., Steyer, J.P., and Angelidaki, I. (2008). Monitoring and control of the biogas process based on propionate concentration using online VFA measurement. *Water Science and Technology* 57**,** 661-666.

Bonacker, L.G., Baudner, S., and Thauer, R.K. (1992). Differential expression of the two methyl-coenzyme M reductases in *Methanobacterium thermoautotrophicum* as determined immunochemically via isoenzyme-specific antisera. *European Journal of Biochemistry* 206**,** 87-92.

Boone, D.R., and Bryant, M.P. (1980). Propionate-degrading bacterium, *Syntrophobacter wolinii* sp. nov. gen. nov., from methanogenic ecosystems. *Applied and Environmental Microbiology* 40**,** 626-632.

Boone, D.R., Johnson, R.L., and Liu, Y. (1989). Diffusion of the interspecies electron carriers H_2 and formate in methanogenic ecosystems and its implications in the measurement of K_m for H_2 or formate uptake. *Applied and Environmental Microbiology* 55**,** 1735-1741.

Brileya, K.A., Camilleri, L.B., Zane, G.M., Wall, J.D., and Fields, M.W. (2014). Biofilm growth mode promotes maximum carrying capacity and community stability during product inhibition syntrophy. *Frontiers in Microbiology* 5**,** 693.

Brown, K.A., Wilker, M.B., Boehm, M., Dukovic, G., and King, P.W. (2012). Characterization of photochemical processes for H_2 production by CdS nanorod-[FeFe] hydrogenase complexes. *Journal of the American Chemical Society* 134**,** 5627-5636.

Brutinel, E.D., and Gralnick, J.A. (2012). Shuttling happens: soluble flavin mediators of extracellular electron transfer in *Shewanella*. *Applied Microbiology and Biotechnology* 93**,** 41-48.

Bryant, M.P., and Boone, D.R. (1987). Isolation and characterization of *Methanobacterium formicicum* MF. *International Journal of Systematic Bacteriology* 37**,** 171-171.

Bryant, M.P., Wolin, E.A., Wolin, M.J., and Wolfe, R.S. (1967). Methanobacillus omelianskii, a symbiotic association of two species of bacteria. *Arch Mikrobiol* 59**,** 20-31.

Buckel, W., and Thauer, R.K. (2013). Energy conservation via electron bifurcating ferredoxin reduction and proton/Na^+ translocating ferredoxin oxidation. *Biochimica et Biophysica Acta* 1827**,** 94-113.

Buyukkamaci, N., and Filibeli, A. (2004). Volatile fatty acid formation in an anaerobic hybrid reactor. *Process Biochemistry* 39**,** 1491-1494.

Calli, B., Mertoglu, B., Inanc, B., and Yenigun, O. (2005). Methanogenic diversity in anaerobic bioreactors under extremely high ammonia levels. *Enzyme and Microbial Technology* 37**,** 448-455.

Cammack, R. (1999). Hydrogenase sophistication. *Nature* 397**,** 214-215.

Candela, T., and Fouet, A. (2006). Poly-gamma-glutamate in bacteria. *Molecular microbiology* 60**,** 1091-1098.

Candela, T., Moya, M., Haustant, M., and Fouet, A. (2009). "*Fusobacterium nucleatum*, the first Gram-negative bacterium demonstrated to produce polyglutamate", in: *Canadian journal of microbiology.* 2009/06/02 ed.).

Caporaso, J.G., Kuczynski, J., Stombaugh, J., Bittinger, K., Bushman, F.D., Costello, E.K., Fierer, N., Pena, A.G., Goodrich, J.K., Gordon, J.I., Huttley, G.A., Kelley, S.T., Knights, D., Koenig, J.E., Ley, R.E., Lozupone, C.A., Mcdonald, D., Muegge, B.D., Pirrung, M., Reeder, J., Sevinsky, J.R., Tumbaugh, P.J., Walters, W.A., Widmann, J., Yatsunenko, T., Zaneveld, J., and Knight, R. (2010). QIIME allows analysis of high-throughput community sequencing data. *Nature Methods* 7**,** 335-336.

Carballa, M., Regueiro, L., and Lema, J.M. (2015). Microbial management of anaerobic digestion: exploiting the microbiome-functionality nexus. *Current Opinion in Biotechnology* 33**,** 103-111.
Carbonero, F., Oakley, B.B., and Purdy, K.J. (2014). Metabolic flexibility as a major predictor of spatial distribution in microbial communities. *PLoS One* 9**,** e85105.
Castelle, C.J., Wrighton, K.C., Thomas, B.C., Hug, L.A., Brown, C.T., Wilkins, M.J., Frischkorn, K.R., Tringe, S.G., Singh, A., Markillie, L.M., Taylor, R.C., Williams, K.H., and Banfield, J.F. (2015). Genomic expansion of domain archaea highlights roles for organisms from new phyla in anaerobic carbon cycling. *Current Biology* 25**,** 690-701.
Ceccaldi, P., Marques, M.C., Fourmond, V., Pereira, I.C., and Leger, C. (2015). Oxidative inactivation of NiFeSe hydrogenase. *Chemical Communications* 51**,** 14223-14226.
Chabriere, E., Charon, M.H., Volbeda, A., Pieulle, L., Hatchikian, E.C., and Fontecilla-Camps, J.C. (1999). Crystal structures of the key anaerobic enzyme pyruvate:ferredoxin oxidoreductase, free and in complex with pyruvate. *Nature structural biology* 6**,** 182-190.
Chang, Y.H., Han, J.I., Chun, J., Lee, K.C., Rhee, M.S., Kim, Y.B., and Bae, K.S. (2002). *Comamonas koreensis* sp. nov., a non-motile species from wetland in Woopo, Korea. *International Journal of Systematic and Evolutionary Microbiology* 52**,** 377-381.
Chen, S., and Dong, X. (2005). *Proteiniphilum acetatigenes* gen. nov., sp. nov., from a UASB reactor treating brewery wastewater. *International Journal of Systematic and Evolutionary Microbiology* 55**,** 2257-2261.
Chen, S., Rotaru, A.E., Liu, F., Philips, J., Woodard, T.L., Nevin, K.P., and Lovley, D.R. (2014). Carbon cloth stimulates direct interspecies electron transfer in syntrophic co-cultures. *Bioresource Technology* 173**,** 82-86.
Chouari, R., Le Paslier, D., Daegelen, P., Ginestet, P., Weissenbach, J., and Sghir, A. (2005). Novel predominant archaeal and bacterial groups revealed by molecular analysis of an anaerobic sludge digester. *Environmental Microbiology* 7**,** 1104-1115.
Clark, M.E., He, Z., Redding, A.M., Joachimiak, M.P., Keasling, J.D., Zhou, J.Z., Arkin, A.P., Mukhopadhyay, A., and Fields, M.W. (2012). Transcriptomic and proteomic analyses of *Desulfovibrio vulgaris* biofilms: carbon and energy flow contribute to the distinct biofilm growth state. *BMC Genomics* 13**,** 138.
Cline, J.D. (1969). Spectrophotometric determination of hydrogen sulfide in natural waters. *Limnology and Oceanography* 14**,** 454-458.
Conrad, R. (1999). Contribution of hydrogen to methane production and control of hydrogen concentrations in methanogenic soils and sediments. *FEMS Microbiology Ecology* 28**,** 193–202.
Cord-Ruwisch, R., Mercz, T.I., Hoh, C.-Y., and Strong, G.E. (1997). Dissolved hydrogen concentration as an on-line control parameter for the automated operation and optimization of anaerobic digesters. *Biotechnology and Bioengineering* 56**,** 626-634.
Costa, K.C., and Leigh, J.A. (2014). Metabolic versatility in methanogens. *Current Opinion in Biotechnology* 29**,** 70-75.
Costa, K.C., Lie, T.J., Jacobs, M.A., and Leigh, J.A. (2013a). H_2-independent growth of the hydrogenotrophic methanogen *Methanococcus maripaludis*. *MBio* 4.
Costa, K.C., Lie, T.J., Xia, Q., and Leigh, J.A. (2013b). VhuD facilitates electron flow from H_2 or formate to heterodisulfide reductase in *Methanococcus maripaludis*. *Journal of Bacteriology* 195**,** 5160-5165.
Costa, K.C., Wong, P.M., Wang, T., Lie, T.J., Dodsworth, J.A., Swanson, I., Burn, J.A., Hackett, M., and Leigh, J.A. (2010). Protein complexing in a methanogen suggests electron bifurcation and electron delivery from formate to heterodisulfide reductase. *Proceedings of the National Academy of Sciences* 107**,** 11050-11055.
Cruz Viggi, C., Rossetti, S., Fazi, S., Paiano, P., Majone, M., and Aulenta, F. (2014). Magnetite particles triggering a faster and more robust syntrophic pathway of methanogenic propionate degradation. *Environmental Science & Technology* 48**,** 7536-7543.

Cypionka, H. (1995). "Solute transport and cell energetics," ed. S. Us.), 151-184.
Da Silva, S.M., Pimentel, C., Valente, F.M., Rodrigues-Pousada, C., and Pereira, I.A. (2011). Tungsten and molybdenum regulation of formate dehydrogenase expression in *Desulfovibrio vulgaris* Hildenborough. *Journal of Bacteriology* 193**,** 2909-2916.
Da Silva, S.M., Voordouw, J., Leitao, C., Martins, M., Voordouw, G., and Pereira, I.A. (2013). Function of formate dehydrogenases in Desulfovibrio vulgaris Hildenborough energy metabolism. *Microbiology* 159**,** 1760-1769.
Daims, H., Brühl, A., Amann, R., Schleifer, K.-H., and Wagner, M. (1999). The domain-specific probe EUB338 is insufficient for the detection of all bacteria: Development and evaluation of a more comprehensive probe set. *Systematic and Applied Microbiology* 22**,** 434-444.
De Bok, F.a.M., Hagedoorn, P.-L., Silva, P.J., Hagen, W.R., Schiltz, E., Fritsche, K., and Stams, A.J.M. (2003). Two W-containing formate dehydrogenases (CO_2-reductases) involved in syntrophic propionate oxidation by *Syntrophobacter fumaroxidans*. *European Journal of Biochemistry* 270**,** 2476-2485.
De Bok, F.a.M., Harmsen, H.J.M., Plugge, C.M., De Vries, M.C., Akkermans, A.D.L., De Vos, W.M., and Stams, A.J.M. (2005). The first true obligately syntrophic propionate-oxidizing bacterium, *Pelotomaculum schinkii* sp. nov., co-cultured with *Methanospirillum hungatei*, and emended description of the genus *Pelotomaculum*. *International Journal of Systematic and Evolutionary Microbiology* 55**,** 1697-1703.
De Bok, F.a.M., Luijten, M.L.G.C., and Stams, A.J.M. (2002a). Biochemical evidence for formate transfer in syntrophic propionate-oxidizing cocultures of *Syntrophobacter fumaroxidans* and *Methanospirillum hungatei*. *Applied and Environmental Microbiology* 68**,** 4247-4252.
De Bok, F.a.M., Roze, E.H., and Stams, A.J.M. (2002b). Hydrogenases and formate dehydrogenases of *Syntrophobacter fumaroxidans*. *Antonie van Leeuwenhoek* 81**,** 283-291.
De Bok, F.a.M., Stams, A.J.M., Dijkema, C., and Boone, D.R. (2001). Pathway of propionate oxidation by a syntrophic culture of *Smithella propionica* and *Methanospirillum hungatei*. *Applied and Environmental Microbiology* 67**,** 1800-1804.
De Vrieze, J., Gildemyn, S., Vilchez-Vargas, R., Jáuregui, R., Pieper, D.H., Verstraete, W., and Boon, N. (2015). Inoculum selection is crucial to ensure operational stability in anaerobic digestion. *Applied Microbiology and Biotechnology* 99**,** 189-199.
Dereli, R.K., Grelot, A., Heffernan, B., Van Der Zee, F.P., and Van Lier, J.B. (2014). Implications of changes in solids retention time on long term evolution of sludge filterability in anaerobic membrane bioreactors treating high strength industrial wastewater. *Water Research* 59**,** 11-22.
Dereli, R.K., Heffernan, B., Grelot, A., Van Der Zee, F.P., and Van Lier, J.B. (2015). Influence of high lipid containing wastewater on filtration performance and fouling in AnMBRs operated at different solids retention times. *Separation and Purification Technology* 139**,** 43-52.
Diender, M., Pereira, R., Wessels, H.J., Stams, A.J.M., and Sousa, D.Z. (2016). Proteomic analysis of the hydrogen and carbon monoxide metabolism of *Methanothermobacter marburgensis*. *Frontiers in Microbiology* 7**,** 1049.
Dolfing, J., Jiang, B., Henstra, A.M., Stams, A.J.M., and Plugge, C.M. (2008). Syntrophic growth on formate: a new microbial niche in anoxic environments. *Applied and Environmental Microbiology* 74**,** 6126-6131.
Dong, X., Plugge, C.M., and Stams, A.J.M. (1994). Anaerobic degradation of propionate by a mesophilic acetogenic bacterium in coculture and triculture with different methanogens. *Applied and Environmental Microbiology* 60**,** 2834-2838.
Dong, X., and Stams, A.J.M. (1995). Evidence for H_2 and formate formation during syntrophic butyrate and propionate degradation. *Anaerobe* 1**,** 35-39.
Duarte, A.G., Santos, A.A., and Pereira, I.A. (2016). Electron transfer between the QmoABC membrane complex and adenosine 5'-phosphosulfate reductase. *Biochimica et Biophysica Acta* 1857**,** 380-386.

El-Zahab, B., Donnelly, D., and Wang, P. (2008). Particle-tethered NADH for production of methanol from CO_2 catalyzed by coimmobilized enzymes. *Biotechnology and Bioengineering* 99**,** 508-514.

Esquivel, R.N., Xu, R., and Pohlschroder, M. (2013). Novel archaeal adhesion pilins with a conserved N terminus. *Journal of Bacteriology* 195**,** 3808-3818.

Fang, H.H.P.C., H. K., Li, Y.Y., and Chen, T. (1994). Performance and granule characteristics of UASB process treating wastewater with hydrolyzed proteins. *Water Science and Technology* 30**,** 55-63.

Ferry, J.G. (1990). Formate dehydrogenase. *FEMS Microbiology Reviews* 7**,** 377-382.

Ferry, J.G., and Lessner, D.J. (2008). Methanogenesis in marine sediments. *Annals of the New York Academy of Sciences* 1125**,** 147-157.

Ferry, J.G., and Wolfe, R.S. (1976). Anaerobic degradation of benzoate to methane by a microbial consortium. *Archives of Microbiology* 107**,** 33-40.

Ferry, J.G., and Wolfe, R.S. (1977). Nutritional and biochemical characterization of *Methanospirillum hungatii*. *Applied and Environmental Microbiology* 34**,** 371-376.

Fotidis, I.A., Karakashev, D., and Angelidaki, I. (2013). The dominant acetate degradation pathway/methanogenic composition in full-scale anaerobic digesters operating under different ammonia levels. *International Journal of Environmental Science and Technology* 11**,** 2087-2094.

Franke-Whittle, I.H., Walter, A., Ebner, C., and Insam, H. (2014). Investigation into the effect of high concentrations of volatile fatty acids in anaerobic digestion on methanogenic communities. *Waste Management* 34**,** 2080-2089.

Garcia Costas, A.M., Poudel, S., Miller, A.F., Schut, G.J., Ledbetter, R.N., Fixen, K.R., Seefeldt, L.C., Adams, M.W.W., Harwood, C.S., Boyd, E.S., and Peters, J.W. (2017). Defining electron bifurcation in the electron-transferring flavoprotein family. *Journal of Bacteriology* 199.

Garcin, E., Vernede, X., Hatchikian, E.C., Volbeda, A., Frey, M., and Fontecilla-Camps, J.C. (1999). The crystal structure of a reduced [NiFeSe] hydrogenase provides an image of the activated catalytic center. *Structure* 7**,** 557-566.

Ge, H., Batstone, D.J., and Keller, J. (2015). Biological phosphorus removal from abattoir wastewater at very short sludge ages mediated by novel PAO clade *Comamonadaceae*. *Water Research* 69**,** 173-182.

Giovannini, G., Donoso-Bravo, A., Jeison, D., Chamy, R., Ruiz-Filippi, G., and Vande Wouwer, A. (2016). A review of the role of hydrogen in past and current modelling approaches to anaerobic digestion processes. *International Journal of Hydrogen Energy* 41**,** 17713-17722.

Goodwin, J.a.S., Finlayson, J.M., and Low, E.W. (2001). A further study of the anaerobic biotreatment of malt whisky distillery pot ale using an UASB system. *Bioresource Technology* 78**,** 155-160.

Goodwin, J.a.S., and Stuart, J.B. (1994). Anaerobic digestion of malt whisky distillery pot ale using upflow anaerobic sludge blanket reactors. *Bioresource Technology* 49**,** 75-81.

Gorby, Y.A., Yanina, S., Mclean, J.S., Rosso, K.M., Moyles, D., Dohnalkova, A., Beveridge, T.J., Chang, I.S., Kim, B.H., Kim, K.S., Culley, D.E., Reed, S.B., Romine, M.F., Saffarini, D.A., Hill, E.A., Shi, L., Elias, D.A., Kennedy, D.W., Pinchuk, G., Watanabe, K., Ishii, S., Logan, B., Nealson, K.H., and Fredrickson, J.K. (2006). Electrically conductive bacterial nanowires produced by *Shewanella oneidensis* strain MR-1 and other microorganisms. *Proceedings of the National Academy of Sciences* 103**,** 11358-11363.

Grabowski, A., Tindall, B.J., Bardin, V., Blanchet, D., and Jeanthon, C. (2005). Petrimonas sulfuriphila gen. nov., sp. nov., a mesophilic fermentative bacterium isolated from a biodegraded oil reservoir. *International Journal of Systematic and Evolutionary Microbiology* 55**,** 1113-1121.

Graham, J., Peter, B., Walker, G.M., Wardlaw, A., and Campbell, E. (2012). "Characterisation of the pot ale profile from a malt whisky distillery," in *Distilled Spirits: Science and Sustainability*.).

Grein, F., Ramos, A.R., Venceslau, S.S., and Pereira, I.A. (2013). Unifying concepts in anaerobic respiration: insights from dissimilatory sulfur metabolism. *Biochimica et Biophysica Acta* 1827**,** 145-160.

Grosskopf, T., Zenobi, S., Alston, M., Folkes, L., Swarbreck, D., and Soyer, O.S. (2016). A stable genetic polymorphism underpinning microbial syntrophy. *The ISME Journal* 10**,** 2844-2853.

Gunsalus, R.P., Cook, L.E., Crable, B., Rohlin, L., Mcdonald, E., Mouttaki, H., Sieber, J.R., Poweleit, N., Zhou, H., Lapidus, A.L., Daligault, H.E., Land, M., Gilna, P., Ivanova, N., Kyrpides, N., Culley, D.E., and Mcinerney, M.J. (2016). Complete genome sequence of *Methanospirillum hungatei* type strain JF1. *Standards in Genomic Sciences* 11**,** 2.

Guo, X.H., Wang, C., Sun, F.Q., Zhu, W.J., and Wu, W.X. (2014). A comparison of microbial characteristics between the thermophilic and mesophilic anaerobic digesters exposed to elevated food waste loadings. *Bioresource Technology* 152**,** 420-428.

Guwy, A.J., Hawkes, F.R., Hawkes, D.L., and Rozzi, A.G. (1997). Hydrogen production in a high rate fluidised bed anaerobic digester. *Water Research* 31**,** 1291-1298.

Hahnke, S., Langer, T., Koeck, D.E., and Klocke, M. (2016). Description of *Proteiniphilum saccharofermentans* sp. nov., *Petrimonas mucosa* sp. nov. and *Fermentimonas caenicola* gen. nov., sp. nov. isolated from mesophilic lab-scale biogas reactors and emended description of the genus *Proteiniphilum*. *International Journal of Systematic and Evolutionary Microbiology*.

Hahnke, S., Maus, I., Wibberg, D., Tomazetto, G., Puhler, A., Klocke, M., and Schluter, A. (2015). Complete genome sequence of the novel *Porphyromonadaceae* bacterium strain ING2-E5B isolated from a mesophilic lab-scale biogas reactor. *Journal of Biotechnology* 193**,** 34-36.

Hamady, M., Walker, J.J., Harris, J.K., Gold, N.J., and Knight, R. (2008). Error-correcting barcoded primers for pyrosequencing hundreds of samples in multiplex. *Nature Methods* 5**,** 235-237.

Hamann, N., Mander, G.J., Shokes, J.E., Scott, R.A., Bennati, M., and Hedderich, R. (2007). A cysteine-rich CCG domain contains a novel [4Fe-4S] cluster binding motif as deduced from studies with subunit B of heterodisulfide reductase from Methanothermobacter marburgensis. *Biochemistry* 46**,** 12875-12885.

Hambourger, M., Gervaldo, M., Svedruzic, D., King, P.W., Gust, D., Ghirardi, M., Moore, A.L., and Moore, T.A. (2008). [FeFe]-hydrogenase-catalyzed H_2 production in a photoelectrochemical biofuel cell. *Journal of the American Chemical Society* 130**,** 2015-2022.

Hansen, T.A. (1994). Metabolism of sulfate-reducing prokaryotes. *Antonie Van Leeuwenhoek International Journal of General and Molecular Microbiology* 66**,** 165-185.

Harmsen, H.J.M., Van Kuijk, B.L.M., Plugge, C.M., Akkermans, A.D.L., De Vos, W.M., and Stams, A.J.M. (1998). *Syntrophobacter fumaroxidans* sp. nov., a syntrophic propionate-degrading sulfate-reducing bacterium. *International Journal of Systematic Bacteriology* 48 Pt 4**,** 1383-1387.

Hattori, S. (2008). Syntrophic acetate-oxidizing microbes in methanogenic environments. *Microbes and environments* 23**,** 118-127.

He, Y., Xu, P., Li, C., and Zhang, B. (2005). High-concentration food wastewater treatment by an anaerobic membrane bioreactor. *Water Research* 39**,** 4110-4118.

Hedderich, R., and Forzi, L. (2005). Energy-converting [NiFe] hydrogenases: more than just H_2 activation. *Journal of Molecular Microbiology and Biotechnology* 10**,** 92-104.

Hedderich, R., Hamann, N., and Bennati, M. (2005). Heterodisulfide reductase from methanogenic archaea: a new catalytic role for an iron-sulfur cluster. *Biological Chemistry* 386**,** 961-970.

Hedderich, R., Koch, J., Linder, D., and Thauer, R.K. (1994). The heterodisulfide reductase from *Methanobacterium thermoautotrophicum* contains sequence motifs characteristic of pyridine-nucleotide-dependent thioredoxin reductases. *European Journal of Biochemistry* 225**,** 253-261.

Hemmingsen, S.M., Woolford, C., Vandervies, S.M., Tilly, K., Dennis, D.T., Georgopoulos, C.P., Hendrix, R.W., and Ellis, R.J. (1988). Homologous plant and bacterial proteins chaperone oligomeric protein assembly. *Nature* 333**,** 330-334.

Herrmann, G., Jayamani, E., Mai, G., and Buckel, W. (2008). Energy conservation via electron-transferring flavoprotein in anaerobic bacteria. *Journal of Bacteriology* 190**,** 784-791.

Hillesland, K.L., Lim, S., Flowers, J.J., Turkarslan, S., Pinel, N., Zane, G.M., Elliott, N., Qin, Y., Wu, L., Baliga, N.S., Zhou, J., Wall, J.D., and Stahl, D.A. (2014). Erosion of functional independence early in the evolution of a microbial mutualism. *Proceedings of the National Academy of Sciences* 111**,** 14822-14827.

Hillesland, K.L., and Stahl, D.A. (2010). Rapid evolution of stability and productivity at the origin of a microbial mutualism. *Proceedings of the National Academy of Sciences* 107**,** 2124-2129.

Hoben, J.P., Lubner, C.E., Ratzloff, M.W., Schut, G.J., Nguyen, D.M.N., Hempel, K.W., Adams, M.W.W., King, P.W., and Miller, A.F. (2017). Equilibrium and ultrafast kinetic studies manipulating electron transfer: A short-lived flavin semiquinone is not sufficient for electron bifurcation. *Journal of Biological Chemistry* 292**,** 14039-14049.

Hochheimer, A., Hedderich, R., and Thauer, R.K. (1998). The formylmethanofuran dehydrogenase isoenzymes in *Methanobacterium wolfei* and *Methanobacterium thermoautotrophicum:* induction of the molybdenum isoenzyme by molybdate and constitutive synthesis of the tungsten isoenzyme. *Archives of Microbiology* 170**,** 389-393.

Hochheimer, A., Linder, D., Thauer, R.K., and Hedderich, R. (1996). The molybdenum formylmethanofuran dehydrogenase operon and the tungsten formylmethanofuran dehydrogenase operon from *Methanobacterium thermoautotrophicum*. Structures and transcriptional regulation. *European Journal of Biochemistry* 242**,** 156-162.

Hochheimer, A., Schmitz, R.A., Thauer, R.K., and Hedderich, R. (1995). The tungsten formylmethanofuran dehydrogenase from *Methanobacterium thermoautotrophicum* contains sequence motifs characteristic for enzymes containing molybdopterin dinucleotide. *European Journal of Biochemistry* 234**,** 910-920.

Holmes, D.E., Shrestha, P.M., Walker, D.J., Dang, Y., Nevin, K.P., Woodard, T.L., and Lovley, D.R. (2017). Metatranscriptomic evidence for direct interspecies electron transfer between *Geobacter* and *Methanothrix* species in methanogenic rice paddy soils. *Applied and Environmental Microbiology* 83**,** e00223-00217.

Huang, H., Wang, S., Moll, J., and Thauer, R.K. (2012). Electron bifurcation involved in the energy metabolism of the acetogenic bacterium *Moorella thermoacetica* growing on glucose or H_2 plus CO_2. *Journal of Bacteriology* 194**,** 3689-3699.

Hug, L.A., Baker, B.J., Anantharaman, K., Brown, C.T., Probst, A.J., Castelle, C.J., Butterfield, C.N., Hernsdorf, A.W., Amano, Y., Ise, K., Suzuki, Y., Dudek, N., Relman, D.A., Finstad, K.M., Amundson, R., Thomas, B.C., and Banfield, J.F. (2016). A new view of the tree of life. *Nat Microbiol* 1**,** 16048.

Ikeda, M., Sato, T., Wachi, M., Jung, H.K., Ishino, F., Kobayashi, Y., and Matsuhashi, M. (1989). Structural similarity among *Escherichia coli* FtsW and RodA proteins and *Bacillus subtilis* SpoVE protein, which function in cell division, cell elongation, and spore formation, respectively. *Journal of Bacteriology* 171**,** 6375-6378.

Imachi, H., Sakai, S., Ohashi, A., Harada, H., Hanada, S., Kamagata, Y., and Sekiguchi, Y. (2007). *Pelotomaculum propionicicum* sp. nov., an anaerobic, mesophilic, obligately syntrophic, propionate-oxidizing bacterium. *International Journal of Systematic and Evolutionary Microbiology* 57**,** 1487-1492.

Imachi, H., Sekiguchi, Y., Kamagata, Y., Hanada, S., Ohashi, A., and Harada, H. (2002). *Pelotomaculum thermopropionicum* gen. nov., sp. nov., an anaerobic, thermophilic, syntrophic propionate-oxidizing bacterium. *International journal of systematic and evolutionary microbiology* 52**,** 1729-1735.

Imachi, H., Sekiguchi, Y., Kamagata, Y., Loy, A., Qiu, Y.L., Hugenholtz, P., Kimura, N., Wagner, M., Ohashi, A., and Harada, H. (2006). Non-sulfate-reducing, syntrophic

bacteria affiliated with *Desulfotomaculum* cluster I are widely distributed in methanogenic environments. *Applied and Environmental Microbiology* 72**,** 2080-2091.

Ishihama, Y., Schmidt, T., Rappsilber, J., Mann, M., Hartl, F.U., Kerner, M.J., and Frishman, D. (2008). Protein abundance profiling of the *Escherichia coli* cytosol. *BMC Genomics* 9**,** 102.

Ishii, S., Kosaka, T., Hori, K., Hotta, Y., and Watanabe, K. (2005). Coaggregation facilitates interspecies hydrogen transfer between *Pelotomaculum thermopropionicum* and *Methanothermobacter thermautotrophicus*. *Applied and Environmental Microbiology* 71**,** 7838-7845.

Jackson, B.E., Bhupathiraju, V.K., Tanner, R.S., Woese, C.R., and Mcinerney, M.J. (1999). *Syntrophus aciditrophicus* sp. nov., a new anaerobic bacterium that degrades fatty acids and benzoate in syntrophic association with hydrogen-using microorganisms. *Archives of microbiology* 171**,** 107-114.

Jarrell, K.F., and Albers, S.V. (2012). The archaellum: an old motility structure with a new name. *Trends in Microbiology* 20**,** 307-312.

Jarrell, K.F., Stark, M., Nair, D.B., and Chong, J.P.J. (2011). Flagella and pili are both necessary for efficient attachment of *Methanococcus maripaludis* to surfaces. *FEMS Microbiology Letters* 319**,** 44-50.

Jing, H., Takagi, J., Liu, J.H., Lindgren, S., Zhang, R.G., Joachimiak, A., Wang, J.H., and Springer, T.A. (2002). Archaeal surface layer proteins contain beta propeller, PKD, and beta helix domains and are related to metazoan cell surface proteins. *Structure* 10**,** 1453-1464.

Joris, B., Dive, G., Henriques, A., Piggot, P.J., and Ghuysen, J.M. (1990). The life-cycle proteins RodA of *Escherichia coli* and SpoVE of *Bacillus subtilis* have very similar primary structures. *Mol Microbiol* 4**,** 513-517.

Junicke, H., Abbas, B., Oentoro, J., Van Loosdrecht, M., and Kleerebezem, R. (2014). Absolute quantification of individual biomass concentrations in a methanogenic coculture. *AMB Express* 4.

Junicke, H., Feldman, H., Van Loosdrecht, M.C., and Kleerebezem, R. (2015). Impact of the hydrogen partial pressure on lactate degradation in a coculture of *Desulfovibrio* sp. G11 and *Methanobrevibacter arboriphilus* DH1. *Applied Microbiology and Biotechnology* 99**,** 3599-3608.

Kaden, J., A, S.G., and Schink, B. (2002). Cysteine-mediated electron transfer in syntrophic acetate oxidation by cocultures of *Geobacter sulfurreducens* and *Wolinella succinogenes*. *Archives of Microbiology* 178**,** 53-58.

Kaster, A.K., Goenrich, M., Seedorf, H., Liesegang, H., Wollherr, A., Gottschalk, G., and Thauer, R.K. (2011a). More than 200 genes required for methane formation from H(2) and CO(2) and energy conservation are present in Methanothermobacter marburgensis and Methanothermobacter thermautotrophicus. *Archaea* 2011**,** 973848.

Kaster, A.K., Moll, J., Parey, K., and Thauer, R.K. (2011b). Coupling of ferredoxin and heterodisulfide reduction via electron bifurcation in hydrogenotrophic methanogenic archaea. *Proceedings of the National Academy of Sciences* 108**,** 2981-2986.

Kato, S. (2015). Biotechnological aspects of microbial extracellular electron transfer. *Microbes and Environments* 30**,** 133-139.

Kato, S., and Watanabe, K. (2010). Ecological and evolutionary interactions in syntrophic methanogenic consortia. *Microbes and Environments* 25**,** 145-151.

Kelly, W.J., Leahy, S.C., Li, D., Perry, R., Lambie, S.C., Attwood, G.T., and Altermann, E. (2014). The complete genome sequence of the rumen methanogen *Methanobacterium formicicum* BRM9. *Standards in Genomic Sciences* 9**,** 15.

Khan, S.T., Horiba, Y., Yamamoto, M., and Hiraishi, A. (2002). Members of the family *Comamonadaceae* as primary poly(3-hydroxybutyrate-co-3-hydroxyvalerate)-degrading denitrifiers in activated sludge as revealed by a polyphasic approach. *Applied and Environmental Microbiology* 68**,** 3206-3214.

Kidby, D.W., and Nedwell, D.B. (1991). An Investigation into the Suitability of Biogas Hydrogen Concentration as a Performance Monitor for Anaerobic Sewage-Sludge Digesters. *Water Research* 25**,** 1007-1012.

Kleerebezem, R., and Stams, A.J.M. (2000). Kinetics of syntrophic cultures: a theoretical treatise on butyrate fermentation. *Biotechnology and Bioengineering* 67**,** 529-543.

Klein, M., Friedrich, M., Roger, A.J., Hugenholtz, P., Fishbain, S., Abicht, H., Blackall, L.L., Stahl, D.A., and Wagner, M. (2001). Multiple lateral transfers of dissimilatory sulfite reductase genes between major lineages of sulfate-reducing prokaryotes. *Journal of Bacteriology* 183**,** 6028-6035.

Kosaka, T., Kato, S., Shimoyama, T., Ishii, S., Abe, T., and Watanabe, K. (2008). The genome of *Pelotomaculum thermopropionicum* reveals niche-associated evolution in anaerobic microbiota. *Genome Research* 18**,** 442-448.

Kosaka, T., Uchiyama, T., Ishii, S., Enoki, M., Imachi, H., Kamagata, Y., Ohashi, A., Harada, H., Ikenaga, H., and Watanabe, K. (2006). Reconstruction and regulation of the central catabolic pathway in the thermophilic propionate-oxidizing syntroph *Pelotomaculum thermopropionicum*. *Journal of Bacteriology* 188**,** 202-210.

Koster, I.W., and Lettinga, G. (1984). The influence of ammonium-nitrogen on the specific activity of pelletized methanogenic sludge. *Agricultural Wastes* 9**,** 205-216.

Kristensen, E., Ahmed, S.I., and Devol, A.H. (1995). Aerobic and anaerobic decomposition of organic matter in marine sediment: Which is fastest? *Limnology and Oceanography* 40**,** 1430-1437.

Kristjansson, J.K., Schönheit, P., and Thauer, R.K. (1982). Different K_s values for hydrogen of methanogenic bacteria and sulfate reducing bacteria: an explanation for the apparent inhibition of methanogenesis by sulfate. *Archives of Microbiology* 131**,** 278-282.

Krogh, A., Larsson, B., Von Heijne, G., and Sonnhammer, E.L.L. (2001). Predicting transmembrane protein topology with a hidden Markov model: Application to complete genomes. *Journal of Molecular Biology* 305**,** 567-580.

Krumholz, L.R., Bradstock, P., Sheik, C.S., Diao, Y., Gazioglu, O., Gorby, Y., and Mcinerney, M.J. (2015). Syntrophic growth of *Desulfovibrio alaskensis* requires genes for H_2 and formate metabolism as well as those for flagellum and biofilm formation. *Applied and Environmental Microbiology* 81**,** 2339-2348.

Kvist, T., Ahring, B.K., and Westermann, P. (2007). Archaeal diversity in Icelandic hot springs. *FEMS Microbiology Ecology* 59**,** 71-80.

Laanbroek, H.J., Abee, T., and Voogd, I.L. (1982). Alcohol conversions by *Desulfobulbus propionicus* Lindhorst in the presence and absence of sulfate and hydrogen. *Archives of Microbiology* 133**,** 178-184.

Larsen, S., Nielsen, L.P., and Schramm, A. (2015). Cable bacteria associated with long-distance electron transport in New England salt marsh sediment. *Environmental Microbiology Reports* 7**,** 175-179.

Le-Clech, P. (2010). Membrane bioreactors and their uses in wastewater treatments. *Applied microbiology and biotechnology* 88**,** 1253-1260.

Lee, S.H., Park, J.H., Kim, S.H., Yu, B.J., Yoon, J.J., and Park, H.D. (2015). Evidence of syntrophic acetate oxidation by *Spirochaetes* during anaerobic methane production. *Bioresource Technology* 190**,** 543-549.

Lens, P.N.L., Visser, A., Janssen, A.J.H., Hulshoff Pol, L.W., and Lettinga, G. (1998). Biotechnological treatment of sulfate-rich wastewaters. *Critical Reviews in Environmental Science and Technology* 28**,** 41-88.

Lenz, O., Ludwig, M., Schubert, T., Bürstel, I., Ganskow, S., Goris, T., Schwarze, A., and Friedrich, B. (2010). H_2 conversion in the presence of O_2 as performed by the membrane-bound [NiFe]-hydrogenase of *Ralstonia eutropha*. *ChemPhysChem* 11**,** 1107-1119.

Li, F., Hinderberger, J., Seedorf, H., Zhang, J., Buckel, W., and Thauer, R.K. (2008). Coupled ferredoxin and crotonyl coenzyme A (CoA) reduction with NADH catalyzed by the butyryl-CoA dehydrogenase/Etf complex from *Clostridium kluyveri*. *Journal of Bacteriology* 190**,** 843-850.

Li, L., He, Q., Ma, Y., Wang, X., and Peng, X. (2016). A mesophilic anaerobic digester for treating food waste: process stability and microbial community analysis using pyrosequencing. *Microbial Cell Factories* 15**,** 65.

Li, L., He, Q., Ma, Y., Wang, X.M., and Peng, X.Y. (2015). Dynamics of microbial community in a mesophilic anaerobic digester treating food waste: Relationship between community structure and process stability. *Bioresource Technology* 189**,** 113-120.

Li, X., Luo, Q., Wofford, N.Q., Keller, K.L., Mcinerney, M.J., Wall, J.D., and Krumholz, L.R. (2009). A molybdopterin oxidoreductase is involved in H2 oxidation in Desulfovibrio desulfuricans G20. *Journal of Bacteriology* 191**,** 2675-2682.

Li, X., Mcinerney, M.J., Stahl, D.A., and Krumholz, L.R. (2011). Metabolism of H_2 by *Desulfovibrio alaskensis* G20 during syntrophic growth on lactate. *Microbiology* 157**,** 2912-2921.

Liao, B.Q., Kraemer, J.T., and Bagley, D.M. (2006). Anaerobic membrane bioreactors: Applications and research directions. *Critical Reviews in Environmental Science and Technology* 36**,** 489-530.

Lie, T.J., Costa, K.C., Lupa, B., Korpole, S., Whitman, W.B., and Leigh, J.A. (2012). Essential anaplerotic role for the energy-converting hydrogenase Eha in hydrogenotrophic methanogenesis. *Proceedings of the National Academy of Sciences* 109**,** 15473-15478.

Lin, H., Peng, W., Zhang, M., Chen, J., Hong, H., and Zhang, Y. (2013). A review on anaerobic membrane bioreactors: Applications, membrane fouling and future perspectives. *Desalination* 314**,** 169-188.

Liu, F., Rotaru, A.-E., Shrestha, P.M., Malvankar, N.S., Nevin, K.P., and Lovley, D.R. (2012). Promoting direct interspecies electron transfer with activated carbon. *Energy & Environmental Science* 5**,** 8982.

Liu, P., and Conrad, R. (2017). Syntrophobacteraceae-affiliated species are major propionate-degrading sulfate reducers in paddy soil. *Environmental Microbiology* 19**,** 1669-1686.

Liu, Y., Balkwill, D.L., Aldrich, H.C., Drake, G.R., and Boone, D.R. (1999). Characterization of the anaerobic propionate-degrading syntrophs *Smithella propionica* gen. nov., sp. nov. and *Syntrophobacter wolinii*. *International Journal of Systematic Bacteriology* 49 Pt 2**,** 545-556.

Liu, Y., and Whitman, W.B. (2008). Metabolic, phylogenetic, and ecological diversity of the methanogenic archaea. *Annals of the New York Academy of Sciences* 1125**,** 171-189.

Losey, N.A., Mus, F., Peters, J.W., Le, H.M., and Mcinerney, M.J. (2017). *Syntrophomonas wolfei* uses an NADH-dependent, ferredoxin-independent [FeFe]-hydrogenase to reoxidize NADH. *Applied Environmental Microbiology* 83.

Lovley, D.R. (1985). Minimum threshold for hydrogen metabolism in methanogenic bacteria. *Applied and Environmental Microbiology* 49**,** 1530-1531.

Lovley, D.R. (2017). Syntrophy goes electric: Direct Interspecies Electron Transfer. *Annual Review of Microbiology* 71**,** 643-664.

Lovley, D.R., Fraga, J.L., Coates, J.D., and Blunt-Harris, E.L. (1999). Humics as an electron donor for anaerobic respiration. *Environmental Microbiology* 1**,** 89-98.

Lovley, D.R., and Klug, M.J. (1983). Sulfate reducers can outcompete methanogens at freshwater sulfate concentrations. *Applied and Environmental Microbiology* 45**,** 187-192.

Lovley, D.R., and Malvankar, N.S. (2015). Seeing is believing: novel imaging techniques help clarify microbial nanowire structure and function. *Environmental Microbiology* 17**,** 2209-2215.

Lu, J., Boeren, S., De Vries, S.C., Van Valenberg, H.J.F., Vervoort, J., and Hettinga, K. (2011). Filter-aided sample preparation with dimethyl labeling to identify and quantify milk fat globule membrane proteins. *Journal of Proteomics* 75**,** 34-43.

Lu, P., Vogel, C., Wang, R., Yao, X., and Marcotte, E.M. (2007). Absolute protein expression profiling estimates the relative contributions of transcriptional and translational regulation. *Nature Biotechnology* 25**,** 117-124.

Lubitz, W., Ogata, H., Rudiger, O., and Reijerse, E. (2014). Hydrogenases. *Chemical Reviews* 114**,** 4081-4148.

Lubner, C.E., Jennings, D.P., Mulder, D.W., Schut, G.J., Zadvornyy, O.A., Hoben, J.P., Tokmina-Lukaszewska, M., Berry, L., Nguyen, D.M., Lipscomb, G.L., Bothner, B., Jones, A.K., Miller, A.F., King, P.W., Adams, M.W.W., and Peters, J.W. (2017). Mechanistic insights into energy conservation by flavin-based electron bifurcation. *Nature Chemical Biology* 13**,** 655-659.

Lucas, R., Kuchenbuch, A., Fetzer, I., Harms, H., and Kleinsteuber, S. (2015). Long-term monitoring reveals stable and remarkably similar microbial communities in parallel full-scale biogas reactors digesting energy crops. *FEMS Microbiology Ecology* 91.

Lupa, B., Hendrickson, E.L., Leigh, J.A., and Whitman, W.B. (2008). Formate-dependent H_2 production by the mesophilic methanogen *Methanococcus maripaludis*. *Applied and Environmental Microbiology* 74**,** 6584-6590.

Luther, G.W., 3rd, Findlay, A.J., Macdonald, D.J., Owings, S.M., Hanson, T.E., Beinart, R.A., and Girguis, P.R. (2011). Thermodynamics and kinetics of sulfide oxidation by oxygen: a look at inorganically controlled reactions and biologically mediated processes in the environment. *Frontiers in microbiology* 2**,** 62.

Lykidis, A., Chen, C.L., Tringe, S.G., Mchardy, A.C., Copeland, A., Kyrpides, N.C., Hugenholtz, P., Macarie, H., Olmos, A., Monroy, O., and Liu, W.T. (2011). Multiple syntrophic interactions in a terephthalate-degrading methanogenic consortium. *The ISME Journal* 5**,** 122-130.

Mancuso, F., Bunkenborg, J., Wierer, M., and Molina, H. (2012). Data extraction from proteomics raw data: an evaluation of nine tandem MS tools using a large Orbitrap data set. *Journal of Proteomics* 75**,** 5293-5303.

Mander, G.J., Pierik, A.J., Huber, H., and Hedderich, R. (2004). Two distinct heterodisulfide reductase-like enzymes in the sulfate-reducing archaeon *Archaeoglobus profundus*. *European Journal of Biochemistry* 271**,** 1106-1116.

Marchaim, U., and Krause, C. (1993). Propionic to Acetic-Acid Ratios in Overloaded Anaerobic-Digestion. *Bioresource Technology* 43**,** 195-203.

Markowitz, V.M., Chen, I.-M.A., Palaniappan, K., Chu, K., Szeto, E., Grechkin, Y., Ratner, A., Jacob, B., Huang, J., Williams, P., Huntemann, M., Anderson, I., Mavromatis, K., Ivanova, N.N., and Kyrpides, N.C. (Version 4.2. November 2013). IMG: the integrated microbial genomes database and comparative analysis system *DOE-JGI, Walnut Creek, USA*.

Marques, M.C., Tapia, C., Gutierrez-Sanz, O., Ramos, A.R., Keller, K.L., Wall, J.D., De Lacey, A.L., Matias, P.M., and Pereira, I.a.C. (2017). The direct role of selenocysteine in [NiFeSe] hydrogenase maturation and catalysis. *Nat Chem Biol* 13**,** 544-550.

Martins, M., Mourato, C., Morais-Silva, F.O., Rodrigues-Pousada, C., Voordouw, G., Wall, J.D., and Pereira, I.A. (2016). Electron transfer pathways of formate-driven H_2 production in *Desulfovibrio*. *Applied Microbiology and Biotechnology* 100**,** 8135-8146.

Martins, M., Mourato, C., and Pereira, I.A. (2015). *Desulfovibrio vulgaris* growth coupled to formate-driven H_2 production. *Environmental Science & Technology* 49**,** 14655-14662.

Mathews, D.H., Sabina, J., Zuker, M., and Turner, D.H. (1999). Expanded sequence dependence of thermodynamic parameters improves prediction of RNA secondary structure. *Journal of Molecular Biology* 288**,** 911-940.

Matschiavelli, N., and Rother, M. (2015). Role of a putative tungsten-dependent formylmethanofuran dehydrogenase in *Methanosarcina acetivorans*. *Archives of Microbiology* 197**,** 379-388.

Mattevi, A., Tedeschi, G., Bacchella, L., Coda, A., Negri, A., and Ronchi, S. (1999). Structure of L-aspartate oxidase: implications for the succinate dehydrogenase/fumarate reductase oxidoreductase family. *Structure* 7**,** 745-756.

Maus, I., Stantscheff, R., Wibberg, D., Stolze, Y., Winkler, A., Puhler, A., Konig, H., and Schluter, A. (2014). Complete genome sequence of the methanogenic neotype strain *Methanobacterium formicicum* MF^T. *Journal of Biotechnology* 192 Pt A**,** 40-41.

May, H.D., Patel, P.S., and Ferry, J.G. (1988). Effect of molybdenum and tungsten on synthesis and composition of formate dehydrogenase in *Methanobacterium formicicum*. *Journal of Bacteriology* 170**,** 3384-3389.
Mccarthy, P. (1964). Anaerobic waste treatment fundamentals. Part III: toxic materials and their control. *Public works* 95**,** 91-94.
Mcinerney, M.J., Bryant, M.P., Hespell, R.B., and Costerton, J.W. (1981). *Syntrophomonas wolfei* gen. nov. sp. nov., an anaerobic, syntrophic, fatty acid-oxidizing bacterium. *Applied and Environmental Microbiology* 41**,** 1029-1039.
Mcinerney, M.J., Bryant, M.P., and Pfennig, N. (1979). Anaerobic bacterium that degrades fatty-acids in syntrophic association with methanogens. *Archives of Microbiology* 122**,** 129-135.
Mcinerney, M.J., Rohlin, L., Mouttaki, H., Kim, U., Krupp, R.S., Rios-Hernandez, L., Sieber, J., Struchtemeyer, C.G., Bhattacharyya, A., Campbell, J.W., and Gunsalus, R.P. (2007). The genome of *Syntrophus aciditrophicus*: life at the thermodynamic limit of microbial growth. *Proceedings of the National Academy of Sciences* 104**,** 7600-7605.
Mcinerney, M.J., Sieber, J.R., and Gunsalus, R.P. (2009). Syntrophy in anaerobic global carbon cycles. *Current Opinion in Biotechnology* 20**,** 623-632.
Mcinerney, M.J., Sieber, J.R., and Gunsalus, R.P. (2011). Microbial syntrophy: Genomic sequences reveal systems required to produce hydrogen and formate, plus other hallmarks of the syntrophic lifestyle. *Microbe* 6**,** 479.
Mcinerney, M.J., Struchtemeyer, C.G., Sieber, J., Mouttaki, H., Stams, A.J.M., Schink, B., Rohlin, L., and Gunsalus, R.P. (2008). Physiology, ecology, phylogeny, and genomics of microorganisms capable of syntrophic metabolism. *Annals of the New York Academy of Sciences* 1125**,** 58-72.
Mcmahon, K.D., Stroot, P.G., Mackie, R.I., and Raskin, L. (2001). Anaerobic codigestion of municipal solid waste and biosolids under various mixing conditions - II: Microbial population dynamics. *Water Research* 35**,** 1817-1827.
Mcmahon, K.D., Zheng, D., Stams, A.J.M., Mackie, R.I., and Raskin, L. (2004). Microbial population dynamics during start-up and overload conditions of anaerobic digesters treating municipal solid waste and sewage sludge. *Biotechnology and Bioengineering* 87**,** 823-834.
Mcmurdie, P.J., and Holmes, S. (2013). phyloseq: an R package for reproducible interactive analysis and graphics of microbiome census data. *PLoS One* 8**,** e61217.
Mei, X., Wang, Z., Miao, Y., and Wu, Z. (2017). A pilot-scale anaerobic membrane bioreactor under short hydraulic retention time for municipal wastewater treatment: performance and microbial community identification. *Journal of Water Reuse and Desalination***,** jwrd2017164.
Melamane, X.L., Strong, P.J., and Burgess, J.E. (2007). Treatment of wine distillery wastewater: A review with emphasis on anaerobic membrane reactors. *South African Journal of Enology and Viticulture* 28**,** 25-36.
Meyer, B., Kuehl, J.V., Deutschbauer, A.M., Arkin, A.P., and Stahl, D.A. (2013). Flexibility of syntrophic enzyme systems in *Desulfovibrio* species ensures their adaptation capability to environmental changes. *Journal of Bacteriology* 195**,** 4900-4914.
Milucka, J., Ferdelman, T.G., Polerecky, L., Franzke, D., Wegener, G., Schmid, M., Lieberwirth, I., Wagner, M., Widdel, F., and Kuypers, M.M. (2012). Zero-valent sulphur is a key intermediate in marine methane oxidation. *Nature* 491**,** 541-546.
Mohammadi, T., Sijbrandi, R., Lutters, M., Verheul, J., Martin, N., Den Blaauwen, T., De Kruijff, B., and Breukink, E. (2014). Specificity of the transport of Lipid II by FtsW in *Escherichia coli*. *Journal of Biological Chemistry*.
Mohana, S., Acharya, B.K., and Madamwar, D. (2009). Distillery spent wash: Treatment technologies and potential applications. *Journal of Hazardous Materials* 163**,** 12-25.
Moller, S., Croning, M.D.R., and Apweiler, R. (2001). Evaluation of methods for the prediction of membrane spanning regions. *Bioinformatics* 17**,** 646-653.
Morgan, R.M., Pihl, T.D., Nolling, J., and Reeve, J.N. (1997). Hydrogen regulation of growth, growth yields, and methane gene transcription in *Methanobacterium thermoautotrophicum* ΔH. *Journal of Bacteriology* 179**,** 889-898.

Morikawa, M., Kagihiro, S., Haruki, M., Takano, K., Branda, S., Kolter, R., and Kanaya, S. (2006). Biofilm formation by a *Bacillus subtilis* strain that produces gamma-polyglutamate. *Microbiology* 152**,** 2801-2807.
Moriya, H. (2015). Quantitative nature of overexpression experiments. *Molecular Biology of the Cell* 26**,** 3932-3939.
Morris, B.E., Henneberger, R., Huber, H., and Moissl-Eichinger, C. (2013). Microbial syntrophy: interaction for the common good. *FEMS Microbiology Reviews* 37**,** 384-406.
Mosey, F.E., and Fernandes, X.A. (1989). Patterns of Hydrogen in Biogas from the Anaerobic-Digestion of Milk-Sugars. *Water Science and Technology* 21**,** 187-196.
Mourato, C., Martins, M., Da Silva, S.M., and Pereira, I.a.C. (2017). A continuous system for biocatalytic hydrogenation of CO_2 to formate. *Bioresource Technology* 235**,** 149-156.
Müller, B., Sun, L., Westerholm, M., and Schnürer, A. (2016). Bacterial community composition and *fhs* profiles of low- and high-ammonia biogas digesters reveal novel syntrophic acetate-oxidising bacteria. *Biotechnology for Biofuels* 9**,** 48.
Müller, N., Schleheck, D., and Schink, B. (2009). Involvement of NADH:acceptor oxidoreductase and butyryl coenzyme A dehydrogenase in reversed electron transport during syntrophic butyrate oxidation by *Syntrophomonas wolfei*. *Journal of Bacteriology* 191**,** 6167-6177.
Müller, N., Worm, P., Schink, B., Stams, A.J.M., and Plugge, C.M. (2010). Syntrophic butyrate and propionate oxidation processes: from genomes to reaction mechanisms. *Environmental Microbiology Reports* 2**,** 489-499.
Murto, M., Bjornsson, L., and Mattiasson, B. (2004). Impact of food industrial waste on anaerobic co-digestion of sewage sludge and pig manure. *Journal of Environmental Management* 70**,** 101-107.
Muyzer, G., and Stams, A.J.M. (2008). The ecology and biotechnology of sulphate-reducing bacteria. *Nature Reviews Microbiology* 6**,** 441-454.
Nadell, C.D., Xavier, J.B., and Foster, K.R. (2009). The sociobiology of biofilms. *FEMS Microbiology Reviews* 33**,** 206-224.
Nakanishi-Matsui, M., and Futai, M. (2006). Stochastic proton pumping ATPases: from single molecules to diverse physiological roles. *IUBMB Life* 58**,** 318-322.
Nakanishi-Matsui, M., Sekiya, M., Nakamoto, R.K., and Futai, M. (2010). The mechanism of rotating proton pumping ATPases. *Biochimica et Biophysica Acta* 1797**,** 1343-1352.
Nilsen, R.K., Torsvik, T., and Lien, T. (1996). *Desulfotomaculum thermocisternum* sp. nov., a sulfate reducer isolated from a hot North Sea oil reservoir. *International Journal of Systematic Bacteriology* 46**,** 397-402.
Nobu, M.K., Narihiro, T., Rinke, C., Kamagata, Y., Tringe, S.G., Woyke, T., and Liu, W.T. (2015). Microbial dark matter ecogenomics reveals complex synergistic networks in a methanogenic bioreactor. *The ISME Journal* 9**,** 1710-1722.
Offre, P., Spang, A., and Schleper, C. (2013). Archaea in biogeochemical cycles. *Annual Review of Microbiology* 67**,** 437-457.
Omil, F. (1995). Anaerobic treatment of saline wastewaters under high sulphide and ammonia content. *Bioresource Technology* 54**,** 269-278.
Ortiz-Alvarez, R., and Casamayor, E.O. (2016). High occurrence of *Pacearchaeota* and *Woesearchaeota* (Archaea superphylum DPANN) in the surface waters of oligotrophic high-altitude lakes. *Environmental Microbiology Reports* 8**,** 210-217.
Ozgun, H., Dereli, R.K., Ersahin, M.E., Kinaci, C., Spanjers, H., and Van Lier, J.B. (2013). A review of anaerobic membrane bioreactors for municipal wastewater treatment: Integration options, limitations and expectations. *Separation and Purification Technology* 118**,** 89-104.
Ozturk, S.S., Palsson, B.O., and Thiele, J.H. (1989). Control of interspecies electron transfer flow during anaerobic digestion: dynamic diffusion reaction models for hydrogen gas transfer in microbial flocs. *Biotechnology and Bioengineering* 33**,** 745-757.
Padmasiri, S.I., Zhang, J., Fitch, M., Norddahl, B., Morgenroth, E., and Raskin, L. (2007). Methanogenic population dynamics and performance of an anaerobic membrane

bioreactor (AnMBR) treating swine manure under high shear conditions. *Water Research* 41**,** 134-144.
Paulo, L.M., Stams, A.J.M., and Sousa, D.Z. (2015). Methanogens, sulphate and heavy metals: a complex system. *Reviews in Environmental Science and Bio/Technology* 14**,** 537-553.
Paulson, J.N., Stine, O.C., Bravo, H.C., and Pop, M. (2013). Differential abundance analysis for microbial marker-gene surveys. *Nature Methods* 10**,** 1200-1202.
Pelletier, E., Kreimeyer, A., Bocs, S., Rouy, Z., Gyapay, G., Chouari, R., Riviere, D., Ganesan, A., Daegelen, P., Sghir, A., Cohen, G.N., Medigue, C., Weissenbach, J., and Le Paslier, D. (2008). "*Candidatus* Cloacamonas acidaminovorans": genome sequence reconstruction provides a first glimpse of a new bacterial division. *Journal of Bacteriology* 190**,** 2572-2579.
Peng, X., Zhang, Z., Luo, W., and Jia, X. (2013). Biodegradation of tetrabromobisphenol A by a novel *Comamonas* sp. strain, JXS-2-02, isolated from anaerobic sludge. *Bioresour Technol* 128**,** 173-179.
Pereira, I.A. (2013). An enzymatic route to H_2 storage. *Science* 342**,** 1329-1330.
Pereira, I.A., Ramos, A.R., Grein, F., Marques, M.C., Da Silva, S.M., and Venceslau, S.S. (2011). A comparative genomic analysis of energy metabolism in sulfate reducing bacteria and archaea. *Frontiers in Microbiology* 2**,** 69.
Pereira, I.a.C. (2008). "Respiratory membrane complexes of *Desulfovibrio*," in *Microbial Sulfur Metabolism,* eds. C. Dahl & C.G. Friedrich. (Berlin, Heidelberg: Springer Berlin Heidelberg), 24-35.
Peters, J.W., Miller, A.F., Jones, A.K., King, P.W., and Adams, M.W. (2016). Electron bifurcation. *Current Opinion in Chemical Biology* 31**,** 146-152.
Pires, R.H., Lourenco, A.I., Morais, F., Teixeira, M., Xavier, A.V., Saraiva, L.M., and Pereira, I.A. (2003). A novel membrane-bound respiratory complex from *Desulfovibrio desulfuricans* ATCC 27774. *Biochimica et Biophysica Acta* 1605**,** 67-82.
Plugge, C.M. (2005). Anoxic media design, preparation, and considerations. *Methods in Enzymology* 397**,** 3-16.
Plugge, C.M., Balk, M., and Stams, A.J.M. (2002). *Desulfotomaculum thermobenzoicum* subsp. *thermosyntrophicum* subsp. nov., a thermophilic, syntrophic, propionate-oxidizing, spore-forming bacterium. *International Journal of Systematic and Evolutionary Microbiology* 52**,** 391-399.
Plugge, C.M., Dijkema, C., and Stams, A.J.M. (1993). Acetyl-CoA cleavage pathway in a syntrophic propionate oxidizing bacterium growing on fumarate in the absence of methanogens. *FEMS Microbiology Letters* 110**,** 71-76.
Plugge, C.M., Henstra, A.M., Worm, P., Swarts, D.C., Paulitsch-Fuchs, A.H., Scholten, J.C.M., Lykidis, A., Lapidus, A.L., Goltsman, E., Kim, E., Mcdonald, E., Rohlin, L., Crable, B.R., Gunsalus, R.P., Stams, A.J.M., and Mcinerney, M.J. (2012). Complete genome sequence of *Syntrophobacter fumaroxidans* strain (MPOB^T). *Standards in Genomic Sciences* 7**,** 91-106.
Plugge, C.M., Jiang, B., De Bok, F.a.M., Tsai, C., and Stams, A.J.M. (2009). Effect of tungsten and molybdenum on growth of a syntrophic coculture of *Syntrophobacter fumaroxidans* and *Methanospirillum hungatei*. *Archives of Microbiology* 191**,** 55-61.
Plugge, C.M., Scholten, J.C.M., Culley, D.E., Nie, L., Brockman, F.J., and Zhang, W. (2010). Global transcriptomics analysis of the *Desulfovibrio vulgaris* change from syntrophic growth with *Methanosarcina barkeri* to sulfidogenic metabolism. *Microbiology* 156**,** 2746-2756.
Plugge, C.M., Zhang, W., Scholten, J.C.M., and Stams, A.J.M. (2011). Metabolic flexibility of sulfate-reducing bacteria. *Frontiers in Microbiology* 2**,** 81.
Poweleit, N., Ge, P., Nguyen, H.H., Loo, R.R., Gunsalus, R.P., and Zhou, Z.H. (2016). CryoEM structure of the *Methanospirillum hungatei* archaellum reveals structural features distinct from the bacterial flagellum and type IV pili. *Nature Microbiology* 2**,** 16222.
Prakash, D., Wu, Y., Suh, S.J., and Duin, E.C. (2014). Elucidating the process of activation of methyl-coenzyme M reductase. *Journal of Bacteriology* 196**,** 2491-2498.
Punta, M., Coggill, P.C., Eberhardt, R.Y., Mistry, J., Tate, J., Boursnell, C., Pang, N., Forslund, K., Ceric, G., Clements, J., Heger, A., Holm, L., Sonnhammer, E.L.L.,

Eddy, S.R., Bateman, A., and Finn, R.D. (2012). The Pfam protein families database. *Nucleic Acids Research* 40**,** D290-D301.
Qiu, Y.L., Sekiguchi, Y., Hanada, S., Imachi, H., Tseng, I.C., Cheng, S.S., Ohashi, A., Harada, H., and Kamagata, Y. (2006). *Pelotomaculum terephthalicum* sp. nov. and *Pelotomaculum isophthalicum* sp. nov.: two anaerobic bacteria that degrade phthalate isomers in syntrophic association with hydrogenotrophic methanogens. *Archives of Microbiology* 185**,** 172-182.
Quast, C., Pruesse, E., Yilmaz, P., Gerken, J., Schweer, T., Yarza, P., Peplies, J., and Glockner, F.O. (2013). The SILVA ribosomal RNA gene database project: improved data processing and web-based tools. *Nucleic Acids Research* 41**,** D590-D596.
Rabus, R., Venceslau, S.S., Wohlbrand, L., Voordouw, G., Wall, J.D., and Pereira, I.A. (2015). A post-genomic view of the ecophysiology, catabolism and biotechnological relevance of sulphate-reducing prokaryotes. *Advances in Microbial Physiology* 66**,** 55-321.
Rajagopal, R., Masse, D.I., and Singh, G. (2013). A critical review on inhibition of anaerobic digestion process by excess ammonia. *Bioresource Technology* 143**,** 632-641.
Ramiro-Garcia, J., Hermes, G.D.A., Giatsis, C., Sipkema, D., Zoetendal, E.G., Schaap, P.J., and Smidt, H. (2016). NG-Tax, a highly accurate and validated pipeline for analysis of 16S rRNA amplicons from complex biomes. *F1000Research* 5**,** 1791.
Ramos, A.R., Grein, F., Oliveira, G.P., Venceslau, S.S., Keller, K.L., Wall, J.D., and Pereira, I.A. (2015). The FlxABCD-HdrABC proteins correspond to a novel NADH dehydrogenase/heterodisulfide reductase widespread in anaerobic bacteria and involved in ethanol metabolism in *Desulfovibrio vulgaris* Hildenborough. *Environmental Microbiology* 17**,** 2288-2305.
Reda, T., Plugge, C.M., Abram, N.J., and Hirst, J. (2008). Reversible interconversion of carbon dioxide and formate by an electroactive enzyme. *Proceedings of the National Academy of Sciences* 105**,** 10654-10658.
Regueiro, L., Veiga, P., Figueroa, M., Alonso-Gutierrez, J., Stams, A.J.M., Lema, J.M., and Carballa, M. (2012). Relationship between microbial activity and microbial community structure in six full-scale anaerobic digesters. *Microbiological Research* 167**,** 581-589.
Reguera, G., Mccarthy, K.D., Mehta, T., Nicoll, J.S., Tuominen, M.T., and Lovley, D.R. (2005). Extracellular electron transfer via microbial nanowires. *Nature* 435**,** 1098-1101.
Rinke, C., Schwientek, P., Sczyrba, A., Ivanova, N.N., Anderson, I.J., Cheng, J.F., Darling, A., Malfatti, S., Swan, B.K., Gies, E.A., Dodsworth, J.A., Hedlund, B.P., Tsiamis, G., Sievert, S.M., Liu, W.T., Eisen, J.A., Hallam, S.J., Kyrpides, N.C., Stepanauskas, R., Rubin, E.M., Hugenholtz, P., and Woyke, T. (2013). Insights into the phylogeny and coding potential of microbial dark matter. *Nature* 499**,** 431-437.
Robinson, W.E., Bassegoda, A., Reisner, E., and Hirst, J. (2017). Oxidation-state-dependent binding properties of the active site in a Mo-containing formate dehydrogenase. *Journal of the American Chemical Society* 139**,** 9927-9936.
Romsaiyud, A., Songkasiri, W., Nopharatana, A., and Chaiprasert, P. (2009). Combination effect of pH and acetate on enzymatic cellulose hydrolysis. *Journal of Environmental Sciences* 21**,** 965-970.
Rotaru, A.-E., Shrestha, P.M., Liu, F., Shrestha, M., Shrestha, D., Embree, M., Zengler, K., Wardman, C., Nevin, K.P., and Lovley, D.R. (2014). A new model for electron flow during anaerobic digestion: direct interspecies electron transfer to *Methanosaeta* for the reduction of carbon dioxide to methane. *Energy & Environmental Science* 7**,** 408-415.
Rotaru, A.-E., Stryhanyuk, H., Calabrese, F., Musat, F., Shrestha, P.M., Weber, H.S., Snoeyenbos-West, O.L.O., Hall, P.O.J., Richnow, H.H., Musat, N., and Thamdrup, B. (2017). Conductive particles enable syntrophic acetate oxidation between *Geobacter* and *Methanosarcina* from coastal sediments. *bioRxiv*.
Rotaru, A.E., Shrestha, P.M., Liu, F., Ueki, T., Nevin, K., Summers, Z.M., and Lovley, D.R. (2012). Interspecies electron transfer via hydrogen and formate rather than direct

electrical connections in cocultures of *Pelobacter carbinolicus* and *Geobacter sulfurreducens*. *Applied Environmental Microbiology* 78**,** 7645-7651.
Ruff, A., Szczesny, J., Zacarias, S., Pereira, I.a.C., Plumeré, N., and Schuhmann, W. (2017). Protection and reactivation of the [NiFeSe] hydrogenase from *Desulfovibrio vulgaris* Hildenborough under oxidative conditions. *ACS Energy Letters* 2**,** 964-968.
Rupakula, A., Kruse, T., Boeren, S., Holliger, C., Smidt, H., and Maillard, J. (2013). The restricted metabolism of the obligate organohalide respiring bacterium *Dehalobacter restrictus*: lessons from tiered functional genomics. *Philosophical Transactions of the Royal Society of London B* 368**,** 20120325.
Sadaie, T., Sadaie, A., Takada, M., Hamano, K., Ohnishi, J., Ohta, N., Matsumoto, K., and Sadaie, Y. (2007). Reducing sludge production and the domination of *Comamonadaceae* by reducing the oxygen supply in the wastewater treatment procedure of a food-processing factory. *Bioscience, Biotechnology, and Biochemistry* 71**,** 791-799.
Saito, Y., Aoki, M., Hatamoto, M., Yamaguchi, T., Takai, K., and Imachi, H. (2015). Presence of a Novel Methanogenic Archaeal Lineage in Anaerobic Digesters Inferred from <I>mcrA</I> and 16S rRNA Gene Phylogenetic Analyses. *Journal of Water and Environment Technology* 13**,** 279-289.
Sakai, K., Kitazumi, Y., Shirai, O., Takagi, K., and Kano, K. (2017). Direct electron transfer-type four-way bioelectrocatalysis of CO_2/formate and NAD^+/NADH redox couples by tungsten-containing formate dehydrogenase adsorbed on gold nanoparticle-embedded mesoporous carbon electrodes modified with 4-mercaptopyridine. *Electrochemistry Communications* 84**,** 75-79.
Santos, A.A., Venceslau, S.S., Grein, F., Leavitt, W.D., Dahl, C., Johnston, D.T., and Pereira, I.A. (2015). A protein trisulfide couples dissimilatory sulfate reduction to energy conservation. *Science* 350**,** 1541-1545.
Schink, B. (1997). Energetics of syntrophic cooperation in methanogenic degradation. *Microbiology and Molecular Biology Reviews* 61**,** 262-280.
Schink, B. (2015). Electron confurcation in anaerobic lactate oxidation. *Environmental Microbiology* 17**,** 543.
Schink, B., Montag, D., Keller, A., and Müller, N. (2017). Hydrogen or formate: Alternative key players in methanogenic degradation. *Environmental Microbiology Reports*.
Schink, B., and Stams, A.J.M. (2013). "Syntrophism among prokaryotes," ed. S.B. Heidelberg.), 471-493.
Schlindwein, C., Giordano, G., Santini, C.L., and Mandrand, M.A. (1990). Identification and expression of the *Escherichia coli fdh*D and *fdh*E genes, which are involved in the formation of respiratory formate dehydrogenase. *Journal of Bacteriology* 172**,** 6112-6121.
Schmidt, A., Müller, N., Schink, B., and Schleheck, D. (2013). A proteomic view at the biochemistry of syntrophic butyrate oxidation in *Syntrophomonas wolfei*. *PLoS One* 8**,** e56905.
Schmidt, J.E., and Ahring, B.K. (1995). Interspecies electron transfer during propionate and butyrate degradation in mesophilic, granular sludge. *Applied and Environmental Microbiology* 61**,** 2765-2767.
Schnürer, A., Zellner, G., and Svensson, B.H. (1999). Mesophilic syntrophic acetate oxidation during methane formation in biogas reactors. *FEMS Microbiology Ecology* 29**,** 249-261.
Scholten, J.C.M., and Conrad, R. (2000). Energetics of syntrophic propionate oxidation in defined batch and chemostat cocultures. *Applied and Environmental Microbiology* 66**,** 2934-2942.
Schut, G.J., and Adams, M.W. (2009). The iron-hydrogenase of *Thermotoga maritima* utilizes ferredoxin and NADH synergistically: a new perspective on anaerobic hydrogen production. *Journal of Bacteriology* 191**,** 4451-4457.
Seitz, H.-J., Schink, B., and Conrad, R. (1988). Thermodynamics of hydrogen metabolism in methanogenic cocultures degrading ethanol or lactate. *FEMS Microbiology Letters* 55**,** 119-124.

Sekiguchi, Y., Kamagata, Y., Nakamura, K., Ohashi, A., and Harada, H. (2000). *Syntrophothermus lipocalidus* gen. nov., sp. nov., a novel thermophilic, syntrophic, fatty-acid-oxidizing anaerobe which utilizes isobutyrate. *International journal of systematic and evolutionary microbiology* 50 Pt 2**,** 771-779.

Serrano, A., Perez-Castineira, J.R., Baltscheffsky, M., and Baltscheffsky, H. (2007). H^+-PPases: yesterday, today and tomorrow. *IUBMB Life* 59**,** 76-83.

Setzke, E., Hedderich, R., Heiden, S., and Thauer, R.K. (1994). H_2: heterodisulfide oxidoreductase complex from *Methanobacterium thermoautotrophicum*. Composition and properties. *European Journal of Biochemistry* 220**,** 139-148.

Shao, M.F., Zhang, T., and Fang, H.H. (2010). Sulfur-driven autotrophic denitrification: diversity, biochemistry, and engineering applications. *Applied microbiology and biotechnology* 88**,** 1027-1042.

Sheik, C.S., Sieber, J.R., Badalamenti, J.P., Carden, K., and Olson, A. (2017). Complete genome sequence of *Desulfovibrio desulfuricans* strain G11, a model sulfate-reducing, hydrogenotrophic, and syntrophic partner organism. *Genome Announcements* 5.

Shimoyama, T., Kato, S., Ishii, S., and Watanabe, K. (2009). Flagellum mediates symbiosis. *Science* 323**,** 1574.

Shrestha, P.M., and Rotaru, A.E. (2014). Plugging in or going wireless: strategies for interspecies electron transfer. *Frontiers in Microbiology* 5**,** 237.

Shrestha, P.M., Rotaru, A.E., Aklujkar, M., Liu, F., Shrestha, M., Summers, Z.M., Malvankar, N., Flores, D.C., and Lovley, D.R. (2013). Syntrophic growth with direct interspecies electron transfer as the primary mechanism for energy exchange. *Environmental Microbiology Reports* 5**,** 904-910.

Sieber, J.R., Crable, B.R., Sheik, C.S., Hurst, G.B., Rohlin, L., Gunsalus, R.P., and Mcinerney, M.J. (2015). Proteomic analysis reveals metabolic and regulatory systems involved in the syntrophic and axenic lifestyle of *Syntrophomonas wolfei*. *Frontiers in Microbiology* 6**,** 115.

Sieber, J.R., Le, H.M., and Mcinerney, M.J. (2014). The importance of hydrogen and formate transfer for syntrophic fatty, aromatic and alicyclic metabolism. *Environmental Microbiology* 16**,** 177-188.

Sieber, J.R., Mcinerney, M.J., and Gunsalus, R.P. (2012). Genomic insights into syntrophy: the paradigm for anaerobic metabolic cooperation. *Annual Review of Microbiology* 66**,** 429-452.

Sieber, J.R., Sims, D.R., Han, C., Kim, E., Lykidis, A., Lapidus, A.L., Mcdonnald, E., Rohlin, L., Culley, D.E., Gunsalus, R., and Mcinerney, M.J. (2010). The genome of *Syntrophomonas wolfei*: new insights into syntrophic metabolism and biohydrogen production. *Environmental Microbiology* 12**,** 2289-2301.

Siegert, I., and Banks, C. (2005). The effect of volatile fatty acid additions on the anaerobic digestion of cellulose and glucose in batch reactors. *Process Biochemistry* 40**,** 3412-3418.

Skouteris, G., Hermosilla, D., López, P., Negro, C., and Blanco, Á. (2012). Anaerobic membrane bioreactors for wastewater treatment: A review. *Chemical Engineering Journal* 198-199**,** 138-148.

Soga, N., Kimura, K., Kinosita, K., Jr., Yoshida, M., and Suzuki, T. (2017). Perfect chemomechanical coupling of FoF1-ATP synthase. *Proceedings of the National Academy of Sciences* 114**,** 4960-4965.

Søndergaard, D., Pedersen, C.N., and Greening, C. (2016). HydDB: A web tool for hydrogenase classification and analysis. *Scientific Reports* 6**,** 34212.

Sousa, D.Z., Smidt, H., Alves, M.M., and Stams, A.J.M. (2007). *Syntrophomonas zehnderi* sp. nov., an anaerobe that degrades long-chain fatty acids in co-culture with *Methanobacterium formicicum*. *International Journal of Systematic and Evolutionary Microbiology* 57**,** 609-615.

Sousa, D.Z., Smidt, H., Alves, M.M., and Stams, A.J.M. (2009). Ecophysiology of syntrophic communities that degrade saturated and unsaturated long-chain fatty acids. *Fems Microbiology Ecology* 68**,** 257-272.

Stams, A.J.M. (1994). Metabolic interactions between anaerobic bacteria in methanogenic environments. *Antonie van Leeuwenhoek* 66**,** 271-294.
Stams, A.J.M., De Bok, F.a.M., Plugge, C.M., Van Eekert, M.H., Dolfing, J., and Schraa, G. (2006). Exocellular electron transfer in anaerobic microbial communities. *Environmental Microbiology* 8**,** 371-382.
Stams, A.J.M., and Dong, X. (1995). Role of formate and hydrogen in the degradation of propionate and butyrate by defined suspended cocultures of acetogenic and methanogenic bacteria. *Antonie van Leeuwenhoek* 68**,** 281-284.
Stams, A.J.M., and Plugge, C.M. (2009). Electron transfer in syntrophic communities of anaerobic bacteria and archaea. *Nature Reviews Microbiology* 7**,** 568-577.
Stams, A.J.M., Plugge, C.M., De Bok, F.a.M., Van Houten, B.H.G.W., Lens, P.N.L., Dijkman, H., and Weijma, J. (2005). Metabolic interactions in methanogenic and sulfate-reducing bioreactors. *Water Science and Technology* 52**,** 13-20.
Stams, A.J.M., Sousa, D.Z., Kleerebezem, R., and Plugge, C.M. (2012). Role of syntrophic microbial communities in high-rate methanogenic bioreactors. *Water Science and Technology* 66**,** 352-362.
Stams, A.J.M., Van Dijk, J.B., Dijkema, C., and Plugge, C.M. (1993). Growth of syntrophic propionate-oxidizing bacteria with fumarate in the absence of methanogenic bacteria. *Applied and Environmental Microbiology* 59**,** 1114-1119.
Steenbakkers, P.J.M., Geerts, W.J., Ayman-Oz, N.A., and Keltjens, J.T. (2006). Identification of pseudomurein cell wall binding domains. *Molecular Microbiology* 62**,** 1618-1630.
Stojanowic, A., Mander, G.J., Duin, E.C., and Hedderich, R. (2003). Physiological role of the F_{420}-non-reducing hydrogenase (Mvh) from *Methanothermobacter marburgensis*. *Archives of Microbiology* 180**,** 194-203.
Stothard, P. (2000). The sequence manipulation suite: JavaScript programs for analyzing and formatting protein and DNA sequences. . *Biotechniques* 28**,** 1102-1104. .
Strittmatter, A.W., Liesegang, H., Rabus, R., Decker, I., Amann, J., Andres, S., Henne, A., Fricke, W.F., Martinez-Arias, R., Bartels, D., Goesmann, A., Krause, L., Puhler, A., Klenk, H.P., Richter, M., Schuler, M., Glockner, F.O., Meyerdierks, A., Gottschalk, G., and Amann, R. (2009). Genome sequence of *Desulfobacterium autotrophicum* HRM2, a marine sulfate reducer oxidizing organic carbon completely to carbon dioxide. *Environmental Microbiology* 11**,** 1038-1055.
Stroot, P.G., Mcmahon, K.D., Mackie, R.I., and Raskin, L. (2001). Anaerobic codigestion of municipal solid waste and biosolids under various mixing conditions - I. Digester performance. *Water Research* 35**,** 1804-1816.
Subhash, Y., Bang, J.J., You, T.H., and Lee, S.S. (2016). Description of *Comamonas sediminis* sp. nov., isolated from lagoon sediments. *International Journal of Systematic and Evolutionary Microbiology* 66**,** 2735-2739.
Suess, D.L., Kuchenreuther, J.M., De La Paz, L., Swartz, J.R., and Britt, R.D. (2016). Biosynthesis of the [FeFe] Hydrogenase H Cluster: A Central Role for the Radical SAM Enzyme HydG. *Inorganic chemistry* 55**,** 478-487.
Summers, Z.M., Fogarty, H.E., Leang, C., Franks, A.E., Malvankar, N.S., and Lovley, D.R. (2010). Direct exchange of electrons within aggregates of an evolved syntrophic coculture of anaerobic bacteria. *Science* 330**,** 1413-1415.
Sun, L., Toyonaga, M., Ohashi, A., Tourlousse, D.M., Matsuura, N., Meng, X.Y., Tamaki, H., Hanada, S., Cruz, R., Yamaguchi, T., and Sekiguchi, Y. (2016). *Lentimicrobium saccharophilum* gen. nov., sp. nov., a strictly anaerobic bacterium representing a new family in the phylum *Bacteroidetes*, and proposal of *Lentimicrobiaceae* fam. nov. *International Journal of Systematic and Evolutionary Microbiology*.
Team, R.C. (2016). "R: A language and environment for statistical computing", (ed.) R.F.F.S. Computing. (Vienna, Austria).
Thauer, R.K. (1998). Biochemistry of methanogenesis: a tribute to Marjory Stephenson. *Microbiology* 144 (Pt 9)**,** 2377-2406.
Thauer, R.K. (2012). The Wolfe cycle comes full circle. *Proceedings of the National Academy of Sciences* 109**,** 15084-15085.
Thauer, R.K., Jungermann, K., and Decker, K. (1977). Energy conservation in chemotrophic anaerobic bacteria. *Bacteriological Reviews* 41**,** 100-180.

Thauer, R.K., Kaster, A.K., Goenrich, M., Schick, M., Hiromoto, T., and Shima, S. (2010). Hydrogenases from methanogenic archaea, nickel, a novel cofactor, and H2 storage. *Annual Review of Biochemistry* 79**,** 507-536.

Thauer, R.K., Kaster, A.K., Seedorf, H., Buckel, W., and Hedderich, R. (2008). Methanogenic archaea: ecologically relevant differences in energy conservation. *Nature Reviews Microbiology* 6**,** 579-591.

Thiele, J.H., Chartrain, M., and Zeikus, J.G. (1988). Control of interspecies electron flow during anaerobic digestion: Role of floc formation in syntrophic methanogenesis. *Applied and Environmental Microbiology* 54**,** 10-19.

Thiele, J.H., and Zeikus, J.G. (1988). Control of interspecies electron flow during anaerobic digestion: Significance of formate transfer versus hydrogen transfer during syntrophic methanogenesis in flocs. *Applied and Environmental Microbiology* 54**,** 20-29.

Tian, H., Fotidis, I.A., Mancini, E., Treu, L., Mahdy, A., Ballesteros, M., Gonzalez-Fernandez, C., and Angelidaki, I. (2017). Acclimation to extremely high ammonia levels in continuous biomethanation process and the associated microbial community dynamics. *Bioresource Technology* 247**,** 616-623.

Tokuda, M., Ohta, N., Morimura, S., and Kida, K. (1998). Methane fermentation of pot ale from a whisky distillery after enzymatic or microbial treatment. *Journal of Fermentation and Bioengineering* 85**,** 495-501.

Tremblay, P.L., Zhang, T., Dar, S.A., Leang, C., and Lovley, D.R. (2012). The Rnf complex of *Clostridium ljungdahlii* is a proton-translocating ferredoxin:NAD^+ oxidoreductase essential for autotrophic growth. *MBio* 4**,** e00406-00412.

Turkarslan, S., Raman, A.V., Thompson, A.W., Arens, C.E., Gillespie, M.A., Von Netzer, F., Hillesland, K.L., Stolyar, S., Lopez Garcia De Lomana, A., Reiss, D.J., Gorman-Lewis, D., Zane, G.M., Ranish, J.A., Wall, J.D., Stahl, D.A., and Baliga, N.S. (2017). Mechanism for microbial population collapse in a fluctuating resource environment. *Molecular Systems Biology* 13**,** 919.

Ueki, A., Akasaka, H., Suzuki, D., and Ueki, K. (2006). Paludibacter propionicigenes gen. nov., sp. nov., a novel strictly anaerobic, Gram-negative, propionate-producing bacterium isolated from plant residue in irrigated rice-field soil in Japan. *International Journal of Systematic and Evolutionary Microbiology* 56**,** 39-44.

Van Den Bogert, B., De Vos, W.M., Zoetendal, E.G., and Kleerebezem, M. (2011). Microarray analysis and barcoded pyrosequencing provide consistent microbial profiles depending on the source of human intestinal samples. *Applied and Environmental Microbiology* 77**,** 2071-2080.

Van Den Bogert, B., Erkus, O., Boekhorst, J., De Goffau, M., Smid, E.J., Zoetendal, E.G., and Kleerebezem, M. (2013). Diversity of human small intestinal *Streptococcus* and *Veillonella* populations. *FEMS Microbiology Ecology* 85**,** 376-388.

Van Kuijk, B.L.M., Hagen, W.R., and Stams, A.J.M. (1998a). "Isolation and properties of the oxygen-sensitive fumarate reductase of the syntrophic propionate-oxidizing bacterium strain MPOB," in *Biochemistry and bioenergetics of syntrophic propionate-oxidizing bacteria*.), 71.

Van Kuijk, B.L.M., Schlosser, E., and Stams, A.J.M. (1998b). Investigation of the fumarate metabolism of the syntrophic propionate-oxidizing bacterium strain MPOB. *Archives of Microbiology* 169**,** 346-352.

Van Kuijk, B.L.M., and Stams, A.J.M. (1995). Sulfate reduction by a syntrophic propionate-oxidizing bacterium. *Antonie van Leeuwenhoek* 68**,** 293-296.

Van Kuijk, B.L.M., and Stams, A.J.M. (1996). Purification and characterization of malate dehydrogenase from the syntrophic propionate-oxidizing bacterium strain MPOB. *FEMS Microbiology Letters* 144**,** 141-144.

Van Kuijk, B.L.M., Van Loo, N.D., Arendsen, A.F., Hagen, W.R., and Stams, A.J.M. (1996). Purification and characterization of fumarase from the syntrophic propionate-oxidizing bacterium strain MPOB. *Archives of Microbiology* 165**,** 126-131.

Venceslau, S.S., Lino, R.R., and Pereira, I.A. (2010). The Qrc membrane complex, related to the alternative complex III, is a menaquinone reductase involved in sulfate respiration. *Journal of Biological Chemistry* 285**,** 22774-22783.

Venceslau, S.S., Stockdreher, Y., Dahl, C., and Pereira, I.A. (2014). The "bacterial heterodisulfide" DsrC is a key protein in dissimilatory sulfur metabolism. *Biochimica et Biophysica Acta* 1837**,** 1148-1164.

Vidal, G., Carvalho, A., Méndez, R., and Lema, J.M. (2000). Influence of the content in fats and proteins on the anaerobic biodegradability of dairy wastewaters. *Bioresource Technology* 74**,** 231- 239.

Vignais, P.M., and Billoud, B. (2007). Occurrence, classification, and biological function of hydrogenases: an overview. *Chemical Reviews* 107**,** 4206-4272.

Vignais, P.M., Billoud, B., and Meyer, J. (2001). Classification and phylogeny of hydrogenases. *FEMS Microbiology Reviews* 25**,** 455-501.

Vincent, K.A., Parkin, A., and Armstrong, F.A. (2007). Investigating and exploiting the electrocatalytic properties of hydrogenases. *Chemical Reviews* 107**,** 4366-4413.

Visser, M., Worm, P., Muyzer, G., Pereira, I.A., Schaap, P.J., Plugge, C.M., Kuever, J., Parshina, S.N., Nazina, T.N., Ivanova, A.E., Bernier-Latmani, R., Goodwin, L.A., Kyrpides, N.C., Woyke, T., Chain, P., Davenport, K.W., Spring, S., Klenk, H.P., and Stams, A.J.M. (2013). Genome analysis of *Desulfotomaculum kuznetsovii* strain 17^T reveals a physiological similarity with *Pelotomaculum thermopropionicum* strain SI^T. *Standards in Genomic Sciences* 8**,** 69-87.

Visweswaran, G.R.R., Dijkstra, B.W., and Kok, J. (2011). Murein and pseudomurein cell wall binding domains of bacteria and archaea - a comparative view. *Applied Microbiology and Biotechnology* 92**,** 921-928.

Von Canstein, H., Ogawa, J., Shimizu, S., and Lloyd, J.R. (2008). Secretion of flavins by *Shewanella* species and their role in extracellular electron transfer. *Applied and Environmental Microbiology* 74**,** 615-623.

Vorholt, J.A., Vaupel, M., and Thauer, R.K. (1997). A selenium-dependent and a selenium-independent formylmethanofuran dehydrogenase and their transcriptional regulation in the hyperthermophilic *Methanopyrus kandleri*. *Molecular Microbiology* 23**,** 1033-1042.

Walker, C.B., He, Z., Yang, Z.K., Ringbauer, J.A., Jr., He, Q., Zhou, J., Voordouw, G., Wall, J.D., Arkin, A.P., Hazen, T.C., Stolyar, S., and Stahl, D.A. (2009). The electron transfer system of syntrophically grown *Desulfovibrio vulgaris*. *Journal of Bacteriology* 191**,** 5793-5801.

Wallrabenstein, C., Gorny, N., Springer, N., Ludwig, W., and Schink, B. (1995a). Pure culture of *Syntrophus buswellii*, definition of its phylogenetic status, and description of *Syntrophus gentianae* sp. nov. *Systematic and Applied Microbiology* 18**,** 62-66.

Wallrabenstein, C., Hauschild, E., and Schink, B. (1994). Pure culture and cytological properties of '*Syntrophobacter wolini*'. *FEMS Microbiology Letters* 123**,** 249-254.

Wallrabenstein, C., Hauschild, E., and Schink, B. (1995b). *Syntrophobacter pfennigii* sp. nov., new syntrophically propionate-oxidizing anaerobe growing in pure culture with propionate and sulfate. *Archives of Microbiology* 164**,** 346-352.

Wan, C.Y., De Wever, H., Diels, L., Thoeye, C., Liang, J.B., and Huang, L.N. (2011). Biodiversity and population dynamics of microorganisms in a full-scale membrane bioreactor for municipal wastewater treatment. *Water Research* 45**,** 1129-1138.

Wang, H., Fotidis, I.A., and Angelidaki, I. (2015). Ammonia effect on hydrogenotrophic methanogens and syntrophic acetate-oxidizing bacteria. *FEMS Microbiology Ecology* 91.

Wang, H., Zhang, Y., and Angelidaki, I. (2016). Ammonia inhibition on hydrogen enriched anaerobic digestion of manure under mesophilic and thermophilic conditions. *Water Research* 105**,** 314-319.

Wang, S., Huang, H., Kahnt, J., Mueller, A.P., Kopke, M., and Thauer, R.K. (2013a). NADP-specific electron-bifurcating [FeFe]-hydrogenase in a functional complex with formate dehydrogenase in *Clostridium autoethanogenum* grown on CO. *Journal of Bacteriology* 195**,** 4373-4386.

Wang, S., Huang, H., Kahnt, J., and Thauer, R.K. (2013b). *Clostridium acidurici* electron-bifurcating formate dehydrogenase. *Applied and Environmental Microbiology* 79**,** 6176-6179.

Wang, S., Huang, H., Moll, J., and Thauer, R.K. (2010). $NADP^+$ reduction with reduced ferredoxin and $NADP^+$ reduction with NADH are coupled via an electron-bifurcating enzyme complex in *Clostridium kluyveri*. *Journal of Bacteriology* 192**,** 5115-5123.

Wang, Y., and Qian, P.Y. (2009). Conservative fragments in bacterial 16S rRNA genes and primer design for 16S ribosomal DNA amplicons in metagenomic studies. *PLoS One* 4.

Wang, Y.Y., Zhang, Y.L., Wang, J.B., and Meng, L. (2009). Effects of volatile fatty acid concentrations on methane yield and methanogenic bacteria. *Biomass and Bioenergy* 33**,** 848-853.

Westerholm, M., Moestedt, J., and Schnürer, A. (2016). Biogas production through syntrophic acetate oxidation and deliberate operating strategies for improved digester performance. *Applied Energy* 179**,** 124-135.

Wofford, N.Q., Beaty, P.S., and Mcinerney, M.J. (1986). Preparation of cell-free extracts and the enzymes involved in fatty acid metabolism in *Syntrophomonas wolfei*. *Journal of Bacteriology* 167**,** 179-185.

Worm, P. (2010). *Formate dehydrogenases and hydrogenases in syntrophic propionate-oxidizing communities: gene analysis and transcriptional profiling.* PhD PhD Thesis.

Worm, P., Fermoso, F.G., Stams, A.J.M., Lens, P.N.L., and Plugge, C.M. (2011a). Transcription of fdh and hyd in *Syntrophobacter* spp. and *Methanospirillum* spp. as a diagnostic tool for monitoring anaerobic sludge deprived of molybdenum, tungsten and selenium. *Environmental Microbiology* 13**,** 1228-1235.

Worm, P., Koehorst, J.J., Visser, M., Sedano-Nunez, V.T., Schaap, P.J., Plugge, C.M., Sousa, D.Z., and Stams, A.J.M. (2014). A genomic view on syntrophic versus non-syntrophic lifestyle in anaerobic fatty acid degrading communities. *Biochimica et Biophysica Acta* 1837**,** 2004-2016.

Worm, P., Stams, A.J.M., Cheng, X., and Plugge, C.M. (2011b). Growth- and substrate-dependent transcription of formate dehydrogenase and hydrogenase coding genes in *Syntrophobacter fumaroxidans* and *Methanospirillum hungatei*. *Microbiology* 157**,** 280-289.

Wu, J.H., Wu, F.Y., Chuang, H.P., Chen, W.Y., Huang, H.J., Chen, S.H., and Liu, W.T. (2013). Community and proteomic analysis of methanogenic consortia degrading terephthalate. *Applied and Environmental Microbiology* 79**,** 105-112.

Wu, L.F., and Mandrand, M.A. (1993). Microbial hydrogenases: primary structure, classification, signatures and phylogeny. *FEMS Microbiology Reviews* 10**,** 243-269.

Xie, F., Ma, H., Quan, S., Liu, D., and Chen, G. (2016). *Comamonas phosphati* sp. nov., isolated from a phosphate mine. *International Journal of Systematic and Evolutionary Microbiology* 66**,** 456-461.

Yadav, R.K., Baeg, J.O., Oh, G.H., Park, N.J., Kong, K.J., Kim, J., Hwang, D.W., and Biswas, S.K. (2012). A photocatalyst-enzyme coupled artificial photosynthesis system for solar energy in production of formic acid from CO2. *Journal of the American Chemical Society* 134**,** 11455-11461.

Yang, W.B., Cicek, N., and Ilg, J. (2006). State-of-the-art of membrane bioreactors: Worldwide research and commercial applications in North America. *Journal of Membrane Science* 270**,** 201-211.

Yano, T. (2002). The energy-transducing NADH: quinone oxidoreductase, complex I. *Molecular Aspects of Medicine* 23**,** 345-368.

Yenigun, O., and Demirel, B. (2013). Ammonia inhibition in anaerobic digestion: A review. *Process Biochemistry* 48**,** 901-911.

Zhang, C., Yuan, Q., and Lu, Y. (2014). Inhibitory effects of ammonia on methanogen mcrA transcripts in anaerobic digester sludge. *FEMS Microbiology Ecology* 87**,** 368-377.

Zhang, P., Yuly, J.L., Lubner, C.E., Mulder, D.W., King, P.W., Peters, J.W., and Beratan, D.N. (2017). Electron bifurcation: Thermodynamics and kinetics of two-electron brokering in biological redox chemistry. *Accounts of Chemical Research* 50**,** 2410-2417.

Zhang, Y., and Gladyshev, V.N. (2005). An algorithm for identification of bacterial selenocysteine insertion sequence elements and selenoprotein genes. *Bioinformatics* 21**,** 2580-2589.

Zheng, K., Ngo, P.D., Owens, V.L., Yang, X.P., and Mansoorabadi, S.O. (2016). The biosynthetic pathway of coenzyme F430 in methanogenic and methanotrophic archaea. *Science* 354**,** 339-342.

Ziganshin, A.M., Schmidt, T., Scholwin, F., Il'inskaya, O.N., Harms, H., and Kleinsteuber, S. (2011). Bacteria and archaea involved in anaerobic digestion of distillers grains with solubles. *Applied Microbiology and Biotechnology* 89**,** 2039-2052.

Zinder, S.H. (1993). "Physiological ecology of methanogens," in *Methanogenesis*. Springer), 128-206.

Zinder, S.H., and Koch, M. (1984). Non-aceticlastic methanogenesis from acetate: acetate oxidation by a thermophilic syntrophic coculture. *Archives of Microbiology* 138**,** 263-272.

Zuker, M. (2003). Mfold web server for nucleic acid folding and hybridization prediction. *Nucleic Acids Research* 31**,** 3406-3415.

Summary

Syntrophic methanogenic associations between acetogenic bacteria and methanogenic archaea are essential for the complete mineralization of organic compounds to methane and CO_2. Propionate and butyrate are important intermediates in anaerobic digestion. In the absence of inorganic electron acceptors these short chain fatty acids can only be degraded if the products acetate, hydrogen and formate, are kept low by methanogens. However, when sulfate is available the conditions change, and propionate and butyrate can be oxidized coupled to sulfate reduction. Several sulfate-reducing bacteria are able to grow in syntrophic associations with methanogens, but others not.

In this thesis, a functional analysis of protein domains was performed on a selected group of bacteria with the ability to grow on short chain fatty acids alone, or in syntrophy with methanogens. Genome analysis revealed that the presence of periplasmic formate dehydrogenases, most probably involved in interspecies electron transfer, differentiated syntrophic from non-syntrophic butyrate and propionate degraders.

Moreover, the metabolic flexibility of the propionate-degrading bacterium *Syntrophobacter fumaroxidans* was investigated. *S. fumaroxidans* can couple propionate oxidation to sulfate reduction or can degrade propionate in syntrophic lifestyle with H_2 and formate scavenging microorganisms. Propionate-grown cultures of *S. fumaroxidans* with sulfate as electron acceptor, or in syntrophy with *Methanospirillum hungatei* or *Desulfovibrio desulfuricans* were studied. We found that *S. fumaroxidans* is prone to oxidize propionate in syntrophy despite the availability of sulfate to grow on its own.

A comparative proteomic analysis of propionate degradation by *S. fumaroxidans* in five growth conditions, including axenic and cocultures, was performed. This analysis gave a thorough overview of the propionate metabolism of *S. fumaroxidans*. Details on the energy conservation mechanisms and electron transfer to syntrophic partners were obtained. The results indicate that confurcating hydrogenases and formate dehydrogenases are important energy converting enzymes in propionate degradation by *S. fumaroxidans*. Moreover, three formate dehydrogenases fulfil an important role in the syntrophic lifestyle. Furthermore, the proteomic profile of *S. fumaroxidans* grown with sulfate revealed in detail the sulfate respiratory pathway of this model bacterium. The abundance of a putatively confurcating protein complex detected only in sulfate-grown cells, is an important finding. This confurcating complex has similarities to heterodisulfide reductases, proteins known to bifurcate electrons in methanogenic archaea. The detection of membrane-associated proteins usually involved in sulfate reduction in all growth conditions leaves room for research on the role of these complexes in electron transfer during syntrophic lifestyle.

Understanding the interactions between propionate-oxidizing syntrophic consortia also involved the investigation of the syntrophic partners of *S. fumaroxidans*. We analysed the proteome of *M. hungatei*, *Methanobacterium formicicum* and *D. desulfuricans* grown in syntrophy and in pure culture with H_2/CO_2 or formate. Although both methanogens can grow on hydrogen and formate, the molecular mechanisms studied in this thesis, points to the use of hydrogen in *M. formicicum*, and of formate in *M. hungatei*, as electron carriers in their metabolism.

Lastly, the microbial community involved in pot ale digestion in an anaerobic membrane bioreactor was analysed using 16S rRNA next-generation sequencing. The robustness of the reactor to high loading tests and the effect on the microbial composition was discussed. Moreover, on-line monitoring of hydrogen in the biogas showed a rapid response to disturbances in the proper performance of the reactor. Thus, our study supports the use of on-line H_2 measurements as an early warning indicator of process instability.

The detailed study and analysis of the molecular mechanisms for energy conservation and interspecies electron transfer discussed in this thesis increases our understanding of electron fluxes occurring in methanogenic syntrophic consortia. These types of analyses are necessary to unravel the black-box ecology of anaerobic biotechnology and the global carbon flux.

Acknowledgements

Formally I want to thank my promotor and co-promotor for working with me along this project. **Caroline**, thank you for giving me the opportunity to join this project and for the supervision and time you dedicated to it. I learned a lot from you since that course of Microbial Physiology that I took while doing my Master's, and later much more during all our meetings and discussions. I remember well when you interviewed me for the position, and you stated that in my CV there were only individual sports and not ones that are played in a team. I never thought about that before, and I am sure that was one of the things that I struggled with during my PhD. But believe me, although I am a slow learner I always kept it in mind and I will be working on it. Thanks for teaching me how to be a researcher, from the theory to the practical and going through the administrative chores.

Fons, although we had many meetings along my PhD, I am especially grateful for the discussions and prompt feedback that you gave about my manuscripts when I had already left the Netherlands. I have always been impressed by your efficient, concrete and fast reply which made the writing process easy despite the distance. Thanks for your directness, scepticism and motivation that always came when it was needed the most.

I would also like to thank **Sjef** Boeren and **Frank** van der Zee for their contributions to this work. You both were very patient and helpful, and I hope you are happy with the resulting work.

More informally I want to acknowledge HER, who is the radioactive material in my very personal Schrödinger's-like thought experiment: To have/haven't met you resulted in the superposition of "finishing this thesis on time" or "not finishing it at all". I guess that now that the box is open we see that the Wageningen interpretation had a third superposed state.

A mis padres y mis hermanos que siempre estuvieron en mi mente y en algunas ocasiones ahí conmigo. Los quiero mucho, espero que podamos estar juntos más seguido.

NEXT PAGE: During these years many people have entered, influenced or only passed by my life. To all those people that form a part of what I am today, thank you and see you along the way!

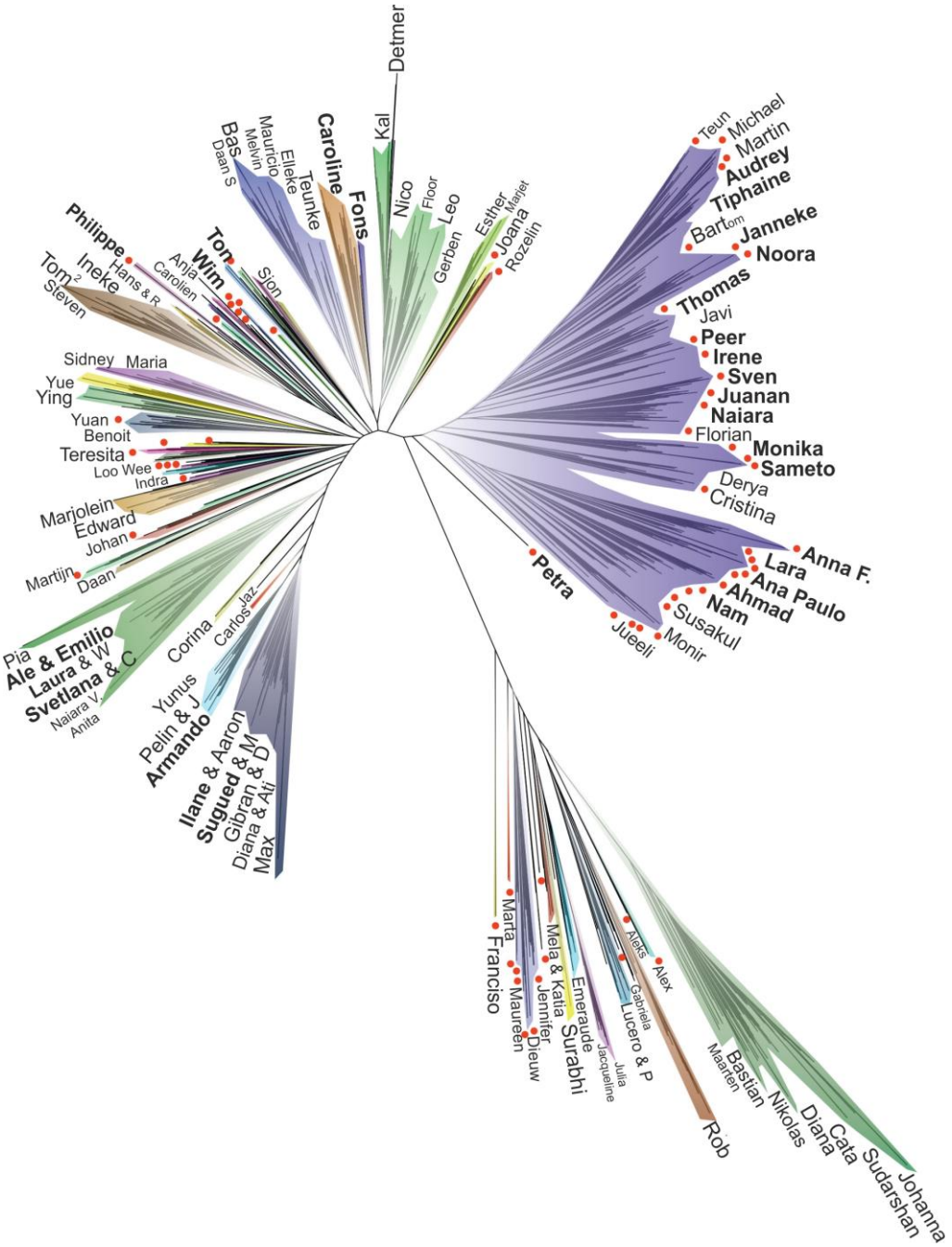

Modified from (Hug et al., 2016)

Disclaimer: No racist intention was meant in the elaboration of this diagram. For all racist interpretation you might infer from it I will argue the Tarantino effect: The racism is already there in your mind.

Netherlands Research School for the
Socio-Economic and Natural Sciences of the Environment

D I P L O M A

For specialised PhD training

The Netherlands Research School for the
Socio-Economic and Natural Sciences of the Environment
(SENSE) declares that

Vicente Tonamellotl Sedano Núñez

born on 11 August 1984 in Mexico City, Mexico

has successfully fulfilled all requirements of the
Educational Programme of SENSE.

Wageningen, 3 April 2018

the Chairman of the SENSE board	the SENSE Director of Education
Prof. dr. Huub Rijnaarts	Dr. Ad van Dommelen

The SENSE Research School has been accredited by the Royal Netherlands Academy of Arts and Sciences (KNAW)

KONINKLIJKE NEDERLANDSE
AKADEMIE VAN WETENSCHAPPEN

The SENSE Research School declares that **Mr Vicente Tonamellotl Sedano Núñez** has successfully fulfilled all requirements of the Educational PhD Programme of SENSE with a work load of 32 EC, including the following activities:

SENSE PhD Courses

- New frontiers in microbial ecology (2013)
- Environmental research in context (2012)
- Research in context activity: 'Co-organizing PhD Study Trip 2013 Laboratories of Microbiology and Systems & Synthetic Biology (USA-Canada, 29 April – 10 May 2013)' (2013)

Other PhD and Advanced MSc Courses

- Advanced Proteomics, Wageningen University (2015)
- Scientific Publishing, Wageningen University (2011)
- Project and Time Management, Wageningen University (2011)
- Techniques for Writing and Presenting Scientific Papers, Wageningen University (2013)

Management and Didactic Skills Training

- Supervising BSc student with thesis entitled 'Reduction of bacterial growth' (2012)
- Assisting practicals of the BSc course 'Microbial Physiology' (2012-2013)
- Assisting practicals of the MSc course 'Research Methods Microbiology' (2012-2014)

Oral Presentations

- *Interspecies electron transfer in fatty acid-degrading communities.* Scientific Spring Meeting KNVM and NVMM, 14 April 2014, Papendal, The Netherlands
- *Electron fluxes in methanogenic microbial communities,* 30 April 2013, New England BioLabs, Ipswich, MA. USA.
- *Metabolic flexibility of Syntrophobacter fumaroxidans*, 7 May 2013, Cornell University, Ithaca, NY. USA.
- *Comparative proteomic analysis of propionate oxidation by S. fumaroxidans*, 10 May 2013, University of Ontario, Oshawa, ON. CANADA.

SENSE Coordinator PhD Education

Dr. Peter Vermeulen

This research is supported by the Dutch Technology Foundation STW, which is part of the Netherlands Organisation for Scientific Research (NWO) and partly funded by the Ministry of Economic Affairs (project number 11603)

Thesis layout: Vicente Sedano

Image in the Chapter titles: Modified section of "Man, Controller of the Universe" by Diego Rivera. 1934. Licensed under the Creative Commons Attribution-Share Alike 3.0 Unported.

Cover design: Digiforce | | ProefschriftMaken

Printed by: Digiforce | | ProefschriftMaken

Financial support from the Laboratory of Microbiology (Wageningen University) for printing this thesis is gratefully acknowledged.